

12

AD

USAAVLABS TECHNICAL REPORT 68-87

FEASIBILITY OF GAS BEARINGS FOR SMALL HIGH-PERFORMANCE AIRCRAFT GAS TURBINES

By

Peter William Curwen

March 1969

AD 684956

**U. S. ARMY AVIATION MATERIEL LABORATORIES
FORT EUSTIS, VIRGINIA**

**CONTRACT DAAJ02-67-C-0026
MECHANICAL TECHNOLOGY INCORPORATED
LATHAM, NEW YORK**

This document has been approved for public release and sale; its distribution is unlimited.



Reproduced by the
CLEARINGHOUSE
for Federal Scientific & Technical
Information Springfield Va. 22151

DDC
RECEIVED
APR 10 1969
RECEIVED

Disclaimers

The findings in this report are not to be construed as an official Department of the Army position unless so designated by other authorized documents.

When Government drawings, specifications, or other data are used for any purpose other than in connection with a definitely related Government procurement operation, the United States Government thereby incurs no responsibility nor any obligation whatsoever; and the fact that the Government may have formulated, furnished, or in any way supplied the said drawings, specifications, or other data is not to be regarded by implication or otherwise as in any manner licensing the holder or any other person or corporation, or conveying any rights or permission, to manufacture, use, or sell any patented invention that may in any way be related thereto.

Trade names cited in this report do not constitute an official endorsement or approval of the use of such commercial hardware or software.

Disposition Instructions

Destroy this report when no longer needed. Do not return it to the originator.

ADDITIONAL TO		
CFSTI	PHOTO SECTION <input checked="" type="checkbox"/>	
DOC	BUFP SECTION <input type="checkbox"/>	
UNANNOUNCED	<input type="checkbox"/>	
JUSTIFICATION		
BY		
SUPERVISION AVAILABILITY CODES		
UNCL	AVAIL. 33	SPECIAL



DEPARTMENT OF THE ARMY
U. S. ARMY AVIATION MATERIEL LABORATORIES
FORT EUSTIS, VIRGINIA 23604

The object of this contractual effort was to determine the feasibility of incorporating gas bearings in a small high-performance aircraft gas turbine engine.

This report was prepared by Mechanical Technology Incorporated under the terms of Contract DAAJ02-67-C-0026. It describes a gas generator designed to incorporate gas bearings and the studies undertaken in the bearing design process. Discussion is presented in areas of selection of bearing type, design of journal and thrust bearings, accommodation of bearing loads, thermal studies and bearing materials.

The study showed that current gas bearing technology is incomplete in the areas of rotor-bearing dynamics and in demonstrated capabilities of bearing structural and coating materials successfully to withstand the operating environment. The results indicate that gas bearing utilization in a small gas turbine engine is feasible in all other aspects.

This report has been reviewed by technical personnel of this Command, and the conclusions and recommendations contained herein are concurred in by this Command.

Task 1G162204A01409
Contract DAAJ02-67-C-0026
USAAVLABS Technical Report 68-87
March 1969

FEASIBILITY OF GAS BEARINGS FOR SMALL HIGH-PERFORMANCE
AIRCRAFT GAS TURBINES

By

Peter William Curwen

Prepared by

Mechanical Technology Incorporated
Latham, New York

for

U. S. ARMY AVIATION MATERIEL LABORATORIES
FORT EUSTIS, VIRGINIA

This document has been approved
for public release and sale; its
distribution is unlimited.

ABSTRACT

Future U.S. Army aircraft missions will require propulsion systems having significantly improved power-to-weight ratio and specific fuel consumption. To obtain these goals, simultaneous increases in engine operating pressures and temperatures are required. These ascending performance conditions, with accompanying high rotational speeds, will impose increasingly severe operating requirements on main engine bearings and seals.

Because of the high temperatures and high speeds, conventional oil lubrication techniques may not be adaptable to the next generation of small engines. If this should be the case, new lubrication methods will be required. One such method is the air-lubricated (gas) bearing. This report presents the results of a comprehensive study, based on existing analytical techniques and test data, to assess the feasibility of, and to identify the problem areas related to, applying gas bearings to an advanced two-spool gas generator. A 4.5-pound-per-second engine having the following gas-generator design-point operating conditions has been studied: turbine inlet temperature, 3000°F; compressor pressure ratio, 18:1; HP-spool speed, 70,000 rpm; and LP-spool speed, 62,800 rpm.

Results of the study show that gas-lubricated journal and thrust bearings can carry the maximum dynamic bearing loads and can be integrated into a practical gas generator configuration. Self-acting pivoted-pad journal bearings and externally pressurized thrust bearings are shown to be the best suited of presently developed bearing types for this application. The HP-spool turbine-end journal bearing (the hottest bearing) will operate somewhere between 1300 and 1500°F at rated-power conditions. Turbine cooling air can be utilized for cooling the journal bearings. Additional pressurization will be required for the thrust bearing supply air. Use of a small regenerative compressor, internally mounted as an integral part of the HP spool, appears to be a feasible way to achieve the required pressure boost.

The most severe operating condition for both the journal and thrust bearings occurs at engine idle during maximum aircraft maneuver and g-load conditions.

The HP spool will behave as a rigid rotor and will not present any balancing problems. The LP spool, however, is highly flexible and will operate close to its fourth flexural critical speed. The flexible nature of the LP spool results from the concentric two-spool engine arrangement, not as a consequence of the gas bearings. Results of the unbalance response analysis show that careful attention to mechanical design, and development of a practical flexible-shaft balancing procedure, may be sufficient to achieve satisfactory LP-spool operation. If not, additional rotor damping will be required.

Two critical areas of feasibility could not be quantitatively assessed because of the lack of proven analytical techniques and sufficient test data. These areas were rotor-bearing system stability, and adequacy of bearing structural and coating materials at the high-temperature high-stress conditions of the HP-spool turbine-end journal bearing. To complete the basic feasibility assessment as rapidly and conclusively as possible, it is recommended that experimental investigations of these two areas be undertaken using full-scale test rigs representative of the HP-spool design presented herein.

FOREWORD

The study reported herein was performed in fulfillment of Contract DAAJ02-67-C-0026 for the U.S. Army Aviation Materiel Laboratories (USAAVLABS), Fort Eustis, Virginia. Mr. L. Bell of USAAVLABS was the technical monitor.

The author gratefully acknowledges the significant contributions to this report made by the following members of MTI's engineering staff:

Mr. H. Pennink, who performed the aerodynamic studies.

Mr. S.F. Murray, who prepared the state-of-the-art summary on gas-bearing materials.

Mr. D.S. Wilson, who performed the externally pressurized journal bearing study and the study of thermal distortion effects on self-acting pivoted-pad bearings.

Mr. H.F. Jones, the lead Project Engineer for this study, who performed most of the conceptual and design-layout studies for the gas generator.

BLANK PAGE

TABLE OF CONTENTS

	<u>Page</u>
ABSTRACT.....	iii
FOREWORD.....	v
LIST OF ILLUSTRATIONS.....	ix
LIST OF TABLES.....	xvii
LIST OF SYMBOLS.....	xix
INTRODUCTION.....	1
Evolution of Gas-Lubricated Machinery Applications.....	1
Conduct of the Feasibility Study.....	4
Terminology.....	4
Report Organization.....	7
DESCRIPTION OF THE GAS-BEARING GAS GENERATOR.....	8
Design Specifications.....	8
Aerodynamic Design.....	10
Evolution of the Rotor-Bearing System Design.....	11
Phase VI Gas-Generator Layout.....	12
JOURNAL BEARING DESIGN STUDIES.....	32
Selection of Journal Bearing Type.....	32
Bearing Loads.....	40
Bearing Ambient Pressures.....	45
Bearing Sizing.....	46
Bearing Thermal Studies.....	58
Isothermal Performance of the Bearings.....	79
Nonisothermal Performance of the Bearings.....	94
Bearing Materials.....	100
THRUST BEARING DESIGN STUDIES.....	106
Thrust Bearing Loads.....	106
Selection of Thrust Bearing Type.....	115
Design of Thrust Bearings.....	119
Thrust Bearing Thermal Analysis.....	123
ROTOR-BEARING SYSTEM DYNAMICS.....	128
Critical Speeds.....	128
Unbalance Response.....	134
Pad Dynamics.....	148
Rotor Stability.....	151

	<u>Page</u>
CONCLUSIONS AND RECOMMENDATIONS.....	153
Specific Conclusions.....	154
Recommendations.....	158
REFERENCES CITED.....	160
APPENDIXES.....	165
I. Aerodynamic Analysis of the Turbine and Compressor Components.....	165
II. Gas-Bearing Materials for High-Temperature Gas Turbines.....	198
III. Analysis of Externally Pressurized Journal Bearings.....	247
IV. Analysis of the Herringbone-Grooved Journal Bearing.....	268
V. Auxiliary Compressor for Thrust Bearing Pressurization.....	270
VI. Summary of Design Layouts Prepared During the Feasibility Study.....	279
DISTRIBUTION.....	286

LIST OF ILLUSTRATIONS

<u>Figure</u>		<u>Page</u>
1	Network Diagram for Feasibility Study of Gas Bearings for Advanced Aircraft Gas Turbines.....	5
2	Phase VI Layout of the Gas-Bearing Gas Generator.....	13
3	Isolated View of the HP Spool and Its Bearings.....	17
4	Isolated View of the LP Spool and Its Bearings.....	19
5	Bearing and Turbine Cooling Flows, Thrust Bearing Supply Flows, and Seal Locations for the Gas Generator.....	21
6	Improved Design Concepts for the HP-Spool Journal and Thrust-Bearing Seals.....	25
7	Power Takeoff Requirements for Driving Gas-Generator Accessories.....	29
8	Torque Requirements Versus HP-Spool Speed for Engine Starting and Accessory Drive.....	30
9	Typical Full-Circular Hybrid Journal Bearing.....	34
10	Herringbone Groove Pattern Applied to Journals of a Small High-Speed Rotor.....	34
11	Typical 4-Pad Pivoted-Pad Journal Bearing With Pivots Supported by Flexures.....	39
12	Operating Load Diagrams for the Gas Generator.....	41
13	Maximum Loads for the HP-Spool Turbine-End Journal Bearing at Sea-Level Flight Conditions.....	42
14	Maximum Loads for the HP-Spool Turbine-End Journal Bearing at 25,000-Foot-Altitude Conditions.....	42
15	Maximum Loads for the LP-Spool Compressor-End Journal Bearing at Sea-Level Landing Conditions.....	44
16	Maximum Loads for the LP-Spool Compressor-End Journal Bearing at 25,000-Foot-Altitude Conditions.....	44
17	Ambient Pressure for the HP- and LP-Spool Journal Bearings, and IP-Spool Speed, as a Function of HP-Spool Speed.....	47

<u>Figure</u>	<u>Page</u>
18 Comparison of Nondimensional Load Capacity Data for 80- and 120-Degree Self-Acting Pads.....	50
19 Effect of Clearance Ratio on Minimum Film Thickness for a Highly-Loaded Self-Acting Pad.....	50
20 Effect of Speed and Diameter on Tangential Stress in the HP-Spool Journals.....	53
21 Tangential Stresses in Helically Grooved Journals at 70,000 RPM.....	54
22 Isothermal Disc Stresses for the HP-Compressor at 70,000 RPM.....	56
23 Effect of Speed and Diameter on Radial Centrifugal Growth of the HP-Spool Journals.....	57
24 Thermal Model for the HP-Spool Turbine-End Bearing.....	61
25 Thermal Model for the LP-Spool Turbine-End Bearing.....	61
26 Journal Bore-Cooling Concept Using Air Flow Through Holes in the Journal Stiffening Rings.....	64
27 Effect of Cooling Technique on HP-Spool Turbine-End Bearing Temperature at Sea-Level, Rated-Power, and Maximum Bearing Load Conditions.....	66
28 Calculated Temperatures for the HP-Spool Turbine-End Bearing at 25,000 Feet Under Engine-Idle and Maximum Bearing Load Conditions.....	69
29 Effect of Cooling Technique on HP-Spool Compressor- End Bearing Temperatures at 25,000 Feet Under Engine- Idle and Maximum Bearing Load Conditions.....	73
30 First Calculation of Temperatures for the LP-Spool Turbine-End Bearing at Sea-Level, Rated-Power, and Maximum Bearing Load Conditions.....	75
31 Second Calculation of Temperatures for the LP-Spool Turbine-End Bearing at Sea-Level, Rated-Power, and Maximum Bearing Load Conditions.....	77
32 Design Configuration for the HP and LP-Spool Pivoted-Pad Journal Bearings.....	82

<u>Figure</u>	<u>Page</u>
33 Pad Radial Clearance at 70°F and Zero Speed as a Function of Flexure Stiffness and Design-Speed Clearance for the HP-Spool Journal Bearings.....	84
34 Performance of the HP-Spool Turbine-End Pivoted-Pad Journal Bearing Under 1-G Load Conditions at a 25,000-Foot Altitude.....	86
35 Performance of the HP-Spool Turbine-End Pivoted-Pad Journal Bearing Under Maximum Load Conditions.....	89
36 Performance of the HP-Spool Pivoted-Pad Journal Bearings for Transient Changes in Speed From Rated-Power Conditions.....	91
37 Effect of a \pm 20-Percent Variation in Bearing Housing Temperature on Performance of the HP-Spool Turbine-End Journal Bearing.....	92
38 Performance of the LP-Spool Compressor-End Pivoted-Pad Journal Bearing Under 1-G Load Conditions.....	95
39 Performance of the LP-Spool Compressor-End Pivoted-Pad Journal Bearing Under Maximum Load Conditions.....	96
40 Maximum Applied Thrust Loads and Thrust Bearing Load Capacity for the HP Spool at Sea-Level Flight and Landing Conditions.....	110
41 Maximum Applied Thrust Loads and Thrust Bearing Load Capacity for the HP Spool at a 25,000-Foot Altitude.....	111
42 Maximum Applied Thrust Loads and Thrust Bearing Load Capacity for the LP Spool at Sea-Level Flight and Landing Conditions.....	112
43 Maximum Applied Thrust Loads and Thrust Bearing Load Capacity for the LP Spool at a 25,000-Foot Altitude.....	113
44 Self-Acting Spiral-Grooved Gas-Lubricated Thrust Bearing Developed for a 50,000 RPM Turbocompressor.....	116
45 Experimentally Determined Performance Map for Self-Acting Spiral-Grooved Gas-Lubricated Thrust Bearings Showing Region of Agreement Between Predicted (Isothermal) and Measured (Nonisothermal) Load Capacity.....	118

<u>Figure</u>	<u>Page</u>
46	Critical Speed Map for the HP Spool..... 129
47	Undamped Mode Shapes for the First and Second Critical Speeds of the HP Spool..... 131
48	Critical Speed Map for the LP Spool..... 132
49	Undamped Mode Shapes for the First and Second Critical Speeds of the LP Spool..... 133
50	Undamped Mode Shapes for the Third and Fourth Critical Speeds of the LP Spool..... 133
51	Effective Dynamic Stiffness Coefficients for the HP-Spool Journal Bearings Under 1-G Load Conditions..... 137
52	Effective Dynamic Damping Parameters for the HP-Spool Journal Bearings Under 1-G Load Conditions..... 138
53	Mass-Moment Unbalance Models Used to Investigate the Unbalance Response Characteristics of the HP Spool..... 139
54	Unbalance Response of the HP-Spool Turbine-End Journal to the Mass-Moment Unbalance Conditions of Figure 53..... 140
55	Mass-Moment Unbalance Models Used to Investigate the Unbalance Response Characteristics of the LP Spool..... 142
56	Unbalance Response of the LP-Spool Turbine-End Journal to the Mass-Moment Unbalance Conditions of Figure 55..... 143
57	Unbalance Response of the LP-Spool Compressor- End Journal to the Mass-Moment Unbalance Conditions of Figure 55..... 146
58	Effective Dynamic Damping Parameters for the LP-Spool Journal Bearings Under 1-G Load Conditions..... 147
59	Natural Frequency Ratios for the Unloaded Pads of the HP-Spool Journal Bearings Under 1-G and Maximum Load Conditions..... 150

<u>Figure</u>		<u>Page</u>
60	Meridional View of Axial and Centrifugal Compressor Stages.....	170
61	Meridional View of Radial and Axial Turbine Stages.....	172
62	Two-Stage Axial Compressor Map.....	173
63	Radial Turbine Characteristic.....	175
64	Axial Turbine Characteristic.....	176
65	Power Turbine Characteristic.....	177
66	HP-Spool Pressure Ratio and Temperature Ratio Characteristics for Three Operating Lines.....	179
67	HP-Spool Compressor Inlet to Turbine Inlet Temperature Ratio.....	180
68	Part-load Speeds at Sea Level.....	183
69	Part-Load Total Pressures at Sea Level.....	184
70	Part-Load Total Temperatures at Sea Level.....	185
71	Total and Static Pressures for the HP-Spool Axial Compressor at Sea Level.....	186
72	Part-Load Static Pressures for the HP-Spool Axial Compressor at Sea Level.....	187
73	Total and Static Pressures for the HP-Spool Centrifugal Compressor at Sea Level.....	188
74	Part-Load Static Pressures for the HP-Spool Centrifugal Compressor at Sea Level.....	189
75	Part-Load Static Pressures for the HP and LP-Spool Turbines at Sea Level.....	191
76	Part-Load Speeds at a 25,000-Foot Altitude.....	192
77	Part-Load Total Temperatures at a 25,000-Foot Altitude.....	193
78	Part-Load Static Pressures at a 25,000-Foot Altitude.....	194
79	Part-Load Blade Forces for the LP-Spool Axial Compressor and Turbine Stages.....	196

<u>Figure</u>		<u>Page</u>
80	Part-Load Blade-Side Impeller Disc Forces for the HP-Spool Radial Compressor and Turbine Stages.....	197
81	Plug and Bushing Set Used for Dimensional Stability Tests.....	202
82	Orifice Erosion Damage Caused by 300°F Steam.....	211
83	High-Temperature Hydrodynamic Bearing Test Rig for Materials Evaluations.....	215
84	Schematic of Bearing-Materials Test Rig.....	216
85	Oscilloscope Traces of Film Thickness Signals From Bearing Materials Test Rig.....	217
86	Bearing Surfaces of Test Pad and Journal After High-Speed Contacts (Plasma-Sprayed Chrome-Oxide Coating on Both Pad and Journal).....	220
87	Bearing Surfaces of Test Pad and Journal After High-Speed Contacts (Nickel-Bonded Tungsten-Carbide Coated Pad Versus Al ₂ O ₃ Coated Journal).....	221
88	Surface of Test Pad After 100 High-Speed Rubs at 48,000 RPM in Ambient Air (Pad Surface Coated With 0.003 Inch of Plasma-Sprayed Chrome Oxide plus 0.0001 Inch of Resin-Bonded MoS ₂).....	223
89	Gas-Bearing Test Machine Mounted on Shock Test Stand.....	224
90	Chrome-Oxide Coated Journal and Hydrodynamic Pivoted-Pad Bearing Segments From Gas-Bearing Test Machine After 1300 Impacts on the Shock Test Stand.....	225
91	Surface Appearance of Chrome-Oxide Coated Pads With Different Density Coatings After Subjecting Both Pads to 100 High-Speed Rubs at 48,000 RPM in Air.....	227
92	Effect of Temperature Cycling on Adherence of Coatings on Hastelloy X (Al ₂ O ₃ and Al ₂ O ₃ + TiO ₂ Coatings; No Undercoating).....	229
93	Effect of Temperature Cycling on Adherence of Stellite and Nickel-Chrome Bonded Chrome Carbide on Hastelloy X.....	230
94	Effect of Orientation on Al ₂ O ₃ Versus Cr ₃ C ₂	233

<u>Figure</u>		<u>Page</u>
95	Al ₂ O ₃ Coated Pad Versus Stellite 6 Coated Journal After High-Speed Rubs at 1400°F in Air.....	235
96	Al ₂ O ₃ Coated Pad Versus Chrome Carbide Coated Journal After High-Speed Rubs at 1400°F in Air.....	236
97	Typical Self-Acting Thrust-Bearing Groove Patterns Formed by Applying Plasma-Sprayed Coatings Through A Mask.....	238
98	Preliminary Electron-Probe Patterns From Cross Section of Stellite Coating on Steel Substrate.....	243
99	Cross Sections of Chrome Carbide Coating Before and After High-Temperature Tests.....	244
100	Inherently Available Supply and Ambient Pressures as a Function of Speed for the Externally Pressurized HP-Spool Turbine-End Journal Bearing.....	251
101	Stability Map for Externally Pressurized Full-Circular Journal Bearings, Based on Pressure Schedules of Figure 100, Showing Effect of Journal Size and Journal Centrifugal Growth.....	253
102	Supply Pressure (With Auxiliary Compressor Boost) and Ambient Pressure as a Function of Speed for the Externally Pressurized HP-Spool Turbine-End Journal Bearing.....	256
103	Temperature of Supply Gas as a Function of Speed for the Externally Pressurized HP-Spool Turbine- End Journal Bearing.....	257
104	Variation in Radial Clearance as a Function of Speed for the Externally Pressurized HP-Spool Turbine-End Journal Bearing.....	259
105	Stability Map and Load Capacity for the Refined Design of the Externally Pressurized HP-Spool Turbine-End Journal Bearing.....	261
106	Achievable Bearing Radial Stiffness (Including Squeeze Film Effects) as a Function of Bearing Radial Clearance.....	264
107	Typical Impeller Configurations for a Regenerative Compressor.....	271

<u>Figure</u>		<u>Page</u>
108	Performance Characteristics of a Typical Regenerative Compressor at Constant Speed.....	273
109	Important Dimensional Parameters of the Regenerative Compressor.....	274
110	Efficiency and Head-Rise Coefficient for a Regenerative Compressor Developed by MTL.....	276

LIST OF TABLES

<u>Table</u>		<u>Page</u>
I	Engine Design Parameters.....	9
II	Leakage Flows Through Gas-Generator Seals at Rated-Power Conditions.....	23
III	Internal Gas Generator Flows at Rated Power.....	26
IV	Minimum Film Thickness Data for 2.625-Inch and 3-Inch Nondistorted Bearings Operating at HP-Spool Maximum Load Conditions.....	51
V	Calculated Node-Point Temperatures for the HP-Spool Turbine-End Bearing Region at Sea-Level Rated-Power Conditions.....	67
VI	Calculated Node-Point Temperatures for the HP-Spool Turbine-End Bearing Region at 25,000 Feet and Engine- Idle Conditions.....	70
VII	Calculated Node-Point Temperatures for the LP-Spool Turbine-End Bearing at Sea-Level Rated-Power Conditions.....	78
VIII	Design Parameters and Material Properties for the HP-Spool Pivoted-Pad Journal Bearings.....	87
IX	Effect of Temperature Gradients on Minimum Film Thickness in the 3-Inch-Diameter HP-Spool Pivoted- Pad Journal Bearings at Maximum Load Conditions.....	98
X	Rupture Strength Data for Several High-Temperature Superalloys.....	101
XI	Maximum Applied Thrust Bearing Loads.....	114
XII	Performance Data for the HP-Spool Thrust Bearings.....	122
XIII	Performance Data for the LP-Spool Thrust Bearings.....	124
XIV	Temperature Rise Data for the Loaded Side of the HP- and LP-Spool Thrust Bearings.....	126
XV	Component Design-Point Conditions.....	168
XVI	Physical Properties of Some Candidate Alloys for High-Speed High-Temperature Gas Bearings.....	205

<u>Table</u>		<u>Page</u>
XVII	Material Combinations Which Were Used In Early Gas Bearing Work.....	213
XVIII	Results of Thermal Cycling Tests for Various Bearing Coating Materials.....	231
XIX	Performance Characteristics of a Preliminary Regenerative Compressor Design.....	277
XX	Summary of Design Sketches for the Gas-Generator Rotor-Bearing System.....	280

LIST OF SYMBOLS

A_s	stator channel flow area, ft^2
a	feeder hole radius, in.
B_{xx}	direct bearing damping coefficient, lb-sec/in.
B_{xy}	cross-coupled bearing damping coefficient, lb-sec/in.
B_{yy}	direct bearing damping coefficient, lb-sec/in.
B_{yx}	cross-coupled bearing damping coefficient, lb-sec/in.
C	radial bearing clearance, in.
C_o	isentropic velocity, ft/sec
C_p	pad radial clearance ($R_p - R_o$) in.
D	bearing diameter, in.
D_i	inside (bore) diameter of journal, in.
D_o	outside diameter of journal, in.
d	blade height, ft
E	modulus of elasticity, lb/in.^2
e	bearing eccentricity, in.
F_{gyro}	gyroscopic force acting on bearing, lb
g	dimensional constant, $386 \text{ lb}_m\text{-in./lb}_f\text{-sec}$
H	isentropic head, ft-lb/lb
h	film thickness, in.
h_p	film thickness at pivot point, in.
I_p	polar mass moment of inertia, in.-lb-sec^2
I_t	transverse mass moment of inertia about rotor mass center, in.-lb-sec^2
K	effective stiffness of bearing, lb/in.
K_b	bearing gas-film stiffness, lb/in.

LIST OF SYMBOLS (Cont'd)

K_f	flexure stiffness, lb/in.
K_{xx}	direct bearing dynamic stiffness coefficient, lb/in.
K_{xy}	cross-coupled bearing dynamic stiffness coefficient, lb/in.
K_{yy}	direct bearing dynamic stiffness coefficient, lb/in.
K_{yx}	cross-coupled bearing dynamic stiffness coefficient, lb/in.
L	bearing length, in.
l	bearing span, in.
M	total rotor mass, lb
m	rotor mass supported by journal bearing, lb
m_c	critical journal bearing mass (for threshold of instability), lb
N	speed, rpm
N_{design}	design speed, rpm
n	number of feeder holes
P_a	bearing ambient pressure, psia
P_s	bearing supply pressure, psia
P_T	total pressure, psia
P_{in}	inlet pressure to regenerative compressor, psia
P_{out}	discharge pressure from regenerative compressor, psia
P_1	axial compressor total inlet pressure, psia
P_2	centrifugal compressor total inlet pressure, psia
P_3	combustor total inlet pressure, psia
P_4	radial turbine total inlet pressure, psia
P_5	axial turbine total inlet pressure, psia

LIST OF SYMBOLS (Cont'd)

P_6	power turbine total inlet pressure, psia
Q	flow, ft ³ /min or lb/sec
Q_{brg}	bearing flow, lb/sec
Q_{seal}	seal leakage flow, lb/sec
Q_{total}	bearing plus seal leakage flow, lb/sec
R	gas constant, in. ² /sec ² -°R
R	bearing radius, in.
R_i	inside (bore) radius of journal or inside radius of thrust bearing, in.
R_o	outside radius of journal or thrust bearing, in.
R_p	radius of pivoted-pad segment, in.
T	bearing supply gas temperature, °R
T_h	temperature of bearing support housing, °F
T_j	temperature of journal, °F
T_p	temperature of pivoted-pad segment, °F
T_T	total temperature, °R
T_{in}	inlet temperature to regenerative compressor, °R
T_{out}	discharge temperature from regenerative compressor, °P.
ΔT	$(T_{\text{in}} - T_{\text{out}})$, °R or °F
T_1	axial compressor total inlet temperature, °R
T_2	centrifugal compressor total inlet temperature, °R
T_3	combustor total inlet temperature, °R
T_4	radial turbine total inlet temperature, °R
T_5	axial turbine total inlet temperature, °R
T_6	power turbine total inlet temperature, °R

LIST OF SYMBOLS (Cont'd)

U	mean peripheral blade speed, ft/sec
U _t	blade-tip peripheral speed, ft/sec
W	net thrust bearing load capacity, lb
W _b	applied journal bearing load, lb
W _p	load on one pivoted-pad segment, lb
\bar{W}_p	nondimensional load on one pivoted-pad segment $(\bar{W}_p = \frac{W_p}{P_a LD})$
W*	load parameter, lb
W _{max design}	maximum applied bearing load at design speed, lb
W ₁	axial compressor inlet flow, lb/sec
W ₂	centrifugal compressor inlet flow, lb/sec
W ₃	combustor inlet flow, lb/sec
W ₄	radial turbine inlet flow, lb/sec
W ₅	axial turbine inlet flow, lb/sec
W ₆	power turbine inlet flow, lb/sec
α_h	coefficient of thermal expansion for bearing support housing, in./in.-°F
α_j	coefficient of thermal expansion for journal, in./in.-°F
α_p	coefficient of thermal expansion for pivoted-pad segment, in./in.-°F
β	angular extent of pivoted-pad segment, rad
γ	ratio of specific heats (c_p/c_v)
δ	a/2C
ϵ	bearing eccentricity ratio (e/C)
ϵ_p	pad eccentricity ratio

LIST OF SYMBOLS (Cont'd)

η	efficiency
θ_p	angular distance from leading edge of pivoted-pad segment to pivot point, rad
$\dot{\theta}$	pitch velocity, rad/sec
Λ	bearing compressibility number, $\Lambda = \frac{6\mu\omega}{P_a} \left(\frac{R}{C}\right)^2$
Λ_c	thrust bearing number, $\Lambda_s = \frac{6\mu\omega(R_o^2 - R_i^2)}{P_a h^2}$
Λ_s	bearing feeding parameter, $\Lambda_s = \frac{6\mu n a^2 \sqrt{RT}}{P_s C^3 \sqrt{1+\delta^2}}$
μ	absolute viscosity, lb-sec/in. ²
ν	Poisson's ratio
ν	vibration frequency, rad/sec
ρ	mass density, lb/in. ³
σ	squeeze film number, $\sigma = \frac{12\mu\nu}{P_a} \left(\frac{R_o}{C}\right)^2$
ϕ	flow coefficient
ψ	head rise coefficient
$\dot{\psi}$	yaw velocity, rad/sec
ω	rotor angular velocity, rad/sec
ω_n	natural frequency, rad/sec
ω_t	threshold speed for the fractional frequency whirl, rad/sec
ω_{nc}	conical mode critical speed, rad/sec
ω_{nt}	translatory mode critical speed, rad/sec

BLANK PAGE

INTRODUCTION

Future U.S. Army aircraft missions will require propulsion systems having significantly improved power-to-weight ratio and specific fuel consumption. To obtain these goals in a small gas turbine, simultaneous increases in engine operating pressures and temperatures are required. To achieve these increases, significant advancements in compressor, turbine, and combustor technology are required and have, to some extent, already been obtained under USAAVLABS advanced development programs. However, these ascending performance conditions, with accompanying high rotational speeds, impose increasingly severe operating requirements on main engine bearings and seals.

There is increasing evidence of problems being encountered with oil-lubricated bearings and associated seals in the current generation of high-performance engines. Because of the inherent degradation characteristics of petroleum-based and synthetic lubricants with increasing temperature, these problems can only become more severe as engine temperatures and speeds continue to increase. Conventional lubrication techniques may not be adaptable to the next generation of small engines. New lubrication methods should therefore be investigated. One such method is the air-lubricated (gas) bearing. Unlike conventional lubricants, the lubricating qualities of air (with respect to bearing load capacity) improve, rather than degrade, with increasing temperature. Accordingly, a feasibility study has been performed to identify the probable advantages and problem areas associated with application of gas bearings to a future class of US Army advanced aircraft gas turbines. This report presents the results of the study.

EVOLUTION OF GAS-LUBRICATED MACHINERY APPLICATIONS

The following brief review of the evolution of gas-bearing machinery applications is given so that the reader may place the present engine feasibility study in proper perspective, and thus better appreciate both the significance and the limitations of the study.

The first requirements for gas-bearing machinery, both in Europe and in the United States, came from governmental atomic energy agencies during the 1955 to 1960 time period. These agencies are, today, the largest users of gas-bearing machinery. A total of 19 machines have been or are presently being used in nuclear test loops in the United States. A considerably larger number of machines are in use in England and Europe.

In 1963, the U.S. National Aeronautics and Space Administration (NASA) began its program to evaluate gas-lubricated gas-turbine machinery for closed-Brayton-cycle space power systems. Four turbomachinery designs for the NASA are currently in various stages of development and test evaluation. An initial 1000-hour test of the first turboalternator has recently been successfully completed at design-point conditions. The U.S. Army has also sponsored gas-bearing simulator work with respect to its interest in the closed Brayton cycle for compact, mobile, terrestrial power plants.

The above-mentioned areas of application are all characterized by the need for noncontaminating, long-lived, maintenance-free, radiation-resistant machinery. Gas-lubricated rotor systems have provided a practical and proven means for satisfying these requirements [1].*

In 1964, the U.S. Navy became interested in the application of process-fluid lubrication as a means of decreasing maintenance, noise, size, and weight of shipboard machinery. Because of the naval shock and vibration environment, an initial investigation was undertaken to assess the ability of gas-bearing machinery to survive low-frequency, large-amplitude vibration, as well as hi-impact shock [2]. The results of this program were quite encouraging, and a continuation of the testing is presently under way to investigate the effects of many repeated hi-impact shocks over an extended period of time [3,4].

Based on results of a design feasibility study performed in 1966, an 800-horsepower forced-draft blower for fire-box pressurization has been designed for the U.S. Navy. This machine will use externally pressurized superheated steam bearings. The bearing steam will be bled from turbine inlet, thus eliminating the need for an external source of pressurized gas [5].

The most recent trend in gas lubrication has been applications involving higher speeds and higher (and lower) temperatures. The reason, of course, for this trend is the ever-present desire for higher performance turbo-machinery of more compact and lighter design. In this case, gas bearings have several inherent attributes which make them logical candidates for these applications.

1. Gas bearings can be operated at considerably higher temperatures than oil- or grease-lubricated bearings. (In fact, the load capacity of gas bearings increases with increasing temperature as a result of the corresponding increase in gas viscosity.) The ability to operate bearings at high temperature permits more compact and simplified machinery arrangements. The only limitations on temperature level are those associated with bearing construction and coating materials.
2. Many thousands of hours of continuous high-speed operation can be expected (and has been demonstrated) from a well-integrated gas bearing machine when the machine is reasonably well isolated from large-amplitude vibrations and shocks. Since the rotor actually spins on a film of gas, the bearings will not, for all practical purposes, wear out. The effects of repeated shocks on long-term performance characteristics are not yet known. Investigations in this respect are presently under way [3].
3. The ability of gas bearings to operate at high temperatures, together with the fact that viscous shear losses are relatively small, greatly simplifies the bearing-region heat transfer problem.

*Numbers in brackets refer to similarly numbered references listed on pages 160 to 164.

Thermal gradient problems along the rotor are likewise alleviated. As a result of the low friction losses, it is possible to design gas-lubricated gas turbines to be completely self-cooled using small flows of compressor bleed gas to cool the bearing regions. This concept has been successfully demonstrated on several turbomachinery developments [6,7].

4. The ability to self-cool a gas-bearing system using small amounts of bleed flow results in considerable simplification of the bearing system auxiliaries. Considerable testing of a 24,000-rpm, 1400°F gas-bearing gas generator, over a wide range of steady-state and transient conditions, has demonstrated that gas lubrication and gas cooling can, in fact, be achieved without the use of any auxiliary components [6]. (This particular machine did require an external source of pressurized gas on the thrust bearing at start-up and shutdown. However, as a result of advancements in bearing materials technology, even this requirement has been eliminated in recent gas-bearing machines delivered to the AEC.) The elimination of auxiliaries, such as oil pumps, oil coolers, buffer seals, oil-gas separators, oil sumps, and associated instruments and controls, greatly simplifies the lubrication system. This results in an inherent potential for increased reliability and decreased weight of gas-lubricated turbomachinery. In military applications, the elimination of engine auxiliaries may also help to make engines less vulnerable to enemy firepower.
5. The total bearing system parasitic losses (including auxiliaries) may be appreciably less for a gas-lubricated machine relative to an oil-lubricated unit. As a specific example, calculated and test data for both oil- and gas-film lubrication systems for a 3,000-HP (rated turbine shaft power) gas generator show that the bearing losses, as a percentage of rated turbine power, are 3.1 percent higher for the oil-lubricated machine [8].

With respect to high-speed operation, a 5-horsepower gas-bearing compressor has been successfully operated at 115,000 rpm. In the area of high-temperature bearings, several technology programs have been conducted for governmental agencies to obtain an initial evaluation of bearing materials and bearing design concepts at temperatures up to 1950°F in inert gases and 1400°F in air [9,10,11]. These are the present-day frontiers of gas-bearing technology for high-performance turbomachinery applications.

The present Army interest in high-performance aircraft engines is an excellent example of the high-speed, high-temperature trend. There is no question that the specified cycle temperatures and rotor speeds create difficult design problems for rolling contact and liquid-film bearings. For a turbine inlet temperature of 3000°F and a compressor temperature rise of 890°F (at an 18 to 1 pressure ratio), the problem of cooling an oil-lubricated turbine bearing is immediately obvious. Furthermore, rotor speeds in the 50,000- to 70,000-rpm range can result in serious oil whip and viscous drag problems in oil bearings, and fatigue life and cage wear

problems in rolling contact bearings. In view of these operational conditions, and considering the rapid advances which have been made in the gas-lubricated turbomachinery field over the past seven years, the impetus for investigating the feasibility of gas lubrication for an advanced Army aircraft engine is clearly evident.

CONDUCT OF THE FEASIBILITY STUDY

The present feasibility study was performed in seven phases as follows:

- Phase I - Establish probable engine design requirements and design-point flow rate
- Phase II - Establish aerodynamic component sizes, engine arrangement concepts, envelope of operating conditions, and bearing requirements
- Phase III - Study bearing types and bearing materials; prepare bearing design data
- Phase IV - Prepare initial engine layouts
- Phase V - Perform engineering analyses and identify problem areas
- Phase VI - Prepare final engine layout(s) and analyses
- Phase VII - Perform critical review and prepare report.

Figure 1 shows the network diagram for the study and identifies specific tasks within each of the above phases. The original program plan was followed quite closely. However, it was necessary to continue the Phase III gas-bearing design studies throughout Phases IV and V for reasons which will become clear in the following chapters.

TERMINOLOGY

The advanced engine concept utilized for this study consists of a two-spool gas generator driving a single-spool free power turbine. However, the present study is limited to feasibility of gas bearings for the gas generator only. In the following chapters the word "engine" is frequently used, but it should be interpreted in the limited sense as referring only to the gas generator.

The terms "gas bearings", "air bearings", and "process-fluid bearings" all mean the same thing in the context of this report. Only air lubrication of the gas generator is considered; the concept of a hybrid bearing system using both air- and oil-lubricated bearings, while possibly feasible and practical, is not considered in this study.

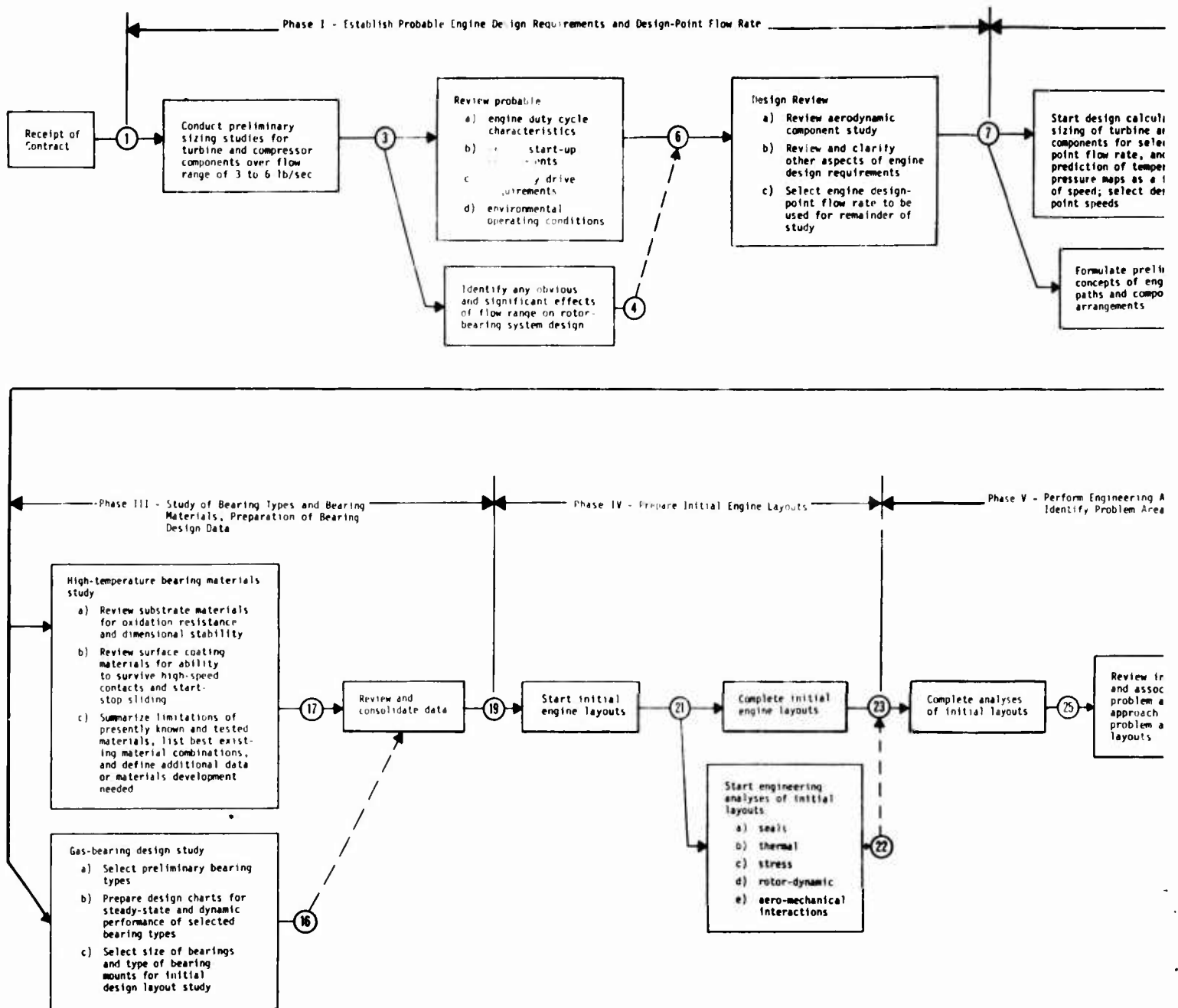
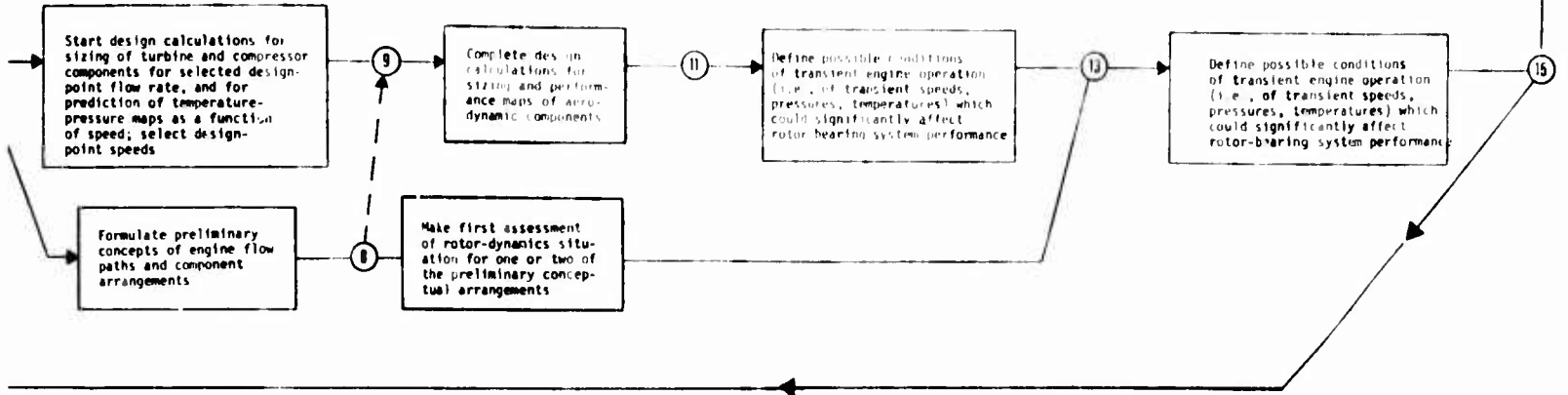


Figure 1. Network Diagram for Feasibility Study of Gas Bearings for Advanced Aircraft Gas Turbines.

A

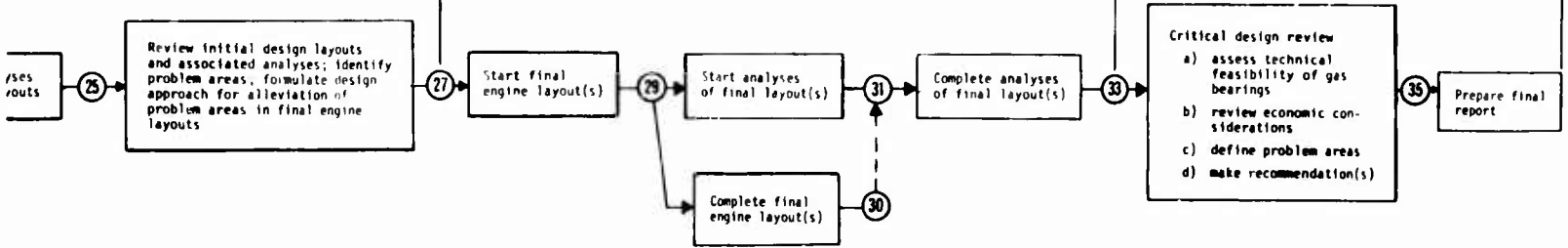
Phase II - Establish Aerodynamic Component Sizes, Engine Arrangement Concepts, Develop of Operating Conditions, and Bearing Requirements



Phase V - Perform Engineering Analyses and Identify Problem Areas

Phase VI - Final Engine Layout(s) and Analyses

Phase VII - Critical Review and Report



B

The term "externally pressurized bearing" (sometimes expressed "hydrostatic bearing") means a bearing in which pressurized lubricant is introduced into the bearing clearance space via suitable orifices or porous materials. The term "self-acting bearing" (sometimes expressed "hydrodynamic bearing") means a bearing with no external pressurization; film pressures are generated solely by viscous-shear pumping of the lubricant as a result of relative motion between the bearing surfaces.

The term "rotor" as used in this report generally refers to a complete rotating assembly of parts. Turbines, compressors, thrust runners, journals, and shafts are typical rotor parts.

The term "LP spool" is frequently used in this report and denotes the gas-generator rotor assembly which carries the low-pressure (LP) axial compressor stages and the low-pressure axial turbine stage.

Similarly, the term "HP spool" denotes the rotor assembly which carries the high-pressure (HP) radial compressor and radial turbine stages.

The term "bearing eccentricity" as used in this report denotes the radial displacement of a shaft journal (sometimes called a bearing journal) from a line (sometimes called a centerline and assumed to be straight) which connects the centers of all labyrinth seals associated with the shaft.

REPORT ORGANIZATION

Organization of this report does not reflect the order in which the feasibility study was conducted. Rather, the Phase VI concept of the gas generator is discussed first. This concept naturally represents the cumulative knowledge gained from the overall study and is the one upon which feasibility conclusions and future program recommendations have been based.

Following the general discussion of the Phase VI gas generator, individual chapters pertaining to journal bearing design, thrust bearing design, and rotor-dynamic evaluations are presented. These chapters, together with the related appendixes, represent the bulk of the study effort and form the technical basis for the feasibility conclusions and recommendations.

DESCRIPTION OF THE GAS-BEARING GAS GENERATOR

Various aspects of the gas-bearing gas-generator design are presented and discussed in the following paragraphs. Primary emphasis is given to the Phase VI engine concept, since this concept represents the accumulated knowledge gained from analytical and layout studies performed during Phases I through V of the program. The overall concept of the gas generator is presented at this point in the report so that the reader can gain an immediate feel for the engine — for the integrated arrangement of parts as well as for the nonconventional and quite advanced aspects of the design. The results of detailed analyses pertaining to specific facets of the rotor-bearing system design are presented and discussed in subsequent chapters and appendixes. A summary of the significant results, conclusions, and recommendations arising from the feasibility study is given in the last chapter.

DESIGN SPECIFICATIONS

The engine design parameters, as specified by USAAVLABS, are listed in Table I. These parameters should be interpreted only as representative conditions for future small gas turbines for U.S. Army aircraft missions. The conditions do not reflect any specific existing requirements, but rather the continual trend toward improved power-to-weight ratio and specific fuel consumption. The simultaneous conditions of temperature and speed for the HP spool are clearly beyond the capability of present-day materials. Depending on the rate of materials and design-technology development, a demonstrator engine operating at these conditions is probably 10 to 15 years away.

The gas bearing design goals specified by USAAVLABS were as follows:

Time before overhaul	1000 hours
Engine starts	2000
Bearing environmental conditions	Per MIL-E-5007C (except for a modified operating load diagram as shown in Figure 12 of this report)
Overspeed capability	10 percent

TABLE I. ENGINE DESIGN PARAMETERS

TABLE I. ENGINE DESIGN PARAMETERS	
<u>Gas Generator</u>	
Configuration	Two-spool
Design-Point Conditions	
Flow rate	3 to 6 lb/sec
Rotational speeds	50,000 to 70,000 rpm
Compressors	Two-stage transonic axial pressure ratio = 3:1 efficiency = 82 %
	Single-stage centrifugal pressure ratio = 6:1 efficiency = 80 %
Combustor	Efficiency = 99 % Pressure loss = 3 %
Turbines	HP-spool single-stage radial inlet temperature = 3000 °F
	LP-spool single-stage axial
	Overall efficiency = 86 %
Compressor bleed flow for turbine cooling	Radial turbine = 5 % Axial Turbine = 2 %
<u>Power Turbine</u>	
	Overall efficiency = 88 %
	HP/lb/sec = 285

AERODYNAMIC DESIGN

Before the bearing-system and rotor-dynamic design studies for the gas generator were begun, it was necessary to establish the weights, sizes, and speeds of the aerodynamic components. In addition, static pressures and blade forces were required as a function of speed and altitude to enable thrust loads to be predicted. Static pressures were also required as a function of speed and altitude to determine ambient and differential pressures which would be available for bearing design purposes.

A detailed summary of the aerodynamic design study is given in Appendix I of this report. To reduce the sizeable amount of aerodynamic analysis required for component optimization, sizing, and performance prediction, extensive use was made of component data provided by USAAVLABS.

During Phase I of the contract, a preliminary aerodynamic study indicated that engine flow rate (within the specified limits of 3-to-6-pounds-per-second) would have no obviously significant effect with respect to either aero-thermo aspects of turbine and compressor design, or mechanical and dynamic aspects of rotor-bearing system design. Accordingly, a 4.5-pound-per-second flow rate was selected for detailed analysis of the gas generator so that minimum extrapolation would be required to extend results of the feasibility study to either extreme of the 3-to-6-pound-per-second flow range. All designs and analysis results presented in this report are based on a 4.5-pound-per-second sea-level design-point flow.

Listed below are several of the pertinent aero-thermo operating characteristics of the Phase VI gas-generator design. Complete aero-thermo performance data are given in Appendix I.

Sea-Level Operating Data

	<u>LP Spool</u>	<u>HP Spool</u>
Speed at rated power, rpm	62,800	70,000
Speed at idle (zero power), rpm	25,000	49,000
Compressor inlet pressure, psia	14.7	-
Compressor discharge pressure, psia		
At rated power	-	264.5
At idle	-	38.0
Turbine inlet temperature, °F		
At rated power	2,500	3,000
At idle	1,140	1,340

25,000-Foot-Altitude Operating Data

	<u>LP Spool</u>	<u>HP Spool</u>
Speed at rated power, rpm	48,000	65,000
Speed at idle (zero power)*, rpm	22,500	45,000
Compressor inlet pressure, psia	7.3	-
Compressor discharge pressure, psia		
At rated power	-	130
At idle	-	18
Turbine inlet temperature, °F		
At rated power	-	2,390
At idle	-	940

EVOLUTION OF THE ROTOR-BEARING SYSTEM DESIGN

To start the rotor-bearing system design studies, an initial selection of self-acting versus externally pressurized journal bearings was required. It was recognized that self-acting pivoted-pad bearings have been used almost exclusively in gas-bearing machinery since 1963. These bearings are favored in most applications because an external source of pressurized gas is not required, and problems of rotor instability can generally be avoided. On the other hand, self-acting bearings have limited load capacity at the conditions of bearing eccentricity ratio (ϵ) normally selected for reliable long-term continuous operation. Hence, when it became evident that maximum bearing loads for the gas generator would be quite high, it was felt that externally pressurized bearings would have the best potential for success. In this instance the requirement for a reliable supply of pressurized air did not appear to be a problem (except perhaps at engine startup), since high pressure ratios (18 to 1 at design speed) would be available from the gas-generator compressor. Accordingly, a comprehensive effort was made during Phases I, II, III, and part of Phase IV, to achieve a feasible rotor-bearing system design using externally pressurized journal bearings.

Results of the analytical and layout studies based on pressurized bearings are presented in detail in Appendix III. In brief, the problem of fractional-frequency whirl (a basically unstable and destructive condition) could not be overcome. Accordingly, an investigation of self-acting

*Subsequent to completing this study, it was pointed out that engine idle speeds at altitude conditions are normally specified to be greater than sea-level idle speed. If this practice had been followed here, the calculated bearing clearances for the 25,000-foot-altitude idle speed condition would have been somewhat larger than are stated in this report. However, the conclusions and recommendations as stated herein would not change as a result of slightly larger idle-speed bearing clearances.

pivoted-pad journal bearings was initiated during Phase IV. It was found that if compressor discharge pressure was used to establish ambient pressure around the bearings, these bearings could theoretically carry the maximum imposed loads at acceptable values of film thickness. This finding, in concert with other well established advantages of pivoted-pad bearings, among these being improved stability, resulted in a redirection of the design and analysis effort to investigate thoroughly the pivoted-pad bearing approach. The detailed results of this investigation are presented in the following chapter of this report. The final Phase VI gas-generator design layout reflects the selection of pivoted-pad journal bearings as being the most feasible of presently developed bearing types for this application.

A listing of the significant design drawings generated during Phases I through VI of the study is given in Table XX of Appendix VI. A brief description of the key features of each design, as well as pertinent remarks about the designs, is also given. A quick scan of Table XX shows that a comprehensive study was made not only of various bearing arrangements but also of various aerodynamic component arrangements.

The Phase VI gas-generator arrangement to be discussed next is not considered to be the best ultimate arrangement. It would be presumptuous to make such a claim. What it does represent is a feasible rotor-bearing system arrangement (with several qualifications) which requires the least amount of new design technology and materials development; that is, it represents the least extension of present gas-bearing state of the art. However, there are at least two other arrangements which seem to offer significant advantages. One of these is a single-shaft, rather than a two-shaft, arrangement. The question here, of course, is whether satisfactory aerodynamic performance could be achieved from a single shaft machine. Because of the possible mechanical advantages which might accrue, this question should be pursued further. The second interesting design concept is a two-spool arrangement using an inverted bearing arrangement for the HP spool. A very compact engine is obtained. This concept would utilize externally pressurized bearings and hence would probably require development of a high-temperature, highly reliable damping mechanism to achieve rotor stability. In this case, the stationary journal might provide a practical coupling means between the bearings and the additional damping elements. However, considerable analysis and component development would be required to assess whether this approach could really be a practical solution.

PHASE VI GAS-GENERATOR LAYOUT

The Phase VI arrangement of the gas generator is shown in Figure 2. A two-spool engine is shown in accordance with the design specification; each spool is independently supported by its own bearings from the engine structure. Figure 2 identifies the significant parts of the gas generator in terms of the nomenclature used throughout this report.

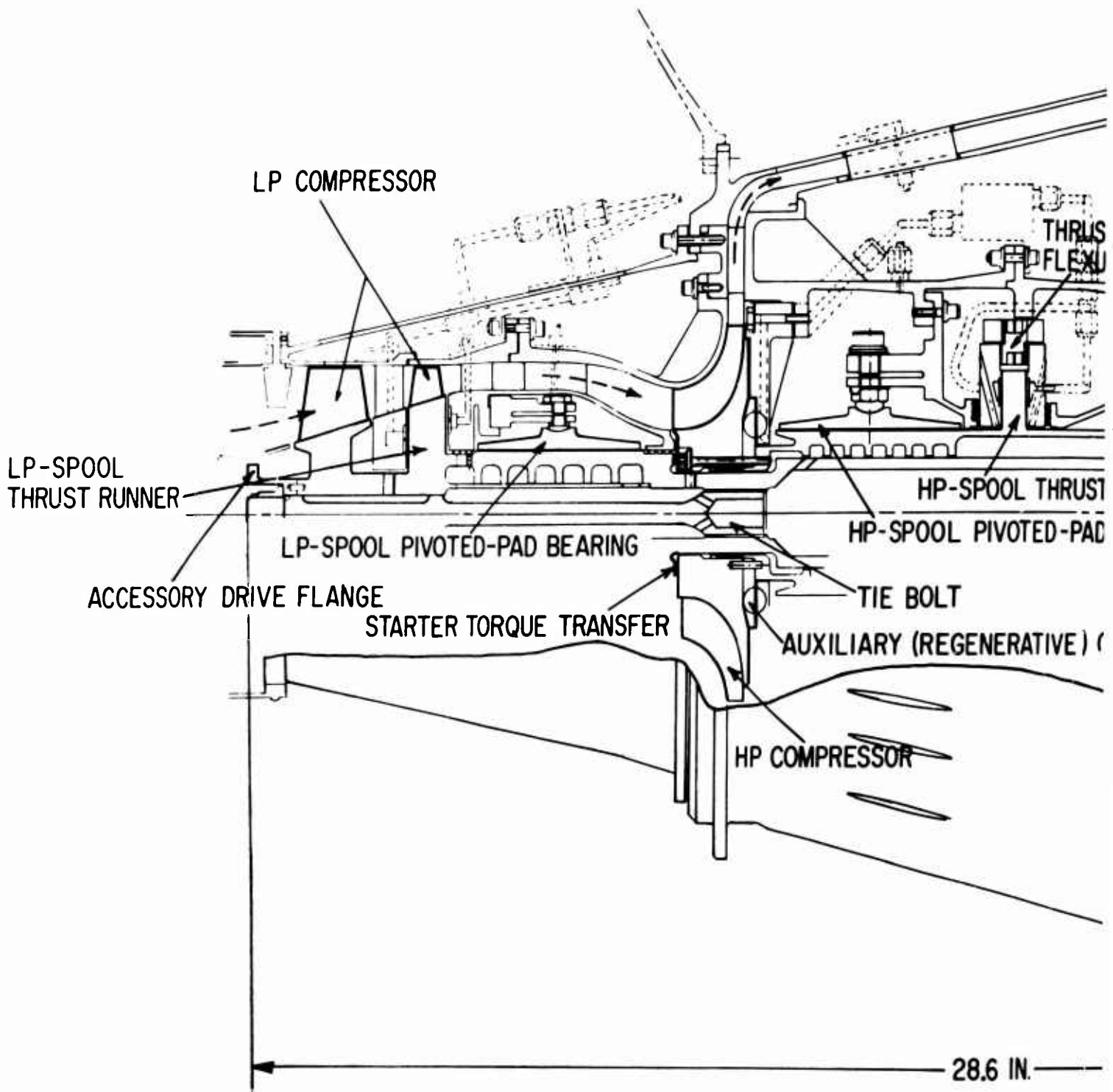
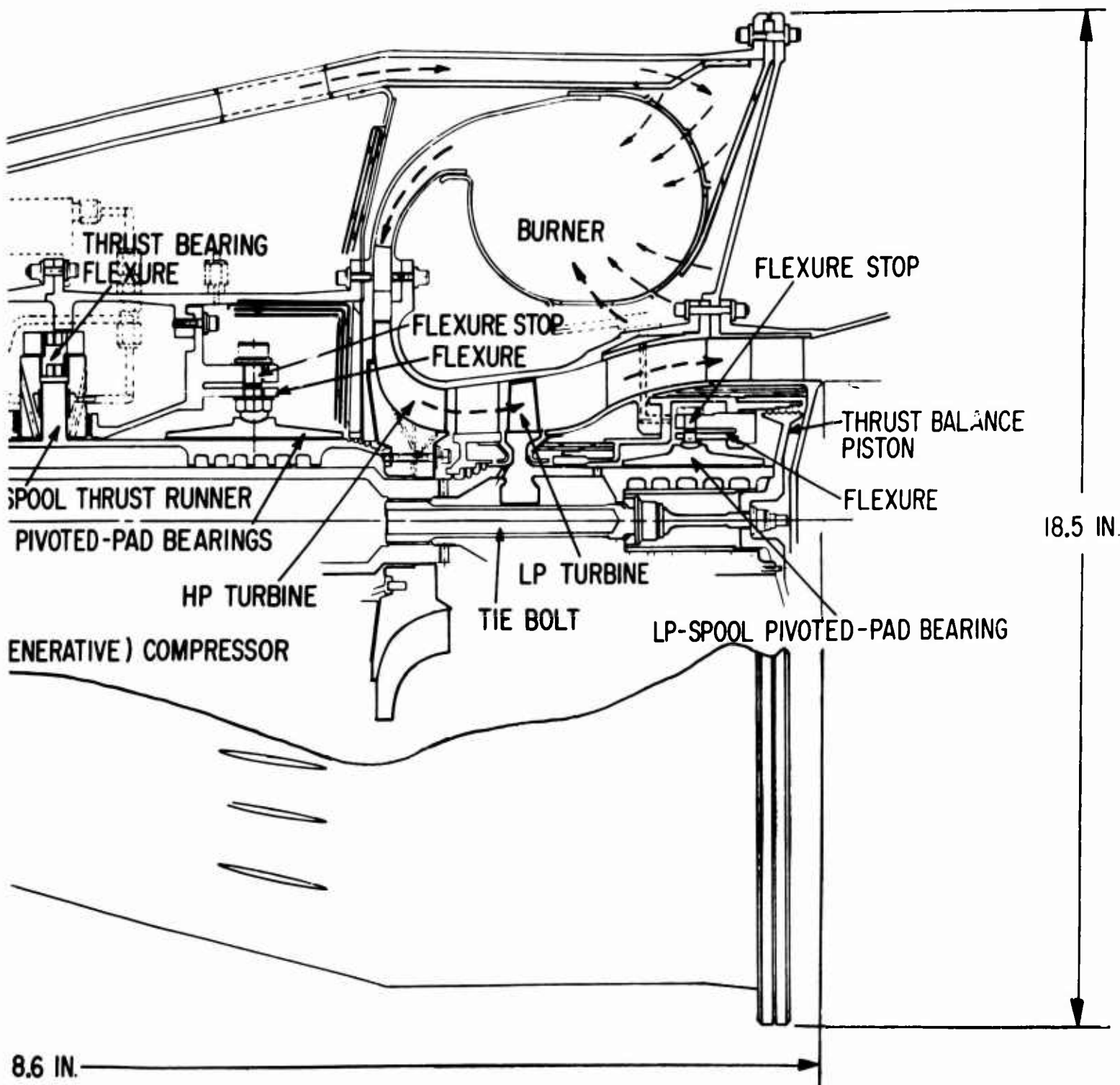


Figure 2. Phase VI Layout of the Gas-Bearing Gas Generator.

A



B

Although primary emphasis of the feasibility study centered on detailed analysis of rotor-bearing system concepts, it was necessary to make a "first cut" layout of the overall engine to identify any significant problems with respect to integrating the rotor-bearing system with the engine. In this regard, Figure 2 represents an initial concept of engine structure and component arrangement which reflects the following important requirements of rotor-bearing system design integration:

1. Maintenance of satisfactory bearing and seal alignment under all engine operation conditions.

Support of the LP-spool turbine-end journal bearing presents the most difficult alignment problem. This bearing is located inside the exhaust ducting for the LP turbine and hence must be supported relative to the HP-spool bearings via hot turbine shrouds and relatively hot engine casings. Symmetry of shroud and casing design, as well as radial and circumferential temperature gradients, must be achieved.

2. Practical procedures for assembly and disassembly of the bearings, rotors, and engine casings.

Component designs and assembly procedures must allow alignment and clearances of the bearings and seals to be quickly achieved, easily checked, and reliably retained. Design and assembly concepts must also assure that rotor-assembly concentricity and squareness tolerances are met. It is clear from Figure 2 that assembly of the LP spool is more complex than assembly of the HP spool and will require more attention to design detail. This situation is similar to that encountered with conventional two-spool engines, except that a generally higher degree of precision will be needed because of the high speeds and the use of gas bearings.

3. Provision for in-place balancing of the completely assembled HP and LP spools on gas bearings.

Because of the high rotor speeds and the small amount of bearing damping, in-place balancing of the complete spool assemblies is believed to be essential. The engine casing arrangement of Figure 2 permits the HP spool to be final-balanced in its fully assembled condition at an early stage of overall engine assembly. (Appropriate fixtures would, of course, be needed to hold the LP-spool mid-shaft section within the bore of the HP shaft.) Once the HP spool is balanced, it would not need to be disassembled.

Following several intermediate engine assembly steps, the LP spool would be completely assembled and balanced. (A special gas-bearing fixture would be used to support the spool so that access to the turbine and compressor discs could be readily attained.) Upon completion of the balancing operation, disassembly and re-assembly of the two axial compressor stages would be required to

complete the engine assembly. A final trim of the in-place balance condition could then be made, if necessary, on the first-stage axial compressor disc.

The HP spool behaves as a rigid shaft and hence should not present any balancing problems. The LP spool, however, is quite flexible and will require advanced balancing techniques. This is discussed further in the "Rotor Dynamics" chapter of this report.

4. Provision for various internal flow passages.

The overall engine design must be compatible with internal flow requirements for bearing and turbine cooling, bearing cavity pressurization, seal-leakage flows, bearing and seal venting, and thrust bearing pressurization. These various flow paths will be discussed shortly.

Once again the reader is reminded that Figure 2 should not be regarded as the best or final arrangement for the gas generator. It would be unrealistic to assume that an optimized concept for such an advanced engine could result from an initial feasibility study. The alternate aerodynamic component arrangements discussed in the preceding subsection suggest that better arrangements may ultimately be possible. Future detailed analysis of engine structural design, combustor design, aerodynamic component design, et cetera, will undoubtedly result in arrangement modifications. What the data in this report and the arrangement of Figure 2 do provide is an initial indication of the feasibility, size, advantages, and problem areas associated with a gas-bearing gas generator. Certain aspects of the gas-bearing approach definitely require experimental verification before absolute feasibility can be established. These are summarized in the concluding section of this report.

HP-Spool Arrangement

Figure 3 is an isolated view of just the HP spool and its bearings for the Phase VI gas-generator arrangement. Pertinent dimensions and parameters of the rotor are specified in the figure. The HP spool has an overhung single-stage radial compressor mounted at one end of the shaft, and an overhung single-stage radial turbine at the other end. Self-acting pivoted-pad journal bearings are located just inboard from the turbine and compressor wheels. A double-acting externally pressurized thrust bearing is located between the journal bearings. The journal bearing pad segments are individually mounted on cantilever flexures to accommodate journal centrifugal growth and bearing-assembly differential thermal expansions. The thrust bearing stators are also flexure mounted to maintain static alignment of the thrust bearing faces.

A small regenerative compressor is located adjacent to the back-face of the compressor wheel. This compressor provides additional pressurization of supply air for the externally pressurized HP- and LP-spool thrust bearings. A description of the regenerative compressor is given in Appendix V.

BEARING SPAN = 6.5 IN.

ROTOR WEIGHT

ON COMPRESSOR-END JOURNAL BEARING = 6.83 LB

ON TURBINE-END JOURNAL BEARING = 10.75 LB

TOTAL 17.58 LB

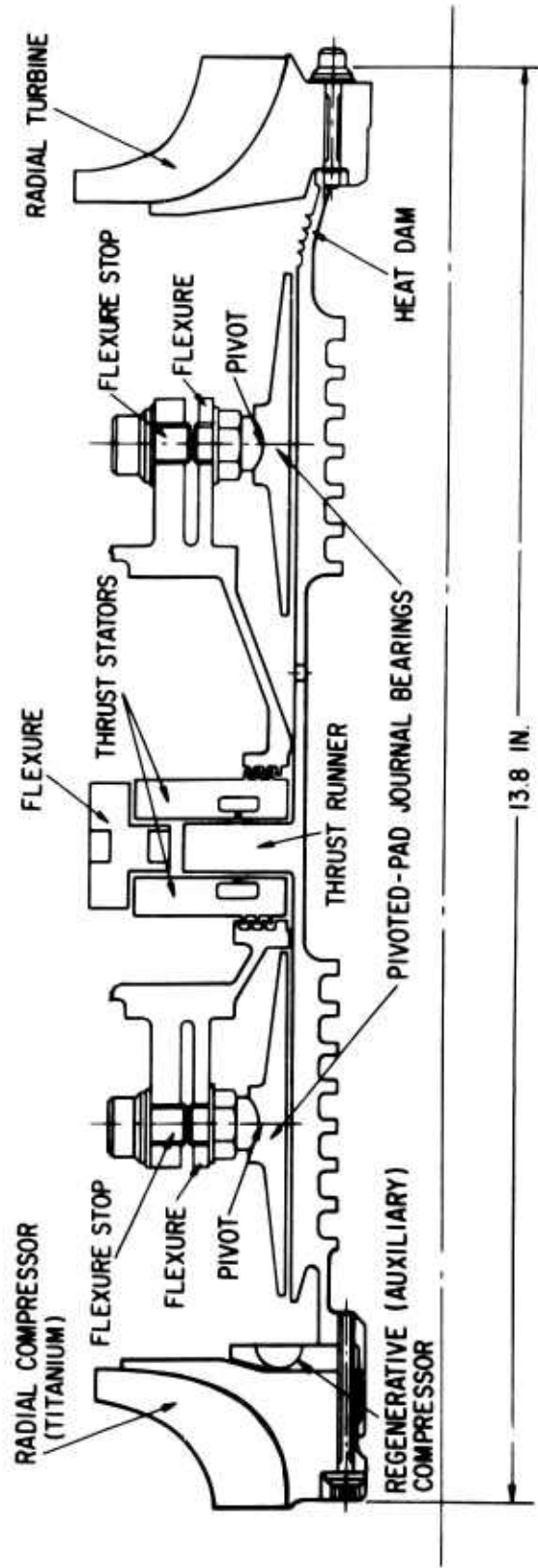


Figure 3. Isolated View of the HP Spool and Its Bearings.

Helically grooved passages are cut into the bore surface of each journal. These grooves form flow passages for the journal bearing cooling air as described in the "Journal Bearing Design Studies" chapter.

The HP turbine is attached to a relatively thin-walled conical section of the shaft which is referred to as the "heat dam". The heat dam provides a significant degree of thermal isolation between the hub of the turbine and the turbine-end journal. Based on the thermal studies presented in the next chapter, the heat dam section should be about 50 percent longer than is shown in Figures 2 and 3. This could be readily accomplished without noticeably changing performance characteristics of either the HP or LP spools.

LP-Spool Arrangement

Figure 4 shows an isolated view of just the LP spool and its bearings. Pertinent dimensions and parameters of the rotor are specified in the figure. A two-stage axial compressor is overhung at one end of the spool. The second-stage compressor disc is used as the thrust runner for a double-acting thrust bearing. Just inboard of the compressor is one of two self-acting pivoted-pad journal bearings. The second journal bearing is located at the other end of the shaft inside the exhaust duct for the LP turbine. The LP single-stage axial turbine is mounted inboard from the turbine-end journal and is separated from the journal by a "heat dam" section of shaft.

The two compressor discs, the turbine section, and the two journals are assembled to the mid-shaft (i.e., the through-shaft) section of the LP spool via locating face splines and axial tie bolts.

The rotor dynamic and mechanical assembly problems are more severe for the LP spool than for the HP spool. As discussed in the "Rotor Dynamics" chapter of this report, the fourth critical speed of the LP spool configuration shown in Figure 4 lies between design speed and overspeed, an unacceptable condition. The requirement for five face splines to achieve mechanical assembly of the spool is undesirable from the standpoints of cost, assembly complexity, and attainment and maintenance of rotor balance. One way to alleviate both of these problems would be to eliminate the reduced diameter sections of the LP shaft at the points where the shaft passes through the bores of the HP compressor and HP turbine. However, this would require an increase in the HP turbine and compressor bore diameters, which in turn would increase the already high centrifugal stresses in these components. Detailed analysis of these stresses would be required to determine if, and by how much, the bore diameters could be increased.

To a less significant extent, the rotor dynamic situation for the LP spool can be improved by lightening and shortening the two end assemblies of the spool as much as possible.

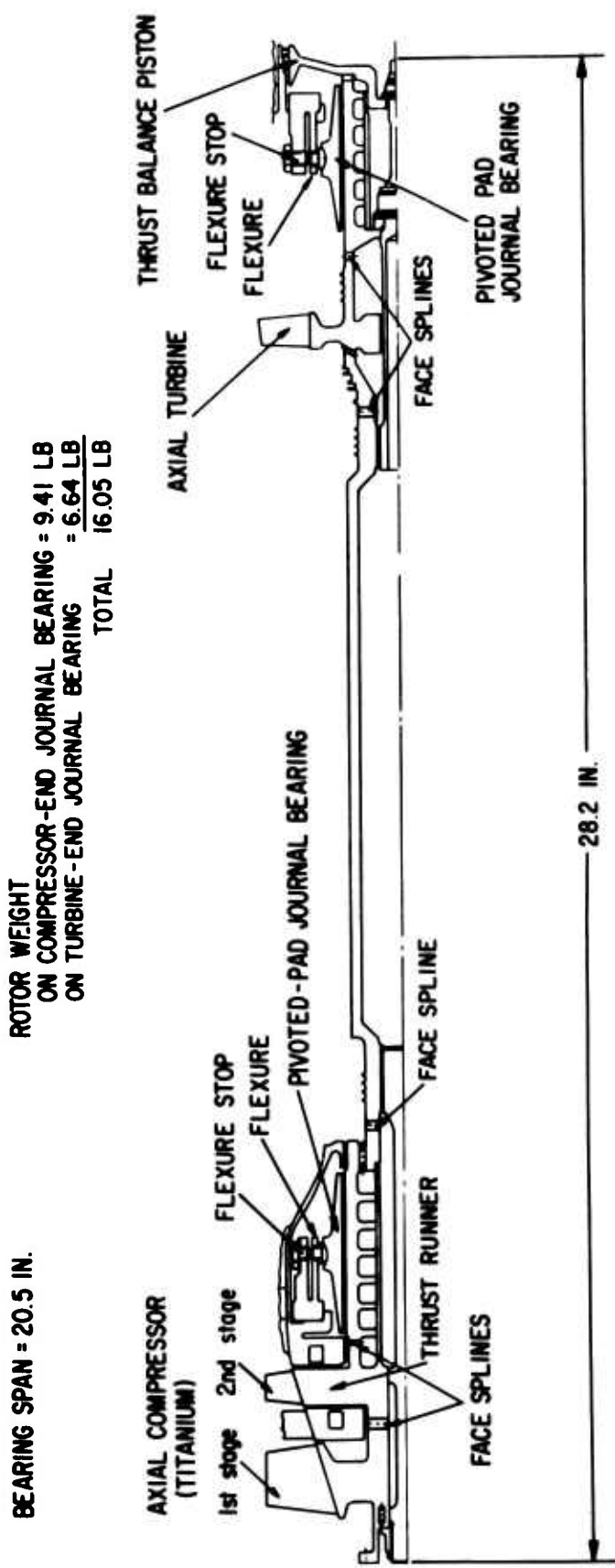


Figure 4. Isolated View of the LP Spool and Its Bearings.

Internal Airflows

Internal airflows in the gas generator fall into three categories:

1. Bleed flows for bearing and turbine cooling
2. Leakage flows from the journal bearing cavities and intershaft seals
3. Supply flows for the externally pressurized thrust bearings.

Figure 5 shows the paths for these various flows. A total of 5 percent of HP-compressor flow is used to cool the HP turbine. The major portion of this flow is also used for cooling the two HP-spool journal bearings and the LP-spool compressor-end journal bearing. Two percent of HP-compressor flow is used to cool the LP turbine. Half of this flow is also used to cool the LP-spool turbine-end journal bearing. These cooling flows are clearly shown in Figure 5.

With respect to Figure 5, unwanted leakage flows occur through seven bearing-cavity labyrinth seals (seals A, B, D₁, D₂, E₁, E₂, and K) and three intershaft seals (seals C, G, and H). Calculated leakage rates for a "first cut" design of the seals (as shown in Figure 5) are listed in Table II. The leakage rates apply to rated-power conditions at any condition of altitude. Altitude has only a second order effect on leakage rates at rated power since bearing cavity and intershaft pressures remain essentially the same, and most of the seals operate at choked flow. Seal design parameters and pressures are also listed in Table II based on the seal configurations shown in Figure 5.

Table II shows that the largest leakages occur across the LP-spool thrust-balance piston (seal K) and across the HP-spool thrust bearing seals (seals D₁, D₂, E₁, and E₂). It does not appear that much can be done to reduce the balance-piston leakage as long as a labyrinth type seal is used. However, by using a face seal instead of a labyrinth seal, the balance-piston leakage could be greatly reduced. Recent analytical and design studies have shown basic feasibility of air-floated noncontacting face seals for jet engine compressors [51, 52]. This type of seal should be evaluated for the balance-piston seal requirement in future studies of this advanced gas-lubricated engine concept.

With respect to the HP-spool thrust-bearing seals, it appears that the leakage rates given in Table II can be significantly reduced. Figure 5 shows the HP thrust bearing located close to the compressor-end journal bearing. This is a carry-over from earlier rotor-bearing system layouts in which turbine-end journal temperatures approach 1600°F and maximum separation of thrust bearing was desirable. However, improved heat transfer concepts were later evolved which reduced journal temperature to the 1200°F to 1400°F region. It thus appears reasonable to centrally locate the thrust bearing between the two journal bearings. The seal configuration can thus

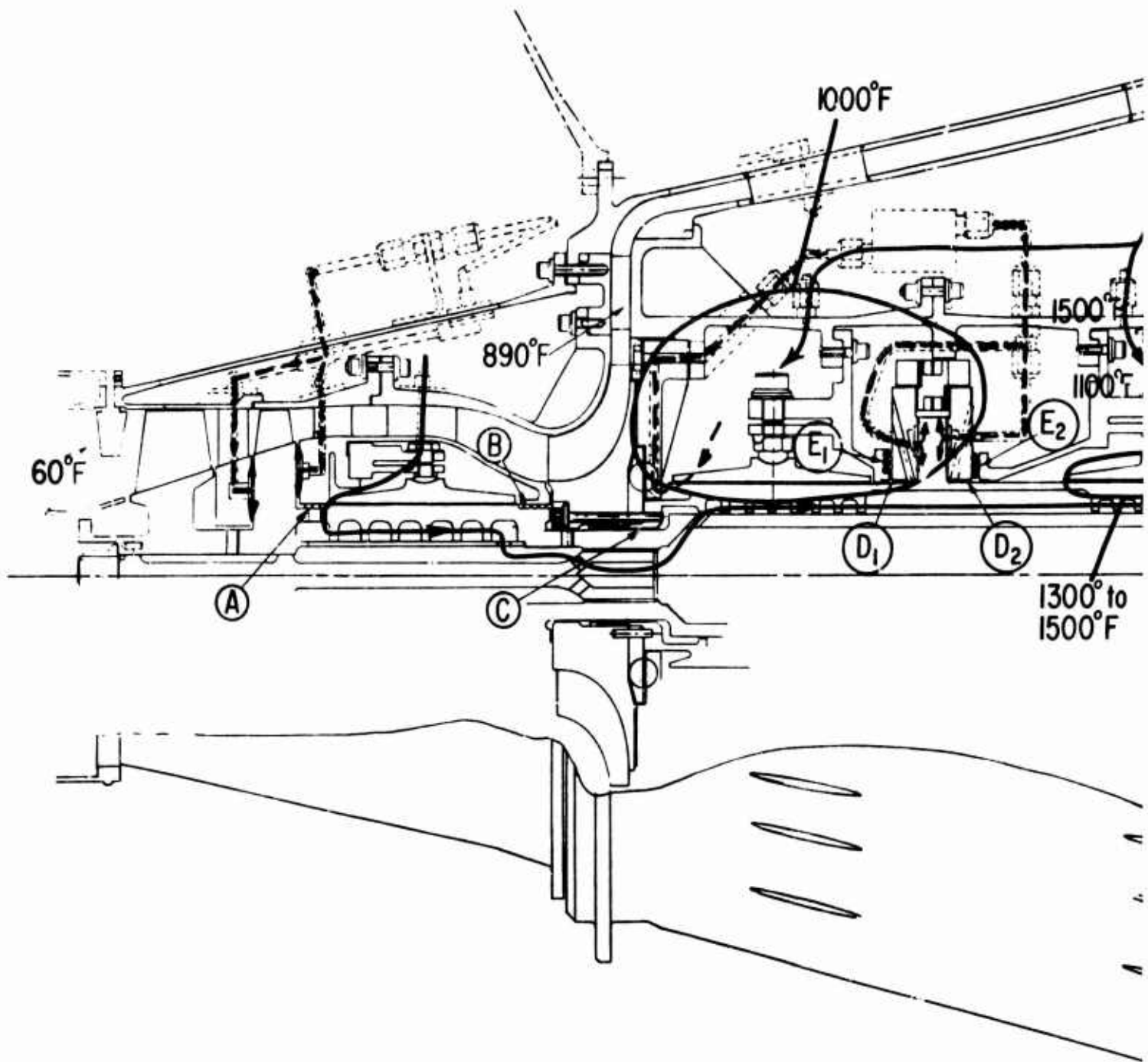
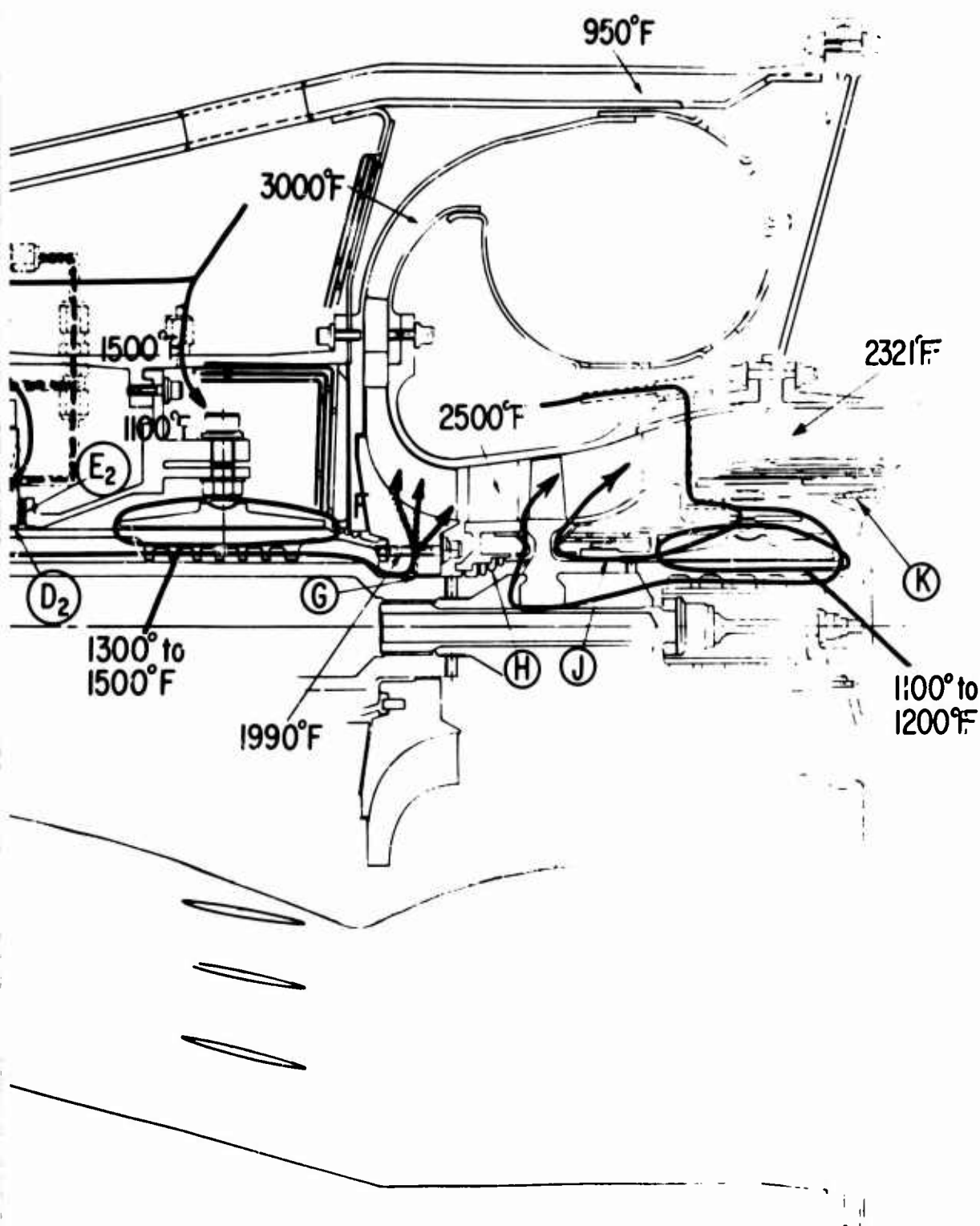


Figure 5. Bearing and Turbine Cooling Flows, Thrust Bearing Supply Flows, and Seal Locations for the Gas Generator.

A



B

TABLE II. LEAKAGE FLOWS THROUGH GAS GENERATOR SEALS AT RATED-POWER CONDITIONS

Seal Identification	Seal Parameters Based on Figure 5		Seal Leakage Flows (lb/sec)			
	Radial Clearance (in.)	Diameter (in.)	Pressures (psia)	For seal arrangement of Figure 5	For optimized design of seal system (estimated)	
			Inlet	Exhaust		
A	0.005	2.2	130	14.7	0.042	0.038
B	0.005	2.2	130	36	0.042	0.038
C	0.007	1.5	130	36	0.035	0.032
D ₁	0.005	3.0	130	14.7	0.050	0.025
D ₂	0.005	3.0	130	14.7	0.050	0.025
E ₁	0.005*	3.6	130	14.7	0.052	0.0
E ₂	0.005*	3.6	130	14.7	0.052	0.0
G	0.010	1.6	130	104	0.034	0.031
H	0.007	2.0	130	104	0.025	0.023
K	0.010	4.2	130	14.7	0.108	0.108
Total leakage for all seals (excluding seals F and J which are used to meter turbine cooling flows)					0.490	0.320

*Axial clearance

be changed to that shown in Figure 6, in which the restriction of seals D_1 and D_2 has been greatly increased.

Even further leakage reduction may be possible. Seals E_1 and E_2 are non-rotating seals. Hence, use of contact-type seals can be considered at these two points. The primary requirement of contact-type seals would be that they not impose excessive restraint on the ability of the thrust stators to self-align to the average plane of the thrust runner via the thrust bearing flexure mounts. Figure 6 shows a possible concept for a flexible contact-type seal. Successful application of a contact-type seal would reduce the leakage through seals E_1 and E_2 to essentially zero.

In addition to leakage rates for the "first cut" seal design, Table II also shows an estimate of leakage rates for an optimized seal system assuming contact-type seals at points E_1 and E_2 .

At rated-power conditions, the following breakdown of internal air flows should be a realistic design goal for the gas-generator configuration of Figure 5:

Bearing and turbine cooling -	0.32 lb/sec
Seal leakage -	0.32
Thrust bearing supply flows -	<u>0.07</u>
	0.71 lb/sec

To put these figures in a better form for comparative evaluation purposes, the various flow rates can be segregated by spool and expressed as a percentage of the rated 4.5-pound-per-second engine flow rate. These data are shown in Table III. It is seen that the thrust bearing flow for each spool, and particularly for the LP spool, is a relatively small portion of the total internal spool flows. The cooling flows for each spool are simply those specified by USAAVLABS. The most significant difference between the two spools is the seal leakage flows. For the HP spool, total seal leakage is slightly over 1 percent. This compares very well with conventional low-pressure single-spool engines. The LP spool has a significantly higher leakage, being approximately 6 percent of engine flow. This is probably higher than leakage rates normally encountered in conventional two-spool engines. The reason for this is twofold:

1. Thrust balance pistons of the type shown in Figure 2 are not generally required in conventional engines. For the gas-generator configuration of Figure 5, leakage through the balance-piston labyrinth seal represents 40 percent of the total seal leakage for the LP spool.
2. The LP spool journal bearing cavities in most conventional engines would operate at essentially LP-spool pressures. In the configuration of Figure 5, the LP-spool bearing cavities are operated at

ALTERNATE CONCEPT
OF CONTACT SEAL
FOR LOCATIONS
 E_1 AND E_2

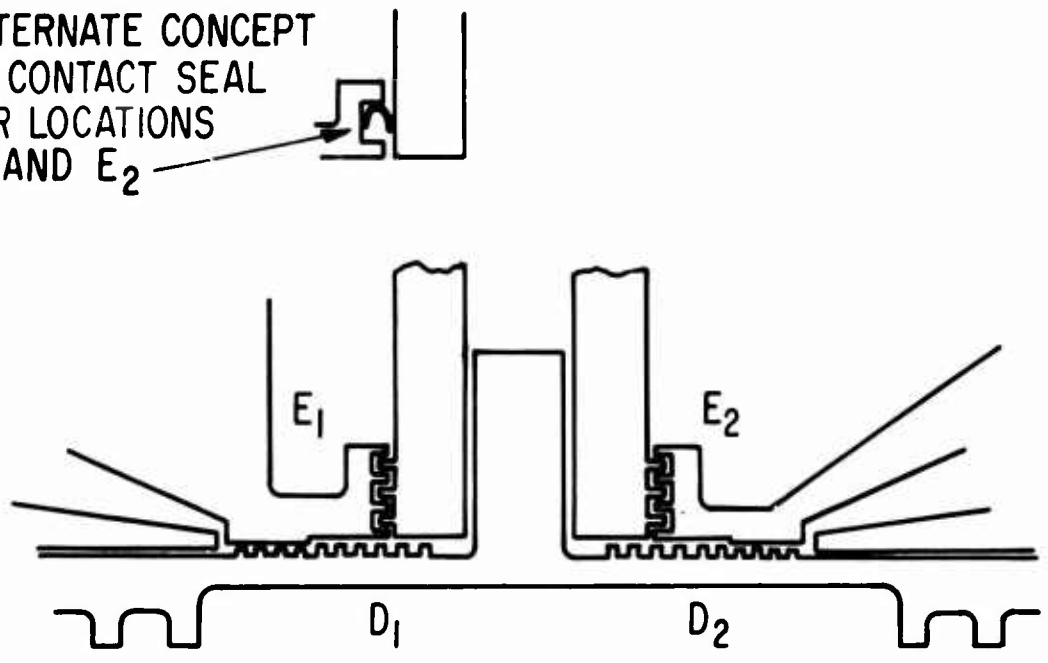


Figure 6. Improved Design Concepts for the HP-Spool Journal and Thrust-Bearing Seals.

HP-spool pressures. Leakage from the compressor-end cavity represents 28 percent of total LP-spool seal leakage.

TABLE III. INTERNAL GAS GENERATOR FLOWS AT RATED POWER (EXPRESSED AS A PERCENTAGE OF RATED ENGINE FLOW [*])		
	Percent of Rated Flow	
	LP Spool	HP Spool
Turbine and bearing cooling	2.0	5.0
Seal leakage	6.0 (Seals A,B,C,G,H,K)	1.1 ^{**} (Seals D ₁ ,D ₂ ,E ₁ ,E ₂)
Thrust bearing flow	0.25	1.3
Total	8.25	7.4
* Rated flow is 4.5 lb/sec		
** Assumes seals E ₁ and E ₂ are contact seals		

Actually, extreme care must be taken when comparing losses for the gas-bearing gas generator and losses for a conventional oil-lubricated engine. The most meaningful comparison is one based on total parasitic losses for the same operating conditions (i.e., the same aerodynamic pressures, temperatures, and speeds). Total parasitic losses should include, in addition to gas-seal losses, bearing losses and all losses associated with bearing system accessories. In the case of the gas-bearing gas generator, the only significant bearing system accessory is the regenerative compressor used to boost thrust bearing supply pressure. In a conventional engine, all losses associated with the lube-oil system should be taken into account, which includes pumping power, cooling-fan power (if required), thermal power removed from the engine by the oil flow, friction losses in the oil seals, and buffer-gas flow if buffered oil seals are used. A recent comparison of oil- and gas-lubricated closed-loop gas-turbine machinery showed total parasitic bearing-system losses for the gas-lubricated system to be significantly less than for the oil-lubricated system [8]. A similar type of study would be required to determine if total LP-spool parasitic losses for the present gas generator are a significant function of the type of lubrication system used.

Temperatures

Also shown in Figure 5 are temperatures at various points within the gas generator. These temperatures correspond to sea-level rated-power engine operation.

A complete thermal analysis of the gas generator was not performed. Hence, except for temperatures of the aerodynamic flow path, the indicated temperatures have been estimated based on thermal analyses performed for the bearing regions (these analyses are summarized in the next chapter). Absolute accuracy of the temperature values is not as important at this point as are general levels of temperature and the severity of the temperature gradients which will exist in the engine.

The significant point with respect to the bearings is that the two turbine-end journal bearings will operate at temperatures above 1000°F. Optimum temperature level for the HP-spool bearing, one that can be obtained via the preferred bearing cooling concept, is 1400° to 1500°F. For the LP-spool bearing, a realistic temperature level is 1100° to 1200°F. The very fact that these levels of bearing temperature can be realistically considered immediately emphasizes an inherent advantage of gas lubrication. It is a well established fact that the lubricating qualities of gas do not degrade with increasing temperatures. In fact, bearing load capacity will increase with increasing temperature due to the increase in gas viscosity.

The only restrictions on the design of high-temperature gas bearings are those associated with the high-temperature properties of bearing structural materials. These restrictions, however, become multivariate as temperature levels rise. A comprehensive summary of the present state of high-temperature gas-bearing material technology is given in Appendix III. Initial testing of bearing materials at 1400°F in air, at speeds of 30,000 rpm, has already been performed with promising results. Extension of existing materials and coating techniques to 1600°F appears to be a reasonable goal for the next five-year period. In addition, the rapid advancements being made in ceramics and cermets, as well as various whisker and yarn reinforced alloys and graphites, may greatly increase the choice of available high-temperature materials as well as increase possible operating temperatures.

From a bearing materials standpoint, therefore, temperature levels of 1200° to 1500°F are considered to be completely reasonable as a design objective for this advanced gas generator. Experimental verification of material feasibility, particularly for the turbine-end journals, should proceed as rapidly as possible using full-scale journal test rigs.

Another important point and possible problem area evident from Figure 5 is the large temperature gradient which will exist between the HP-turbine nozzle ring and the support casing for the HP-spool turbine-end journal bearing. Very careful attention will have to be given to design of the nozzle-ring support means to achieve adequate thermal isolation, acceptable thermal stress levels, and the required accuracy of mechanical alignment.

Figure 5 does not reflect, except very superficially, detailed study of the structural design problems. In all probability, final mechanical design of the nozzle attachment means would be different from that indicated by Figure 5.

The other thermal gradient area which will require careful design analysis is the heat dam section of the HP spool. Aspects of heat dam design are discussed in the next chapter.

Accessory Drive

Power takeoff requirements for driving the gas generator accessories were estimated using data given in Reference 12 and supplemented by USAAVLABS. Accessory power will be required for ignition, electrical accessories, and fuel pumping. Figure 7 shows the estimated accessory power requirements as a function of HP-spool speed.

Only mechanical techniques for power takeoff were investigated. Both direct-drive and geared-drive systems were considered. On the basis of several layout studies, it was concluded that direct-drive systems were more compatible with the concept of a gas-bearing gas generator. Geared takeoff systems would require considerable gear development for reliable operation at the gas-generator operating speeds. Furthermore, gears would require some type of lubrication, perhaps solid but more likely liquid. Lubricant seals would thus be required within the engine and accessory lube pumps, sumps, filters, etc., would be required outside the engine.

The power takeoff system implied by the Phase VI gas-generator layout consists of a quill shaft or other suitable direct connection from a drive flange at the compressor-inlet end of the LP spool to an accessory package mounted in front of the compressor. The accessory package would contain its own bearings (probably oil lubricated) and seals. The accessories would be driven at LP-spool speeds and hence should be reasonably small. If, however, the accessory package becomes too large for efficient ducting of compressor inlet air, a right-angle gearbox, direct-driven from the end of the LP-spool, would have to be developed for transmission of drive power to a side-mounted accessory package.

Starter Drive

Torque required for gas-generator startup is plotted as a function of speed in Figure 8. The total torque includes torque requirements for accessories as well as rotor acceleration torque and sliding-friction torque of the self-acting journal bearings. Lift-off speed was calculated to be 176 rpm for the LP-spool journal bearings and 700 rpm for the HP-spool bearings. The bearing sliding-friction torque produces the two discrete step changes in the low-speed torque characteristic of Figure 8.

The startup torque characteristic of Figure 8 was selected on the basis of data given in Reference 12 to achieve HP-spool light-off speed of 15,000 rpm

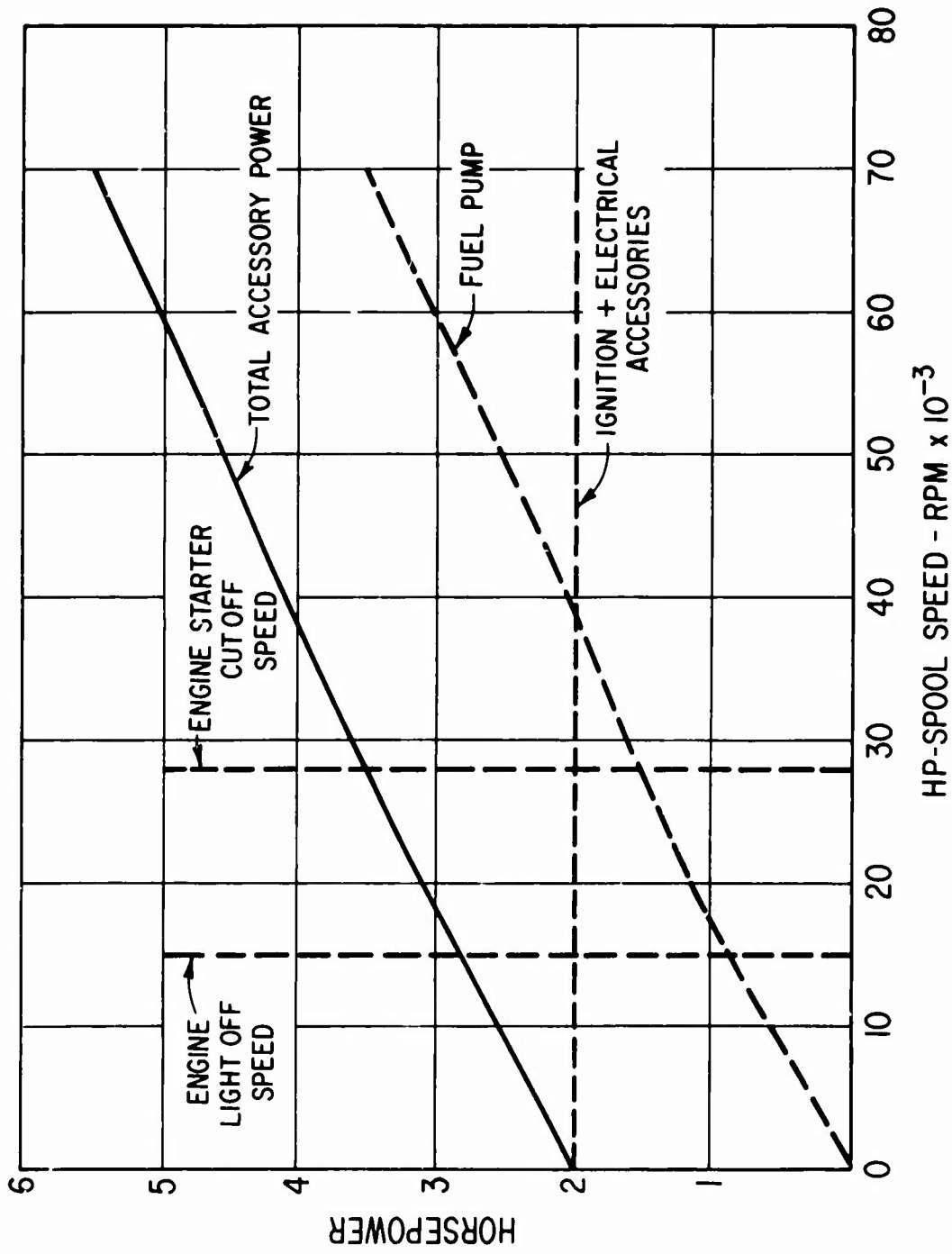


Figure 7. Power Takeoff Requirements for Driving Gas-Generator Accessories.

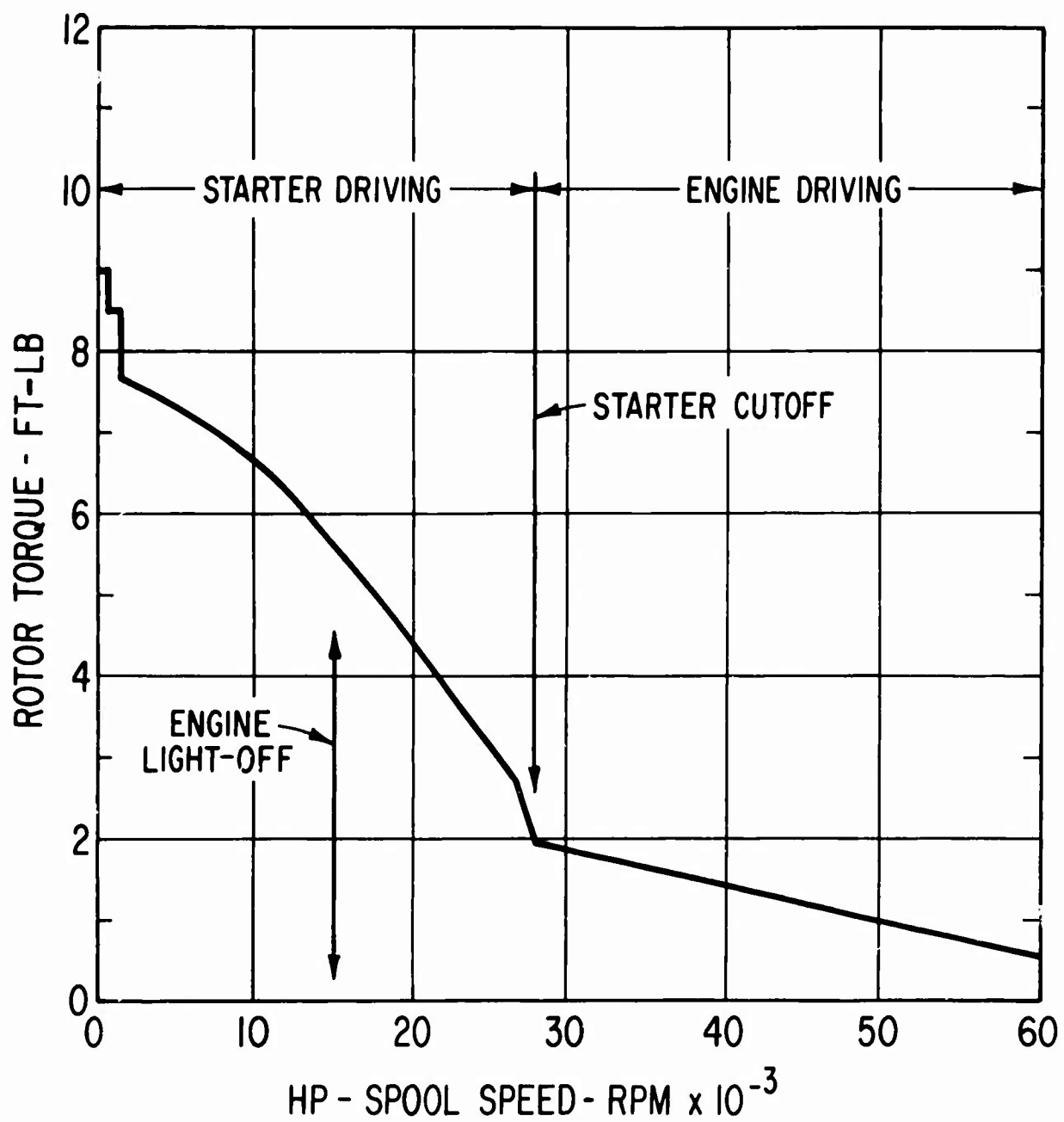


Figure 8. Torque Requirements Versus HP-Spool Speed for Engine Starting and Accessory Drive.

in 7 seconds. Attainment of self-sustaining engine operation would occur 18 seconds from initiation of startup.

Only mechanical techniques for transmitting starter torque to the gas generator were investigated. In spite of an intensive study effort, only one promising transmission concept was evolved. The concept assumes that startup torque is transmitted from a starter motor via the accessory drive train to the LP spool. However, the HP spool must also be driven during startup. To transmit torque from the LP spool to the HP spool, friction or face-serrated drive surfaces on the two spools are brought into mating contact. The LP-spool drive surface is located on the compressor-end journal and mates against a similar drive surface on the hub of the HP-spool radial compressor. During the startup period, an auxiliary air system would be used to pressurize the left-hand side of the LP-spool thrust runner (as seen in Figure 2) thus driving the LP and HP driving surfaces together. At the same time the right-hand side of the HP-spool thrust bearing would also be pressurized so that the combined LP/HP-spool assembly would be floating in the axial direction.

Upon attainment of starter cutoff speed, the auxiliary air supply system and the starter motor would be cut off. The internally contained normal thrust bearing air supply system would then function and supply air to both sides of each thrust bearing. Upon removal of the auxiliary air pressure, the drive surfaces of the LP and HP spools would separate.

Preliminary analysis of this means for coupling the two rotors during start-up indicated that the required torque could be transmitted to the HP spool without slippage if the appropriate sides of the HP and LP thrust bearings were pressurized with air at 80 to 100 psia. The driving faces were assumed to be smoothly surfaced with a coating such as chrome oxide, which has a sliding coefficient of friction of about 0.3.

The above-described concept for mechanically coupling the two rotors during startup appears to be feasible. However, careful control of axial dimensional tolerances between the two rotors will be required. The major disadvantage may be the requirement for an external source of 100-psi air during the startup period. If this proves to be a major logistics problem, it is recommended that serious consideration be given to ways in which conventional air-start equipment (or advanced models of present air-start equipment) might be used to accomplish direct air drive of the HP spool.

JOURNAL BEARING DESIGN STUDIES

Analysis and design of the journal bearings for the gas generator progressed in parallel with evolution of the rotor-bearing system design layouts. This was a natural and inescapable consequence of the many interactions which exist between the aerodynamic, heat transfer, stress analysis, rotor dynamic, and bearing-system design parameters in any advanced type of rotating machine. For reasons of conciseness, however, only the Phase VI version of the journal bearing designs is discussed in detail in this chapter.

The Phase VI journal bearing designs should not be interpreted as final or fully optimized designs ready for detailing, manufacturing, and testing. The intent of the study was not to reach this degree of refinement, but rather to:

1. Identify the types of bearings which should be used.
2. Determine operational feasibility of the bearings for the prescribed gas-generator operating conditions.
3. Identify any specific or potential problem areas which would require new analysis procedures, new component hardware, or advanced test programs to resolve the problem or assess the magnitude of its severity.
4. Identify where additional design and analysis effort would be required to achieve an optimized bearing design which could proceed to the manufacturing and testing phase with a high degree of confidence for success.

SELECTION OF JOURNAL BEARING TYPE

In order to screen and select the most promising journal bearing designs for use in the gas generator, one bearing location was selected for comparative evaluation purposes. For a two-spool engine configuration, having two bearings per spool, a choice of four bearings is available. After considerable initial study, it became evident that the HP-spool turbine-end bearing would encounter the most severe conditions of applied load, environmental temperature, bearing friction heating, rotating mass, and journal centrifugal growth. This bearing was therefore selected for the comparative design and evaluation study.

It also became apparent that conditions for the HP-spool compressor-end bearing would be very similar to the turbine-end bearing except that the environmental temperature would be somewhat lower. On the other hand, the LP-spool journal bearings would operate at considerably less severe conditions, in most respects, relative to the HP-spool bearings. Only the effects of synchronous unbalance response proved to be more severe. This is discussed in the "Rotor Dynamics" section of this report.

The following types of journal bearings were examined during the screening study:

1. Full-circular hybrid bearing^{*}
2. Full-circular self-acting herringbone-grooved bearing
3. Pivoted-pad self-acting bearing
4. Pivoted-pad hybrid bearing

The full-circular self-acting bearing (which is not included in the above list) was quickly eliminated from any serious consideration as a result of its lack of stability at the gas-generator operating conditions. Foil-supported and conformable-surface bearings were not studied because of a general lack of turbomachinery experience with these bearings, as well as a number of readily apparent problem areas.^{**}

Full-Circular Hybrid Bearing

Because of the high Δp available from the HP compressor, it was initially thought that the full-circular hybrid bearing was the most logical candidate for the HP-spool turbine-end bearing. As will be discussed shortly, the maximum bearing load was calculated to be 320 pounds at design speed. For a 3-inch-diameter by 3-inch-long bearing, this would give a unit loading of 35.5 pounds per square inch of projected bearing area. This degree of loading was well within the state of the art for externally pressurized bearings, but considerably greater than existing experience with self-acting bearings. Figure 9 shows a representative example of a full-circular hybrid journal bearing. In this particular bearing, the pressurized gas is fed to the clearance space via two rows of orifices located in planes at the one-quarter and three-quarter length positions along the bearing.

A thorough analysis of the externally pressurized hybrid journal bearing was performed. A detailed summary of the analysis is given in Appendix III. The net result of the analysis was a realization that fractional-frequency whirl instability would be a serious problem. To solve this problem would require (1) additional pressurization of the bearing supply gas as taken from the HP-compressor discharge, and (2) operation of the bearings at radial clearances of 0.001 inch or less.

* For the purpose of this report, a hybrid bearing is defined as an externally pressurized bearing in which self-acting (hydrodynamic) effects have a significant influence on bearing performance.

**Foil-supported and conformable-surface bearings for turbomachinery applications are currently being evaluated, on a bearing technology basis only, by MTI under NASA Contracts NAS 3-9433 and NAS 3-10951. Both analytical and test evaluations are being performed.

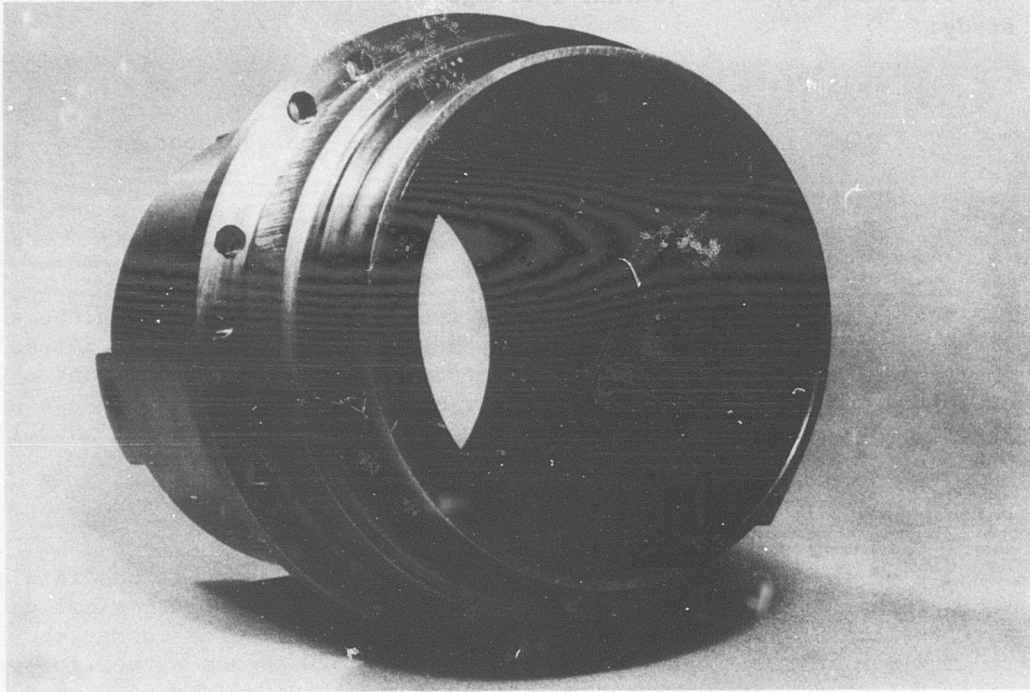


Figure 9. Typical Full-Circular Hybrid Journal Bearing.

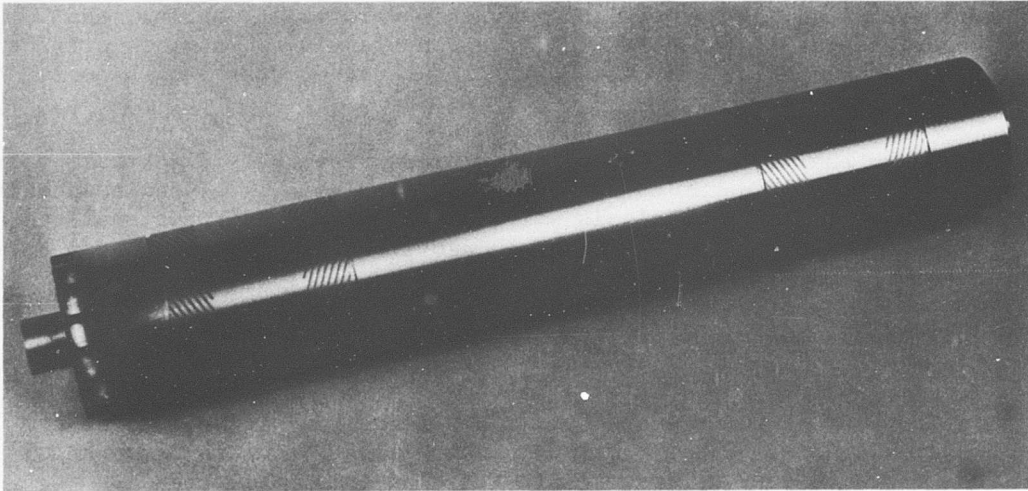


Figure 10. Herringbone Groove Pattern Applied to Journals of a Small High-Speed Rotor.

The problem of obtaining additional pressurization of the bearing supply gas could be solved by incorporating a small regenerative compressor as an integral part of the HP-spool assembly. However, maintenance of a 0.001-inch, or less, radial clearance in the HP-spool bearings proved to be a major problem area because of centrifugal growth of the journal. Assuming a journal radius ratio (R_1/R_0) of 0.433 (this being optimistically smaller than LP-spool design would actually permit), the change in radial clearance due to centrifugal growth, from idle to maximum speed, would be 0.0009 inch. The only way in which this amount of growth could be accommodated, while at the same time maintaining reasonable bearing clearances not exceeding 0.001 inch, would be to have a bearing design which could automatically compensate for centrifugal growth. Several ideas for achieving such a design were proposed and preliminarily evaluated. It was concluded that each concept (not having, to our knowledge, been previously tried) would require considerable design and development effort to determine its feasibility and reliability. Accordingly, rather than continue the study on the assumption that a successful constant-clearance externally pressurized bearing could ultimately be developed, it was decided to investigate fully the feasibility of self-acting types of bearings first.

The use of full-circular hybrid journal bearings for the LP spool was definitely ruled out because of stability problems. Unlike the HP spool, neither centrifugal growth nor bearing supply pressure was the problem. Rather, the LP spool is a highly flexible shaft having its first simply-supported critical speed at 22,000 rpm. Hence, the threshold speed for fractional-frequency whirl would have an upper bound of approximately 44,000 rpm regardless of bearing stiffness (i.e., regardless of supply pressure or radial clearance). Since maximum speed of the LP spool was well above 44,000 rpm, the use of externally pressurized hybrid bearings was accordingly ruled out.

A more complete summary of the analysis of externally-pressurized hybrid journal bearings for the gas generator is given in Appendix III.

Self-Acting Herringbone-Grooved Bearing

The self-acting (hydrodynamic) bearing in its simplest form is a smooth cylindrical (fully circular) sleeve. However, of the various self-acting configurations, this configuration is the most susceptible to fractional-frequency whirl. To improve stability, geometry modifications such as steps, tapered lands, eccentric lobes, or grooves can be added to the bore of the sleeve or the surface of the journal. One of the most effective of these geometry modifications is that which yields the so-called herringbone-grooved journal bearing. A herringbone pattern of grooves, which provides a viscous pumping action, is added to either the bearing sleeve or the journal. Figure 10 shows such a pattern applied to the journals of a small shaft. Reference 13 has shown that this type of pattern results in a minimal reduction of load capacity and a marked improvement in stability.

The application of the herringbone-grooved bearing to the HP-spool turbine-end journal was analyzed. The results of the analysis are summarized in Appendix IV. In brief, the analysis showed that although adequate load capacity could be achieved, a stability problem would again exist due to the change in radial clearance resulting from centrifugal growth. The problem of achieving a more-or-less constant clearance bearing design was essentially the same as discussed in the preceding section for the externally pressurized bearing.

With respect to the LP spool, existing test data and stability analyses for the herringbone-grooved bearing do not extend to the case of a flexible shaft. Since centrifugal growth effects are much less severe on the LP-spool journals, it intuitively appeared that stable operation might be possible. However, without documented support for this intuitive feel, and recognizing that serious stability problems would exist with the HP-spool, it was decided to defer a final decision on the herringbone-grooved bearing until a thorough investigation of other types of bearings was completed.

Self-Acting Pivoted-Pad Bearing

A further improvement in the stability of self-acting bearings is provided by constructing the bearing in three or more circular-arc segments and supporting each segment on a pivot. This construction gives rise to the pivoted-pad (sometimes called the tilting-pad) journal bearing. By virtue of the pivot, each pad (segment) can individually align itself to the rotating journal to provide an inlet gas wedge for generation of hydrodynamic pressures. The center of pressure of the gas film will tilt the pad to an angle of attack that results in an equilibrium of forces acting on the pad. At the equilibrium position, the center of pressure of the gas film will be over the pivot point. This results in a highly stable bearing configuration with respect to fractional-frequency whirl. However, because of the circumferential interruptions caused by the edges of the individual pads, some load capacity is lost relative to a full-circular sleeve bearing.

Stability characteristics of the self-acting pivoted-pad bearing are not yet well understood from a theoretical standpoint. The problem is currently the subject of several small initial investigations. There is, however, a limited amount of experimental data [7]. It has been observed that the threshold speed for fractional-frequency whirl occurs when rotor speed exceeds 4 to 5.5 times the first critical speed of the rotor-bearing system. By contrast, the threshold speed of full-circular self-acting and hybrid bearings occurs at a factor of approximately two times the first critical speed. Thus, for comparable values of bearing stiffness, it appears that the pivoted-pad bearing can operate stably at 2 to 2.75 times higher speeds than the full-circular types of bearings.

A preliminary threshold speed analysis was made for the HP spool supported by pivoted-pad bearings. Consideration of the experimental data of Reference 7 led to the following stability criterion: For stable operation,

shaft speed should not exceed five times the first critical speed of the rotor-bearing system at any given operating condition. Based on this criterion, the threshold analysis indicated that stable operation would be possible with a small margin of safety.

An initial check of the bearing load capacity was then made. The case of a 320-pound bearing load applied directly through the pivot of a single pad was examined. Two calculations of minimum pad film thickness were made using theoretical design data for ideal (nondistorted) bearing geometry as obtained from two sources [14, 15]. Excellent agreement between the two values of film thickness was obtained. Equally as important, the calculated results indicated that the 320-pound bearing load could be carried at a film thickness of 0.69 mil, which is only slightly less than the "usual" operating films in present-day gas-bearing turbomachinery.

It was recognized that distortion of the bearing geometry, such as would be produced by temperature gradients, might significantly reduce the film thickness. Accordingly, an initial estimate of the bearing temperature gradients was made. (Later thermal studies showed these initially estimated gradients to be excessively large.) The single pad data were then recalculated using a newly developed computer program in which thermal distortions resulting from specified temperature gradients are first calculated, and then the gas-lubrication equations are solved based on the distorted bearing geometry. The pad film thickness for the distorted condition dropped to 0.18 mil, slightly less than the 0.2-mil-minimum film thickness criterion which had been established based on actual gas-bearing turbomachinery operating experience at comparable film conditions.*

Since the preliminary calculations indicated that the self-acting pivoted-pad bearing could operate stably and could, with adequate control of bearing distortions, carry the maximum bearing load at reasonable film thicknesses, it was decided to perform a more rigorous analysis of this type of bearing. Presentation and discussion of the design requirements and calculated performance of pivoted-pad bearings for both the LP and HP spools are the primary subjects of this section of the report.

In addition to their better stability characteristics, self-acting pivoted-pad bearings have a number of practical advantages, and they have been used in most motor-driven and all turbine-driven gas-bearing machinery built to date. However, in all instances, the bearing loads have been less than 10 pounds per square inch of projected bearing area. It was thus a

* It should be understood that it is not recommended practice to operate gas-bearing turbomachinery at 0.2-mil film thicknesses. We do not consider this to be a comfortable condition. However, since the maximum gas-generator bearing loads should occur only occasionally (if at all), and would probably be applied for only short durations of time, the 0.2-mil minimum film criterion seems reasonable. Ultimately, however, the reasonableness of this criterion must be proven by extensive test data under representative gas-generator maximum load conditions.

pleasant surprise to find that the bearings could, at least under ideal conditions, carry loads up to 35 pounds per square inch with reasonable film thicknesses. Listed below are several of the design advantages of the pivoted-pad bearing:

1. As a result of the individual pivot-mounted pads, the bearing is self-aligning. Misalignment between the two bearing support housings, as might be caused by thermal or mechanical distortions, has virtually no effect on bearing performance.
2. The bearing appears to be self-cleaning due to the interruptions created by adjacent edges of the pads which permit debris to escape. Pivoted-pad bearings have been operated in relatively dirty environments, with no attempt at cleaning or filtering the ambient gas, with no known failures. In one instance, acceptance testing of a 50-HP gas-bearing helium circulator by the AEC required introduction of carbon-graphite powder into the compressor inlet during operation of the machine. The machine passed this test without any observable effect on bearing performance. After the test, the machine was dismantled for inspection. Carbon-graphite powder was found throughout the pivoted-pad journal bearing cavities as well as in the thrust bearing cavity.

Unfortunately, no studies have been performed to quantitatively determine the effects of various types of dirt and debris on the performance of gas bearings. Until such studies are made (with specific emphasis on aircraft engine environmental conditions), only intuitive statements based on extrapolation of existing qualitative experience can be made about the possible effects of dirt on gas bearings in aircraft engines. This is clearly one area where quantitative evaluations must eventually be made.

3. Distortions caused by linear axial temperature gradients along the journal, or differential axial gradients along both the pads and the journal, cause very little loss in load capacity. This is due to the ability of the pads to adjust individually to the cone angle of the journal.
4. Techniques of flexure mounting one or more of the pads have resulted in bearing designs which can accommodate appreciable amounts of journal centrifugal growth, plus differential thermal expansion between the journal and bearing support housing, without excessive loss or increase in film thickness. This is a particularly important consideration in the gas-generator design.

Figure 11 shows a typical 4-pad pivoted-pad bearing with pivots supported by individual beam type flexures. The holes in the pads were for the purpose of instrumentation to monitor bearing performance during development testing.

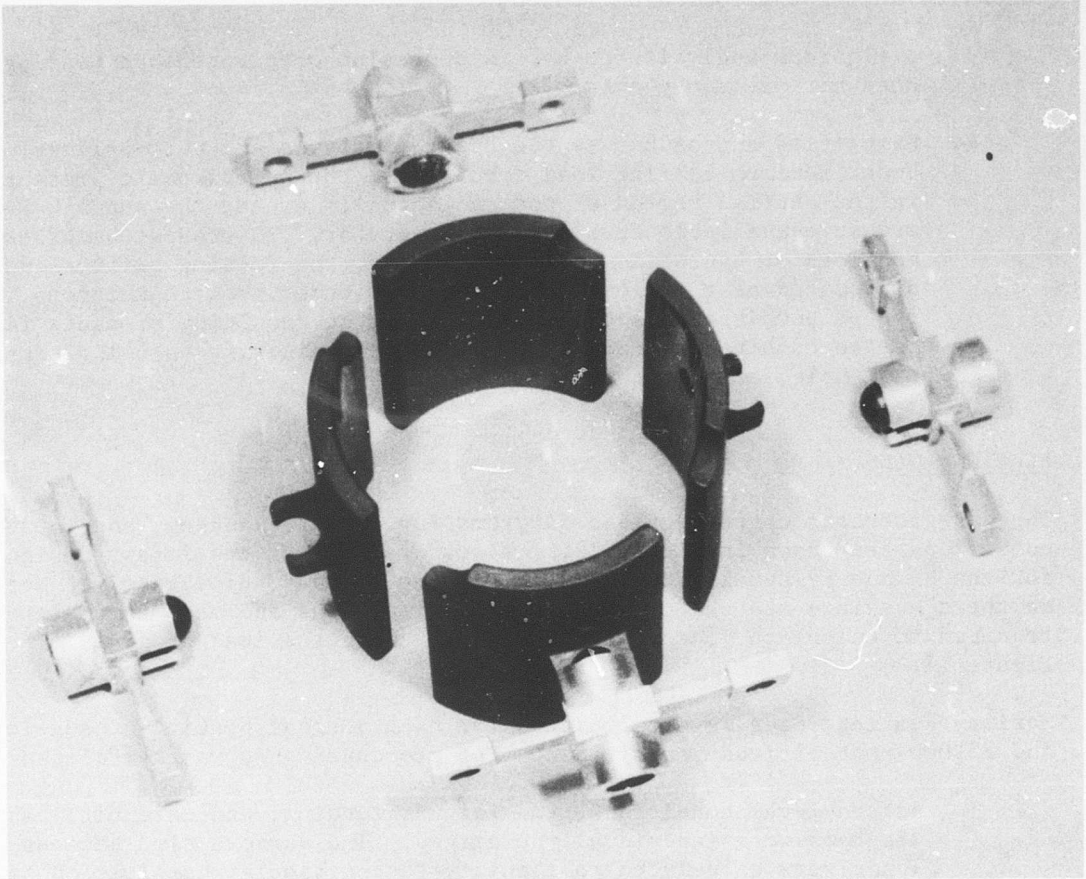


Figure 11. Typical 4-Pad Pivoted-Pad Journal Bearing
With Pivots Supported by Flexures.

Hybrid Pivoted-Pad Bearing

A brief study was made to assess whether the load capacity of pivoted-pad bearings could be increased by supplying pressurized gas to the clearance space through suitable feeding orifices. The results of this study were inconclusive for the following reasons:

1. A rigorous analysis for hybrid operation of pivoted-pad bearings does not presently exist.
2. Simplified approaches to the hybrid analysis are not applicable. Under maximum bearing load conditions, the hydrodynamic pressures in the central region of the pad actually exceed the supply pressure available from the gas generator. To prevent backflow and loss of hydrodynamic load capacity, the feeding orifices must be located near the edges of the pad. Under these conditions it is not possible to accurately predict the resulting pressure field due to combined hydrodynamic and hydrostatic effects using simple hand-calculation techniques.

BEARING LOADS

The gas-generator operating load diagrams for flight, landing, and catapult conditions are shown in Figure 12. Layout drawings of the latest designs for the HP and LP spools are shown in Figures 3 and 4 respectively. Noted on these drawings are the pertinent rotor dimensions and mass parameters required to calculate journal bearing loads using the load diagrams of Figure 12.

Maximum bearing loads were calculated for each journal bearing at sea-level and 25,000-foot-altitude conditions. The procedure used was as follows:

1. At sea-level conditions, the flight, landing, and catapult load diagrams were individually examined. The various simultaneous loads were calculated to identify the particular combination of operating condition and simultaneous loads which would produce the highest bearing load. In all cases, total bearing load was calculated as the vector sum of the simultaneously acting vertical and side force components. The maximum value of total vector load so obtained was the value retained for design analysis purposes.
2. At a 25,000-foot altitude, only the flight load diagram needed to be examined. The procedure outlined above was used to determine the maximum vector load for bearing design purposes.

HP-Spool Bearing Loads

Figures 13 and 14 show the calculated bearing loads at sea-level and at 25,000 feet altitude, respectively, for the HP-spool turbine-end bearing. The load components are plotted as dashed lines, while the maximum

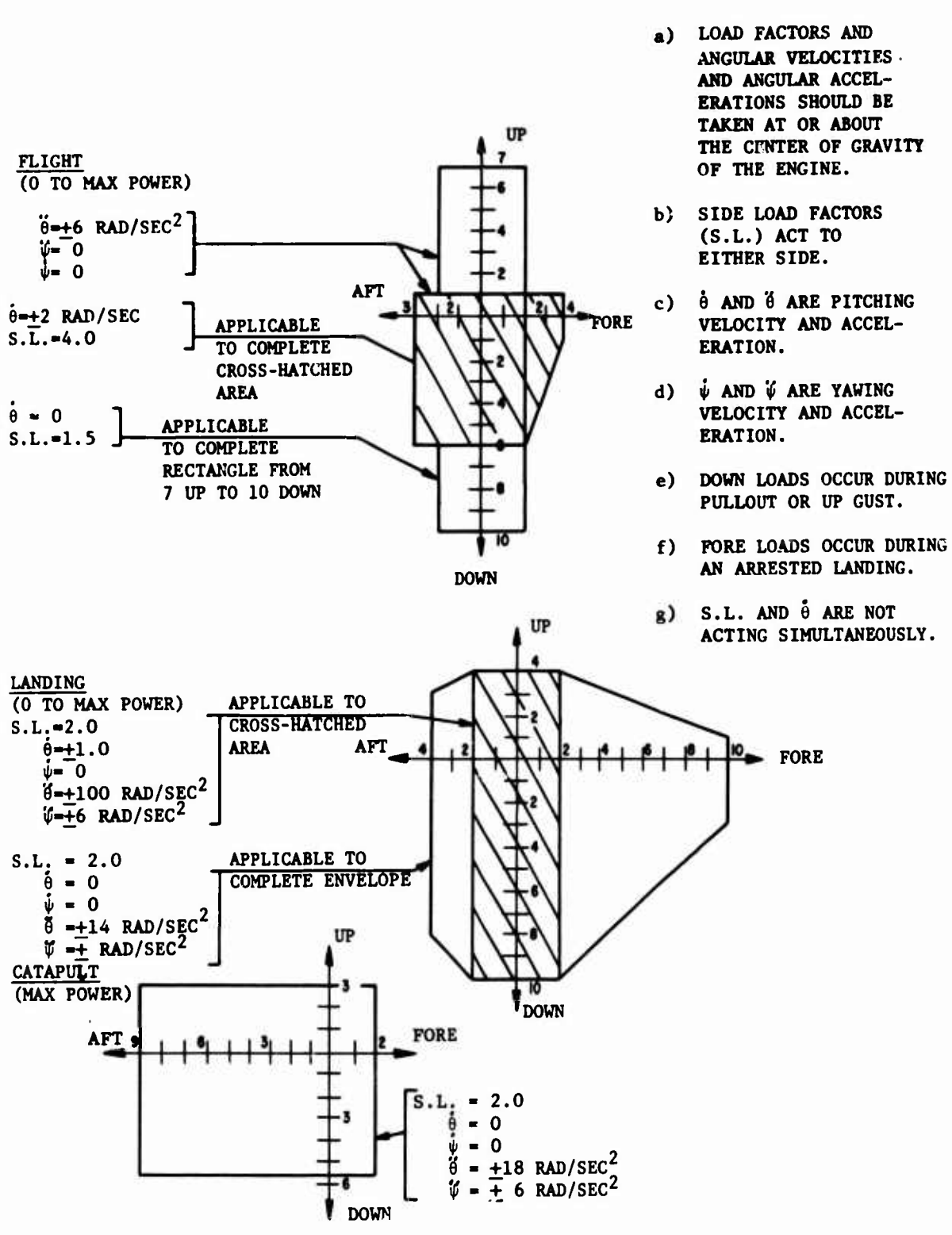


Figure 12. Operating Load Diagrams for the Gas Generator.

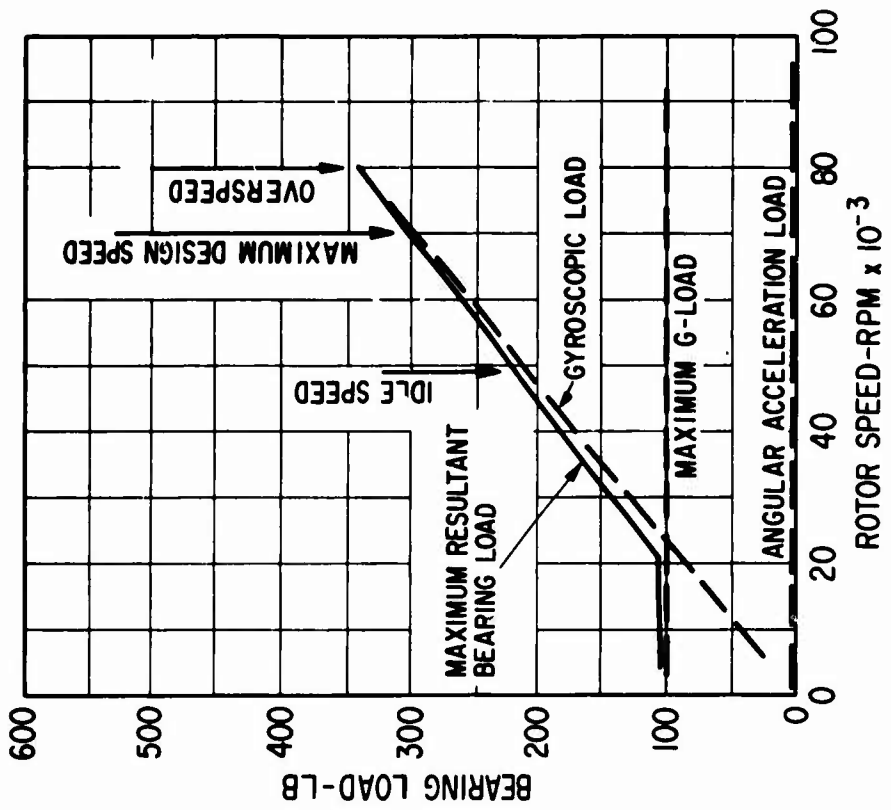


Figure 13. Maximum Loads for the HP-Spool Turbine-End Journal Bearing at Sea-Level Flight Conditions.

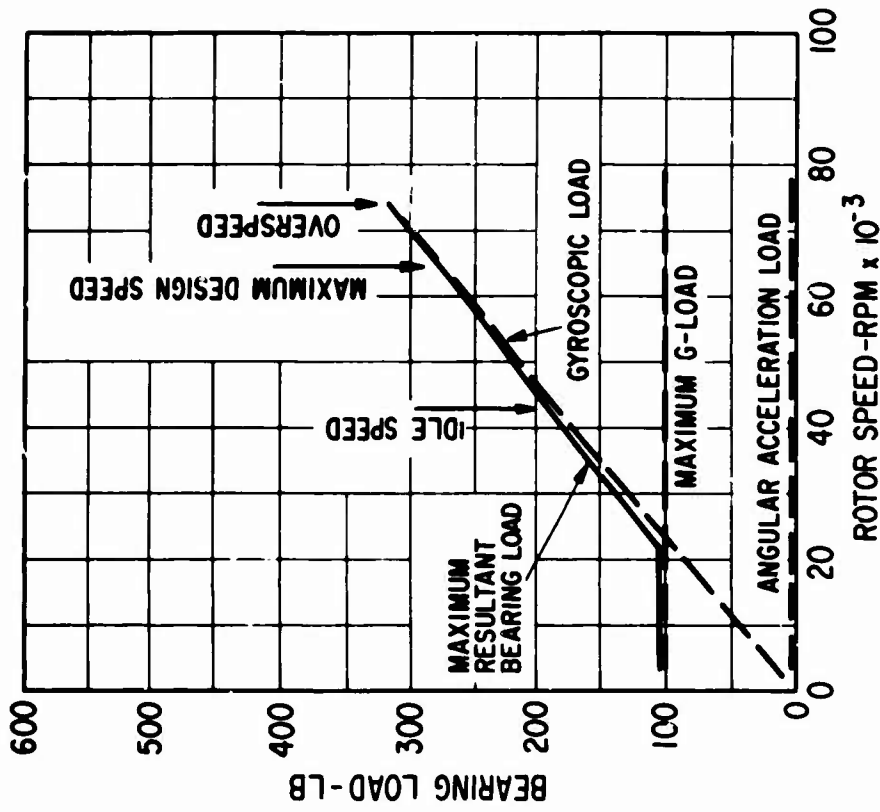


Figure 14. Maximum Loads for the HP-Spool Turbine-End Journal Bearing at 25,000-Foot-Altitude Conditions.

resultant bearing load is shown as a solid line. It should be noted that the plotted component load values are maximum values, but that these maximum values do not all act simultaneously. For example, the load diagram of Figure 12 shows that vertical loads during flight are limited to 6 g's when they occur simultaneously with the ± 2 radians per second pitch velocity. Above 20,000 rpm, these two simultaneous conditions define a larger resultant bearing load than does the specified maximum 10-g vertical load condition acting by itself. However, below 20,000 rpm the 10-g vertical load, by itself, is larger than that produced by the simultaneous 6-g acceleration and the ± 2 radians per second pitch rate.

It is seen from Figures 13 and 14 that the gyroscopic load is by far the most significant load in the operating range of the HP spool. Consequently, both of the HP-spool bearings must be designed for the same maximum bearing loads even though the compressor-end bearing carries approximately 37 percent less rotating mass than does the turbine-end bearing. For this reason, the plots of maximum load for the turbine-end bearing (Figures 13 and 14) apply also to the compressor-end bearing.

The gyroscopic force is given by the following equation:

$$F_{\text{gyro}} = \frac{I_p \dot{\theta} \omega}{l} \quad (1)$$

where

- F_{gyro} = gyroscopic force acting on the bearing, lb
- I_p = polar mass moment of inertia of the rotor, in.-lb-sec²
- $\dot{\theta}$ = pitch velocity, rad/sec
- ω = rotor speed, rad/sec
- l = bearing span, in.

It is clear from Equation (1) that maximizing the bearing span (l) to the greatest practical extent will minimize the gyroscopic forces.

At sea-level design and overspeed conditions, the maximum resultant HP-spool bearing loads are 300 and 345 pounds respectively. At 25,000 feet, these loads drop to 280 and 320 pounds respectively, as a result of the decreased shaft speeds.

LP-Spool Bearing Loads

Figures 15 and 16 show the maximum bearing loads for the LP-spool compressor-end bearing at sea-level and 25,000 feet, respectively. Description of these curves is the same as given above for the HP spool. However, there are three significant differences between these curves and the HP-spool load curves:

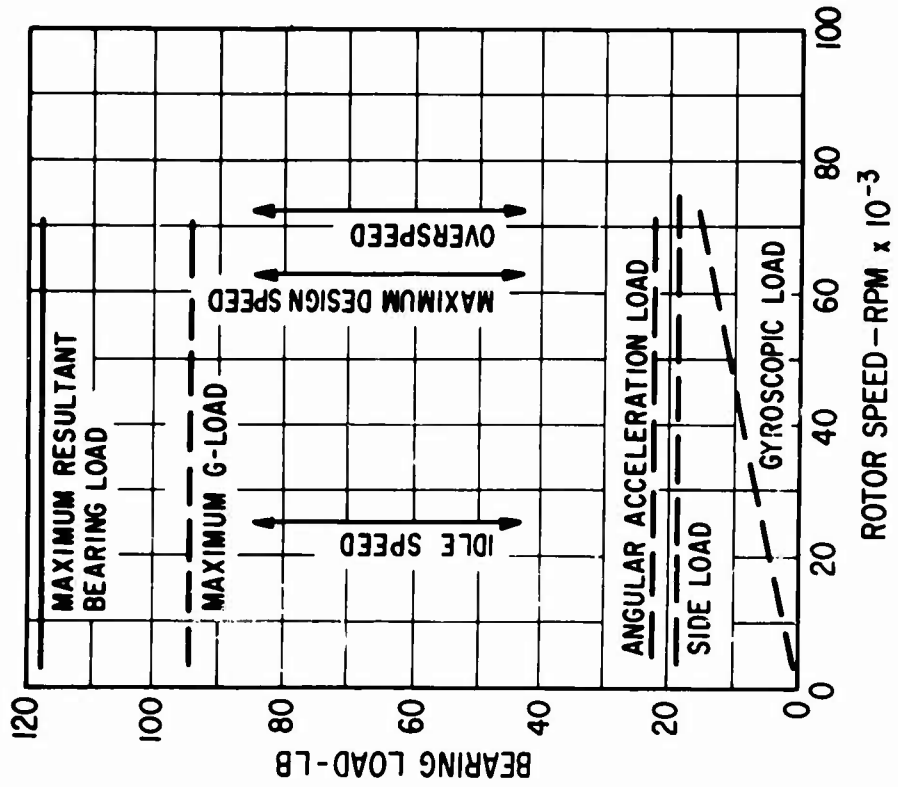


Figure 15. Maximum Loads for the LP-Spool Compressor-End Journal Bearing at Sea-Level Landing Conditions.

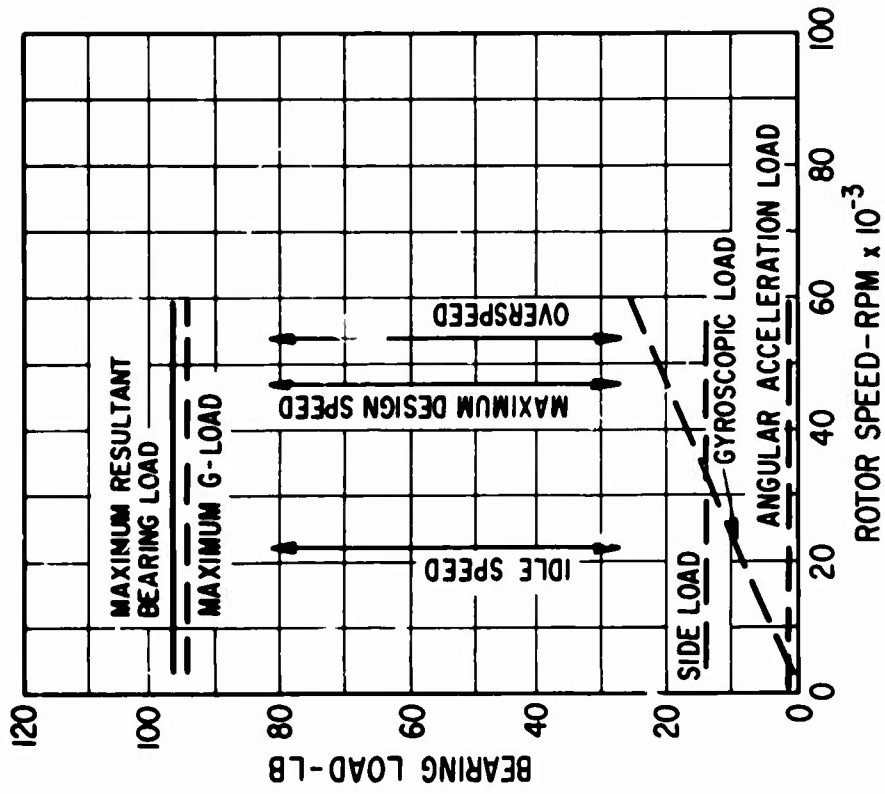


Figure 16. Maximum Loads for the LP-Spool Compressor-End Journal Bearing at 25,000-Foot-Altitude Conditions.

1. Because of the long bearing span and the reduced polar moment of inertia for the LP spool, the gyroscopic forces are sufficiently small that they do not contribute to the maximum resultant bearing load. Maximum load is thus independent of shaft speed. It is a function only of the maximum acceleration g's and the rotating mass. Consequently, since the LP-spool bearings do not carry equal amounts of rotating mass, curves of maximum bearing load were required for each bearing.
2. At sea level, the landing condition produces a larger bearing load than does the flight condition.
3. The maximum compressor-end bearing load is 118 pounds, which is roughly one-third that of the HP-spool bearings.

The load curves for the LP-spool turbine-end journal bearing have the same form as those for the compressor-end bearing. However, maximum load values are less due to the smaller rotor mass supported by the bearing. At sea-level landing and 25,000 foot-altitude conditions, the maximum turbine-end bearing loads are 84 and 71 pounds, respectively.

BEARING AMBIENT PRESSURES

As the bearing study proceeded, it became more and more evident that the most severe operating condition for the journal bearings was engine idle at 25,000 feet with maximum loads imposed. The reason for this was the low levels of pressure within the gas generator at idle and near-idle conditions. To alleviate this problem as much as possible, it was decided that both the HP- and LP-spool journal bearing cavities should be operated at HP-compressor discharge pressure. This, however, introduced a new problem; namely, overpressurization of the bearing cavities when operating at or near rated output power. In other words, at rated design conditions, HP-compressor discharge pressure was more than adequate for bearing load capacity. In fact, the excess available pressure would be a problem due to excessive labyrinth seal leakage from the four bearing cavities. Any increase in bearing ambient pressure beyond that required for good bearing operation would result in unnecessary gas-generator performance penalty.

It was therefore decided that pressure in the bearing cavities should not be allowed to rise above some maximum limit. Definition of this limiting maximum value would be a function of the HP-turbine design. A portion of the leakage from the HP-spool turbine-end bearing cavity must be pumped up the back face of the turbine disc and then discharged into the main turbine flow stream. If this is not done, leakage of high-temperature turbine gas into the bearing cavity would result. A thorough study of the head-rise capability of the turbine for pumping the back-face leakage flow was not made. Rather, 130 psia was estimated to be the minimum suction pressure at which such pumping could occur.

It is clearly in the best interest of overall gas-generator efficiency to keep ambient pressures in the bearing cavities as low as possible, consistent with satisfactory operation of the bearings. Maximum head-rise capability from the HP turbine should thus be an objective, even perhaps to the extent of incorporating a small high-pressure-ratio regenerative or viscous drag compressor into the back face of the turbine. However, if it should result that a 130-psia suction pressure is not sufficient for turbine pumping, the maximum bearing cavity pressure limit should be increased. While such an increase would improve bearing performance as well as turbine pumping capability, these improvements would occur at the expense of increased bearing cavity leakage flows and, hence, decreased efficiency of the gas generator.

Figure 17 shows plots of bearing ambient pressure at sea-level and 25,000 feet altitude as a function of HP-spool speed. Also plotted is LP-spool speed versus HP-spool speed. These plots were used for the self-acting pivoted-pad bearing analyses, the results of which will be presented shortly. It should be remembered that the same value of ambient pressure was assumed to be supplied to both the LP- and HP-spool journal bearing cavities.

The ambient pressure curves of Figure 17 represent 90 percent of HP-compressor discharge pressure up to the point at which 130 psia is reached. HP-spool speeds corresponding to the 130 psia point are 63,500 and 65,800 rpm at seal level and 25,000 feet, respectively. Above these speeds, a pressure-limiting control system is assumed to hold the bearing cavity pressures at a constant 130 psia.

BEARING SIZING

For the HP-spool application, there were three highly interacting facets to the basic task of establishing the size of the self-acting pivoted-pad journal bearings. These were load capacity, journal stress, and journal centrifugal growth. Load capacity, of course, increases with increasing bearing diameter. So also does journal stress and journal centrifugal growth, the former being proportional to diameter squared and the latter to diameter cubed. Because of these strong interactions, the effects of diameter on load capacity, stress, and centrifugal growth were studied simultaneously. However, for the sake of conciseness, these effects are discussed separately in this report, and only final results of the studies are presented.

Most of the following discussion of bearing performance pertains to the HP-spool journal bearings. As mentioned previously, the HP-spool bearings operate under considerably more severe conditions than do the LP-spool bearings. Accordingly, most of the design and analysis effort was devoted to these bearings. However, sufficient calculations were made for the LP-spool bearings to permit valid assessment of feasibility, basic size requirements, and specific problem areas.

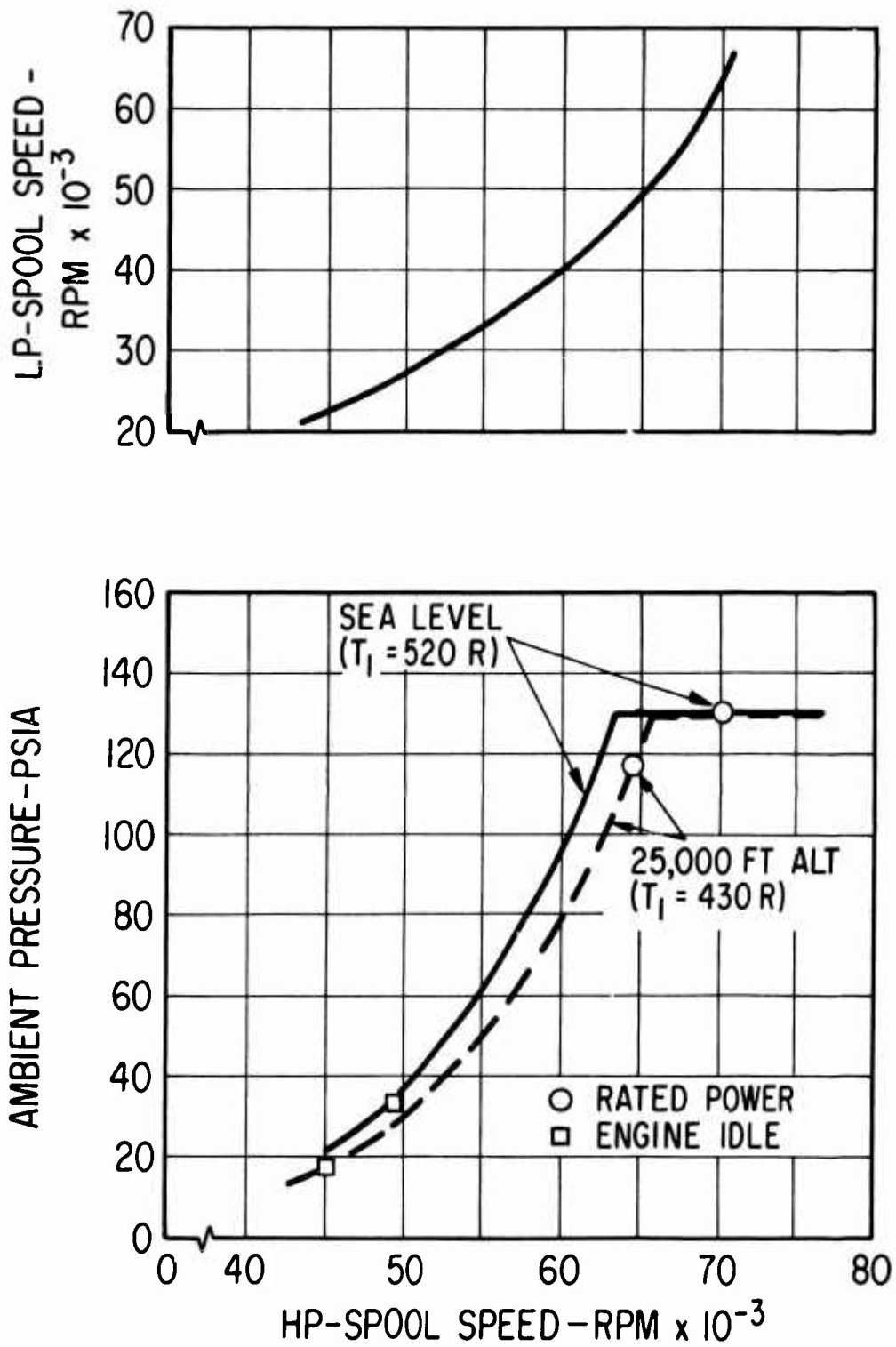


Figure 17. Ambient Pressure for the HP- and LP-Spool Journal Bearings, and LP-Spool Speed, as a Function of HP-Spool Speed.

Load Capacity

Self-acting pivoted-pad gas bearings have, to date, been built with either three or four pads (circular-arc segments). It was recognized that under the maximum load conditions of Figures 13 and 14, minimum film thicknesses would be quite small, particularly if significant thermal distortions should exist. Accordingly, the question as to whether a three- or a four-pad bearing should be used was answered by determining which configuration would have the greater film thickness at the maximum load condition.

The most severe condition for a pivoted-pad bearing occurs when the bearing load acts directly through one of the bearing pivots. Accordingly, single-pad data (based on ideal geometry) for an 80-degree and a 120-degree arc length were compared. Figure 18 shows plots of nondimensional load (\bar{W}_p) versus compressibility number (Λ) for 80- and 120-degree pads operating at high values of pad eccentricity ratio (ϵ_p). For the HP spool, compressibility number varies from approximately 0.6 to 2.5. Figure 18 shows that for a given pad load, the pad eccentricity ratio for a 120-degree pad will be from 6 to 14 percent lower than that for an 80-degree pad, depending on the compressibility number. While the difference in values of eccentricity ratio may appear small, it should be remembered that pivot-point film thickness is a function of pad eccentricity ratio in the following manner:

$$h_p = C_p (1 - \epsilon_p \cos \phi_p)^* \quad (2)$$

where

h_p = film thickness at pivot point, in.

C_p = radial clearance of pad, in.

ϵ_p = pad eccentricity ratio

ϕ_p = pad attitude angle, rad

*Minimum film thickness in a pivoted-pad bearing does not occur at the pivot point, except for the limiting case where pad eccentricity ratio (ϵ_p) approaches unity (i.e., where the journal approaches rubbing contact with the pad). However, when ϵ_p is greater than 0.8, the minimum film point is very close to the pivot point and the film thickness at both points is almost the same. Accordingly, a high-eccentricity-ratio bearing design is evaluated on the basis of its pivot-point film thickness, since under static overload conditions it would be the pivot point at which rubbing contact would first be made.

Accordingly, when the pad is operating at conditions of high eccentricity ratio, a small reduction in eccentricity ratio will mean a large increase in pivot-point film thickness. For example, assume a bearing running condition for which \bar{W}_p is 5.7 and Λ is 1.5. For an 80-degree pad, Figure 18 shows ϵ_p to be 0.85. However, for a 120-degree pad operating at the same conditions of \bar{W}_p and Λ , ϵ_p is found to be 0.80. Using Equation 2 (and charts given in Reference 24 to obtain values of ϕ_p), it can be shown that the pivot-point film thickness for the 120-degree pad will be more than 55 percent greater than that for the 80-degree pad.

After it was determined that a three-pad bearing should be used, a study was performed to determine the bearing diameter (D) and the optimum clearance ratio (C_p/R) for the HP-spool bearings. To maintain reasonable bearing proportions, an L/D ratio of 1.08 was selected. Single-pad calculations for various diameter values were then made for the following conditions:

$$\begin{aligned}
 P_a &= 130 \text{ psia} \\
 W_p &= 370 \text{ lb} \\
 N &= 70,000 \text{ rpm} \\
 \mu &= 5.0 \times 10^{-9} \text{ lb-sec/in.}^2 \\
 \beta &= 110 \text{ deg.} \\
 \theta_p / \beta &= 0.65
 \end{aligned}$$

Figure 19 shows the resulting values of minimum film thickness as a function of clearance ratio for a 3-inch-diameter bearing. It is seen that the value of minimum film thickness reaches a maximum at a clearance ratio of 0.0015. At clearance ratio values of 0.001 and 0.002, the film thickness is reduced approximately 7.1 percent from its maximum value.

Journal stress and centrifugal growth considerations indicated that 3 inches was the largest bearing diameter that could realistically be considered for the HP spool in the light of existing and near-future technology. To assess the feasibility of a smaller diameter bearing, single-pad calculations were made for a 2.625-inch-diameter bearing as a function of speed and altitude. A comparison of single-pad data (assuming ideal bearing geometry) for the 2.625- and 3-inch diameter bearings is given in Table IV. It is seen that the 2.625-inch bearing does satisfy the 0.2 mil minimum film thickness criterion throughout the operating range. However, at the 25,000-foot-altitude engine-idle condition, there is no margin with respect to the minimum film criterion.

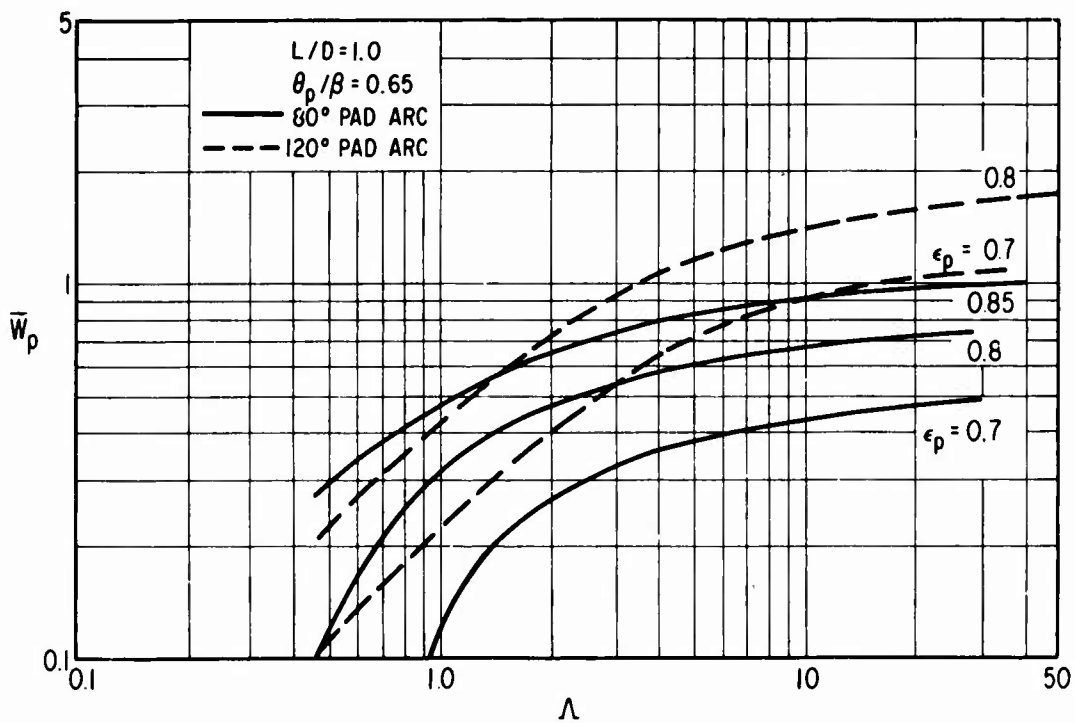


Figure 18. Comparison of Nondimensional Load Capacity Data for 80- and 120-Degree Self-Acting Pads.

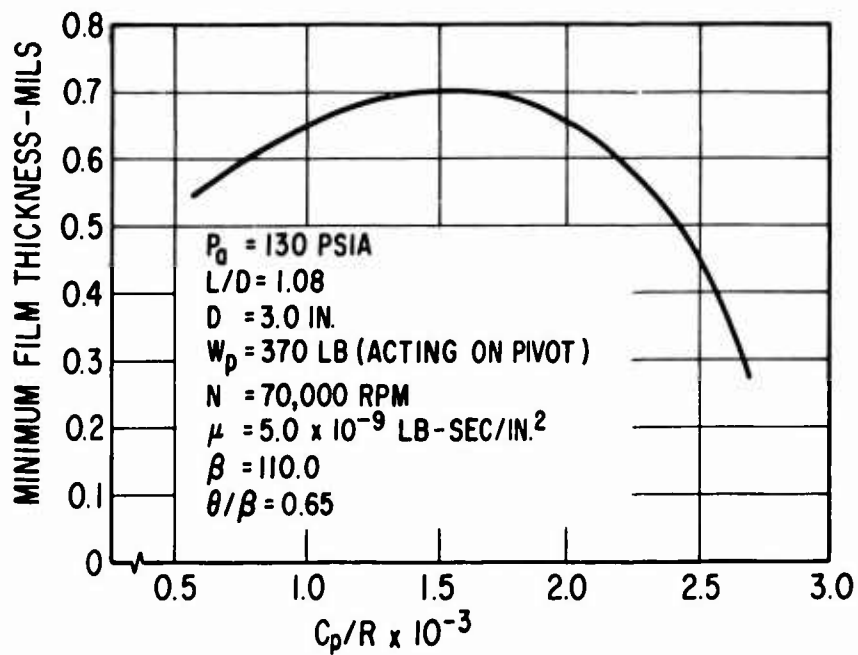


Figure 19. Effect of Clearance Ratio on Minimum Film Thickness for a Highly-Loaded Self-Acting Pad

TABLE IV. MINIMUM FILM THICKNESS DATA FOR 2.625-INCH AND 3-INCH
 NONDISTORTED BEARINGS OPERATING AT HP-SPOOL MAXIMUM
 LOAD CONDITIONS

($L/D = 1.08$, $C_p/R = 0.0013$, $\beta = 110^\circ$, $\theta/\beta = 0.65$)

Percent of Rated Power	Speed (rpm)	Ambient Pressure (psia)	Total Load on Loaded Pad (lb)	Minimum Film Thickness of Loaded Pad (mils)	
				2.625-Inch Diameter	3-Inch Diameter
<u>Sea level</u>					
100	70,000	130	370	0.5	0.69
0	49,000	36	285	0.3	0.38
<u>25,000 Feet</u>					
100	64,500	118	345	0.45	0.60
0	45,000	18	237	0.20	0.25

The results of Table IV were the first quantitative indication that engine idle would be the most severe bearing condition, particularly at 25,000 feet altitude. Accordingly, the 3-inch-diameter bearing was selected for further study, since this bearing did have film thickness in excess of the minimum criterion throughout the operating range. At this point in the study, an indication of excess film was considered to be essential for two reasons. First, as a result of journal centrifugal growth, the actual C_p/R value of the bearing would vary with speed over a considerable range:

from high values at low speeds to low values at high speeds. Accordingly, it would be impossible to operate the bearing at its optimum C_p/R value

under all conditions, and some loss of film thickness would thus result. Second, it was known that the effects of bearing geometry distortions could result in considerable reductions in clearance. The effects of C_p/R variations and geometry distortions on the performance of the 3-inch-diameter bearing are discussed on page 55.

Journal Stress

The ID and OD tangential stresses (also referred to as circumferential stresses) due to centrifugal forces in a uniform hollow rotating journal are shown in Figure 20. Two journal sizes are shown: a 3-inch and a 2.625-inch diameter. The ratio of bore diameter to bearing diameter (R_i/R_o) was held constant at 0.667. Maximum journal stress occurs at the

bore and is 81,000 psi and 62,000 psi for the 3-inch and 2.625-inch journals, respectively, at sea-level design speed. Average tangential stress for the 3-inch journal is 64,500 psi. At the sea-level overspeed condition, average tangential stress in the 3-inch journal increases to 88,000 psi.

For bearing cooling purposes, short-pitch helical grooves would be cut into the bore surface of the journals. These grooves are shown in Figures 2, 3, and 4. The effect of the grooves is to increase the tangential stresses. A calculation of the groove effect was made for the 3-inch journal, assuming the effect of the small helix angle to be negligible. Figure 21 shows the results of this calculation at design speed. It is seen that the maximum and minimum tangential stresses are approximately 10.5 percent higher than those for a uniform journal. Average tangential stress is 71,400 psi, as compared to the 64,500 psi stress for the uniform journal.

The criterion for journal stress must, of course, assure a reliable 1000-hour life of the bearing. The question as to whether a 71,400-psi average tangential stress can be reliably sustained for 1000 hours is dependent solely upon the temperature at which the journal will operate and the strength of the journal material at this temperature. This question is discussed further in the "Bearing Materials" subsection of

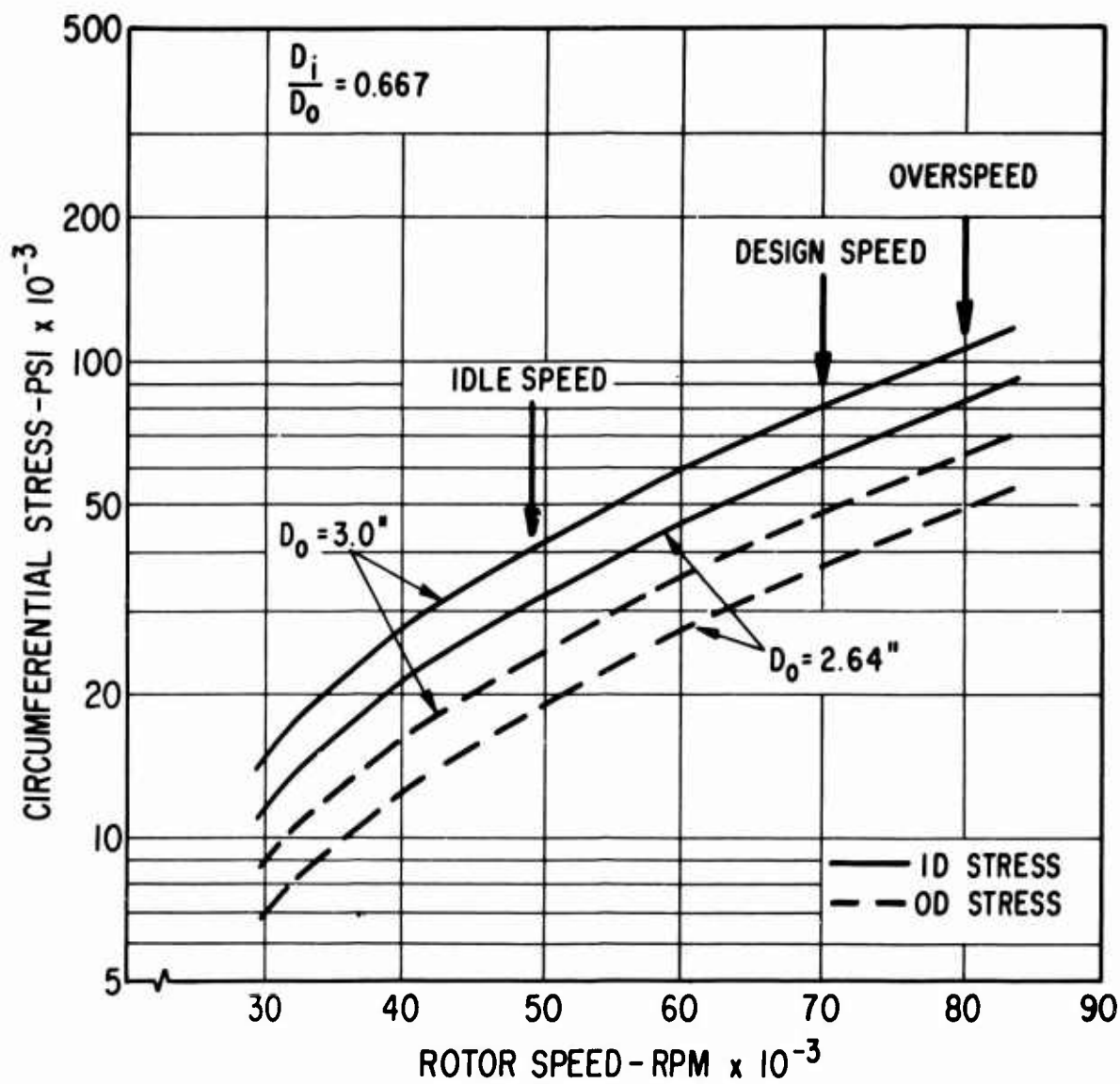


Figure 20. Effect of Speed and Diameter on Tangential Stress in the HP-Spool Journals.

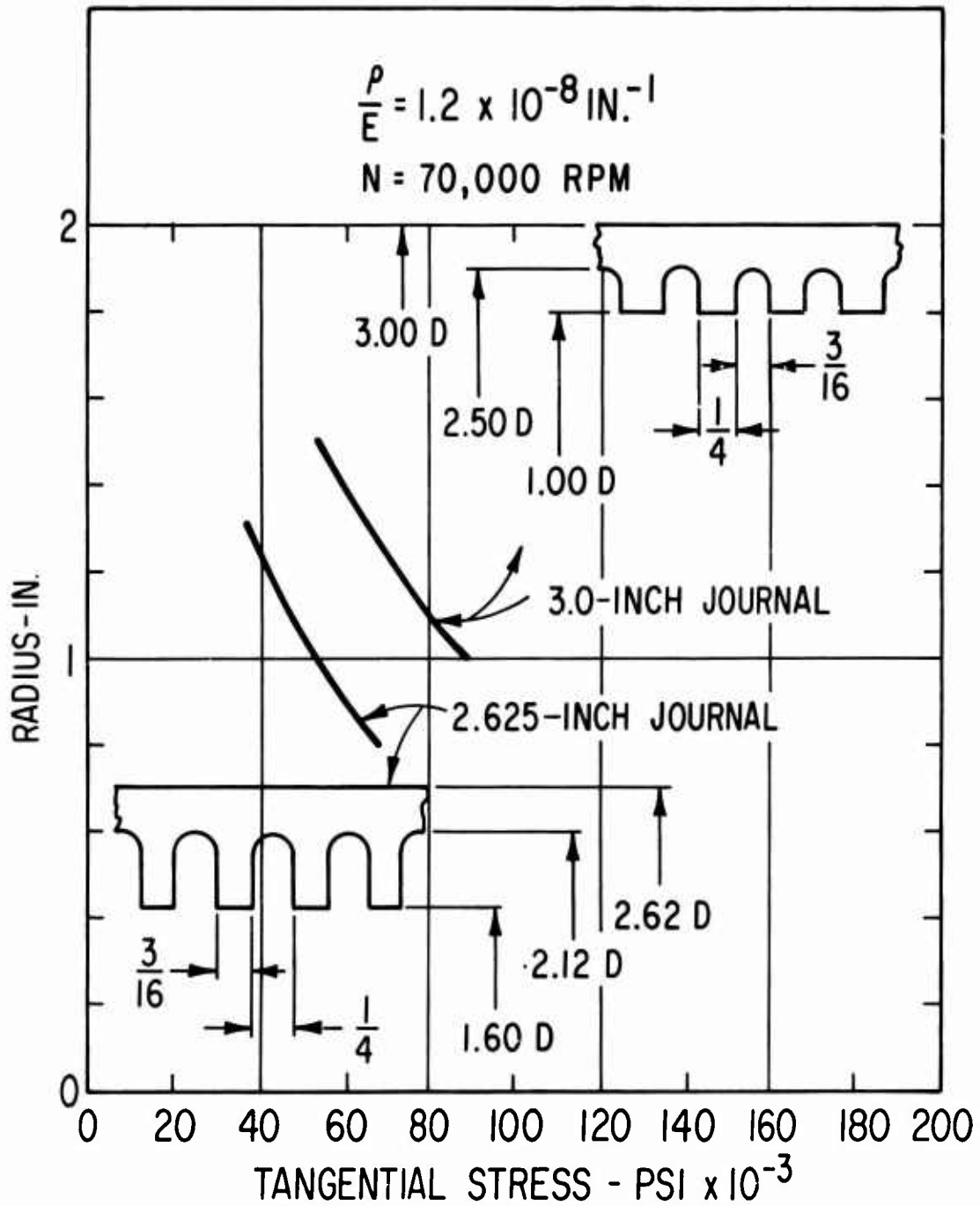


Figure 21. Tangential Stresses in Helicallly Grooved Journals at 70,000 RPM.

this chapter.

At this point, however, journal stress can be compared with turbine and compressor stresses. Figure 22 shows the isothermal radial and tangential stresses which will occur in the HP-compressor at design speed. It is seen that the average tangential stress is about 98,000 psi. Since the HP turbine is about the same size as the compressor, it also will run at comparable stress levels. However, the turbine will run with metal temperatures above 2000°F. Accordingly, the stresses for the 3-inch-diameter journal are quite conservative in comparison to both the compressor and turbine stresses.

Journal Centrifugal Growth

Radial growth of the 2.625- and 3-inch journals due to the centrifugal forces is shown in Figure 23. From sea-level idle to overspeed, the change in radius for the 3-inch journal would be 2.5 mils. The implication of this amount of radial change is twofold:

1. Bearing radial clearance (C_p/R) will vary — neglecting for the moment any changes due to differential thermal expansions — by at least 250 percent from its minimum to maximum value. This emphasizes the point made earlier, with respect to Figure 19, that optimum (maximum) bearing film thickness can be achieved over only a limited portion of the total speed range.
2. For good dynamics of the pivoted-pad segments, sufficient gas film pressures must act upon the pads at all times. This can be accomplished by maintaining normal bearing film thicknesses in the range of 0.8 to 1.2 mils. However, since radial growth of the 3-inch journal exceeds the required film thicknesses several times over, it is essential that some means of externally accommodating at least 80 percent of the centrifugal growth be provided. This has been done, as is discussed in the "Isothermal Performance" subsection, by individually mounting each pad on a mechanical flexure.

LP-Spool Bearing Sizing

Sizing of the LP-spool journal bearings was essentially dictated by the results of the HP-spool bearing studies and the space limitations imposed by the gas-generator gas-flow passages. Two-inch diameter bearings, having a length-to-diameter ratio of 1.5, were ultimately established as the maximum size bearing which could realistically be accommodated. Calculations of single-pad performance, similar to those made for the HP-spool bearings, indicated that the minimum film thickness criterion of 0.2 mil could be met. In the interest of brevity, results of these calculations are not presented here. A quantitative discussion of the LP-spool bearings is presented in the "Isothermal" subsection of this chapter.

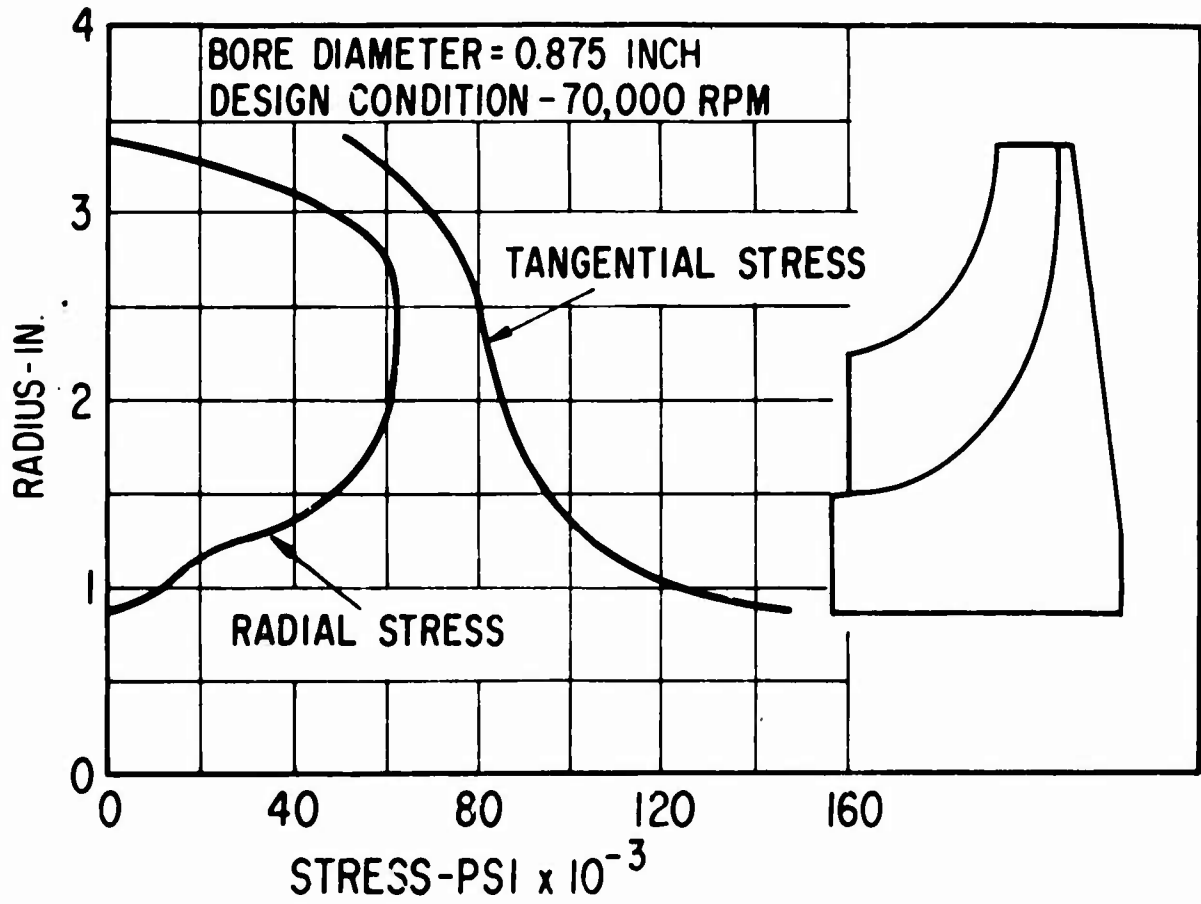


Figure 22. Isothermal Disc Stresses for the HP-Compressor at 70,000 RPM.

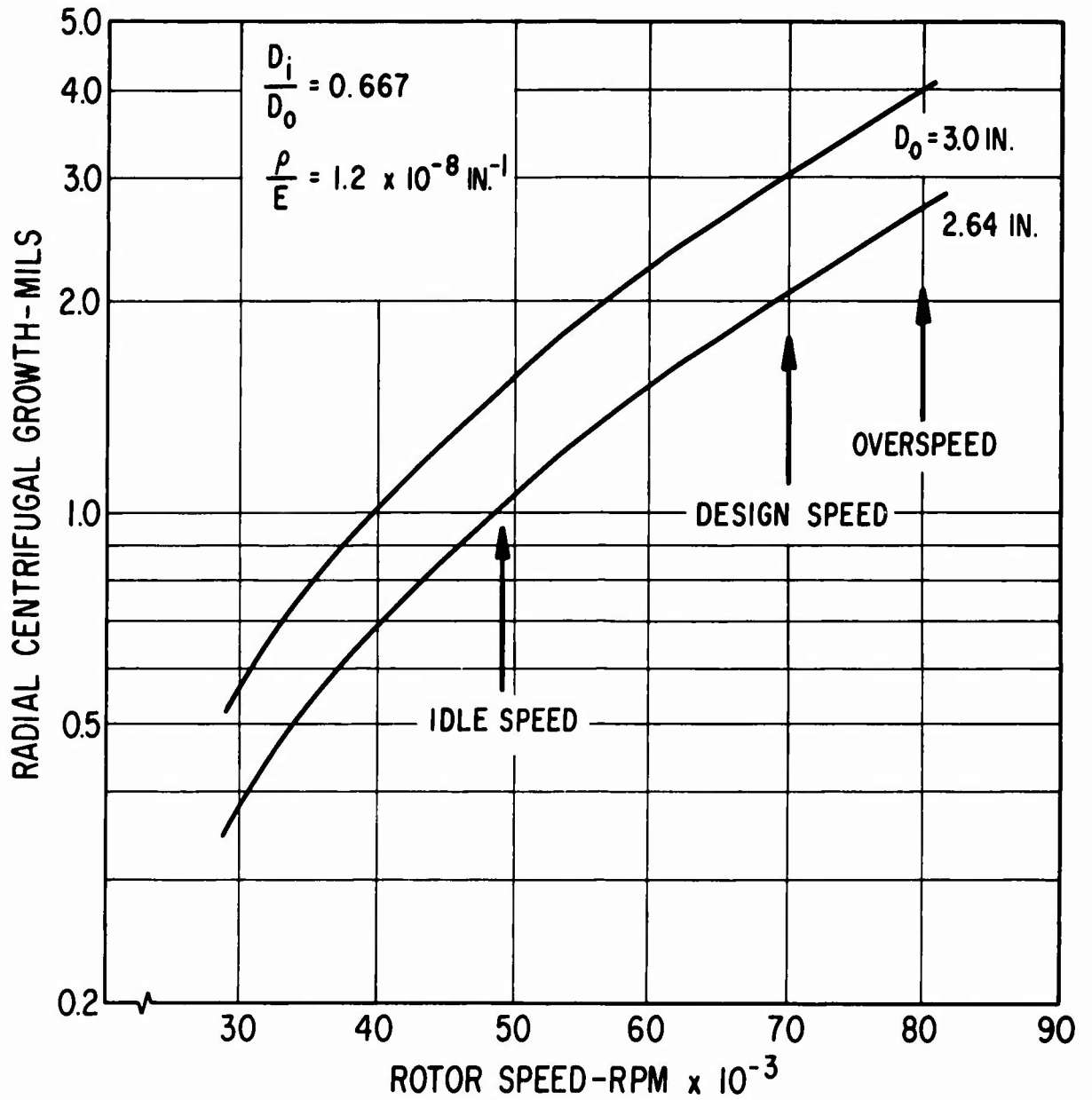


Figure 23. Effect of Speed and Diameter on Radial Centrifugal Growth of the HP-Spool Journals.

Stress levels in the LP-spool journals will be approximately 55 percent lower than those in the HP-spool journals. Centrifugal growth will be reduced by approximately 70 percent relative to the HP spool. Consequently, achievement of a 1000-hour life, optimization of bearing performance, and accommodation of centrifugal growth present considerably less difficulties with the LP-spool bearings.

BEARING THERMAL STUDIES

Performance of a fully assembled pivoted-pad bearing is strongly influenced by temperature conditions within the bearing. From a fundamental standpoint, high-temperature operation of gas-lubricated bearings is inherently feasible since gas viscosity, and hence bearing load capacity (i.e., film thickness for a given load), increases with increasing temperature. However, from a practical standpoint, fluid-film bearings generate heat due to shearing of the lubricant film. Heat generated within the lubricant film is commonly referred to as bearing friction losses. If the friction losses are not removed, bearing temperatures will, of course, continue to rise. This will give rise to an exponential thermal runaway condition, since friction losses generally increase at about the same rate as load capacity (i.e., as film thickness) due to increasing viscosity with temperature.

Bearing friction losses must, of course, be removed from the bearing regions. However, the manner in which they are removed is of equal importance. If the losses are removed in such a way as to cause large temperature gradients within the bearing, thermal distortions of the bearing surfaces will result. These distortions may significantly reduce bearing load capacity (i.e., bearing film thickness). This in turn will increase bearing friction losses and further exaggerate the thermal distortions. Thus, even with removal of bearing friction heat, it is still possible to encounter a condition of thermal runaway and ultimate bearing failure.

Clearly then, one objective of good bearing design must be to remove bearing friction losses in a manner which will not result in excessive thermal distortions. A second objective must be to achieve temperature levels which are compatible with the bearing materials, from both a strength and a corrosion standpoint. Finally, the bearing temperature levels must be compatible with the rest of the rotor-bearing system in the sense that excessive temperature gradients, and hence thermal stresses, are not created between adjacent parts.

In order to perform both isothermal and nonisothermal bearing performance calculations, it was first necessary to determine the approximate thermal conditions which could be achieved in the bearing regions. To do this, preliminary calculations of bearing friction losses were made. Two heat transfer techniques for removing these losses were then investigated using MTI computer program PN 060. The resulting average temperatures of the journals, pads, and bearing-support housings were then used to calculate bearing isothermal performance. For the nonisothermal performance

calculations, actual temperature gradients in the pads and journal were used.

Bearing Friction Losses

Preliminary calculations of bearing friction losses were made on the basis of single-pad data under maximum load conditions. The friction loss values used for the thermal calculations are listed below:

HP-Spool Bearings

<u>Operating Condition</u>	<u>Friction Loss Per Bearing - HP</u>
Sea level, rated power (70,000 rpm)	2.87
Sea level, engine idle (49,000 rpm)	1.32
25,000-foot altitude, rated power (64,000 rpm)	2.24
25,000-foot altitude, engine idle (45,000 rpm)	1.21

Subsequent calculations of bearing performance indicated that the above values of friction loss were slightly high for normal maximum load operation (see Figure 35). However, the values are representative of losses which could occur during the thermal transient period following a sudden change in engine speed, or if, for some reason, the temperature of the bearing-support housing should drop 20 percent from its nominal operating temperature (see Figure 36).

LP-Spool Bearings

<u>Operating Condition</u>	<u>Friction Loss Per Bearing - HP</u>
Sea level, rated power (62,800 rpm)	1.026
Sea level, engine idle (25,000 rpm)	0.214
25,000-foot altitude, rated power (47,000 rpm)	0.613
25,000-foot altitude, engine idle (22,500 rpm)	0.18

All of the preceding values of friction loss are about twice as high as were subsequently obtained from the bearing performance calculations (see Figure 39). The discrepancy was traced to an error in calculation of the compressibility numbers for the single-pad data. As a result of this error, the computed thermal gradients for the LP-spool bearings are more severe than would actually exist with the correct (smaller) values of friction loss. Temperature levels are also somewhat high. In other words, the error in friction loss value exaggerated the bearing thermal results. However, the practical consequences of the error were actually insignificant. The LP-spool bearing losses are sufficiently small that there is no problem in obtaining essentially isothermal conditions at acceptable temperature levels.

Thermal Analysis Models

A small number of nodes were used in formulating the thermal models of the bearing regions. Furthermore, each bearing region was analyzed individually. The reason for these simplifications was to minimize the amount of computer program input data preparation, thus making it easy to change the thermal models so that different heat transfer techniques could be quickly evaluated.

The thermal models are adequate for feasibility study purposes; that is, for identifying and resolving the basic heat transfer problems and for establishing the range of bearing temperature levels with reasonable accuracy. However, the final bearing system design for an actual prototype engine should include a more comprehensive thermal analysis. As a minimum, each end of the gas generator should be accurately modeled so that thermal interactions between the two turbine-end bearings and the two compressor-end bearings are accounted for. Additionally, the HP-spool should be modeled in its entirety so that interactions between the thrust bearing and the two journal bearings are included.

The thermal model for the HP-spool turbine-end bearing is shown in Figure 24. In all, 36 nodes were used. The journal, pads, and gas film were represented by 18 nodes, the cooling-air flow path by 10 nodes, and the turbine and interconnecting structure by the remaining 8 nodes. Since the primary purpose of the model was to facilitate the calculation of bearing temperatures, a very simple representation was used for the air-cooled turbine. The blade cooling nodes were derived assuming 19 blades with a 0.032-inch-wide cooling passage. The only purpose of the turbine nodes was to obtain a reasonably accurate value of the turbine hub temperature at the point where the turbine is attached.

The thermal model used for the HP-spool compressor-end bearing was essentially the same as that used for the turbine-end bearing except for minor modifications in flow path and geometry.

The thermal model for the LP-spool turbine-end bearing is shown in Figure 25. In all, 52 nodes were used. The journal, pads, and gas film

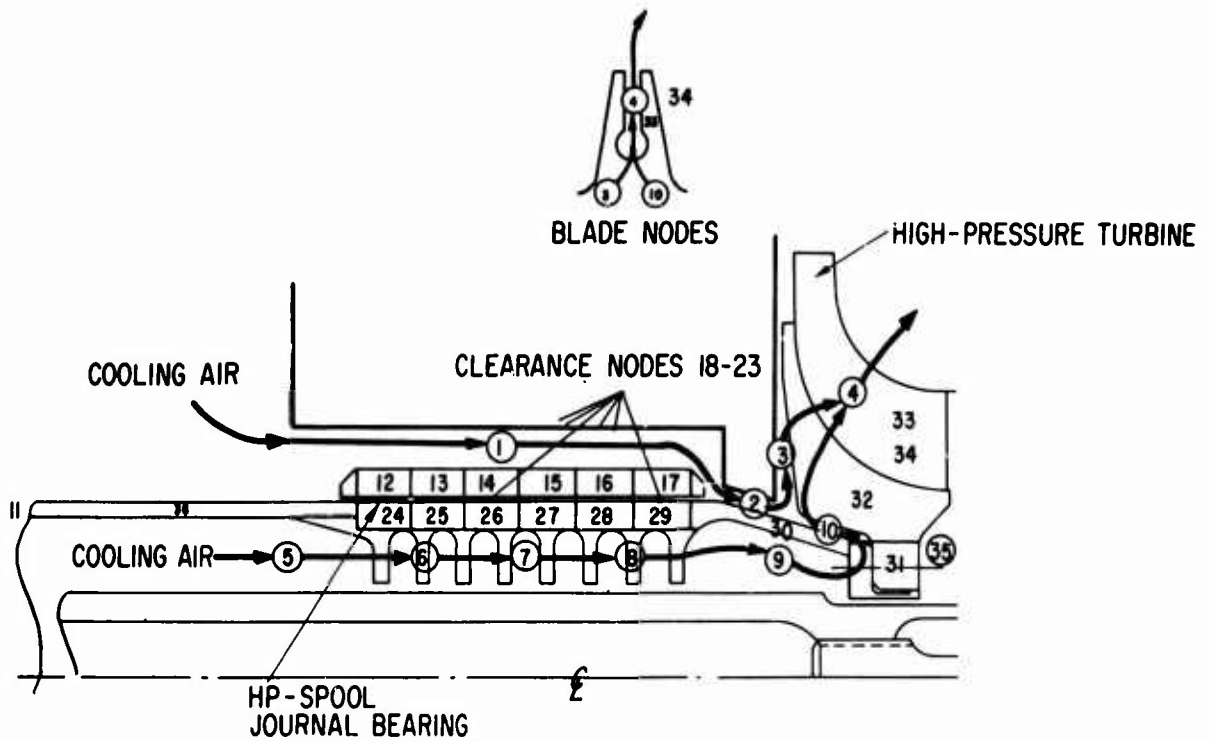


Figure 24. Thermal Model for the HP-Spool Turbine-End Bearing.

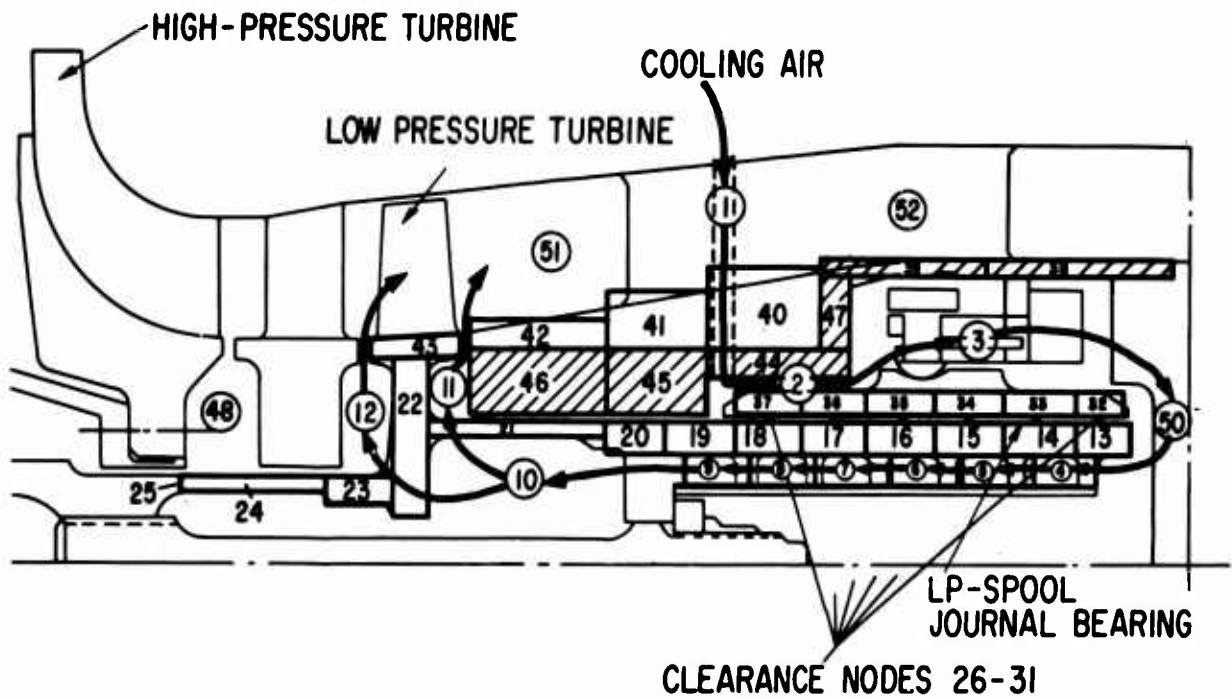


Figure 25. Thermal Model for the LP-Spool Turbine-End Bearing.

were again represented by 18 nodes. The cooling-air flow path was represented by 13 nodes, the turbine discharge flow by 2 nodes, the turbine and connecting structure by 8 nodes, and the turbine discharge ducting and insulation material located around the bearing by 9 nodes.

No thermal model was made for the LP-spool compressor-end journal bearing. Friction losses in this bearing were essentially the same as for the turbine-end bearing. Essentially the same cooling technique would be used. The only difference in the two bearings would be temperature level, the compressor-end bearing being somewhat cooler. Since very satisfactory thermal results were obtained for the turbine-end bearing, it was not necessary for feasibility purposes to repeat these calculations for the compressor-end bearing.

In all of the thermal calculations, it was assumed that the thermal conductivity of the journals, pads, and shaft sections was 25 BTU/hr-ft-°F. Thermal conductivities of the turbine discs and the fiberfelt insulation were assumed to be 16.7 and 0.167 BTU/hr-ft-°F, respectively.

Cooling Concept

A major objective of the feasibility study was to determine if the bearings could be air cooled using compressor discharge gas. This would represent the simplest and most reliable cooling concept since there would be no requirement for auxiliary fluids or equipment. Elimination of auxiliary requirements is a very significant advantage which can frequently be realized with process-fluid lubricated machinery. A further advantage occurs with respect to air cooling the two turbine-end bearings. Since both the HP and LP turbines require cooling air for blade cooling, cooling of the turbine-end bearings with this same air accomplishes the bearing cooling function with very little additional penalty in engine performance. Figure 5 illustrates the manner in which the same flow of air can be used for both bearing and turbine cooling.

Implementation of the air cooling concept is most easily accomplished by using axial flows of air over the outside surfaces of the pivoted-pad bearing segments and through the bore of the journals. Based on prior developments of gas-cooled machinery, it was known that mechanical design considerations usually result in bore cooling being the most effective heat transfer mode. To obtain high values for the forced-convection heat transfer film coefficients, it is necessary to achieve high relative velocities of the cooling gas. This implies that the cooling-gas flow passages must have a fairly small cross-section area. A mechanically attractive means for obtaining small cross-section flow area around the outside surfaces of pivoted-pad segments has not yet been demonstrated, although several technically (and perhaps practically) feasible concepts have been proposed. On the other hand, there are several relatively simple means for achieving small flow passages on the inside surface of a rotating journal, two of which have been successfully proven in field operation of gas-bearing machinery.

Two means for obtaining high flow velocities through the journal bore were investigated. One method is illustrated in Figure 26; it consists of eight circumferentially-spaced 1/8-inch-diameter holes drilled through the journal stiffening rings. (Journal stiffening rings were used as a minimum-weight means to reduce centrifugal growth of the journals.) Cooling flow from compressor discharge entered the holes at one end of the journal. Axial flow through the holes in successive stiffening rings was sustained by an HP-turbine-induced pressure drop. Although this concept represents a simple means for obtaining high flow velocities, these velocities exist only within the holes. Effective heat transfer area is therefore quite limited.

The second means for obtaining high flow velocities consisted of using helically-grooved circumferential passages under the journals. By keeping the pitch distance between adjacent grooves sufficiently small, the journal stiffening-ring effect could be maintained. Flow of cooling gas through the grooves was accomplished in the same manner as described for the stiffening-ring holes. Although flow velocity through the grooves was significantly less than that obtained through the holes, higher heat transfer rates were nonetheless obtained for the grooved geometry because of the greatly increased effective heat transfer area.

Cooling Flow Rates

Discussions with USAAVLBAS personnel resulted in preliminary estimates of turbine cooling flow requirements at rated-power conditions. These estimates were 5 percent and 2 percent of gas-generator flow for HP-turbine and LP-turbine cooling, respectively. A total of 7 percent of design-point compressor flow was thus allotted to turbine cooling. (This estimate of turbine-cooling bleed flow was included in the aerodynamic turbine and compressor sizing calculations of Appendix I.) For part-load engine operation, the same percentages of actual gas-generator flow were assumed for turbine cooling requirements.

Initial thermal calculations for the turbine-end bearings were made assuming bearing cooling flow to be equal to the required turbine cooling flow for the particular spool. Division of cooling flow within each bearing was also assumed to be equal; that is, 50 percent of the flow was assumed to pass through the journal bore and the remaining 50 percent was assumed to pass over the outside surfaces of the pads. This latter flow was not intended to be particularly effective for bearing cooling, but rather to provide a continuous circulation of air through the bearing cavity for environmental temperature control purposes. This was considered to be particularly important for the turbine-end bearings which are located in close proximity to high-temperature turbine flow passages.

Two additional thermal calculations were made for lesser flow rates of cooling air. In one case the cooling flow for the LP-spool turbine-end bearing at sea-level rated-power conditions was reduced from 2 percent to 1 percent of compressor flow. The second case was a calculation of HP-

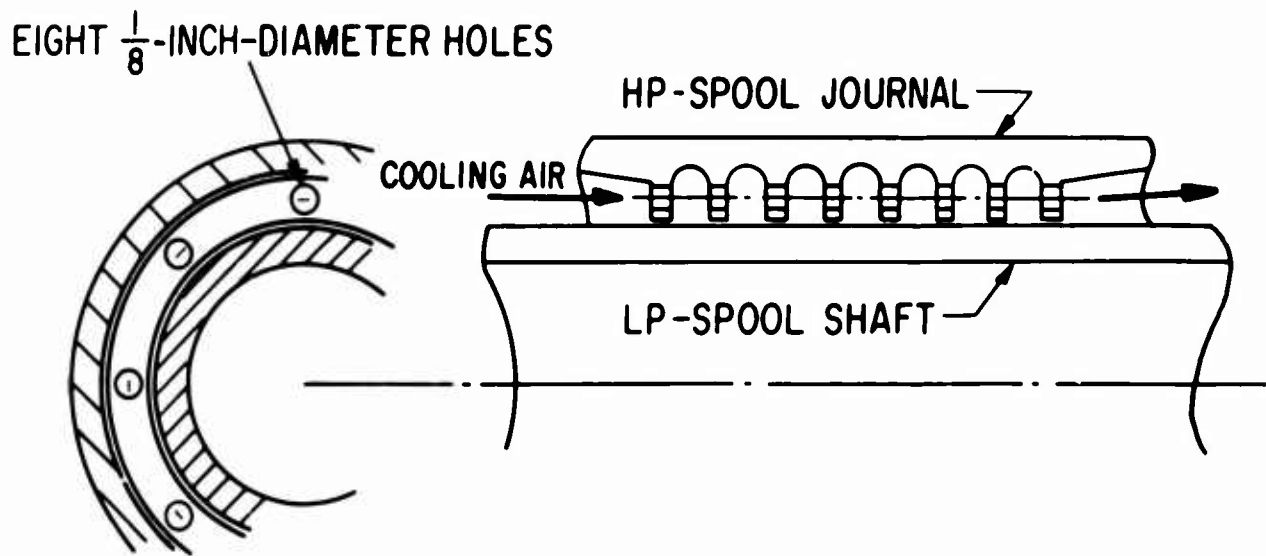


Figure 26. Journal Bore-Cooling Concept Using Air Flow Through Holes in the Journal Stiffening Rings.

spool compressor-end bearing temperatures at engine-idle and at an altitude of 25,000 feet. Flow rate in this instance was taken to be 2 percent of compressor flow. An equal split of cooling air within each bearing was again assumed for each calculation.

Since bearing cavity pressurization and bearing cooling would both be accomplished with the same flow of compressor discharge air, pressure of the cooling air flowing through the bearing cavities and entering the journal bores was assumed to follow the bearing ambient pressure curves shown in Figure 17.

HP-Spool Turbine-End Bearing Temperatures

Calculated temperatures for the HP-spool turbine-end bearing are plotted in Figure 27 for the conditions of sea-level flight at maximum bearing load and rated power (70,000 rpm). A tabulation of all node-point temperatures for the thermal model of Figure 27 is given in Table V. Thermal input conditions for this calculation were as follows:

Bearing friction loss	2.87 HP (equally distributed over nodes 18 to 23)
Cooling-air inlet temperature	1000 ^o F (at nodes 1 and 5)
Total cooling-air flow	0.225 lb/sec (5 percent of rated gas-generator flow)
Surface temperature of the turbine blades	2700 ^o F (node 34)
Turbine windage heating	9000 BTU/hr (heat input at node 3)
Assumed shaft boundary temperature	1000 ^o F (node 11)

The upper portion of Figure 27 shows bearing temperatures, with and without radiation heat transfer, for axial flow of cooling air through the eight circumferentially spaced holes in the journal stiffening rings. Radiation effects were calculated assuming a 1200^oF temperature for the bearing support structure and surrounding casings. Since the bearing runs hotter than the surrounding structure, radiation heat transfer helps to cool the bearing. Peak journal temperature is approximately 1540^oF when radiation heat transfer is included. In the absence of radiation effects (that is, if temperatures of the surrounding structure should approach those of the bearing), peak journal temperature would increase to approximately 1630^oF. Pad temperatures are 20 to 80 degrees higher than journal temperatures, depending on axial position along the bearing and whether or not radiation cooling is significant.

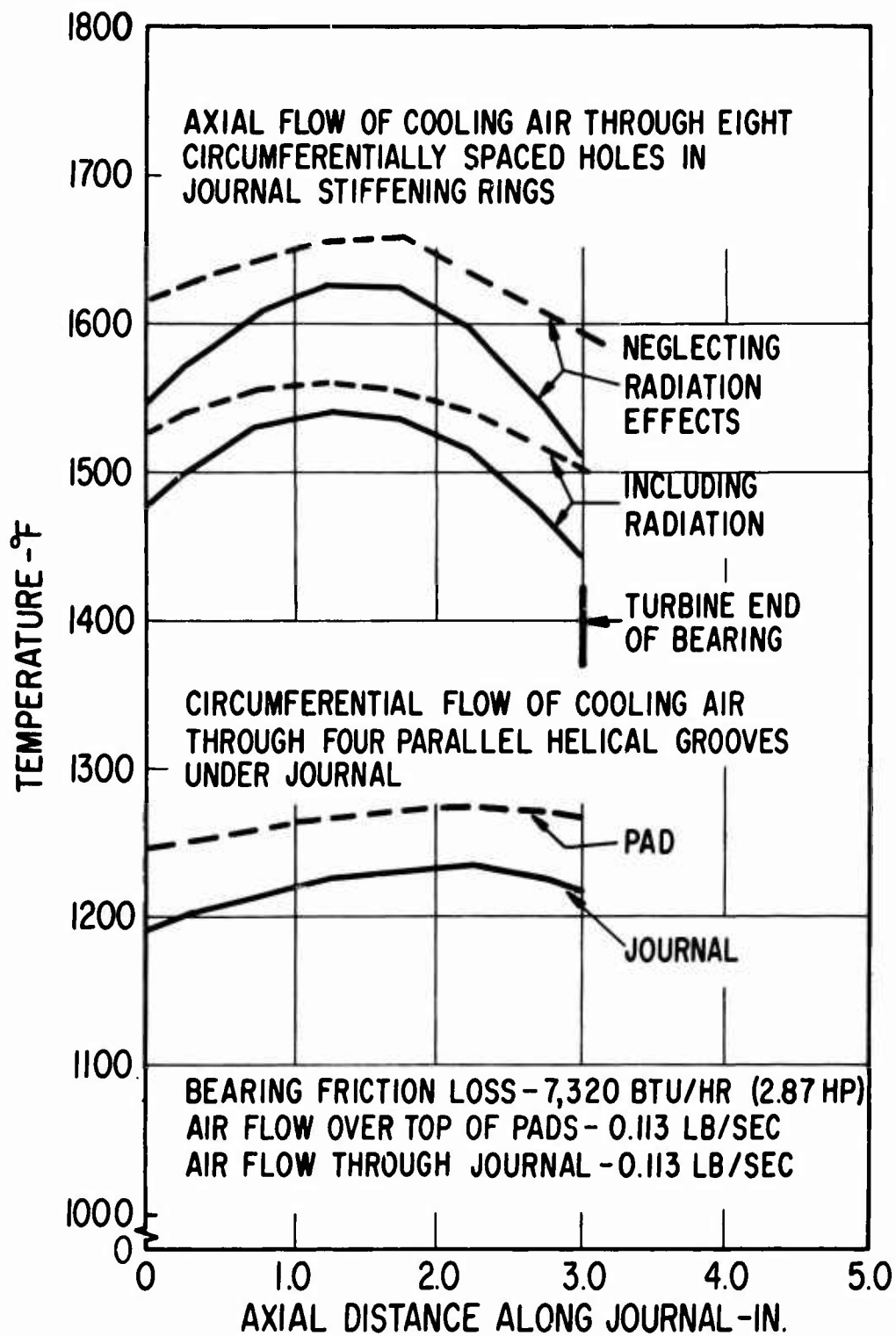


Figure 27. Effect of Cooling Technique on HP-Spool Turbine-End Bearing Temperatures at Sea-Level, Rated-Power, and Maximum Bearing Load Conditions.

TABLE V. CALCULATED NODE-POINT TEMPERATURES FOR THE
HP-SPOOL TURBINE-END BEARING REGION AT
SEA-LEVEL RATED-POWER CONDITIONS

Temperatures - °F			
Node No. (Nodes are defined on Figure 24)	Journal Cooled Via Circumferentially Spaced Holes in Journal Stiffening Rings		Journal Cooled Via Helically Grooved Flow Passages Under Journal
	Without Radiation Heat Transfer	With Radiation Heat Transfer	
	1	1000*	1000*
2	1032	1030	1030
3	1193	1191	1192
4	2241*	2240*	2242*
5	1000*	1000*	1000*
6	1015	1013	1020
7	1030	1026	1041
8	1044	1038	1059
9	1056	1052	1071
10	1150*	1146*	1158*
11	1000*	1000*	1000*
12	1624	1540	1251
13	1642	1555	1258
14	1655	1562	1266
15	1659	1558	1270
16	1632	1542	1272
17	1602	1519	1270
18	1621	1543	1250
19	1649	1567	1260
20	1664	1576	1269
21	1665	1572	1274
22	1638	1554	1276
23	1594	1519	1271
24	1570	1499	1201
25	1609	1531	1214
26	1625	1542	1225
27	1623	1538	1230
28	1596	1518	1232
29	1538	1470	1224
30	1138	1133	1135
31	1990	1989	1991
32	2035	2034	2036
33	2575	2574	2575
34	2700*	2700*	2700*
35	2500*	2500*	2500*
36	1115	1100	1040

* Program input values.

The lower portion of Figure 27 shows temperatures for circumferential flow of cooling air through helical grooves under the journal. Radiation heat transfer was neglected in this case, since bearing temperatures are only slightly higher than the surrounding casing and support-structure temperatures. Peak journal temperature is approximately 1230°F. The pads are about 50 degrees hotter than the journal.

It is seen from Figure 27 that axial temperature gradients in the journal and pads are greatly reduced when helically grooved flow passages are used for bore cooling. This, as well as the lower levels of temperature, is due to the increased radial heat transfer through the journal into the cooling gas resulting from the increased heat transfer area provided by the grooves. The reduced temperature gradients significantly improve bearing performance, as discussed in the "Nonisothermal Bearing Performance" subsection of this chapter. The lower temperature levels are also desirable from the standpoint of creep strength and corrosion resistance of the journal materials. However, lower journal temperatures do increase the axial temperature gradient across the "heat dam" section of the shaft between the journal and the turbine. Higher heat-dam gradients result in higher thermal stresses at the two ends of the dam.

Temperatures of the HP-spool turbine-end bearing were not calculated for the 25,000-foot-altitude rated-power condition (64,000 rpm). At this condition, bearing friction losses would be 22 percent less than at sea level. Supply pressure for the bearing cooling air, however, would be reduced less than 10 percent relative to the sea-level condition. Differential pressure for sustaining cooling flow would actually increase slightly. Accordingly, the bearing temperature gradients at 25,000 feet would be slightly less than at sea-level. Temperature levels would be significantly lower. Hence, sea-level flight represents a slightly more severe thermal condition at rated-power conditions.

At engine idle speed, bearing friction loss at 25,000 feet is only 9 percent less than the sea-level loss. Supply pressure for the bearing cooling air, however, is reduced by 45 percent at 25,000 feet. Consequently, at idle speed, the 25,000-foot-altitude condition is the more severe thermal condition.

Figure 28 shows calculated temperatures for the HP-spool turbine-end bearing under conditions of maximum bearing load and engine idle (45,000 rpm) at 25,000 feet altitude. Node-point temperatures corresponding to the thermal model of Figure 28 are given in Table VI. Thermal input conditions for this calculation were as follows:

Bearing friction loss	1.21 HP (equally distributed over nodes 18 to 23)
Cooling-air inlet temperature	290°F (at nodes 1 and 5)
Total cooling-air flow	0.0306 lb/sec (5 percent of gas-generator flow)

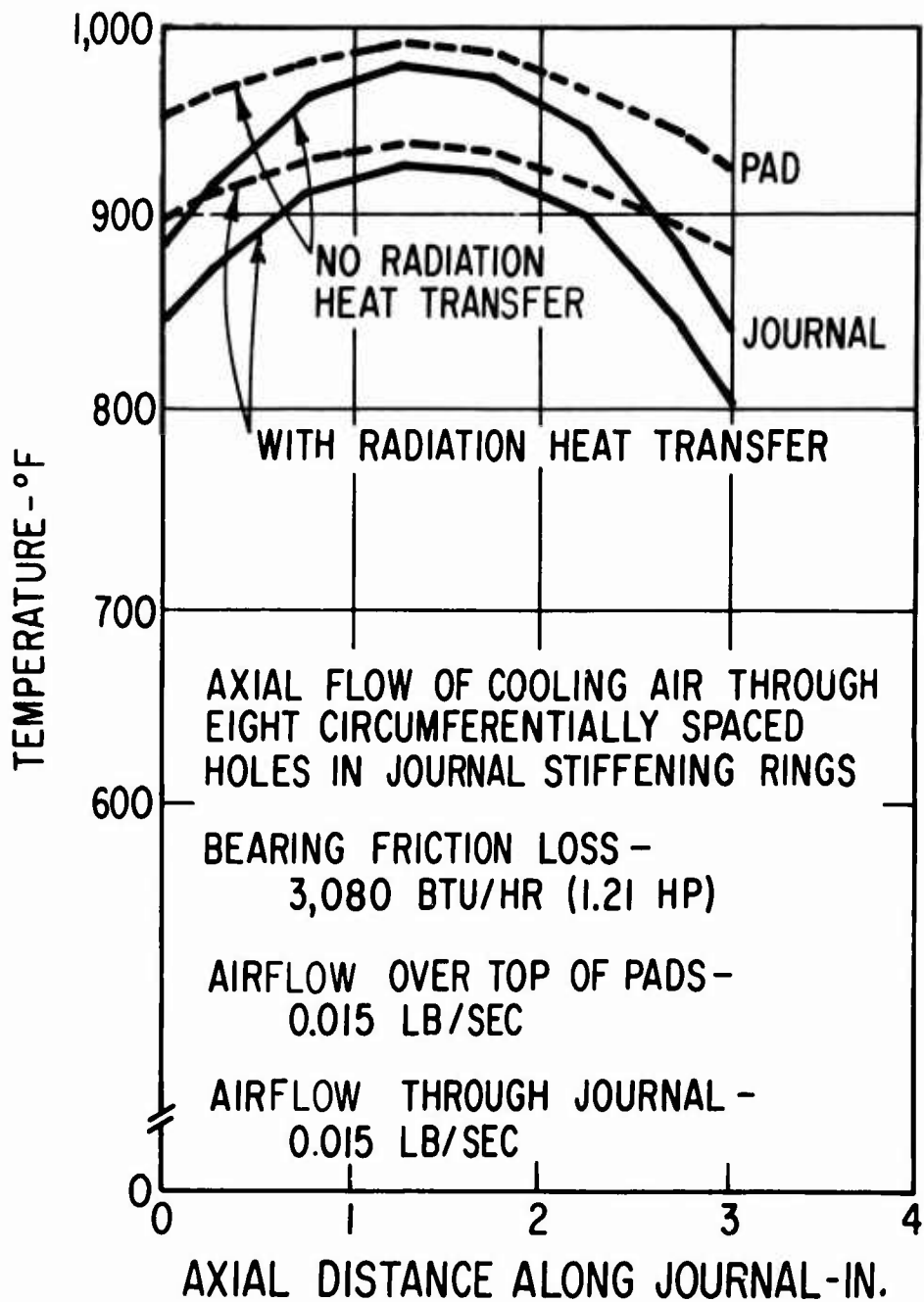


Figure 28. Calculated Temperatures for the HP-Spool Turbine-End Bearing at 25,000 Feet Under Engine-Idle and Maximum Bearing Load Conditions.

TABLE VI. CALCULATED NODE-POINT TEMPERATURES FOR THE
HP-SPOOL TURBINE-END BEARING REGION AT
25,000 FEET AND ENGINE-IDLE CONDITIONS

Node No. (Nodes are defined on Figure 24)	Temperatures - °F	
	Journal Cooled Via Circumferentially Spaced Holes in Journal Stiffening Rings	
	Without Radiation Heat Transfer	With Radiation Heat Transfer
1	290*	290*
2	382	379
3	511	508
4	800	798
5	290*	290*
6	311	309
7	332	328
8	350	345
9	390	384
10	498	492
11	350*	350*
12	966	914
13	981	929
14	990	937
15	984	932
16	966	915
17	942	894
18	957	909
19	988	937
20	1000	948
21	994	943
22	971	922
23	929	884
24	918	872
25	963	914
26	979	929
27	973	924
28	945	899
29	884	843
30	500	491
31	703	700
32	737	735
33	884	884
34	890*	890*
35	865*	865*
36	430	421

* Program input values.

Surface temperature of the turbine blades	890°F (node 34)
Turbine windage heating	770 BTU/hr (heat input at node 3)
Assumed shaft boundary temperature	350°F (node 11)

Bearing temperatures, with and without radiation heat transfer, are shown in Figure 28 for the case of axial flow of cooling air through the eight holes in the journal stiffening rings. Radiation effects were calculated assuming a 350°F temperature for the bearing support structure and surrounding casings. The radiation transfer again acts to cool the bearing. Peak journal temperature ranges for 925°F to 980°F, depending on whether or not radiation heat transfer is significant.

Comparison of Figures 27 and 28 shows that temperatures of the turbine-end bearing are appreciably lower at idle speed than at design speed. However, the temperature gradient within the journal at idle is slightly larger than the design-speed gradient. Thus, for a given method of journal bore cooling, and a constant percentage of cooling flow, the bearing temperature gradients remain roughly the same throughout the HP-spool operating range.

The turbine-end bearing temperatures at idle speed were not calculated for the case of circumferential flow of cooling air through helical grooves under the journal. However, lower temperature levels and reduced gradients would be expected, as was the case at rated power (Figure 27) and, as will be shown next, likewise for the compressor-end bearing at a 25,000-foot altitude and idle speed.

HP-Spool Compressor-End Bearing Temperatures

A calculation of temperatures was made for the HP-spool compressor-end journal bearing under conditions of maximum bearing load and idle speed (45,000 rpm) at a 25,000-foot altitude. At the time that this calculation was made, the back face of the radial compressor disc was being evaluated as a possible location for one of the HP-spool thrust bearings. Accordingly, the thermal model of Figure 24 could be used as a reasonably good representation of the compressor end of the HP spool by simply adjusting the various nodal coefficients. The thermal input conditions for the calculation were as follows:

Bearing friction loss	1.21 HP (equally distributed over nodes 18 to 23)
Cooling-air inlet temperature	290°F (at nodes 1 and 5)
Total cooling-air flow	0.0123 lb/sec (two percent of gas-generator flow)

Surface temperature of the compressor blades	220°F (node 34)
Thrust bearing friction loss	5350 BTU/hr (heat input at node 3)
Assumed shaft boundary temperature	350°F (node 11).

Note that only 2, rather than 5, percent of compressor bleed was assumed for the total cooling flow. Figure 29 shows calculated temperatures for the two modes of cooling gas flow. It is again seen that flow through helically grooved passages under the journal gives lower temperature levels and smaller temperature gradients than does axial flow through circumferentially spaced holes in the journal stiffening rings. Comparison of Figures 28 and 29 shows that temperature levels in the compressor-end journal bearing for 2 percent cooling flow are about the same as those in the turbine-end bearing for 5 percent flow. At the same time, temperature gradients in the compressor bearing are larger than those in the more liberally cooled turbine bearing.

Summary of Bearing Cooling for the HP Spool

It is clear from the preceding discussions and figures that helical-grooved flow passages under the journals are the preferred method of bearing cooling, primarily because of the smaller temperature gradients which result and, to a lesser extent, because of the lower temperature levels. It is also evident that there is considerable flexibility to adjust bearing temperature level by varying cooling air flowrate through the journals. It is also clear that total turbine cooling flow is more than sufficient for cooling purposes. Assumed flow through the journals in all of the preceding calculations was one-half or less of the 5 percent flow required for turbine cooling.

The temperature conditions shown on Figures 27 through 29 should not be rigorously interpreted as actual temperature conditions for the Phase VI gas-generator layout, since the thermal analyses were performed prior to the Phase VI layout study. Rather, the thermal results should be considered primarily as proof of the feasibility of the air-cooling concept for removal of bearing friction losses.

Final optimization of the cooling concept — which will involve detailed design of the helical-grooved passages, determination of proper distribution of cooling-gas flow, optimum cooling gas preheat, and so forth — would be performed during the detail-design phase of a gas-generator development program. As mentioned previously, a considerably more complete thermal model will be required to accurately assess the interactions between adjacent bearing regions and engine casings.

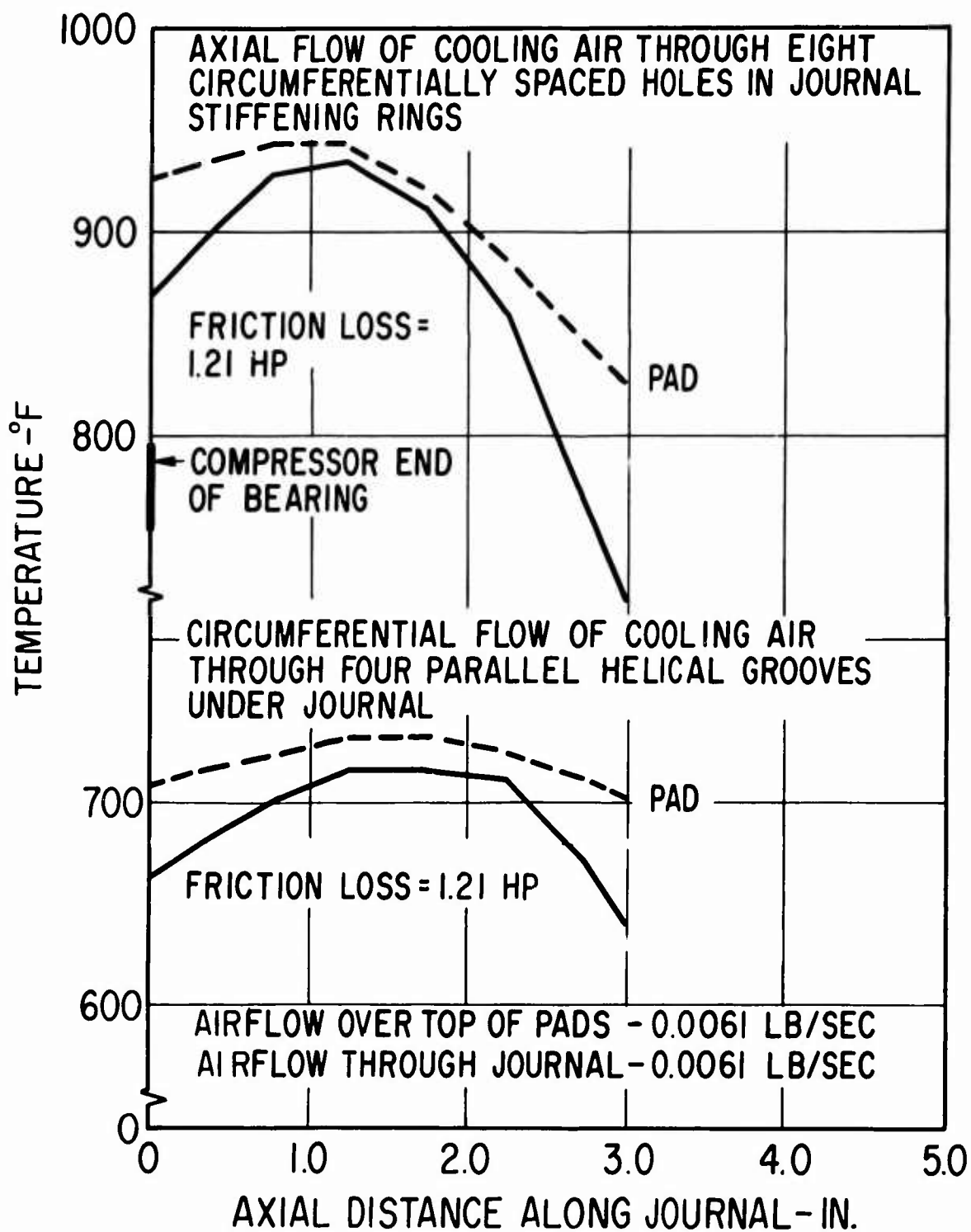


Figure 29. Effect of Cooling Technique on HP-Spool Compressor-End Bearing Temperatures at 25,000 Feet Under Engine-Idle and Maximum Bearing Load Conditions.

LP-Spool Turbine-End Bearing Temperatures

Results of the first calculation of LP-spool turbine-end bearing temperatures are plotted in Figure 30 for conditions of sea-level flight at maximum bearing load and rated power (62,800 rpm). Thermal input conditions for the calculation (based on the thermal model of Figure 25) were as follows:

Bearing friction loss	1.026* (equally distributed over nodes 26 to 31)
Cooling-air inlet temperature	1000°F (at node 1)
Total cooling-air flow	0.09 lb/sec (2 percent of rated gas-generator flow)
Hub temperature of LP-turbine inlet nozzle ring	2400°F (node 49)
Temperature of turbine blades and turbine exit gas	2320°F (node 51)
Temperature of turbine exit gas flowing over the bearing cavity	2240°F (node 52)
Assumed shaft boundary temperature under the bore of the HP-spool turbine	2000°F (node 25)

* The reader is again reminded that this friction loss value is erroneously high by a factor of approximately two (see explanation on page 76). Correct values of bearing friction loss are given in Figures 38 and 39.

Figure 30 shows bearing temperatures, with and without radiation heat transfer, for circumferential flow of cooling air through helical grooves under the journal. Radiation effects were calculated assuming a 2230°F temperature for the bearing support and surrounding casings. Unlike the HP-spool results, the LP-spool turbine-end bearing runs cooler than the surrounding structure, and radiation transfer heats, rather than cools, the bearing. Peak journal temperature is approximately 1210°F when radiation effects are included. In the absence of radiation, peak journal temperature drops to 1160°F.

The most significant feature about Figure 30 is the nature of the pad temperature gradients. It is seen that pad gradients are considerably more severe than journal gradients and that pad temperatures actually drop below journal temperatures at the turbine end of the bearing. This is a generally undesirable condition. The thermal model of Figure 25 indicates the source of the problem. It is seen that cooling air flow

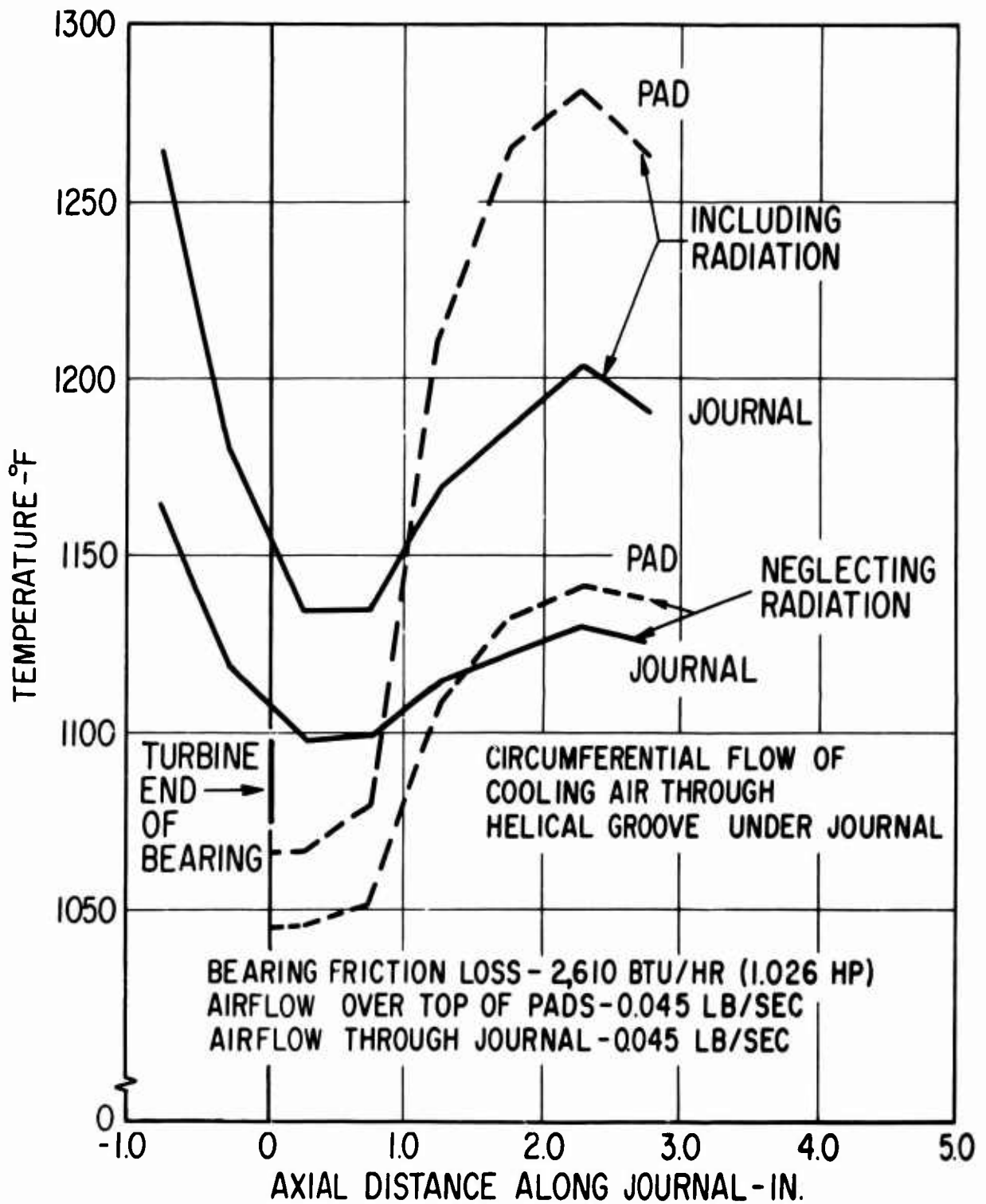


Figure 30. First Calculation of Temperatures for the LP-Spool Turbine-End Bearing at Sea-Level, Rated-Power, and Maximum Bearing Load Conditions.

enters the bearing cavity through a rather narrow annulus, where the inner surface of the annulus is formed by the top surface of the pads. Because of the relatively high flow velocities in this annulus, there is a relatively good heat transfer path from the turbine end of the pads to the cooling gas. This results in excessive cooling of the pads.

The solution to the above problem is shown in the cooling flow path arrangement of Figure 5. The narrow annular passage over the pads has been removed. In addition, the cooling gas enters the bearing cavity well above the pads. The resulting bearing temperatures, with and without radiation heat transfer, are shown in Figure 31. A tabulation of all node-point temperatures for the thermal model of Figure 25 is given in Table VII. Thermal input data for this calculation were the same as previously listed.

It is seen from Figure 31 that the problem of severe pad gradients was greatly alleviated. It is also seen that if the radiation heat transfer can be blocked, essentially isothermal conditions can be obtained in the bearing. With maximum radiation transfer, the journal still remains essentially isothermal, while a mild gradient exists in the pad. The Phase VI engine layout implies the use of some radiation shielding. However, this is not too critical since radiation effects are not severe.

Since the bearing friction loss used for the above calculations was roughly twice as high as will actually exist, it is seen that the bearing will essentially assume the temperature of the cooling gas. The use of helical-grooved cooling passages under the journal thus gives a very satisfactory means for cooling the bearing. Nearly isothermal conditions will exist, and the temperature level will be between 1000° and 1200° F. As a result of these conclusions, it was deemed unnecessary to perform any additional thermal calculations for the LP-spool journal bearings. There is no question that these bearings can be very effectively cooled using a portion of turbine cooling air.

HP-Spool Heat Dam

The "heat dam" is a thin-walled section of the shaft having a relatively high thermal resistance. (Figure 3 shows the location of the heat dam. The dam is represented by node 30 of the thermal model shown in Figure 24.) Its function is to thermally isolate the bearing from the turbine. The problem in heat dam design is to achieve safe stress levels under the combined action of heat-dam centrifugal and thermal strains, and attachment forces resulting from centrifugal and thermal growths of the HP turbine. Successful application of the heat-dam concept has been made to several gas-bearing machines. In one instance of a 24,000-rpm turbocompressor, the heat dam was designed to have a 10,000-hour life for a gradient of 480 degrees per inch [16]. More recently, a 60,000-rpm gas-bearing turbocompressor was designed with a heat-dam gradient of 510 degrees per inch and an average temperature of 660° F [7]. Still another gas-bearing turbomachine is currently being developed with a 600-degree-

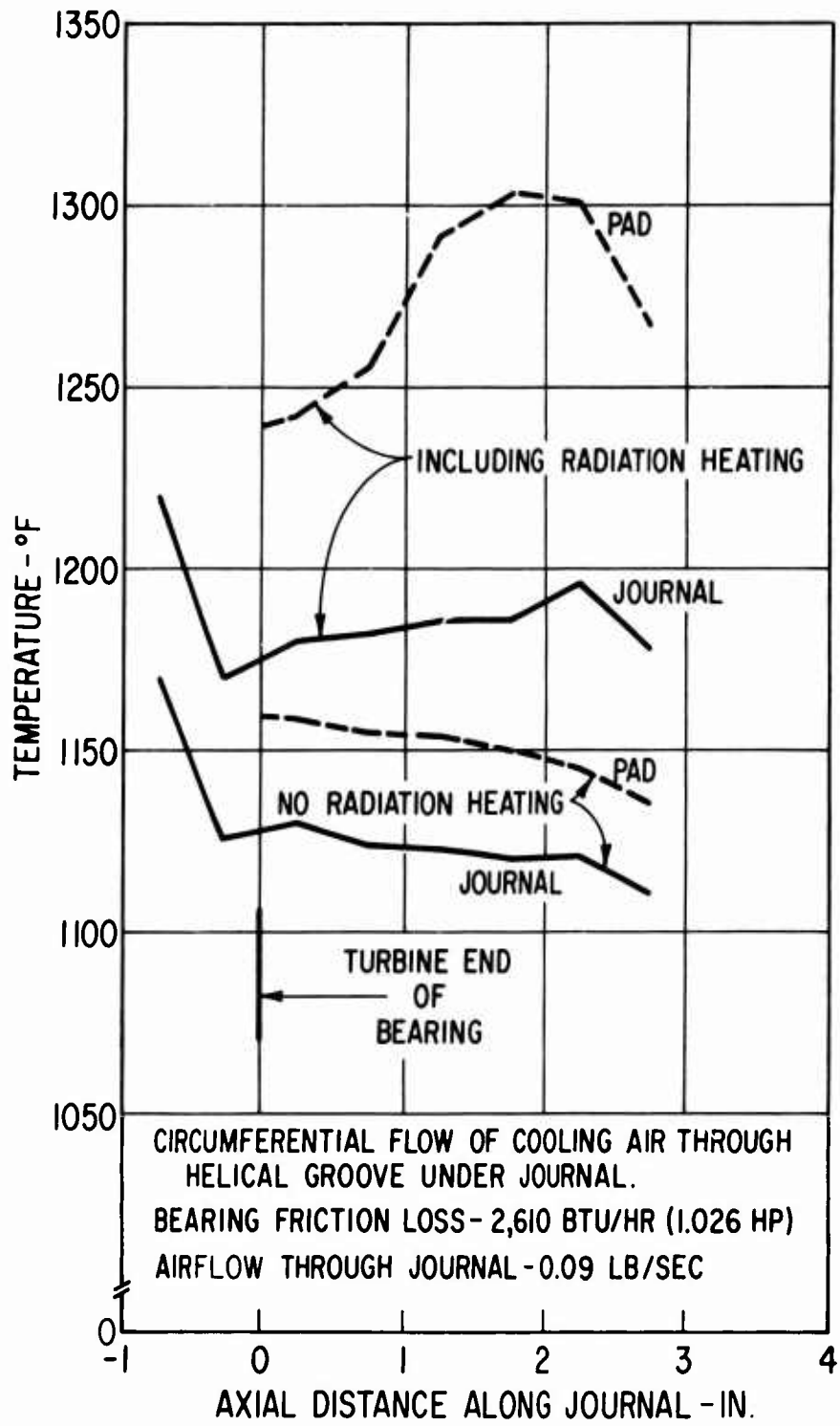


Figure 31. Second Calculation of Temperatures for the LP-Spool Turbine-End Bearing at Sea-Level, Rated-Power, and Maximum Bearing Load Conditions.

TABLE VII. CALCULATED NODE-POINT TEMPERATURES
FOR THE LP-SPOOL TURBINE-END BEARING
REGION AT SEA-LEVEL RATED-POWER
CONDITIONS

Node No.	Temperature** (°F)	Node No.	Temperature** (°F)
1	1000*	27	1150
2	1008	28	1151
3	1070	29	1154
4	1081	30	1157
5	1086	31	1160
6	1091	32	1134
7	1096	33	1146
8	1101	34	1150
9	1105	35	1154
10	1109	36	1156
11	1217	37	1159
12	1319	38	2233
13	1115	39	2233
14	1123	40	2232
15	1120	41	2309
16	1123	42	2318
17	1127	43	2363
18	1129	44	1620
19	1126	45	1964
20	1172	46	1895
21	1320	47	1913
22	1614	48	2500
23	1646	49	2400*
24	2241	50	1074*
25	2000*	51	2320*
26	1140	52	2240*

*Program input values.

**Assuming no radiation heating of bearing.

Journal cooled via helically grooved flow passages under journal.
Nodes are defined on Figure 25.

per-inch gradient and an average temperature of 900°F.

For a 1.5-inch-long heat dam, the calculated heat-dam temperature gradients for the HP spool (corresponding to the thermal conditions used for the temperature calculations of Figure 27) were as follows:

<u>Bearing cooling flow arrangement</u>	<u>Heat dam temperature gradient (end-to-end) (°F/in.)</u>
Axial flow through holes in journal stiffening rings	346
Circumferential flow through helical grooves under the journal	512

Thus, the HP-spool heat-dam gradients are within current practice. However, average heat-dam temperatures range from 1600° to 1730°F, which are, of course, much higher than those that exist in current machinery.

A stress analysis was not made for the heat-dam section. Such an analysis is highly dependent upon the turbine design, which in itself will be a challenging task. However, it is obvious that the heat-dam stress situation must be carefully analyzed and assessed during the early stages of actual gas-generator design. If the temperature gradients for a 1.5-inch-long dam are too high, the dam length can be increased somewhat without significantly affecting the rotor-bearing system performance of the HP spool. Length of the LP spool, however, might have to be increased, and this increase would have a detrimental effect on LP-spool rotor dynamics.

Finally, it is obvious that if oil-lubricated bearings were considered for this engine, the turbine-end bearings would have to be cooled to much lower temperatures than those presented herein for a gas-lubricated engine. Accordingly, the axial temperature gradient in the HP-spool heat dam for an oil-lubricated engine would be much greater (for the same heat dam length) than would exist in a gas-bearing engine. To reduce the heat-dam gradient to an acceptable value (i.e., a value which will be dictated by the maximum allowable thermal stress in the heat dam), it is clear that greater separation of the HP-spool turbine and turbine-end bearing will be required for the oil-lubricated engine than for the gas-lubricated engine.

ISOTHERMAL PERFORMANCE OF BEARINGS

MTI computer program PN 409 was used to study the performance of the completely assembled pivoted-pad journal bearings. This program assumes ideal (isothermal) bearing geometry in the sense that the pad and journal surfaces remain cylindrical at all times. Except for this one limitation, the program is quite complete and includes the following features:

1. Thermal expansion effects of the journal, the pads, and the bearing support housing are accurately treated. Different temperatures and coefficients of expansion can be assigned to each of these three bearing elements. In addition, a linear radial temperature gradient can be assigned to the pads.
2. The effect of journal centrifugal growth is included in the analysis.
3. Flexure mounting of one or more of the pads can be specified. This feature permits simulation of a deflection-limiting stop on the loaded pad.
4. Either extreme of bearing load condition can be selected; that is, load applied directly through a pivot or midway between adjacent pivots.
5. Effects of pivot stiffness are also included. Any one of three pivot geometries may be selected: ball-on-flat, ball-in-spherical-seat, or ball-in-cylindrical-seat.
6. Bearings with three to twelve pad segments can be investigated.

Output from the program includes the following:

1. Pad mass and inertia properties
2. Bearing setup data
3. Bearing eccentricity
4. Bearing friction loss
5. Journal centrifugal growth
6. Four bearing stiffness parameters for use in rotor-response calculations. These are the effective direct and cross-coupling stiffnesses of the bearing, and they include the effects of flexure and pivot stiffness, as well as pad mass and gas-film stiffness and damping.
7. Four bearing damping parameters for use in rotor-response calculations. Again, these are the effective direct and cross-coupling damping coefficients of the bearing, and include the same effects as mentioned above.
8. The following output is given for each pad:
 - a. Pad load
 - b. Pivot film thickness

- c. Friction loss
- d. Flexure deflection
- e. Pivot stress
- f. Eight gas-film stiffness coefficients for translatory and angular pad motions
- g. Eight gas-film damping coefficients for translatory and angular pad motions
- h. Four resonant frequencies and amplification factors corresponding to the radial, pitch, roll and yaw degrees of freedom of the pad.
- i. Additional pad parameters, such as preload, attitude angle, compressibility number, dimensionless pad load, etc.

It should be noted that program PN 409 is a very powerful (and accurate) design tool. Without it, a meaningful study of pivoted-pad bearings for this advanced gas-generator application would have been, for all practical purposes, impossible.

Concept of Pivoted-Pad Bearing Design

The basic concept of the pivoted-pad journal bearing designs for both the HP- and LP-spools is shown in Figures 2 and 32. Each bearing has three pads. Each pad has an arc length (β) of 110 degrees and a pivot location ratio (θ_p/β) of 0.65. The pivots are of the nonconforming ball-in-spheri-

cal-seat type. The ball and seat radii were selected to maintain safe hertzian contact stress levels under the maximum condition of applied pad load (W_p). Based on very successful field operation of motor-driven

gas-bearing machinery [1], as well as test data from a high-temperature pivot technology program [9], maximum hertzian contact stress was limited to 125,000 psi.

Cantilever-beam-type flexures are used. A deflection-limiting mechanical stop is provided for each flexure to prevent excessive deflection and overstressing of the flexures when the bearings are highly loaded. During normal operation, the flexures would not be seated against the stops. The flexures have been designed for a maximum bending stress of 60,000 psi. Determination of flexure stiffness is discussed in the next subsection.

All but one of the above design concepts and design parameters have been demonstrated in actual gas-bearing machinery, the single exception being the use of flexure stops. However, pivoted-pad bearing operation has never been demonstrated at the high values of bearing load, journal

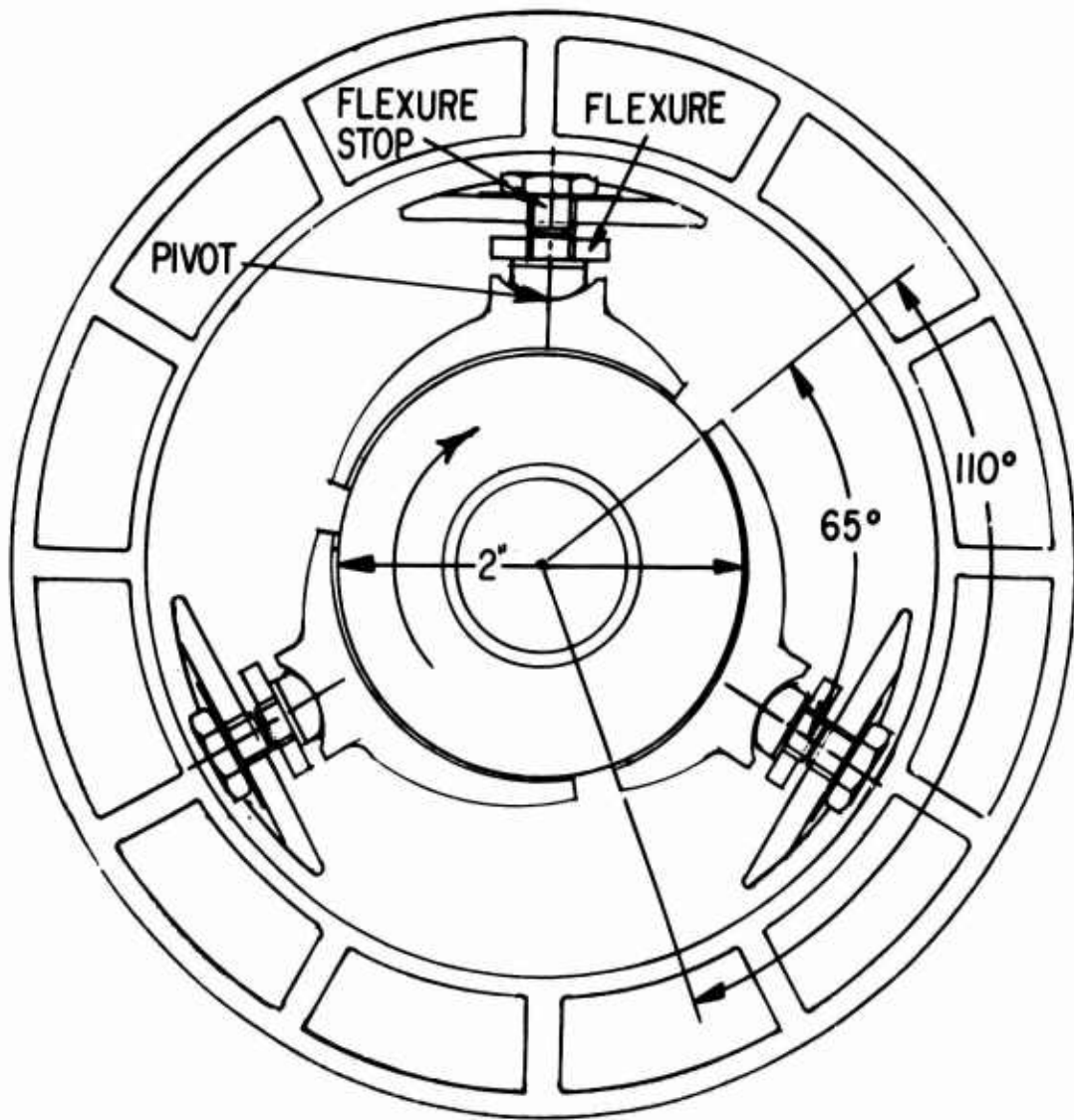


Figure 32. Design Configuration for the HP- and LP-Spool Pivoted-Pad Journal Bearings.

surface velocity, or bearing temperatures of this gas-generator application. Although the design concepts and the performance analyses indicate that pivoted-pad bearings should be able to operate satisfactorily under the required conditions, test data are definitely needed to substantiate these indications.

Determination of Flexure Stiffness

Because of the large amount of journal centrifugal growth and the relatively high bearing temperatures (and hence thermal expansions), it was recognized that each pad in the HP-spool bearings would have to be mounted on a relatively soft flexure. However, while in principle the flexure should be made as soft as possible, there are practical limitations. First, the flexure deflections must be limited to reasonable values and safe stress levels. Second, if the flexure is made too soft, it will force the pad against the journal at low and zero speeds, thus causing severe rubbing during startup and shutdown, as well as greatly increasing startup breakaway torque. This problem can be overcome by providing either externally pressurized lift-off orifices within the pad, or by assembling the flexure in a preloaded condition against a mechanical stop which prevents the flexure from forcing the pad into the journal. Both of these solutions entail undesirable mechanical complexity. Consequently, a study was made for the HP-spool bearings to determine if a flexure stiffness value could be obtained which would accommodate the centrifugal growth and thermal expansion effects, and still result in clearance between the pads and journals at the zero-speed room-temperature condition.

Figure 33 shows the results of the flexure stiffness study. Flexure stiffness is plotted against pad radial clearance at 70°F and zero speed for three values of bearing diametral clearance at sea-level design-speed conditions. The calculations were made using program PN 409 and include effects of centrifugal growth and thermal expansions at the design-speed condition. Based on bearing heat transfer studies (discussed in the "Bearing Thermal Studies" subsection of this chapter), design-speed journal, pad, and bearing-support temperatures were specified to be 1500°F and 1100°F respectively. Bearing load was 10 pounds (gravity load) acting through a pivot.

It is seen from Figure 33 that for a given value of flexure stiffness, zero-speed pad clearance is a strong function of design-speed diametral clearance. A change of 0.1 mil in design-speed clearance results in a 1- to 2-mil change in zero-speed clearance. Selection of design-speed diametral clearance is a trade-off between low gas-film stiffness at large clearances and high bearing friction loss at small clearances. A compromise value of 2.6 mils was selected. A value of pad radial clearance between 1.5 and 2.0 mils at zero speed and 70°F was felt to be practical. Selection having been made of design-speed and zero-speed clearances, a flexure stiffness of 15,000 pounds per inch was obtained from Figure 33.

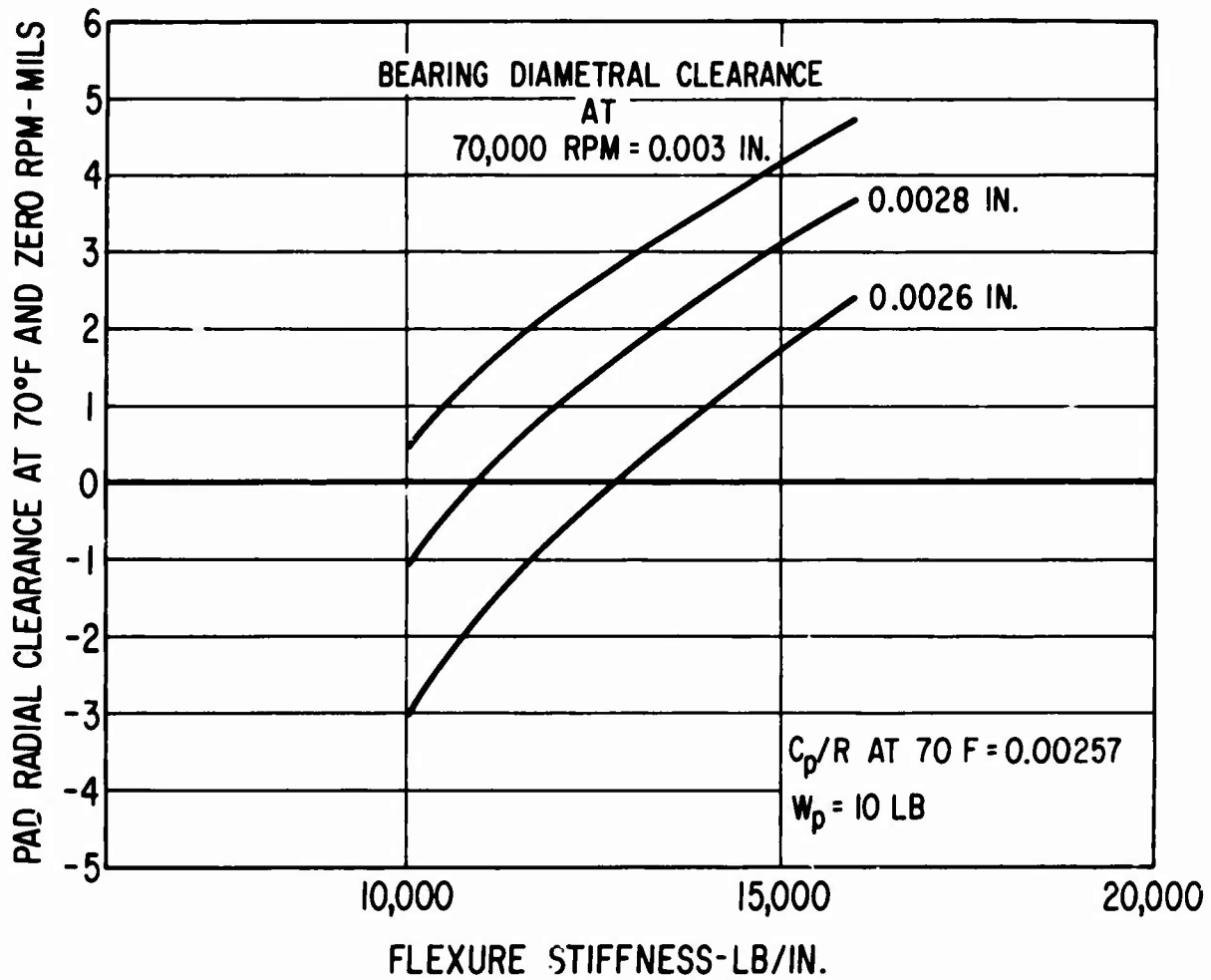


Figure 33. Pad Radial Clearance at 70°F and Zero Speed as a Function of Flexure Stiffness and Design-Speed Clearance for the HP-Spool Journal Bearings.

The 15,000-pound-per-inch stiffness value obtained for the HP-spool bearings should be close to optimum. The flexure sizes shown on Figures 2 and 32 are based on this stiffness. A flexure stiffness study was not, however, performed for the LP-spool bearings. Rather, the same stiffness value as determined for the HP-spool was used for the LP-spool bearing calculations. Because of the smaller centrifugal growth of the LP-spool bearings, it appears that the flexure stiffness should be greater than 15,000 pounds per inch in order to achieve higher values of gas-film stiffness at design speed. Before proceeding with a test evaluation of the LP-spool bearings, further calculations should be made to determine optimum flexure stiffness.

HP-Spool Bearings

There are many design parameters which must be defined for program PN 409 in order to perform the bearing calculations. Among these are material properties for the journal, pads, and bearing-support housing. The material properties in turn are a function of temperature. Accordingly, any changes in materials or temperature levels, as a result of future refinements to the heat transfer or mechanical design of the HP and LP-spool assemblies, should be checked for their effect on the detailed design and performance of the bearings.

The bearing performance results presented here are based upon one combination of material properties as defined in Table VIII. Other fixed properties of the bearing design are also given in Table VIII. The journal and pad material was assumed to be IN-100 (nickel base) alloy. Properties of this alloy at 1600°F were used. For the bearing support housing, Hastelloy X at 1100°F was assumed. The most significant effect of a future material change would be if the journal, for purposes of higher strength, were to be made from a more advanced material such as coated TZM, TAZ-8A [17], or a boron or silicon-carbide whisker or a graphite-yarn reinforced material. In this case, the modulus of elasticity, the thermal expansion coefficient, and perhaps the density would be significantly different, and a new set of bearing performance calculations would have to be made.

1-G Bearing Load

Performance of the HP-spool turbine-end bearing under normal 1-g load conditions is shown in Figure 34. Bearing load in this case is 10 pounds. The most severe 1-g condition has been assumed; namely, load acting through a pivot at 25,000 feet altitude. For this and all subsequent calculations, the ambient pressure versus speed characteristics given in Figure 17 have been used.

The principal conclusion to be drawn from Figure 34 is that under normal 1-g load conditions, excellent film thickness will be maintained in the pivoted-pad bearings throughout the HP-spool speed range.

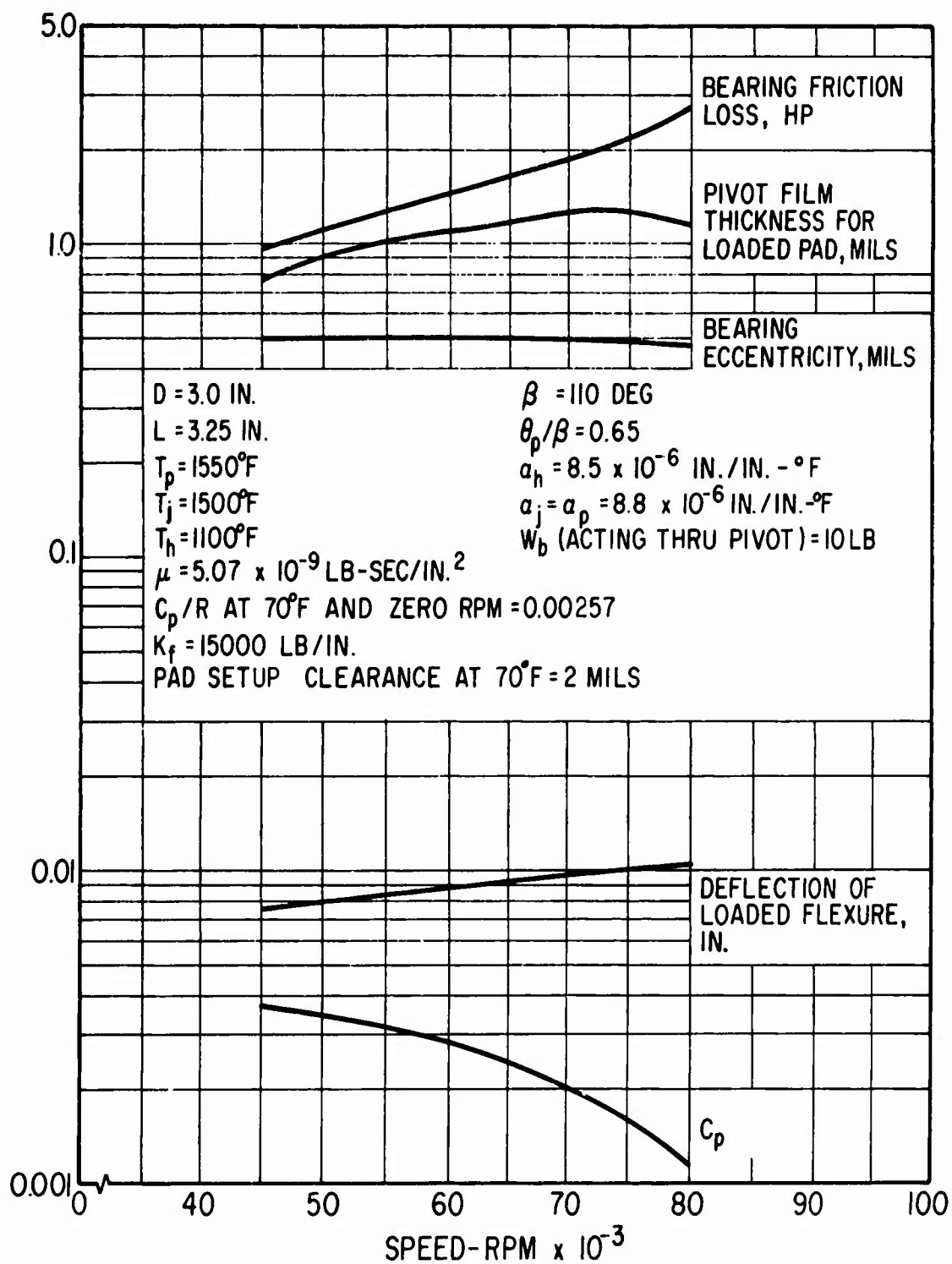


Figure 34. Performance of the HP-Spool Turbine-End Pivoted-Pad Journal Bearing Under 1-G Load Conditions at a 25,000-Foot Altitude.

TABLE VIII. DESIGN PARAMETERS AND MATERIAL PROPERTIES FOR THE HP-SPOOL PIVOTED-PAD JOURNAL BEARINGS

Bearing configuration	Three pads per bearing, each pivot supported by a flexure
Journal diameter (D)	3.0 in.
Bearing length-to-diameter ratio (L/D)	1.08
Pad arc length (β)	110.0 deg
Pivot location from leading edge of pad (θ_p/β)	0.65
Pad clearance ratio at zero speed and 70°F (C_p/R)	0.00385
Setup clearance (radial) per pad at 70°F (with journal concentrically located in bearing)	0.002 in.
Individual pad mass	0.51 lb _m
Individual pad mass-moment of inertia about roll axis	0.63 lb _m -in. ²
Individual pad mass-moment of inertia about pitch axis	0.55 lb _m -in. ²
Individual flexure stiffness	15,000 lb _f /in.
Thermal expansion coefficients	
Journal and pads	8.8×10^{-6} in./in.-°F
Bearing support housing	8.5×10^{-6} in./in.-°F
Additional properties of journal material at 1500°F	
Density	0.28 lb _m /in. ³
Young's modulus	2.4×10^7 psi
Poisson's ratio	0.3
Flexure stop setting at zero speed and 70°F	0.013 in.

Minimum film thickness of 0.76 mil occurs at the 45,000-rpm idle speed. At all speeds above 55,000 rpm, the film thickness is greater than 1.0 mil. The gradual drop-off in film thickness as speed is reduced is primarily due to the large value of bearing clearance ratio (C_p/R) at low speeds. Figure 34 verifies the single-pad data of Figure P 19 in that optimum clearance ratio occurs in the range of 0.001 to 0.002. The bearing compressibility number (Λ) at 45,000 and 75,000 rpm is 1.23. The maximum variation in Λ between these two speeds is a 29 percent reduction at 55,000 rpm.

Maximum Bearing Load

Figure 35 shows performance of the HP-spool turbine-end bearing under maximum load conditions as defined by Figures 13 and 14. The journal and bearing support temperatures shown on Figure 35 are estimated steady-state temperatures at any given speed. The viscosity function, however, is based on a conservative estimate of the gas film temperatures in the compressor-end bearing. In other words, Figure 35 represents a conservative calculation of film thickness for both the turbine and compressor-end bearings.

Film thickness is plotted for both sea-level and 25,000-foot altitude conditions. Minimum values of film thickness again occur at idle speed. At 49,000 rpm (sea-level idle) the film is 0.42 mil. At 45,000 rpm (25,000 feet idle), the film drops to about 0.3 mil. Thus, under the most severe conditions of maximum load applied through a pivot, film thickness exceeds the 0.2-mil minimum film thickness criterion for all conditions of HP-spool operation (assuming, of course, ideal bearing geometry in the sense that all bearing surfaces remain cylindrical).

Under maximum load conditions, the loaded pad (or pads) would be bottomed against the flexure stop(s). Figure 35 shows that actual bearing eccentricity with the flexure(s) bottomed would be a maximum of 8 mils at 45,000 rpm and a minimum of 2.1 mils at 80,000 rpm. (Under 1-g loading, an essentially constant eccentricity of 0.5 mil was obtained.) Thus, labyrinth seals around the HP-spool shaft would require an operating radial clearance of not less than 8 mils. If this amount of clearance should prove to be excessive from the standpoint of labyrinth leakage, flexure stiffness could be increased somewhat (and the flexure stop setting reduced) to decrease the maximum bearing eccentricity.

Effect of Transient Power Changes

During engine operation, sudden changes in power demand may occur. This will cause rapid changes in speed and pressure levels. Temperature levels, however, will change slowly.

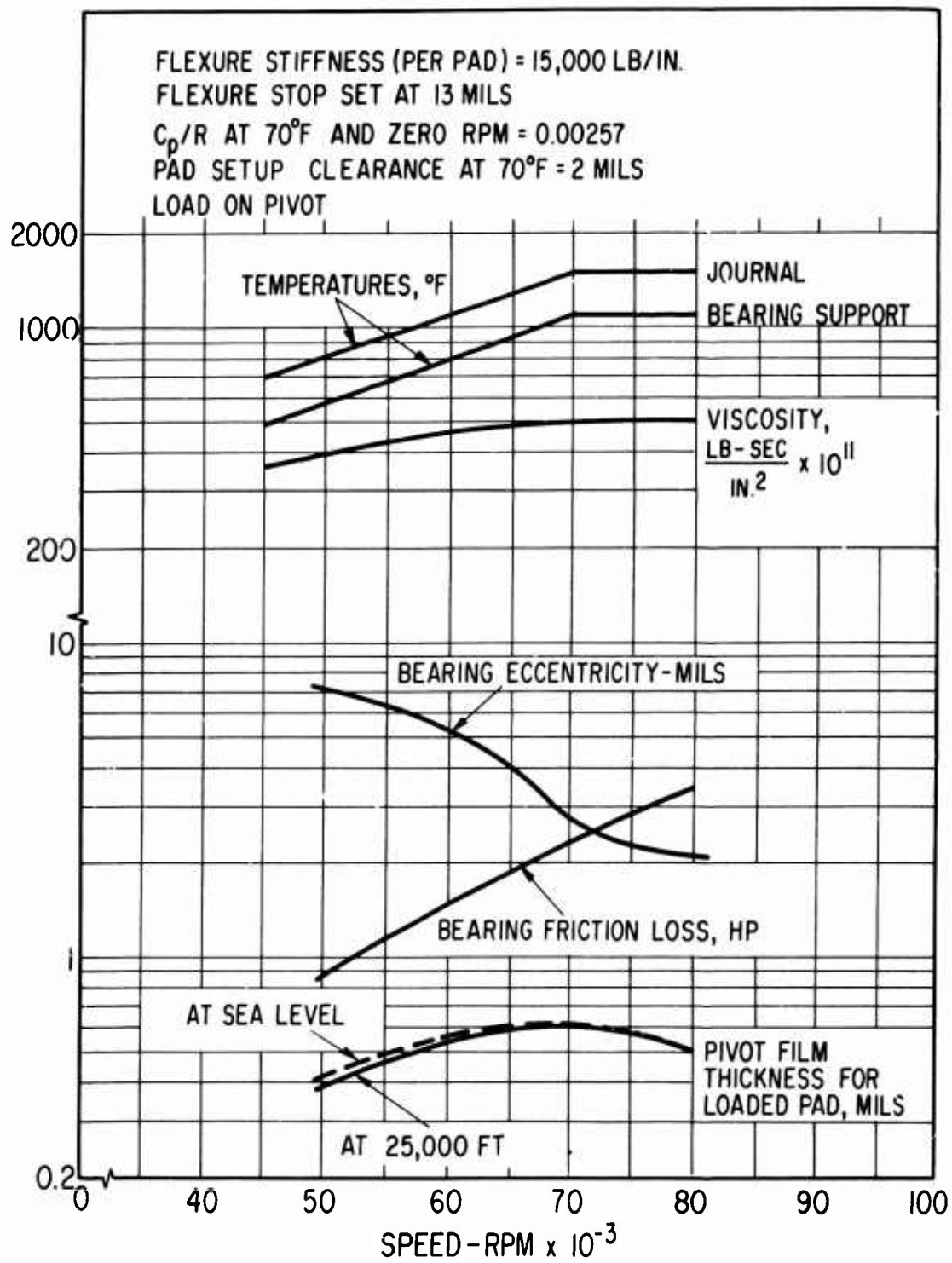


Figure 35. Performance of the HP-Spool Turbine-End Pivoted-Pad Journal Bearing Under Maximum Load Conditions.

The effect of sudden power changes was investigated by calculating bearing performance, under maximum load conditions, over the complete range of speed and corresponding pressures while maintaining constant temperature conditions. Temperatures of 1500° F, 1550° F, and 1100° F were used for the journal, pads, and bearing-support housing respectively. These temperatures are indicative of rated-power conditions.

Figure 36 shows the result of the transient investigation. Relative to steady-state performance, it is seen that a decrease of about 50 microinches in film thickness occurs at the 25,000-foot idle-speed condition. Above 55,000 rpm there is essentially no effect of the transient condition on film thickness.

Figure 36 also shows the effect of direction of load application on bearing performance. It is seen that film thickness increases between 40 and 140 microinches when the load is applied midway between pivots. The greatest increase in film thickness occurs at the idle speeds. These data verify that the most severe operating condition occurs when bearing loads are applied through a pivot.

Tolerance to Temperature Variations

In a compact high-speed high-temperature engine, it is difficult to calculate temperature levels within 10 percent accuracy. Furthermore, a fairly wide range of temperature variation may occur due to normal variations in engine operation. Accordingly, it is highly desirable to have a bearing design which is inherently insensitive to reasonably large temperature variations.

A study of bearing tolerance to temperature variations was made. The most severe operating conditions were assumed; namely, maximum bearing load applied through a pivot at 25,000 feet altitude. Journal and pad temperatures were held constant at 1500° F and 1550° F respectively. The bearing support temperature was varied for 900° F to 1350° F, or about ± 20 percent from the 1100° F nominal temperature estimated for rated-power operation.

Figure 37 shows the result of this study. The maximum variation in film thickness due to the 450° F range in housing temperature is about 0.17 mil and occurs at idle speed. The actual diametral growth of the bearing-support housing from 900° F to 1350° F is 14.4 mil (at the pivot circle radius of 1.9 inches). Analysis of the calculated bearing clearance of 900° F and 1350° F shows that the unloaded flexures accommodate approximately 88 percent of the diametral housing expansion. The remaining 12 percent is accommodated by the gas film, with the unloaded pads (which operate at films in excess of 1.0 mil) providing most of this accommodation.

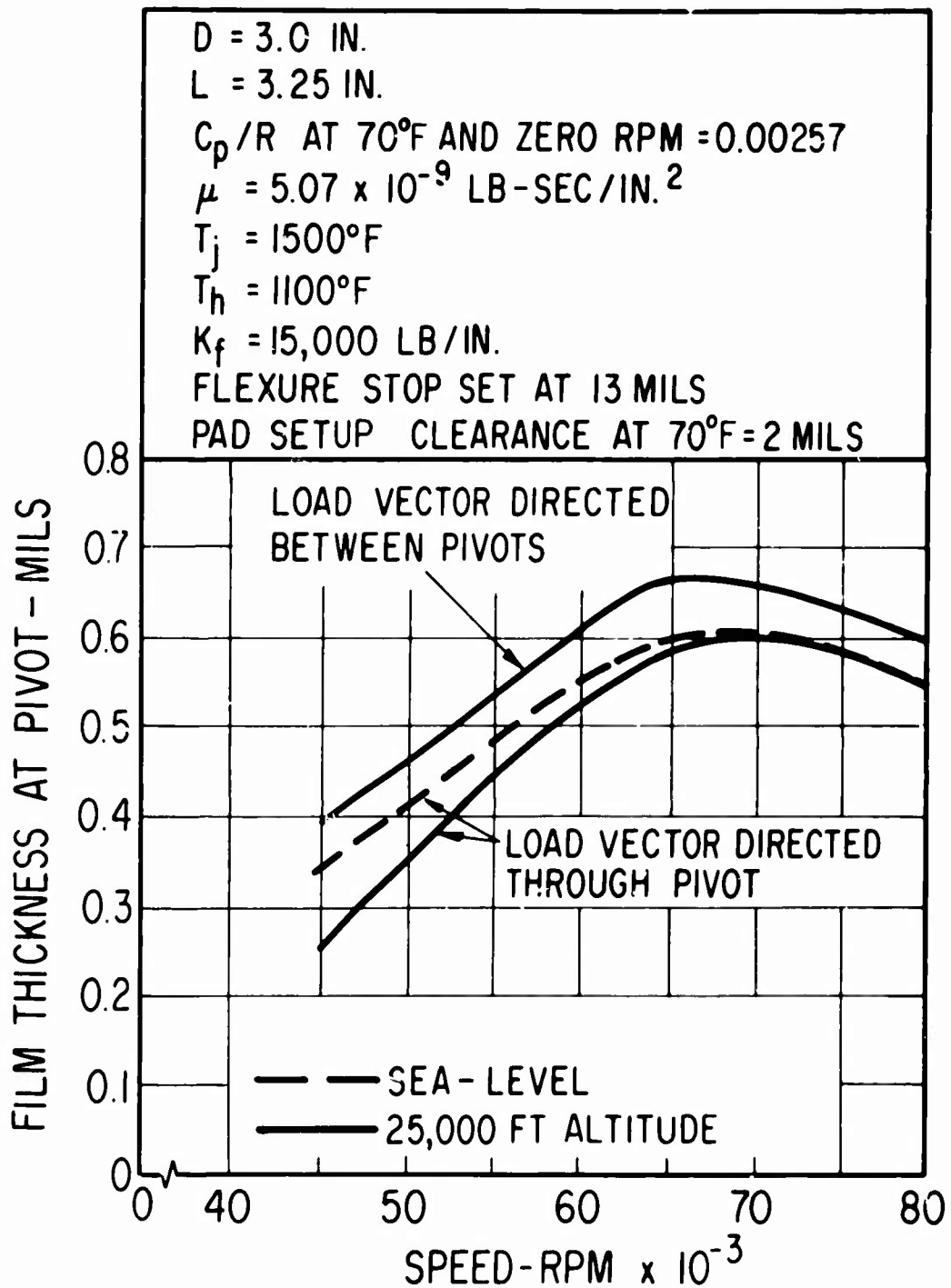


Figure 36. Performance of the HP-Spool Pivoted-Pad Journal Bearings for Transient Changes in Speed From Rated-Power Conditions.

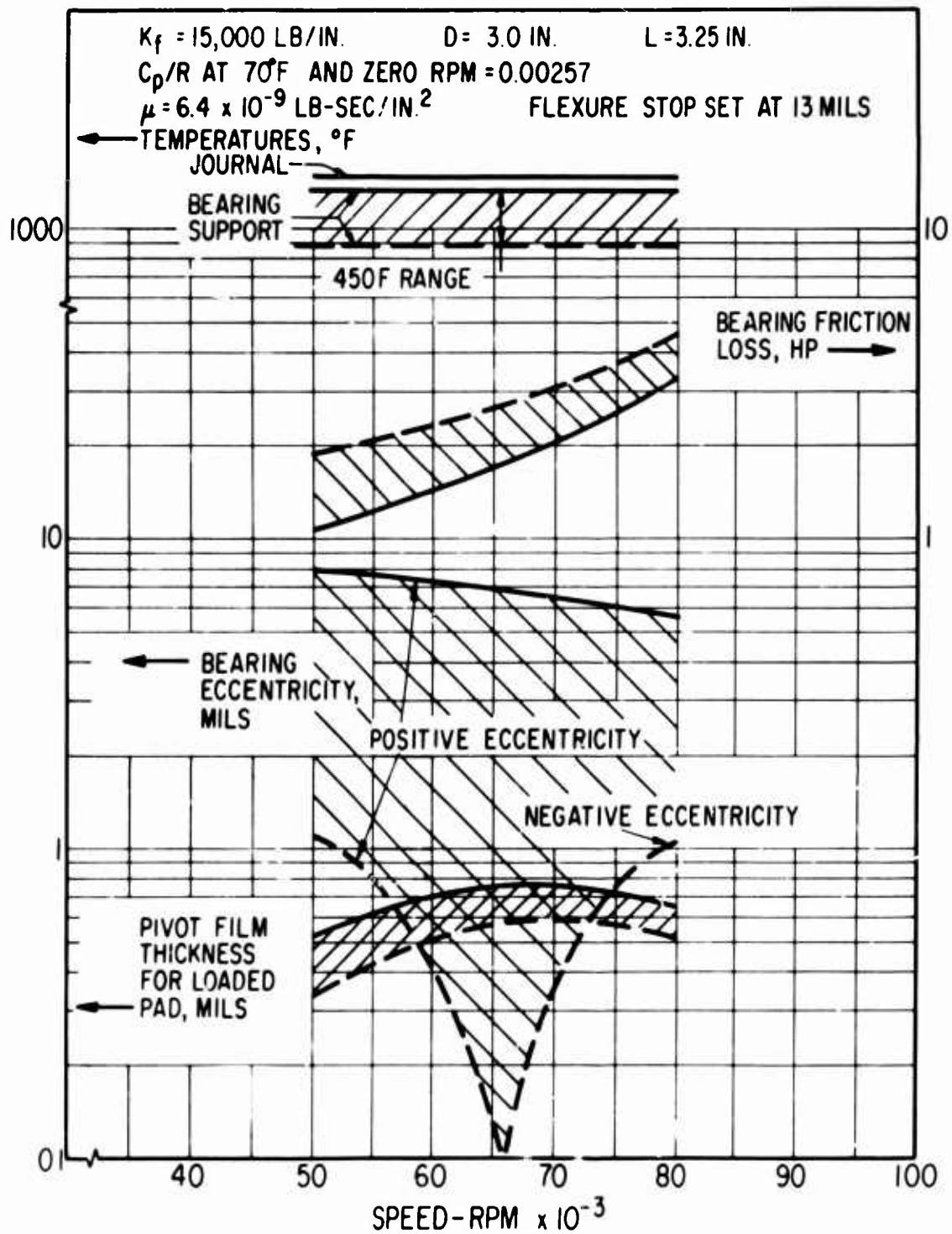


Figure 37. Effect of a ± 20 -Percent Variation in Bearing Housing Temperature on Performance of the HP-Spool Turbine-End Journal Bearing.

Figure 37 also shows maximum bearing eccentricity occurring at idle speed. For a 1350° F housing temperature, eccentricity slightly exceeds 8 mils. At 900° F, the eccentricity is reduced to about 1.1 mils. This reduction in eccentricity, when added to the slight reduction in film thickness for the loaded pad, reflects almost exactly the radial thermal contraction of the housing from 1350° to 900° F.

It is concluded from Figure 37 that the flexure-supported pivoted-pad bearing can be designed to be tolerant of a reasonably wide range of temperature variations. For the specific example of ± 20 percent variation in support-housing temperature, and with the bearing operating under its most severe condition, film thickness exceeded the minimum film thickness criterion throughout the operating range of the HP-spool.

LP-Spool Bearings

As mentioned previously, the LP-spool bearings were not examined in as much detail as were the HP-spool bearings. No effort was made to determine optimum flexure stiffness, nor was clearance ratio or flexure stop setting fully optimized. Since temperature levels, centrifugal growth, centrifugal stress, and bearing friction loss were less severe than for the HP-spool bearings, sufficient calculations were made only to verify that the LP-spool bearings could indeed carry the maximum loads.

1-G Bearing Load

The LP-spool compressor-end bearing is the most highly loaded bearing under both 1-g and maximum load conditions. It was therefore selected for analysis purposes. A constant value of gas-film viscosity based on a 500° F film temperature was used. Since a heat transfer analysis of the compressor-end journal bearing was not performed, the 500° F film temperature was estimated on the basis of a 440° F discharge temperature from the HP compressor at sea-level engine-idle conditions. (It will be recalled that (1) the bearing cavities are pressurized from HP-compressor discharge, and (2) maximum compressor-end bearing load occurs at the sea-level landing condition.) The 500° F film temperature should be realistic for idle-speed conditions and should result in progressively more conservative calculations of film thickness as speed is increased (as HP-compressor discharge rises).

Although bearing loads and gas-film viscosity were based on compressor-end bearing conditions, the performance calculations were made using turbine-end temperatures for the journal, pads, and bearing-support housing. In this way, the maximum conditions of load and temperature for both of the LP-spool bearings could be assessed in one series of calculations.

Figure 38 shows performance of the LP-spool compressor-end bearing under its normal 1-g loading of 10 pounds. It is seen that film thickness is 0.97 mil at engine idle and increases to 1.4 mils at design speed of 62,800 rpm. Bearing eccentricity is less than 1.0 mil. Variation in bearing clearance ratio is quite small, from 0.00148 at idle to 0.00108 at design speed. This reflects the relatively small amount of journal centrifugal growth, being only 0.55 mil radially at 65,000 rpm.

In spite of the nonoptimal nature of the design, load capacity characteristics of the LP-spool bearings under normal 1-g conditions must certainly be considered excellent.

Maximum Bearing Load

Figure 39 shows performance of the compressor-end bearing under two maximum load conditions: sea-level landing and flight at 25,000 feet altitude. In both cases the loads are applied through a pivot. In terms of minimum film thickness, it is seen that the landing condition is slightly more severe.

Minimum film thickness again occurs at engine idle conditions. At sea-level idle (25,000 rpm), the film thickness is 0.25 mil. At 25,000 feet idle (22,500 rpm), the film reduces to 0.24 mil. These minimum films again satisfy, with a small amount of margin, the 0.20-mil minimum film thickness criterion. It is probable that the margin of film thickness could be increased by optimization of the bearing design parameters.

NONISOTHERMAL PERFORMANCE OF THE BEARINGS

The bearing performance results presented thus far pertain to ideal bearing geometry in the sense that pad and journal surfaces remain cylindrical at all times. In actual fact this condition can only be approximated. Some deviation from truly cylindrical geometry will occur because of manufacturing tolerances, elastic deflections of the pad and journal due to gas-film pressures, and thermal distortions of the pad and journal due to temperature gradients within the bearing.

With present manufacturing techniques, 50-microinch tolerances have readily been obtained on 3.5-inch-diameter journals and pads. With the recently introduced air-bearing precision spindles, 1- to 10-microinch tolerances can be obtained and will probably become fairly commonplace in the gas-bearing field within the next several years. Hence, manufacturing tolerance requirements for the gas-generator bearings do not pose any basic problems.

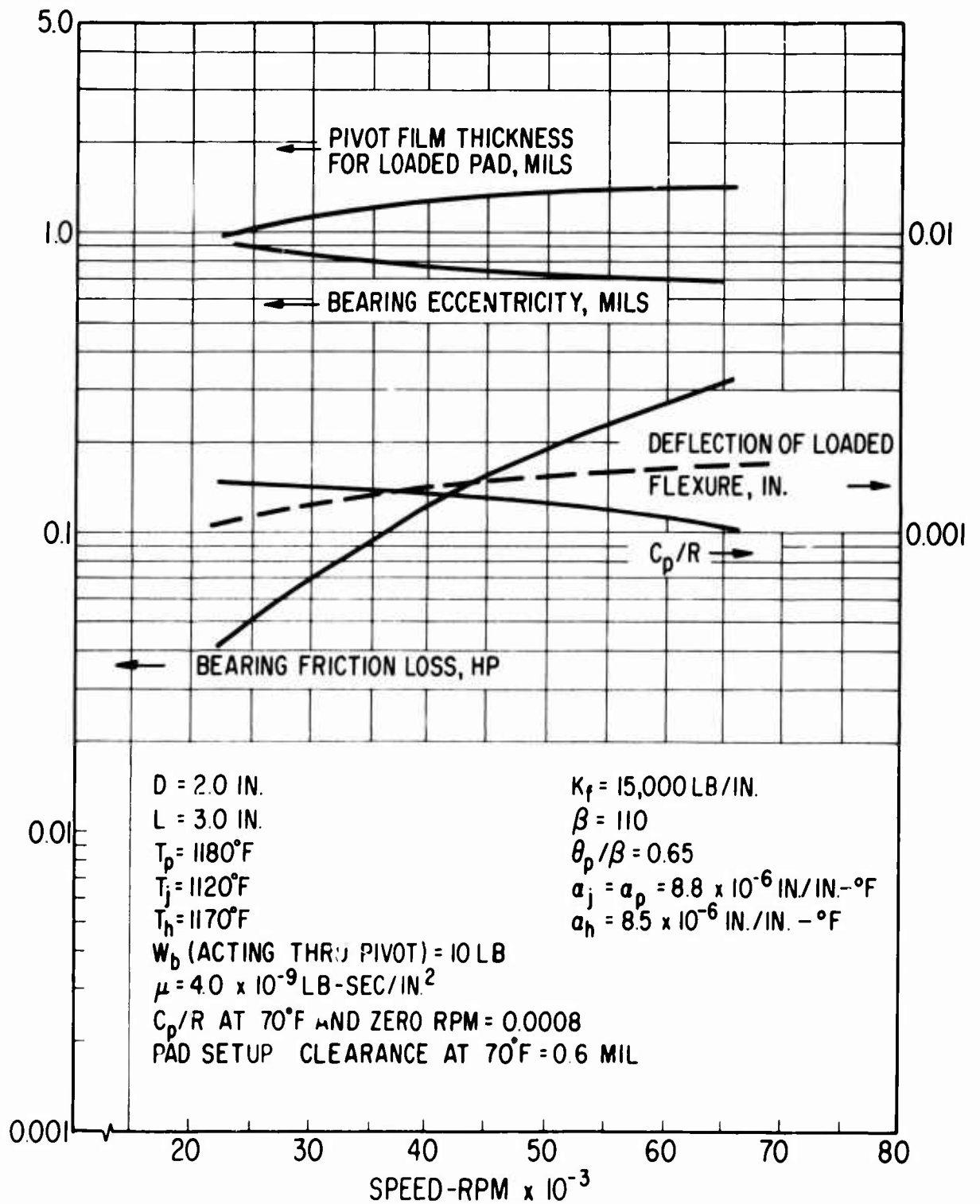


Figure 38. Performance of the LP-Spool Compressor-End Pivoted-Pad Journal Bearing Under 1-G Load Conditions.

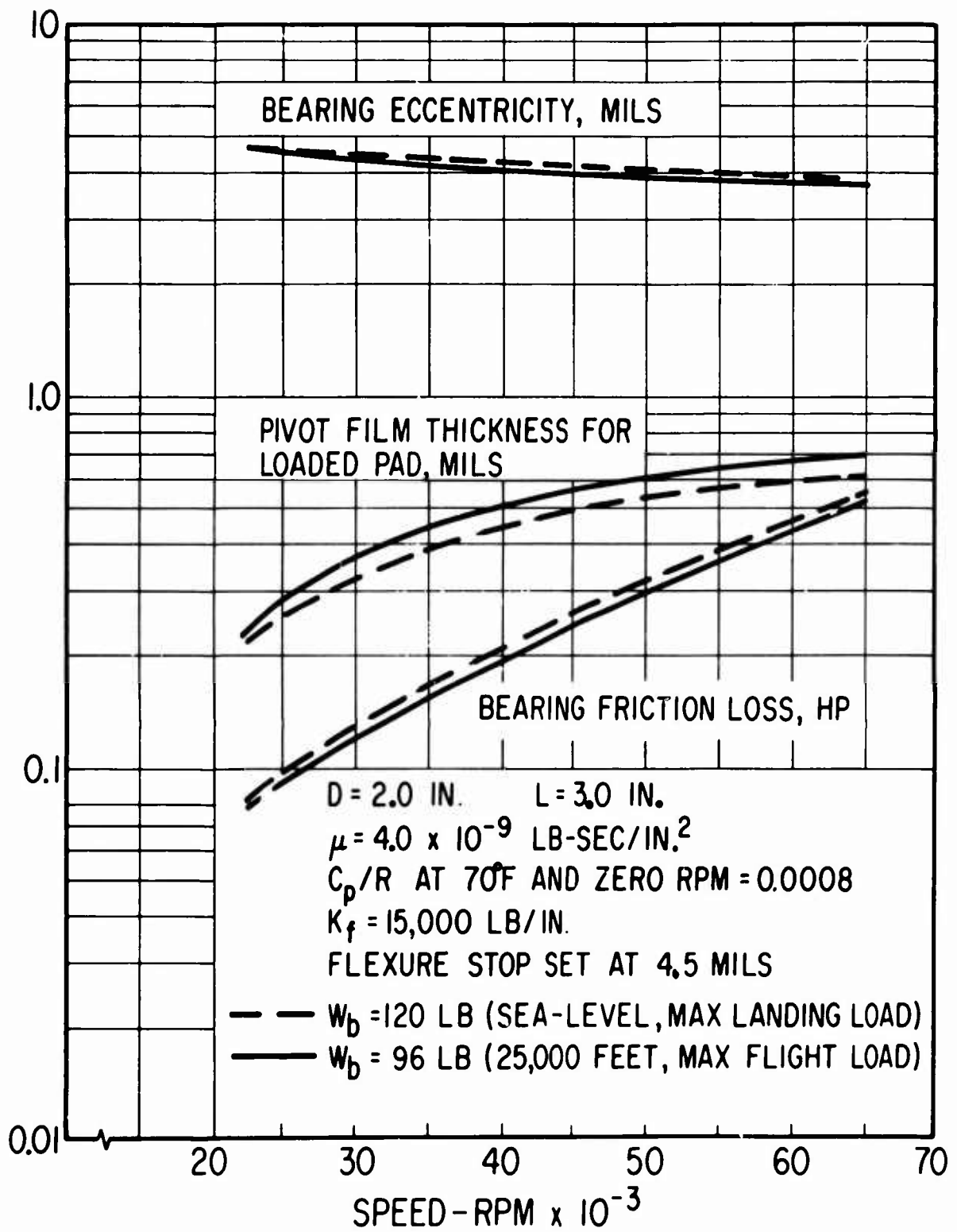


Figure 39. Performance of the LP-Spool Compressor-End Pivoted-Pad Journal Bearing Under Maximum Load Conditions.

At maximum load conditions, peak gas-film pressures will reach 350 to 400 pounds per square inch for the HP-spool journal bearings. Careful mechanical design will be required to assure that these pressures do not cause excessive elastic distortion of the pads. In this case the requirement for high mechanical rigidity will be in opposition to the requirement for minimum pad roll and pitch inertia. Minimum pad inertia is desirable from a pad dynamics standpoint (this is discussed in the "Rotor Dynamics" chapter). Current practice of making uniform thickness pads may not be adequate to meet the high-rigidity, low-inertia requirements. Tapered thickness pads, as shown in Figure 32, or thin-walled rib-stiffened pads may be required. The question of mechanical distortions due to gas-film pressures was not investigated. While the writer has an intuitive belief that these distortions can be adequately controlled by good mechanical design, this belief must be subjected to rigorous design study and elastic-deflection analysis during the next phase of feasibility demonstration.

The problem of thermal distortions is far more significant than the above mentioned distortions because of manufacturing tolerances and pressure-induced deflections. (The thermal distortions referred to here are those which cause the journal and pad surfaces to deviate from cylindrical geometry. The effects of gross changes in temperature levels, and the resulting differential thermal expansions, between the various parts of the bearing were accounted for in the preceding isothermal calculations. Deviations from cylindrical geometry can be caused only by temperature variations (gradients) within the journals or pads.) A quantitative initial assessment of the thermal distortion problem was made using a newly developed computer program in which thermal distortions resulting from specified temperature gradients are first calculated, after which the gas-lubrication equations are solved based on the distorted bearing geometry.

HP-Spool Bearings

Temperature gradients given in Figures 27, 28, and 29 were used to calculate nonisothermal performance of the HP-spool journal bearings. Calculations were made for conditions of maximum bearing load as defined by Figures 13 and 14. Results of the calculations are given in Table IX. It is unfortunate that time and funds did not permit a series of iterative heat transfer and nonisothermal bearing performance calculations to be made. An iterative procedure would have produced convergence to an optimized heat transfer design which, in turn, would have permitted a final assessment of nonisothermal bearing performance to be made. However, since only one set of heat transfer and nonisothermal performance calculations was possible, a degree of engineering judgement is required to estimate ultimate nonisothermal performance of an optimized design.

First of all, Table IX shows very clearly the appreciable performance difference which results from the two techniques of journal bore cooling. At sea-level rated-power conditions, the minimum bearing film thickness drops from an isothermal value of 0.69 mil to a value of 0.178 mil when the journal is cooled via axial flow of air through holes in the journal

TABLE IX. EFFECT OF TEMPERATURE GRADIENTS ON MINIMUM FILM THICKNESS IN THE 3-INCH-DIAMETER HP-SPOOL PIVOTED-PAD JOURNAL BEARINGS AT MAXIMUM LOAD CONDITIONS

Percent of Rated Power	Speed (rpm)	Ambient Pressure (psia)	Total Load on Pad (lb)	Isothermal		Temperature Gradient Condition	Cooling Flow Through Journal (lb/sec)	Cooling Flow (percent of engine flow)	Nonisothermal Film Thickness at Pivot (mils)
				Film Thickness at Pivot (mils)	Film Thickness at Pivot (mils)				
<u>Sea level</u>									
100	70,000	130	370	0.69	0.69	{ Fig. 27* Fig. 27**	0.113 0.113	2.5 2.5	0.437 0.178
0	49,000	36	285	0.38	0.38	Fig. 29*	0.006	1.0	0.168
<u>25,000 feet</u>									
100	64,500	118	345	0.60	0.60	Fig. 27*	0.113	2.5	0.395
10	50,000	30	288	0.35	0.35	Fig. 29*	0.006	1.0	0.131
0	45,000	18	237	0.25	0.25	Fig. 28**	0.015	2.5	0.095

* Circumferential flow of cooling air through helical grooves under journal.

** Axial flow of cooling air through circumferentially spaced holes in journal stiffening rings.

stiffening rings. However, for the case of circumferential cooling flow through helical grooves, the film drops to only 0.437 mil. At 25,000-foot rated-power conditions, the ideal film of 0.6 mil drops to 0.395 mil for the helical-groove cooling concept. Thus, Table IX positively establishes that satisfactory nonisothermal bearing performance can be achieved for the HP spool, at rated and near-rated power conditions, when helical-groove cooling-flow passages are used. The minimum film thickness remains considerably greater than the 0.2 mil minimum film criterion.

Now compare the sea-level zero-power and the 25,000-foot 10-percent power conditions. It is seen that isothermal minimum film thickness is essentially the same for both conditions (about 0.35 mil). Nonisothermal bearing performance for these two conditions was checked using the temperature gradients of Figure 29 for the case of helical-grooved cooling passages. It is seen that the nonisothermal minimum film for both conditions drops to approximately 0.15 mil, which is less than the minimum film criterion. Thus idle and near-idle operation, as identified previously, is the most severe operating condition.

Notice, however, that only 1 percent of engine flow rate was assumed to be flowing through the journal for the gradient condition of Figure 29. Notice also that the actual gradient condition for 1 percent flow through the helical cooling passages is quite similar to the gradient for 2.5 percent of axial flow through holes in the journal stiffening rings (Figure 27). Hence, it seems reasonable to conclude that considerably smaller gradients would have been realized if a 2.5-percent flow rate, rather than a 1-percent rate, had been used for the calculation of Figure 29. The writer believes that at the higher flow rate, the nonisothermal film thickness values would have exceeded 0.2 mil at the sea-level zero-power and the 25,000-foot 10-percent power conditions.

Finally, consider the 25,000-foot zero-power condition. Isothermal film thickness was 0.25 mil. Nonisothermal performance was calculated for the case of 2.5 percent axial flow through holes in the journal stiffening rings. This again is a severe temperature gradient condition which results in a nonisothermal film thickness of 0.095 mil. This is decidedly too small. There is little doubt, however, that the use of helical cooling passages would increase the film to well above 0.15 mil. Whether or not it would exceed 0.2 mil is difficult to estimate since the isothermal film thickness is only 0.25 mil. Hence, the 25,000-foot zero-power condition is the only condition which the writer feels might not meet the minimum film thickness criterion.

It is clear from the results of Table IX and the above discussion that the influence of thermal distortion on maximum load capacity of the bearings is very strong. The heat transfer design must utilize helical (or similar type) journal cooling passages, and it must be optimized to produce as nearly isothermal conditions as possible. In this regard, it appears desirable to increase the proportion of HP-turbine cooling air flowing through the HP-spool journals. A flow of 3.5 to 4.0 percent through the journals (with the remaining 1.5 to 1.0 percent flowing through the turbine-end journal bearing cavity) would seem to be in order. This

higher flow rate might well assure satisfaction of the 0.2-mil minimum film thickness criterion at the 25,000-foot engine-idle condition.

The cooling-air flow path shown in Figure 5 is basically amenable to the journal cooling flow requirements. However, a thorough hydraulic analysis of the flow path was not performed. Such an analysis should be made during the next development phase.

LP-Spool Bearings

The heattransfer results for the HP-spool journal bearings show that essentially isothermal conditions can be obtained in the bearing journals and pads without difficulty. Consequently, nonisothermal bearing calculations were not performed.

BEARING MATERIALS

The following paragraphs summarize existing data relative to structural and coating materials for gas-lubricated journal bearings. The data are discussed in terms of the HP-spool turbine-end bearing since this bearing has, by far, the most severe material problems.

Material considerations are crucial to the success of any gas-bearing application and will be decidedly so with respect to advanced engines of the type being considered here. Very reliable material combinations have been developed which are suitable for temperatures up to 700° or 800°F. These materials have been, and are being, applied to present-day AEC, NASA, and commercial gas-bearing turbomachinery. Laboratory testing and evaluation of materials at 1400°F was started in 1966. A comprehensive summary of the current state of the art for gas-bearing materials is given in Appendix II of this report.

Journal Structural Materials

At sea-level rated-power conditions, average tangential stress in the 3-inch diameter HP-spool journals will be approximately 71,400 psi. It is not yet clear just what the temperature of the turbine-end journal will be since this will depend on how much temperature drop can be taken across the turbine heat dam. For a heat transfer standpoint, however, it appears feasible to design the journal cooling concept to achieve a design-point temperature anywhere in the range of 1200° to 1500°F.

Data pertaining to 100- and 1000-hour rupture strengths of high-temperature nickel-base superalloys and one refractory alloy (TZM) are given in Table X. It is obvious from these data that there is no alloy available today which can operate for 1000 hours at 1500°F under the HP-spool journal-stress conditions. At 1400°F three materials have a 1000-hour rupture strength in excess of 71,000 psi: MAR-M200, IN-100, and TRW-1900. In

TABLE X. RUPTURE STRENGTH DATA FOR SEVERAL HIGH-TEMPERATURE SUPERALLOYS

100-Hour Rupture Strength*					
Alloy	(psi x 10 ⁻³)				
	1200°F	1300°F	1400°F	1500°F	1600°F
IN 100-cast	—	—	91	73	55
713 C-cast	—	—	83	60	43
MAR-M200-cast	—	—	94	72	58
TRW 1900-cast	—	107	90	74	57
Udimet 700-bar	—	98	79	58	42
Rene 41-bar	—	96	64	38	23
TZM** cast	78	—	72	—	71

1000-Hour Rupture Strength*					
Alloy	(psi x 10 ⁻³)				
	1200°F	1300°F	1400°F	1500°F	1600°F
IN 100-cast	—	—	75	55	37
731 C-cast	—	88	65	44	28
MAR-M200-cast	—	—	84	60	43
TRW 1900-cast	108	91	75	58	43
Udimet 700-bar	102	83	62	43	29
Rene 41-bar	100	74	40	24	14
TZM** cast	74	—	70	—	62

* All data are from Reference 18 except TZM data, which were obtained from Reference 19.

** TZM would, of course, have to be coated to prevent rapid oxidation at the temperatures listed above.

an actual engine application, however, it is obvious that the 1000-hour stress-rupture value cannot be used as a design criterion when 1000 hours of reliable bearing life are required. Hence, of the above-mentioned three materials, only MAR-M200 might have a chance of being a satisfactory journal material for a 1000-hour life requirement.

If 100 hours of life could be considered acceptable for the HP-spool turbine-end journal, then MAR-M200, IN-100, and TRW-1900 might all be adequate for 1400^oF service.

If journal operating temperature were held at 1300^oF or less, the above three materials would almost certainly be acceptable, from a stress standpoint, for 1000 hours of reliable bearing operation.

In summary, superalloys are presently available which can meet the HP-spool journal-stress requirements for a 1000-hour life if journal temperature does not exceed 1300^oF. For a 1400^oF journal temperature, the life requirement would probably have to be reduced to 100 to 200 hours. MAR-M200 appears to be the most promising candidate material, with IN-100 and TRW-1900 next in preference.

As pointed out in Appendix II, adequate high-temperature strength, while being a necessary material requirement, is not in itself sufficient to assure satisfactory gas-bearing operation. Other material characteristics which have a direct influence on gas-bearing feasibility and design are:

1. Dimensional stability
 - a. Metallurgical variations or changes
 - b. High-temperature creep
2. Corrosion and erosion resistance
3. Compatibility of thermal expansion rates
4. Sliding compatibility under both start and stop conditions and during high-speed contacts
5. Fabrication procedures
6. Thermal conductivity

Each of the above aspects is discussed in detail in Appendix II.

Initial testing of gas-bearing materials in air at 1400^oF has been accomplished with encouraging results. This work is described in Appendix II. However, the testing was performed using a 1.5-inch-diameter test journal at speeds to 30,000 rpm. Since resulting journal stresses were low, Hastelloy X was used as the journal structural material because of its good oxidation resistance. Hastelloy X cannot be considered for

the present HP-spool journal. Accordingly, there are no experimental data at the present time for any of the potentially suitable superalloys with respect to (1) dimensional stability and (2) corrosion and erosion resistance for gas-bearing applications. As pointed-out in Appendix II, the data that do exist for superalloys have been obtained with respect to high-temperature turbine requirements. These data are not sufficient or detailed enough for gas-bearing design purposes. It will be mandatory that test data be obtained for the candidate superalloys at operating conditions of the HP-spool turbine-end journal before a final decision as to immediate or near-future feasibility of gas bearings for advanced aircraft engines can be made.

Journal Coating Materials

None of the superalloys which are candidate structural materials for the HP-spool bearings have good sliding compatibility. For this reason, surface coatings will be required. An additional advantage of coatings which has been observed is their apparent ability to provide an increased measure of corrosion protection for the structural material.

The status of coating experience is discussed in detail in Appendix II. In brief, one series of tests has been performed at 1400^oF in air. Both start-stop sliding tests and momentary-contact tests at 30,000 rpm have been performed. Results have been encouraging. However, it is clear that much coating development and testing will still be required before high-temperature gas bearings can be applied to advanced aircraft engines. Development and testing of high-temperature coatings are equally as important as testing of the journal structural materials.

Pad, Pivot, and Flexure Materials

Stresses in the pads will be less severe than those in the journals. Accordingly, if a satisfactory structural material can be found for the journals, the same material can be used for the pads.

The bearing surfaces of the pads will also have to be coated for good sliding compatibility. This is discussed in Appendix II.

Two pivot material combinations have been tested at 1400^oF in argon with very good results. Hertzian contact stress during these tests was 200,000 psi. Tests were conducted for 12 hours at a fretting frequency of 1000 hertz. The test program is described in Reference 20 and summarized in Reference 21. The two pivot material combinations were as follows.

1. Titanium carbide (Kennametal 162 B) ball and flat
2. Stellite Star J flat and a Stellite 19 ball

The titanium-carbide combination is preferred from a high-temperature

strength standpoint. However, there is a significant difference between the thermal expansion coefficients for titanium carbide and for the various superalloys from which the pads and pivot screws would be made. Consequently, a detailed design study would be required to determine if the ball and socket elements of the pivot could be reliably attached to the structural materials of the bearing.

Differential thermal expansions would not be a problem with a stellite pivot combination, since the expansion coefficient of stellite is similar to those of the superalloys. However, the high-temperature strength of stellite is not as high as that of titanium carbide. Nonetheless, there was no significant difference in the 12-hour test results at 1400° F for the titanium carbide and stellite pivots at a 200,000-psi stress level. Since nominal pivot-contact stresses can be held to the order of 125,000 psi in the gas-generator bearing design, the stellite material may be satisfactory.

It is the opinion of MTI's material technologists that both titanium carbide and stellite should perform satisfactorily in air at 1500° F for a 1000-hour period. Again, however, test data must be obtained to confirm this opinion before a final feasibility assessment can be made relative to application of pivoted-pad journal bearings to advanced high-temperature engines.

With respect to flexure materials, the HP-spool turbine-end journal flexures will operate under the most severe combination of temperature and stress conditions. Under normal 1-g bearing loads, these flexures will be deflected approximately 10 mils. Under maximum bearing loads, deflection of the loaded flexures will increase to 13 mils, at which point the flexure stops will prevent any further deflection.

At the maximum 13-mil deflected position, the maximum bending stress in the flexure will be 60,000 psi. Under normal 1-g load conditions, the mean maximum bending stress will drop to 46,000 psi. However, under normal conditions there will be a small amount of once-per-rev dynamic flexure motion due to residual shaft unbalance. A very conservative allowance of ± 1.0 mil was used to establish a dynamic (fatigue) stress requirement for the flexures.

Accordingly, under normal 1-g load conditions, a cyclic flexure stress condition of 41,400 to 50,600 psi was established. At maximum bearing load conditions a static stress of 60,000 psi was defined.

Design plots of alternating stress versus mean stress for combined conditions of fatigue and creep were constructed using the method of Tapsell [22]. The reversed bending (zero mean stress) endurance stress was assumed to be 40 percent of the ultimate tensile stress at the temperature of interest. This value was plotted as the ordinate-axis intercept. The abscissa intercept was taken as the 1000-hour creep-rupture strength, also at the temperature of interest. A straight line was then used to connect these two points. This procedure for constructing allowable stress curves under combined conditions of fatigue and creep has so far been found to

be conservative.

Stress curves were constructed for several of the superalloys at 1200°F and 1400°F. If flexure temperature can be held at or below 1200°F, which is felt to be a realistic goal, either Rene 41 or Udimet 700 alloy would provide a high margin of safety under the imposed flexure stress conditions. If flexure temperature should fall in the 1300° to 1400°F range, MAR-M200 would provide the best strength properties, with IN-100 a close second. These materials would have about a 20-percent margin of safety. However, since the allowable stress curves were based on 1000-hour creep-rupture data, testing of the flexures would be required to determine if a 20-percent safety margin would be sufficient at 1400°F.

Since it should be possible to maintain flexure temperatures at 1200°F or less, flexure stresses do not appear to be a problem.

THRUST BEARING DESIGN STUDIES

The term "thrust bearing" as used in this report connotes the capability to carry only unidirectional loads acting parallel to (and usually coincident with) the axis of a shaft. In the gas generator, axial thrust loads can act in either direction depending upon the engine's operating condition. Consequently, four thrust bearings are required, two each for the HP and LP spools.

Like the journal bearings, analysis and design of the thrust bearings progressed in parallel with the rotor-bearing system design layouts. In the interest of brevity, only final results of the thrust bearing studies are presented here. It should again be noted that the word "final" is not meant to connote fully optimized bearing designs, but rather that the results permit conclusions to be drawn pertaining to feasibility of gas-lubricated thrust bearings for the gas-generator application.

THRUST BEARING LOADS

The first step in the thrust bearing design study was to establish thrust loads as a function of gas-generator operating conditions. The total load acting on a given bearing arises from two independent types of forces: (1) differential pressure forces resulting from pressure gradients generated by, or imposed upon, the aerodynamic components, and (2) inertia force reactions resulting from the various acceleration rates specified on the Operating Load Diagrams of Figure 12. Accurate prediction of the maximum resultant thrust loads for all possible gas-generator operating conditions would clearly have been a difficult and costly task, particularly since the design layout of the gas generator was continually being revised up to the conclusion of the feasibility study. Accordingly, only four operating conditions were selected for calculation of thrust loads: rated power and engine idle at sea level, and rated power and engine idle at 25,000 feet altitude. Straight-line plots, obtained by joining the rated-power and engine-idle points, were then used to define thrust load as a function of output power. The nature of the thrust-bearing load capacity curves gives reasonable assurance that this simplified procedure for defining the applied load curves is adequate for the purpose of establishing thrust bearing feasibility. However, if actual development of a gas-bearing gas generator is undertaken in the future, the nature of the applied thrust loads should be more accurately determined as a function of engine power.

Aerodynamic Loads

The net aerodynamic thrust loads acting on the HP and LP spools result from (1) pressure forces acting on the compressor and turbine discs and (2) blade pressure forces. Blade forces for the LP-spool axial turbine and compressor stages, and the blade-side disc forces for the HP-spool radial turbine and compressor impellers, were calculated during the aerodynamic analysis phase. The procedures used to calculate these forces are explained in Appendix I.

LP-spool blade forces are plotted as a function of shaft horsepower in Figure 79. Disc forces for the HP-spool components are plotted in Figure 80.

The differential pressure force acting on each of the various turbine and compressor discs is a function of the location of compressor and turbine seals. Net aerodynamic thrust acting on a complete spool assembly is therefore also a function of the seal locations. Because of the continual changes to the gas-generator layout drawing during the design evolution process, it was impractical to attempt a thorough analysis of optimal seal locations based on rigorous calculation of differential pressure forces. Instead, it was hypothesized that the seal systems, with augmentation from thrust balance pistons if necessary, could be designed to achieve nearly complete balancing of the aerodynamic forces at one condition of engine operation. Sufficient study was then made of each spool to confirm that at least one completely balanced condition could be theoretically achieved. When, as with the LP spool, it became apparent that one of several operating conditions could be selected for the fully balanced condition, sufficient study was then made to determine which condition should be selected such that thrust loads over the remaining range of engine operation would be acceptable.

It was realized, of course, that perfect balance could never be obtained in practice and that it would be necessary to define a tolerance for the "balanced" condition. This tolerance was defined to be 4 percent of the maximum aerodynamic force component (per spool) acting in any one direction. To illustrate the application of this tolerance, consider the case of the HP spool. It was established that this spool should, and could, be balanced at sea-level rated-power operation. Approximate locations for the seals were defined, and the aerodynamic force components were calculated for sea-level rated-power operation. These were found to be 5,000 pounds toward the turbine and 4,976 pounds toward the compressor. The two forces were thus theoretically balanced within 24 pounds. However, application of the thrust balance tolerance gave a possible thrust load variation equal to 4 percent of 5,000 pounds, or 200 pounds. The maximum applied aerodynamic thrust load was therefore defined to be 224 pounds, and was assumed to act in either direction.

With respect to the LP spool, it was found that the aerodynamic loads could also be balanced at sea-level rated-power conditions using a simple seal system. However, calculated values of thrust load at idle speed were found to be considerably higher than the load that could be supported by a practical thrust bearing. Accordingly, a thrust balance piston was added to the turbine end of the shaft with one face vented to atmospheric pressure and the opposite face exposed to bearing cavity pressure. The balance piston is clearly seen at the right-hand end of the LP spool in Figure 2. With the balance piston in place and seal locations approximately defined, the calculated aerodynamic force components at sea-level idle were 420 pounds toward the compressor and 387 pounds toward the turbine. The two forces were thus theoretically balanced within 33 pounds. However, application of the thrust balance tolerance gave a possible thrust load variation equal to 4 percent of 420 pounds, or 17 pounds. The maximum applied aerodynamic thrust load was thus defined to be 51 pounds and was also assumed

to act in either direction.

Having established the "balanced condition" seal arrangements and aerodynamic thrust loads for the HP and LP spools, thrust loads at the remaining conditions of engine operation were determined as follows: The maximum applied aerodynamic thrust load was taken to be either 4 percent of the maximum aerodynamic force component acting in any one direction, or the actual value of calculated unbalanced aerodynamic force, whichever was greater.

A brief study was made to see if it would be advantageous to purposely introduce an aerodynamic bias force to ensure that maximum values of thrust load would always act in one direction. In this way the need for a second thrust bearing for each spool would be greatly reduced, perhaps to the point of requiring only a bumper bearing to handle any small reversals of thrust such as might occur during engine startup and shutdown. It was found, however, that maximum thrust loads would be appreciably higher in this case and would require a significant increase in bearing diameter. Since thrust bearing friction losses increase as the fourth power of diameter, the increased problems of heat transfer and thermal distortion were severe. The trade-off thus favored two small bearings designed to handle the smaller bidirectional thrust loads.

A final comment is in order at this point about the 4-percent tolerance figure used in the procedure for establishing maximum aerodynamic thrust loads. Traditionally, the problem of achieving satisfactory balance of aerodynamic forces in gas-bearing machinery has been a difficult one because of the reduced load capacity of gas bearings relative to oil-film and rolling-element bearings. In terms of normal machinery design practice, the 4-percent tolerance factor is low. A 10-percent tolerance would be more representative.

For the present study, the 4-percent tolerance factor was selected to favor the thrust bearings at engine-idle conditions. Because of the low air pressures available at idle, thrust bearing load capacity is severely reduced. However, above 50 percent of rated engine power, a 6-percent tolerance factor could have been used. For comparison, the largest gas-bearing turbocompressor built to date (50 gas horsepower, Reference 16) has been operated at thrust loads equal to 5 percent or less of the maximum aerodynamic force component. Thus, although the aerodynamic thrust balancing requirements for gas-bearing machinery are stringent, they have not, to date, proven impractical. However, particular effort is demanded in the design of the aerodynamic components to ensure that the basic aerodynamic forces are kept as small as possible.

Inertia Loads

The gas-generator operating load diagrams of Figure 12 were used to calculate the maximum thrust bearing inertia loads due to the various simultaneously acting acceleration rates. However, since the journal bearing span was large relative to the thrust bearing diameter, it was assumed that the gyroscopic, side, and yaw accelerations would not impose any loads on the

thrust bearings. These loads would be carried entirely by the journal bearings.

HP-Spool Total Thrust Loads

The calculated aerodynamic and acceleration thrust load components, as well as the combined total thrust loads, for the HP spool are tabulated in Table XI for the three different flight conditions. Positive values of load may be interpreted as acting toward the turbine; negative values, acting in the opposite direction. However, since the aerodynamic loads may actually occur in either direction, depending on where a particular engine operates within the plus and minus tolerance band for thrust balance, it has been assumed that the combined total loads may also act in either direction.

Based on the data of Table XI, straight-line plots of maximum applied thrust load were drawn for the HP spool as a function of gas-generator output power. The plots for sea-level landing and sea-level flight conditions are shown in Figure 40. The 25,000-foot-altitude flight condition is shown in Figure 41. Since it was assumed that the maximum applied loads may act in either direction, only the absolute values of thrust load are plotted.

LP-Spool Total Thrust Loads

The calculated aerodynamic and acceleration thrust loads, as well as the combined total thrust loads, for the LP spool are also tabulated in Table XI for the three different flight conditions. Based on the data of Table XI, straight-line plots of maximum applied thrust line were drawn for the LP spool as a function of gas-generator output power. The plots for sea-level landing and sea-level flight conditions are shown in Figure 42. The 25,000-foot-altitude flight condition is shown in Figure 43.

Because of the effect of the LP-spool thrust balancing piston, definite directions can be ascribed to the various total load values. This means that the two LP-spool thrust bearings probably do not have to be the same size. However, this possibility was not studied in detail. For feasibility purposes, it was assumed that the total loads could act in either direction and that both bearings should therefore be the same size. Consequently, only the absolute values of thrust load are plotted in Figures 42 and 43.

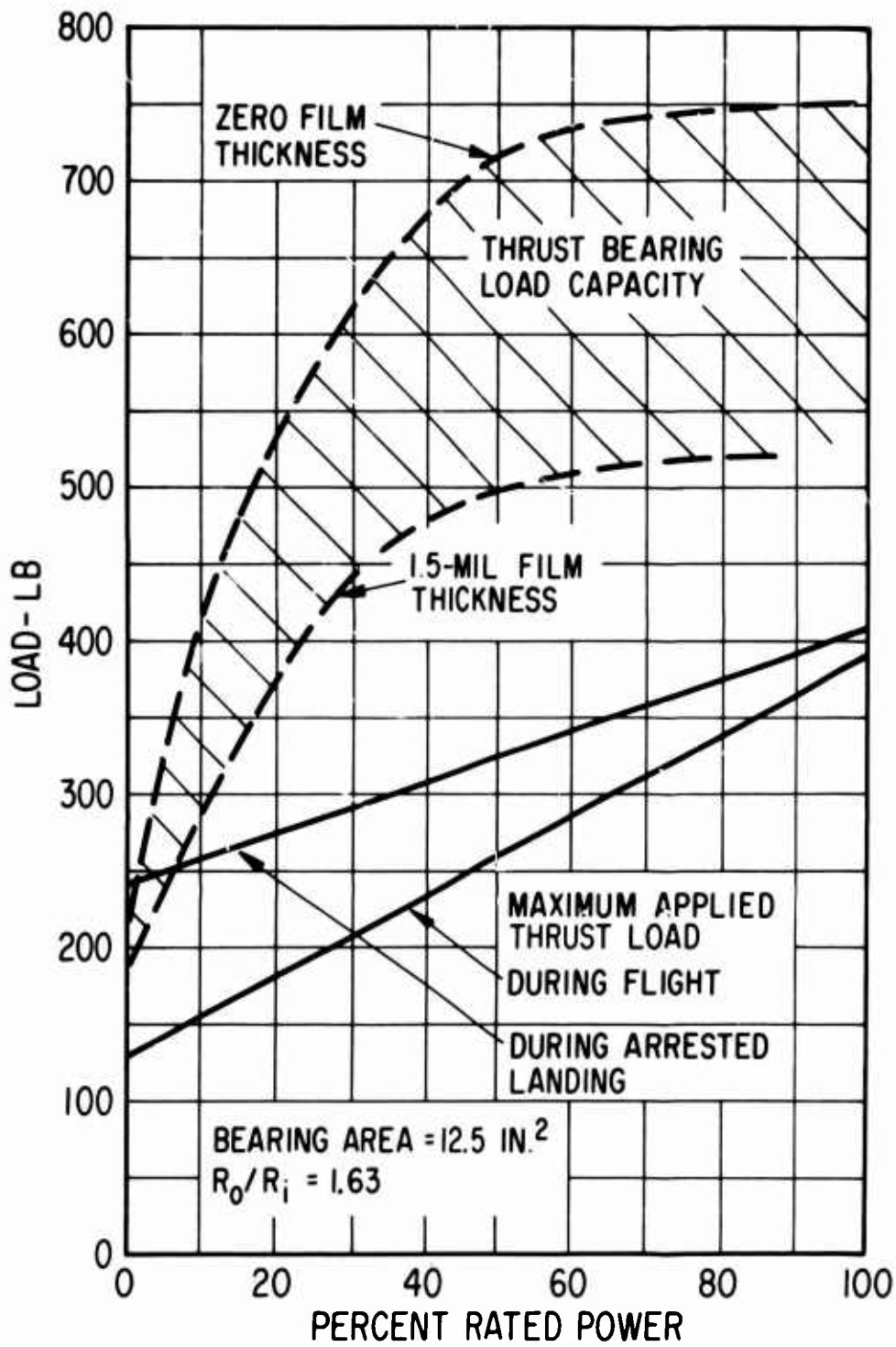


Figure 40. Maximum Applied Thrust Loads and Thrust Bearing Load Capacity for the HP Spool at Sea-Level Flight and Landing Conditions.

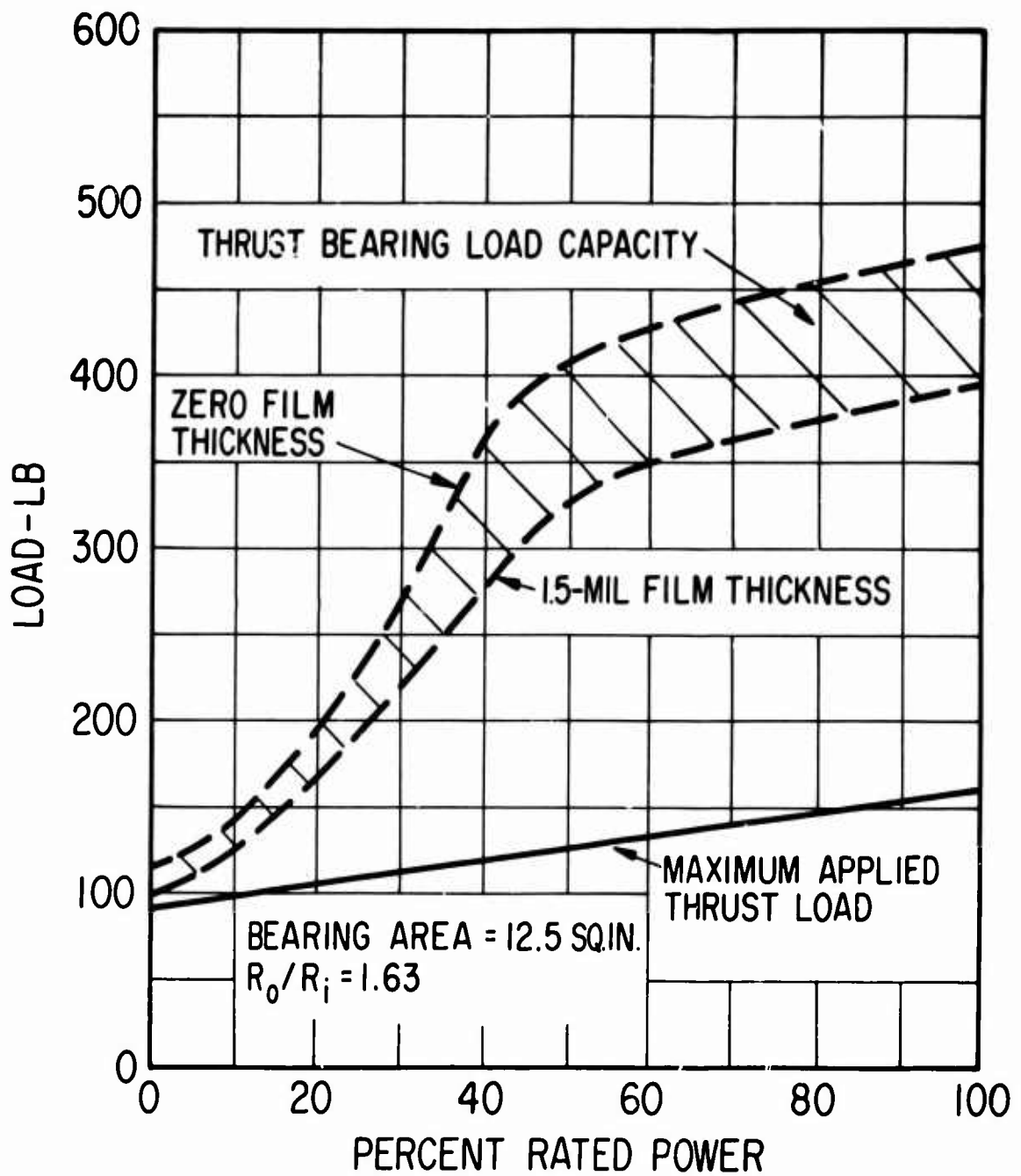


Figure 41. Maximum Applied Thrust Loads and Thrust Bearing Load Capacity for the HP Spool at a 25,000-Foot Altitude.

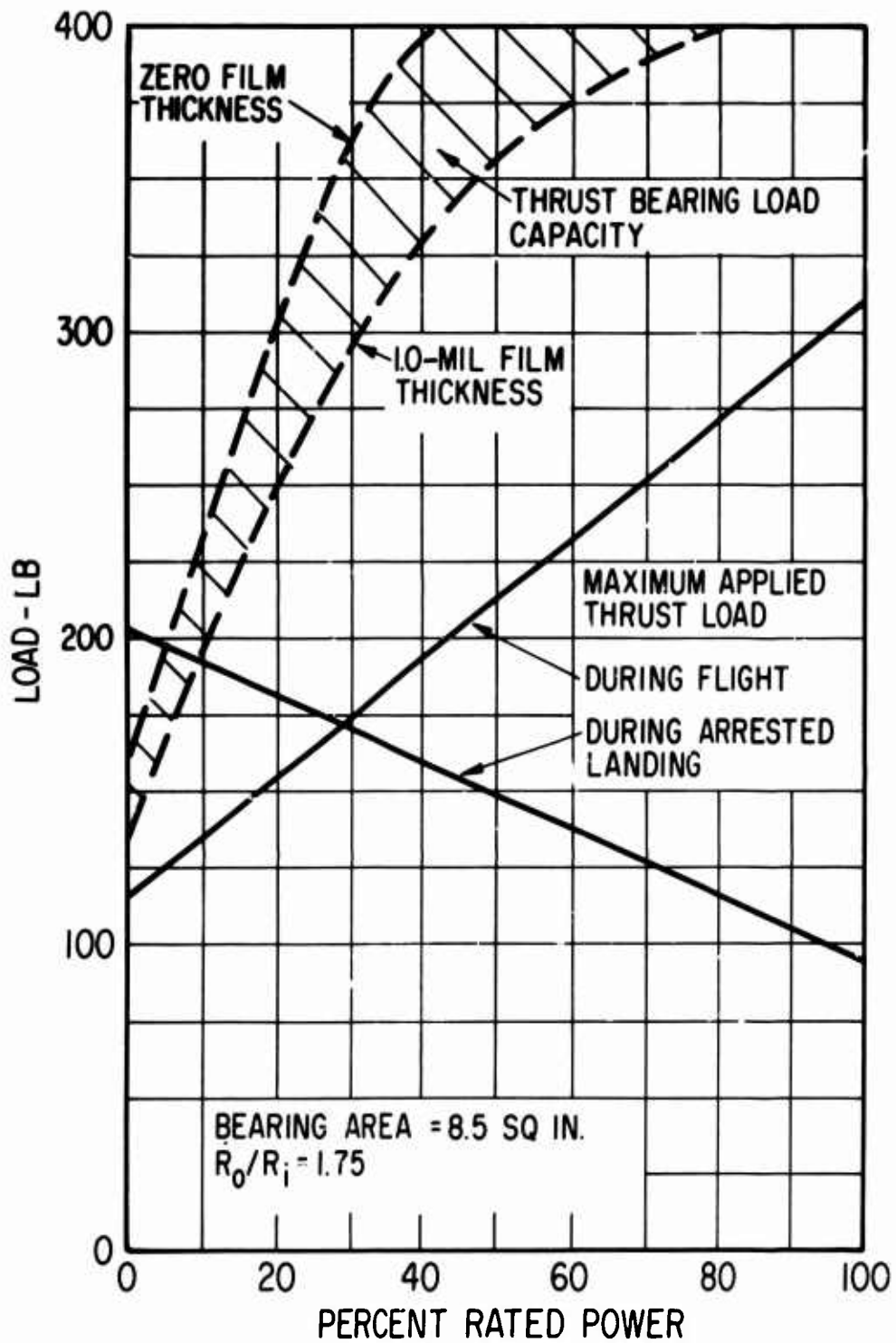


Figure 42. Maximum Applied Thrust Loads and Thrust Bearing Load Capacity for the LP Spool at Sea-Level Flight and Landing Conditions.

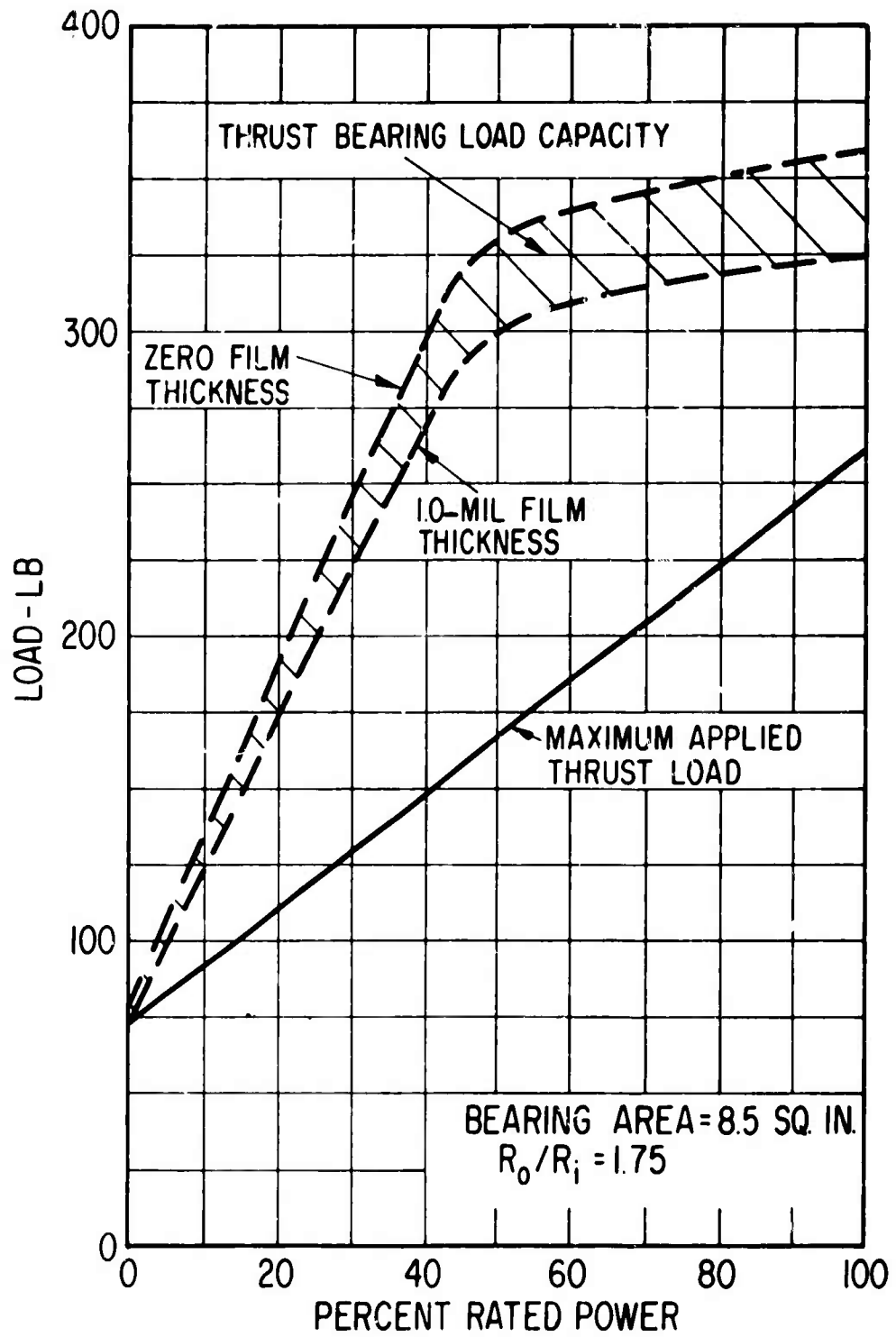


Figure 43. Maximum Applied Thrust Loads and Thrust Bearing Load Capacity for the LP Spool at a 25,000-Foot Altitude.

TABLE XI. MAXIMUM APPLIED THRUST BEARING LOADS

Flight Condition	Percent of rated engine power	HP-Spool Loads (lb.)		LP-Spool Loads (lb.)	
		Aerodynamic Acceleration	Total	Aerodynamic Acceleration	Total
Sea-level landing	0	± 53	-185	± 50	-155
	100	±224	-185	+249	-155
Sea-level flight	0	± 53	± 74	± 50	- 62
	100	±224	±166	+249	+ 62
25,000-foot altitude flight	0	± 18	± 74	± 11	- 62
	100	± 88	± 74	+217	+ 46
Minus forces are directed from the turbines toward the compressors. Plus forces are oppositely directed.					

SELECTION OF THRUST BEARING TYPE

Thrust bearings may be grouped into three general categories:

1. Self-acting (hydrodynamic)
2. Externally pressurized (hydrostatic)
3. Hybrid (a combination of self-acting and externally pressurized)

Within each category there are many possible variations [23]. Accordingly, an initial screening study was performed to determine which types of thrust bearings were best suited for the gas-generator application.

Survey of Self-Acting Thrust Bearings

A brief investigation was made of the three most frequently used self-acting types of thrust bearings: the spiral-grooved, the stepped, and the pivoted-pad bearings. On the basis of equal bearing size, equal values of minimum film thickness, and optimum bearing geometry, it was found from design data given in Reference 24 that the spiral-grooved bearing had over 1.6 and 2.3 times the load capacity of the stepped and pivoted-pad bearings, respectively, at the sea-level operating conditions of the gas generator. Figure 44 shows a representative spiral-grooved thrust bearing stator. This particular bearing was successfully developed under NASA contract [7] for a small 50,000-rpm (design speed) gas-bearing turbocompressor. An externally pressurized bearing section was also provided in the seal region of the spiral groove pattern to carry very high thrust forces which would occur during injection start of the turbocompressor.

Operating characteristics of the spiral-grooved bearing were examined at the design-speed and idle-speed maximum thrust load conditions of the HP spool. Based on a bearing area of 12.5 square inches, the unit loads at these conditions were 32.8 and 19.2 pounds per square inch respectively. It was found that the bearing could theoretically carry these loads. However, the film thickness at both idle and design speed would be only 0.6 mil. The bearing friction losses would range from 1.6 horsepower at idle to 2.75 horsepower at design speed.

In a self-acting thrust bearing, the amount of gas which is pumped through the clearance space is insufficient for adequate cooling of the bearing. Most of the friction losses must be transferred from the film into the thrust runner and/or stator, and then from these parts into a suitable heat sink. It is inherent in this heat transfer process that some of the heat will be conducted axially through the thickness dimension of the thrust runner and/or stator. Such axial conduction causes thermal crowning of the thrust bearing surfaces, which in turn causes a reduction in thrust bearing film thickness at the inner diameter of the bearing. The amount of thermal distortion and loss of film thickness is dependent upon the amount of heat generated in the film, the actual heat-transfer paths through the runner and stator parts, and the ratios of thermal expansion coefficient

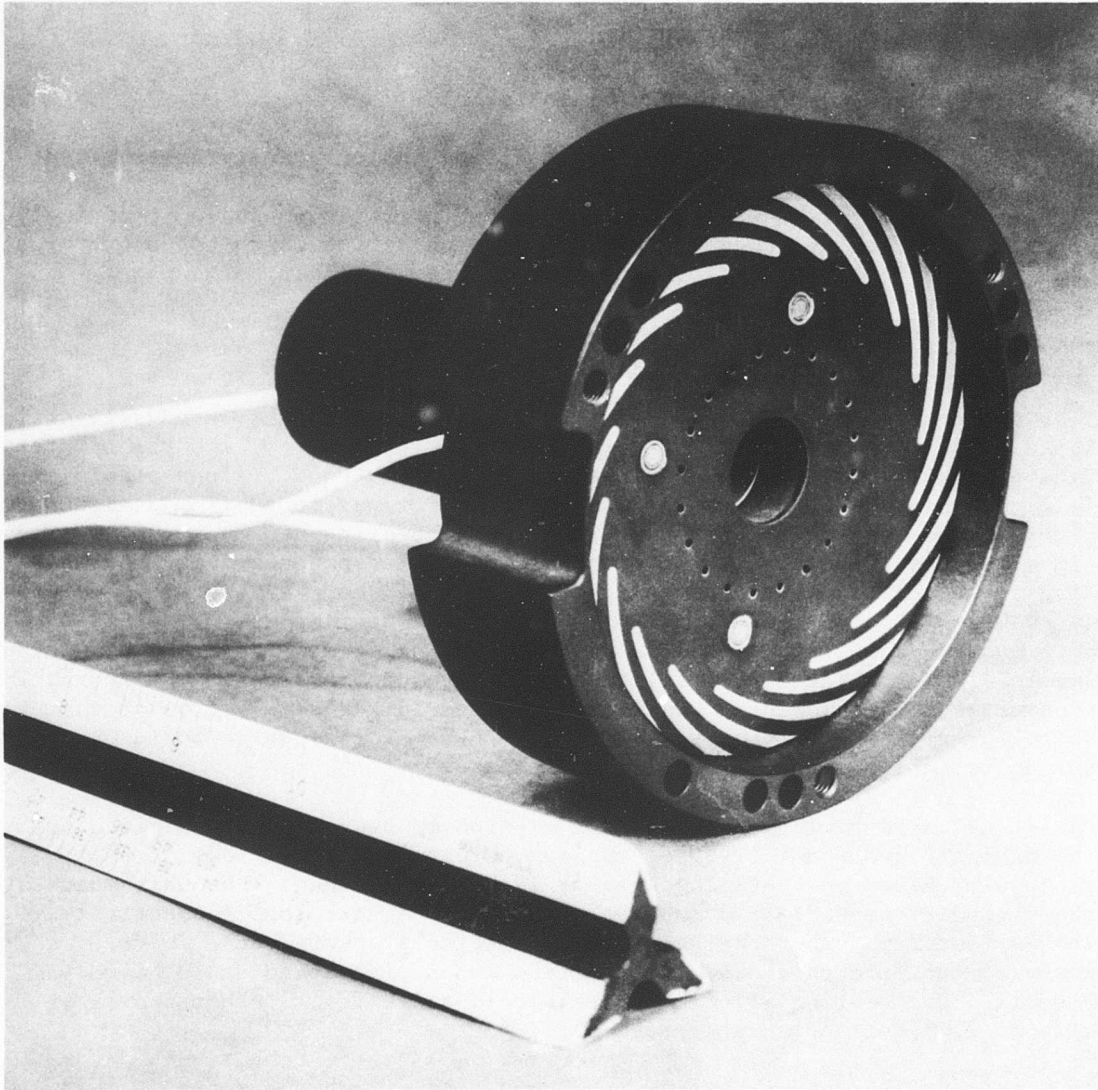


Figure 44. Self-Acting Spiral-Grooved Gas-Lubricated Thrust Bearing Developed for a 50,000 RPM Turbocompressor.

to thermal conductivity coefficient for the bearing materials. The effect of thermal expansion to thermal conductivity ratio on load capacity of spiral-grooved bearings has been theoretically investigated for the case of axial transfer of all bearing losses through the stator [25]. It was shown that when the bearing is made from conventional materials, such as alloy steel or aluminum, the loss in load capacity at small film conditions can be quite significant as a result of the thermal distortions.

- Several gas-bearing machines have been built with spiral-grooved thrust bearings and subjected to careful calibration of bearing load versus film thickness. In all of these tests, it was noted that the measured load capacity was equal to or slightly greater than the calculated capacity at large values of film thickness (that is, at low loads). However, as load on the bearings was progressively increased, a point was always reached where the measured load capacity would start to become smaller than the calculated value. For further increases in load, the deficiency in load capacity continued to increase. The primary reason for the load deficiency was thermal distortion due to increased friction losses at the small film-thickness (high-load) conditions.

Figure 45 shows two curves of film thickness (h) versus load parameter (W^*) based on the above-mentioned test data. One curve applies to liquid-cooled thrust bearings and the other to gas-cooled bearings. The curves are based upon test data from four different bearing designs. The data points represent the most highly loaded operating conditions at which agreement was obtained between measured and calculated (isothermal) load capacity. The region to the left of any given curve thus represents operating conditions at which the measured load capacity would be less than that calculated due to distortion effects.

Returning now to the HP-spool thrust bearing, the values of W^* would be 1145 and 1635 at idle speed and design speed respectively, based on the calculated (nondistorted) 0.6-mil film thickness value. Entering Figure 45 with these values shows that the bearing would be operating very much in the deficit load region. In other words, actual film thickness at maximum load conditions would drop well below 0.6 mil due to thermal distortions. Since, for various reasons, MTI does not consider even a 0.6 mil-film thickness to be practical for a high-speed 5-inch-diameter bearing, it was concluded that self-acting thrust bearings were not feasible for the gas generator.

• Survey of Externally Pressurized Thrust Bearings

In an externally pressurized thrust bearing, the flow of gas through the clearance space is understandably greater than with a self-acting bearing. The gas can therefore materially aid in removing bearing friction losses. Accordingly, initial calculations for an externally pressurized HP-spool thrust bearing were made on the basis of 16 square inches of bearing area. (Throughout the thrust bearing studies, inner diameter of the bearing was maintained the same as the HP-spool journal bearing diameters. This allows the thrust stators to be made in one piece, and greatly simplifies fabrication and assembly of the rotor-bearing system parts.) Supply pressure for

	N-RPM	R ₀ -IN.	R _i -IN.	Λ _c	STATOR COOLED BY	REF
▼	20,300	3.31	1.4	8.6	GAS	[]
●	13,300	2.687	1.125	5.3	GAS	[]
■	17,500	"	"	6.3	GAS	[]
▲	50,400	1.625	0.69	14.6	LIQUID	[]
×	30,100	"	"	10.5	LIQUID	[]
◆	12,000	3.5	1.4	15.1	LIQUID	[]

NOTE: ALL BEARINGS COOLED BY AXIAL HEAT TRANSFER THROUGH AN ALUMINUM STATOR

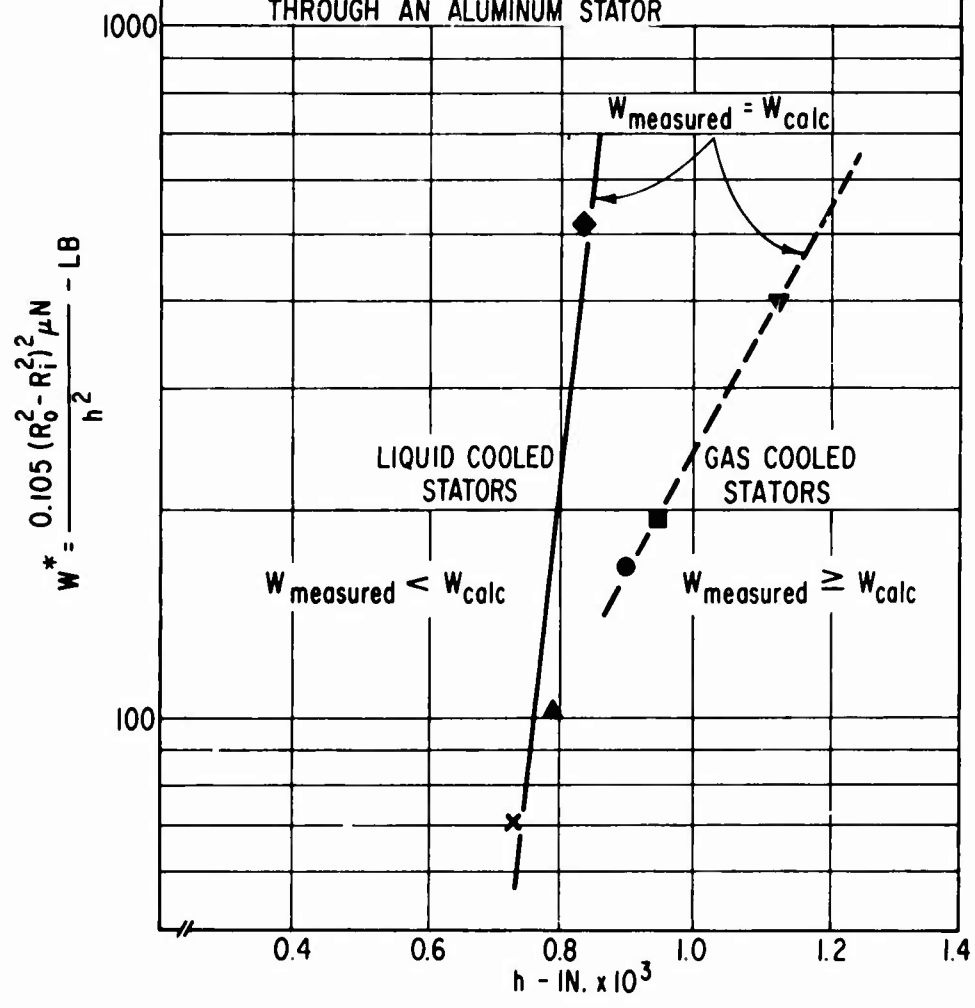


Figure 45. Experimentally Determined Performance Map for Self-Acting Spiral-Grooved Gas-Lubricated Thrust Bearings Showing Region of Agreement Between Predicted (Isothermal) and Measured (Nonisothermal) Load Capacity.

the bearing was assumed to be discharge pressure from the HP-spool compressor. Bearing ambient (or discharge) pressure was assumed to be atmospheric pressure (i.e., LP-spool compressor inlet pressure). In this way, maximum available differential pressure from the gas generator was made available to the thrust bearing.

Briefly stated, results of the survey calculations showed that externally pressurized thrust bearings could not carry the maximum applied thrust loads at sea-level conditions using available supply pressure from the HP compressor. At 25,000 feet altitude, a film thickness of 1.0 mil could be achieved for gas-generator output power levels in excess of 15 percent of rated power. At idle conditions, however, the bearing again could not carry the maximum thrust load.

Calculations for the LP-spool thrust bearings, using a bearing area of 8.5 square inches, showed the same results as for the HP-spool bearings. LP-spool bearing area was limited by the size of the LP-compressor discs, since these discs represented the most logical location for the thrust bearings.

Study of the load capacity problem revealed that the bearing supply pressure would have to be boosted by a factor of approximately 1.7 to achieve satisfactory film thickness at engine idle conditions. Without a pressure boost, the concept of gas-lubricated thrust bearings for the gas generator is not feasible unless some means for obtaining even better balance of the aerodynamic and acceleration thrust forces is found. Accordingly, a review was made of ways in which the required pressure boost might be obtained. The most promising approach appears to be incorporation of a small regenerative boost compressor as an integral part of the HP-spool assembly. Figure 2 shows a regenerative compressor incorporated on the back side of the HP-compressor impeller. The compressor is drawn to accurate scale for supplying pressurized gas to the HP and LP-spool thrust bearings. A description of the regenerative compressor concept, and an initial analysis of its application to this requirement, is given in Appendix V. It need only be stated here that regenerative compressors have been very successfully developed by MTI for several specialized applications and one commercial production application. The technology of this compressor is reasonably well developed, although improvements are still being made.

DESIGN OF THRUST BEARINGS

Based on the assumption that a regenerative boost compressor would be incorporated into the HP-spool assembly, a detailed design study of externally pressurized thrust bearings was made for both the HP and LP spools. It was assumed that the pressure-boost factor for the regenerative compressor would vary from 1.7 to 1.5 as engine power was increased from zero to rated power at sea-level conditions.* At 25,000 feet altitude, a variation in pressure boost from 1.7 to 1.4 was used. Subsequent analysis

*Pressure-boost factor is the pressure ratio across the regenerative compressor.

of the regenerative compressor (see Appendix V) indicated that these pressure-boost assumptions should be conservative estimates of the compressor performance. Adequate margin should therefore exist in the concept of the thrust bearing system to account for such practical matters as pressure drop in the feed lines between the regenerative compressor and bearings, and pressure losses due to valves or actuators if a thrust bearing flow-control system is required.

The regenerative compressor will, of course, be effective only when the HP spool is rotating. If engine startup is accomplished using a mechanical drive system as described on page 28, it will be necessary to pressurize the thrust bearings from an external source of air, such as an auxiliary compressor, a pressurized bottle, or bleed flow from another engine or APU. However, if an air-start system is used, it may be feasible to accomplish startup without an auxiliary pressure source (assuming, of course, that the engine is oriented horizontally). This would depend upon the low-speed pressure-rise characteristic of the regenerative compressor and the magnitude of the air-start thrust loads. If the loads are sufficiently small, and the low-speed pressure rise is sufficiently high, it may be possible to achieve gas-film lubrication during most of the startup interval. Technical feasibility of this approach would have to be established by a detailed design analysis. Practical feasibility would depend on the availability of bearing surface coatings which could survive brief periods of possible sliding contact without damage. As discussed in Appendix II, considerable data already exist which indicate that this latter requirement can be satisfied.

One point is clear: There is a strong interaction between the thrust bearings and the method of engine startup. Method of startup in turn interacts with aircraft operational and accessory requirements. The question of startup technique must be carefully considered from all points of view in any future specification for a gas-bearing gas generator. Additional study would be required to clearly establish which startup technique, if any, would be most compatible with the particular engine application.

HP-Spool Thrust Bearings

Procedures and design data given in Reference 24 were used to design the HP-spool thrust bearings. Although two bearings are needed, they have identical load capacity requirements. Only one bearing design study was therefore performed.

Several design iterations were required to establish a satisfactory bearing size. The first design was based on a bearing area of 16 square inches. The design had high load capacity, but also high friction loss — approximately 3 horsepower. This amount of heat generation could not be adequately removed via gas flow through the bearing.

Bearing area was next reduced to 11 square inches. Because of the fourth-power effect of bearing radius, removal of friction losses was not a problem. However, bearing load capacity was slightly low. The final design

thus converged to an area of 12.5 square inches.

The thrust bearing design was optimized at engine idle conditions, this having been identified as the most severe operating condition for the bearing. The following design parameters were established:

- Number of feeding holes (n): 40
- Radius of feeding holes (a): 0.030 in.
- Inner radius of bearing (R_i): 1.55 in.
- Outer radius of bearing (R_o): 2.53 in.

Bearing load capacity was calculated as a function of engine power for two film thickness conditions; 1.5 mils and essentially zero film. The 1.5 mil value was selected as being a very practical film thickness and one which should have ample margin for thermal distortion effects. The zero film calculation gave a measure of load capacity margin. The load capacity calculations accounted for the fact that an opposed thrust bearing configuration would be used; that is, the net load capacity would be the difference in pressure forces acting on the two faces of the thrust runner.

Results of the load capacity calculations at sea level and a 25,000-foot altitude are plotted in Figures 40 and 41 respectively. It is seen that with one exception, the bearing can carry the maximum imposed loads at all conditions with a film thickness of 1.5 mils. The one exception is the condition of arrested landings at less than 10 percent engine power. The bearing cannot carry the maximum arresting load unless engine power is maintained at 10 percent or more of rated power.

Figures 40 and 41 show that the thrust bearing has considerable excess load capacity when the engine is operated above 24 percent of rated power. Therefore, it did not seem reasonable to strive for increased load capacity at the arrested-landing low-engine-power condition. Rather, it is suggested that the engine operating manual be written to favor this condition. Specifically, for arrested landings the engine must be operated at not less than 15 percent of rated power during the brief period of maximum arresting deceleration.

The catapult launch condition presents no problem since it is already specified that the engine will be operating at maximum power during launch.

Pertinent operating characteristics of the HP-spool thrust bearings are summarized in Table XII. It is seen that maximum air flow through the loaded bearing will be approximately 0.4 percent of rated engine flow. Since this flow is vented to atmosphere, there is no way in which it can be utilized for other than thrust bearing cooling purposes. The unloaded thrust bearing would, of course, operate at a much larger clearance, depending on the total axial float in the thrust bearing assembly. Air flow through the unloaded bearing would therefore be much higher, perhaps to the point of choked flow through the feeding holes. Such large flow is

TABLE XII. PERFORMANCE DATA FOR THE HP-SPOOL THRUST BEARINGS

Regenerative Compressor										Bearing Performance*		
Percent of Rated Engine Power	P _{in} (psia)	P _{out} (psia)	T _{in} (°F)	T _{out} (°F)	Shaft Speed (rpm)	h (mils)	μ $\left(\frac{\text{lb-sec}}{\text{in.}^2} \times 10^9 \right)$	Λ _s	W ^{**} (lb)	Q (lb/sec)	Friction (hp)	
												Sea Level
0	36	61	460	860	49,000	1.5	3.88	3.6	180	0.0036	0.67	
20	90	144	540	940	59,000	1.5	4.11	1.67	373	0.012	0.75	
50	130	195	790	1190	66,000	1.5	4.7	1.51	500	0.017	1.26	
100	130	195	890	1290	70,000	1.5	5.1	1.71	520	0.014	1.54	
25,000-Foot Altitude												
0	18	30.6	290	690	45,000	1.5	3.35	5.77	100	0.0015	0.45	
10	30	48	415	815	50,000	1.5	3.75	4.36	172	0.0043	0.64	
50	78	117	540	940	60,000	1.5	4.15	2.07	330	0.0084	0.91	
100	117	165	665	1065	64,500	1.5	4.5	1.65	398	0.013	1.16	

* Performance data pertains to loaded thrust bearing only.

** W is net load capacity for the double-acting thrust bearing arrangement.

basically undesirable: first, because it may impose an excessive performance penalty on the engine; second, because it may excessively cool the unloaded face of the thrust runner thus causing it to thermally distort. To alleviate both of these problems, it may be desirable to have a control system which can automatically reduce flow through the unloaded bearing.

LP-Spool Thrust Bearings

The LP-spool thrust bearings were designed in the same manner as the HP-spool bearings. The design was optimized at engine idle conditions, and the following design parameters were established:

Number of feeding holes (n): 20

Radius of feeding holes (a): 0.012 in.

Inner radius of bearing (R_i): 1.2 in.

Outer radius of bearing (R_o): 2.05 in.

Bearing load capacity was calculated as a function of engine power for two film thickness conditions: 1.0 mil and essentially zero film. Because of the smaller diameter and smaller friction losses relative to the HP-spool bearings, a 1.0-mil film thickness was felt to be practical for the LP-spool thrust bearings.

Results of the load capacity calculations at sea level and 25,000 feet are plotted in Figures 42 and 43 respectively. It is again seen that the arrested landing condition at less than 10 percent rated power is the only condition at which the bearing could not carry the applied loads. However, as with the HP spool, this problem can be overcome by specifying that the engine be operated at not less than 15 percent of rated power during the arresting action.

Pertinent operating characteristics of the LP-spool thrust bearings are summarized in Table XIII. It is seen that maximum air flow through the loaded bearing would be approximately 0.07 percent of rated engine flow. This is less than 20 percent of the flow through the loaded HP-spool bearing. The problem of excessive flow through the unloaded bearing will likewise be greatly reduced relative to the HP-spool bearing.

Thrust Bearing Thermal Analysis

Extensive calculations of temperatures in the thrust bearing regions using multinode thermal models were not performed. Rather, a simplified and conservative approach was used to estimate temperature rise of the thrust bearings. It was assumed that all thrust bearing friction losses would be removed by air flows emanating from the bearings and from labyrinth seals associated with the bearings. This approach neglected any heat transfer

TABLE XIII. PERFORMANCE DATA FOR THE LP-SPOOL THRUST BEARINGS

Regenerative Compressor		Bearing Performance*									
Percent of Rated Engine Power	P _{in} (psia)	P _{out} (psia)	T _{in} (°F)	T _{out} (°F)	Shaft Speed (rpm)	h (mils)	$\mu \left(\frac{\text{lb-sec}}{2 \text{ in.}} \times 10^9 \right)$	Λ_s	W ^{**} (lb)	Q (lb/sec)	Friction (hp)
0	36	61	460	860	25,100	1.0	3.88	6.0	132	0.001	0.1
20	63	144	540	940	32,600	1.0	4.11	3.8	250	0.0016	0.17
50	130	195	790	1190	52,000	1.0	4.7	2.37	360	0.0023	0.52
100	130	195	890	1290	62,800	1.0	5.1	3.1	415	0.0031	0.82
25,000-Foot Altitude											
0	18	30.6	290	690	22,500	1.0	3.35	9.0	72	0.0004	0.07
10	30	48	415	815	27,300	1.0	3.75	7.2	121	0.0006	0.15
50	78	117	540	940	40,000	1.0	4.15	3.5	300	0.0027	0.27
100	117	165	665	1065	48,000	1.0	4.5	3.2	324	0.0033	0.42

* Performance data pertains to loaded thrust bearing only.

** W is net load capacity for the double-acting thrust bearing arrangement.

from the gas films via the thrust runners. For instance, the thrust runner for the LP spool is the disc of the second-stage axial compressor. Consequently, there should be quite a significant transfer of bearing friction losses from the film into the runner and, hence, through the compressor blades into the main stream of compressor flow. With respect to the HP-spool runner, heat conduction into the shaft and forced-convection transfer from the outer rim should also be significant.

A second aspect of conservatism was built into the temperature rise calculations. All friction losses for the HP- and LP-spool thrust bearings were based on a 1.5- and 1.0-mil film thickness, respectively, for the loaded bearings. Actually, the theoretical film thicknesses approach these values at the idle-speed maximum-load conditions only. Larger films and lower friction losses would be obtained, even under maximum load conditions, at rated or near-rated power conditions.

A summary of the temperature rise calculations for the HP-spool loaded thrust bearing is given in Table XIV. It was found that bearing flow alone was not sufficient to hold bearing temperature rise to reasonable values. Accordingly, additional air flow was obtained by passing leakage flow from the HP-spool journal bearing cavities through cooling passages in the thrust bearing stators. Labyrinth seal leakage from the bearing cavities was calculated using data given in Reference 29. A four-throttle high-low optimum seal geometry was selected. Fifty percent of the calculated leakage was then assumed to be effective for thrust bearing cooling purposes. It is seen from Table XIV that reasonable levels of bearing temperature rise were obtained. However, because of the conservative analysis approach, it is felt that an optimized heat transfer design and rigorous thermal analysis would indicate still smaller values of temperature rise.

The heat generated in the unloaded film of the HP-spool bearing, assuming a film thickness of 3 mils, would be about half that generated in the loaded film. At sea-level rated-power conditions, the temperature rise of the unloaded face of the thrust runner would be about 34 degrees, while that of the loaded face would be about 68 degrees. A 34-degree axial gradient would thus exist across the runner. Assuming a thermal expansion coefficient of 0.000088 inch per inch per degree Fahrenheit, the thrust runner would crown by approximately 0.55 mil. By insulating the outside surfaces of the stators, it should be possible to hold stator crowning to 0.3 mil or less. Total thrust bearing distortion would thus amount to 0.85 mil. Recent experimental data obtained by MTI under Air Force contract have shown that film thickness of externally pressurized bearings reduces by approximately 60 percent of the total thermal distortion [30].

Minimum film thickness in the thermally distorted HP-spool thrust bearing would thus be approximately 1.0 mil, a still acceptable film.

Although the above calculation of thermal distortion is somewhat pessimistic, it does illustrate the importance of maintaining low axial temperature gradients in the thrust bearing members. Temperature rise is important only from the standpoint of material strength and corrosion. Axial gradients, however, directly affect bearing performance. The low-temperature condition

TABLE XIV. TEMPERATURE RISE DATA FOR THE LOADED SIDE OF THE HP- AND LP-SPOOL THRUST BEARINGS						
Percent of Rated Engine Power	Cooling Flows (lb/sec)			Friction loss (Btu/min)	Temperature Rise of Cooling Air (°F)	
	$Q_{br'g.}$	Q_{seal}	Q_{total}			
<u>Sea Level</u>						
0	0.0036	0.015	0.0186	28.4	98	
100	0.014	0.047	0.061	65.3	67.5	
<u>25,000-Foot Altitude</u>						
0	0.0015	0.008	0.0095	19.1	129	
100	0.013	0.049	0.062	49.2	51	
<u>LP-Spool Thrust Bearing</u>						
<u>Sea Level</u>						
0	0.001	-	0.001	4.25	272	
100	0.003	-	0.003	34.8	745	
<u>25,000-Foot Altitude</u>						
0	0.0004	-	0.0004	3.0	480	
100	0.0033	-	0.0033	17.9	350	

on the unloaded side of the thrust runner again indicates why it may be desirable to reduce flow through the unloaded bearing clearance. Reduced flow would raise the film temperature of the unloaded face and hence reduce the thermal distortion.

A summary of the temperature rise calculations for the LP-spool loaded thrust bearing is given in Table XIV. In this case the temperature rise is based on bearing flow only. It is seen that the small values of bearing flow result in quite high values of temperature rise. However, as mentioned previously, actual temperature rise should be greatly less due to heat transfer from the second-stage compressor blades into the compressor flow stream. Additionally, the thrust bearing flow rate could easily be increased by a factor of three by using more feeding holes of slightly larger diameter. Accordingly, cooling of the LP-spool thrust bearing was not felt to be a problem. However, the cooling scheme would again have to be optimized for minimal axial temperature gradients in the thrust runner and stators.

The above thermal analysis results serve only to illustrate that it should be feasible to obtain satisfactory cooling of the thrust bearings. However, final design of any developmental or prototype bearing system must be based on a more rigorous thermal analysis. Optimization of thermal design to achieve compatible temperature levels and acceptable temperature gradients can be done only via accurate thermal models. These models should include interactions with the journal bearing thermal conditions when close coupling exists between the thrust and journal bearing parts.

ROTOR-BEARING SYSTEM DYNAMICS

The static load carrying capability of journal and thrust bearings for the gas generator has been examined in considerable detail in preceding sections of this report. The strong interactions of bearing thermal conditions upon bearing performance and properties of the bearing materials have been stressed. However, there is still another very important aspect of rotor-bearing system performance which must be carefully examined in any feasibility study of an advanced gas-bearing machine; namely, the dynamic aspect of rotor-bearing system performance. Since gas bearings have very low inherent damping capacity relative to oil-film bearings, a gas-lubricated rotor is generally more prone to exhibit resonant unbalance response amplitudes at rotor critical speeds, and to encounter various modes of rotor-bearing system instability. Because of the complete lack of boundary lubrication in a gas bearing, any condition which could result in repeated bearing contacts, whether induced by resonant unbalance response, instability, or externally applied vibration and shock, must be avoided if at all possible.

Considerable analysis was performed to gain insight into the dynamic characteristics of both the HP and LP spools for the gas generator. Critical speeds, response to unbalance, and other results of the dynamics study are presented in the following subsections of this chapter. These results pertain only to the Phase VI configurations of the HP and LP spools as depicted in Figures 3 and 4.

CRITICAL SPEEDS

The first step in the rotor dynamics study was to assess the critical speed characteristics of the HP and LP spools. MTI computer program PN 315V was used for this purpose. This program computes rotor-system undamped transverse natural frequencies (critical speeds) and corresponding mode shapes, taking into account the stiffness and mass characteristics of both the rotor and the bearings.

HP-Spool Critical Speeds

The HP spool was modeled using 15 rotor mass stations. Gyroscopic stiffening effects of the compressor, turbine, and thrust bearing discs were included. Variation in shaft dynamic modulus of elasticity as a function of temperature was also included.

The computed critical speed map for the HP spool is shown in Figure 46. It is seen that the first two critical-speed curves are straight lines having a slope of one-half, thus indicating a square root function of bearing stiffness. This means that the HP spool behaves as a rigid body in its first two critical-speed modes throughout the realizable range of bearing stiffness. The third critical speed, which in this case would be the first

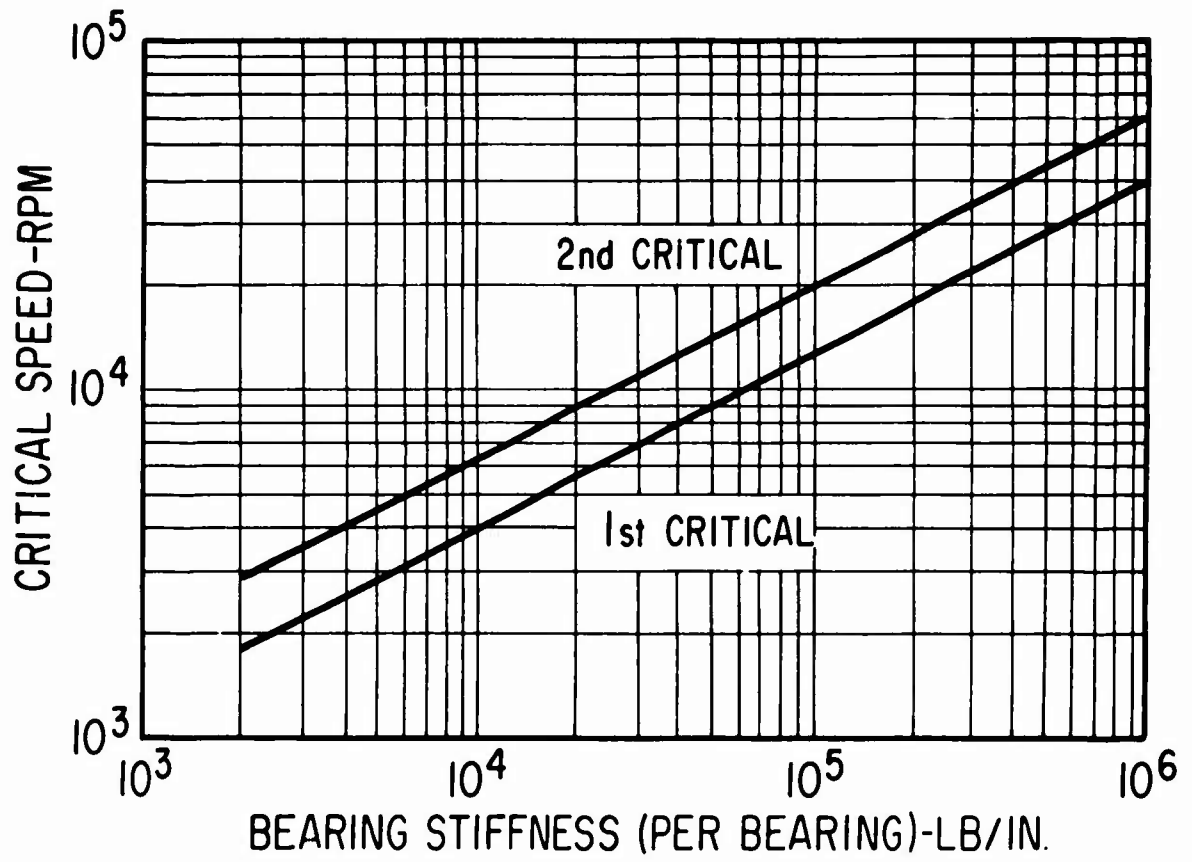


Figure 46. Critical Speed Map for the HP Spool.

bending critical of the rotor, was found to occur at about 140,000 rpm, well above the 80,000-rpm overspeed limit for the HP spool.

The undamped mode shapes for the HP spool are plotted in Figure 47. These plots confirm that the shaft behaves as a rigid body. The nodal point for the first critical speed mode occurs between the bearing locations. This type of mode is frequently referred to as a conical response mode. The nodal point for the second mode occurs outside the bearing span, this being the commonly used criterion for identifying a translatory response mode.

The principal fact learned from the HP-spool critical-speed analysis was that the spool would behave as a rigid body. This is a highly desirable condition for any rotating machine, and most certainly for a gas-bearing machine. The implications of a rigid-body condition are (1) that the rotor can be balanced using simple two-plane balancing techniques, and (2) that no difficulty should be encountered in achieving a degree of balance which will be satisfactory for reliable gas bearing operation.

LP-Spool Critical Speeds

The LP spool was modeled using 26 rotor mass stations. Gyroscopic stiffening effects of the compressor and turbine discs were again included, as was variation in shaft dynamic modulus of elasticity in accordance with the estimated profile of shaft temperature. In addition, the effect of different shaft materials having significantly different values of dynamic modulus was investigated. TZM was selected as a representative refractory alloy having high values of modulus, while IN-100 was selected as a representative high-strength superalloy having more conventional modulus values.

The computed critical-speed map for the LP spool is shown in Figure 48. It is seen that within the speed range of the LP spool (sea-level overspeed is 69,000 rpm), four critical speeds are encountered, with the fourth critical occurring in the vicinity of design speed and overspeed. The first two critical speeds represent rigid-body criticals at low values of bearing stiffness only (less than 10,000 pounds per inch). For the normal range of bearing stiffness values (between 20,000 and 100,000 pounds per inch) the first two critical-speed curves indicate that shaft bending will occur.

Figures 49 and 50 show the calculated mode shapes for the four critical speeds corresponding to a bearing stiffness (per bearing) of 60,000 pounds per inch. Figure 49 confirms that the first two critical speeds do contain appreciable shaft bending. The third and fourth modes are essentially pure shaft bending. The bearings do not influence these criticals except at high values of stiffness (greater than 100,000 pounds per inch).

It is apparent that the LP spool is a highly flexible shaft from a rotor dynamic standpoint, and must operate through three to four flexural criticals. This is due to the relatively long length and small diameter required to pass the shaft through the HP spool. In early layouts of the two-spool arrangement, the LP spool was even longer and of smaller diameter. This resulted in the third and fourth critical speeds being approximately 20,000 and

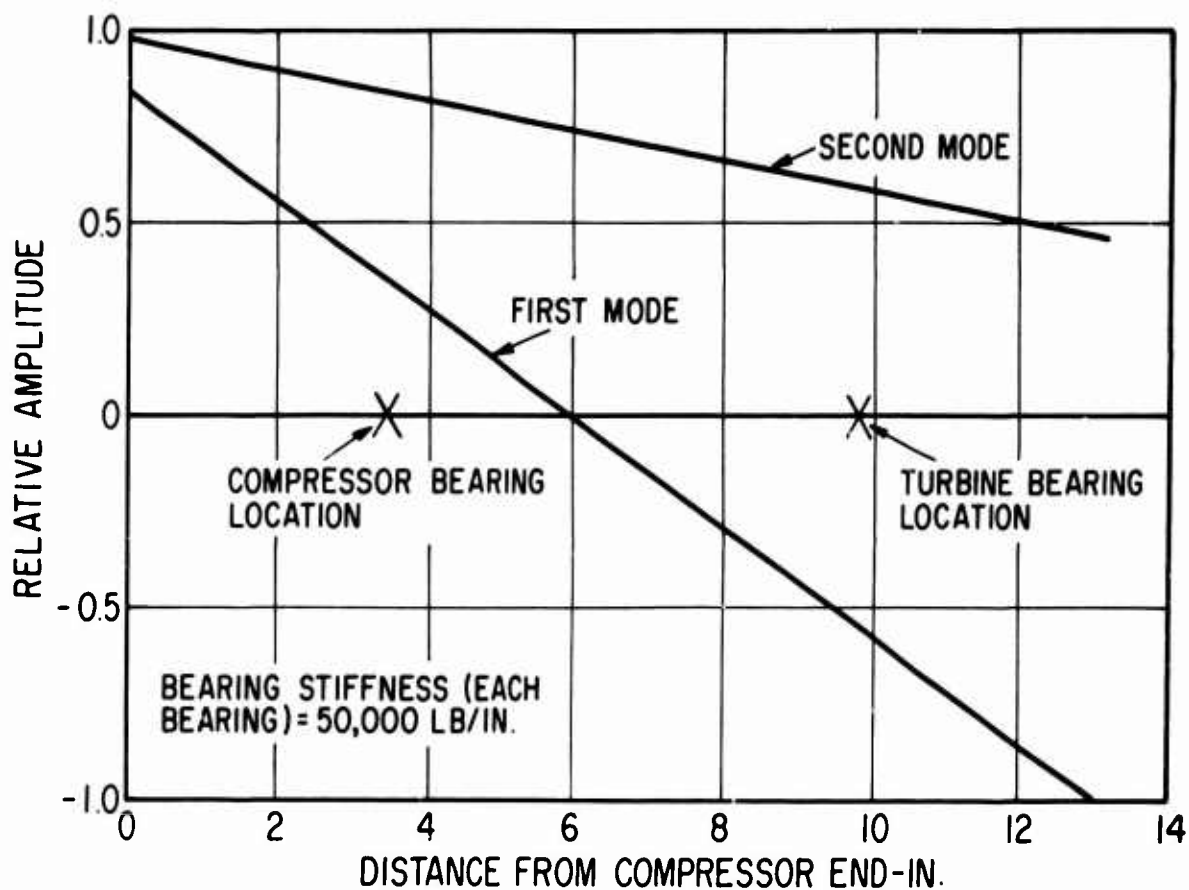


Figure 47. Undamped Mode Shapes for the First and Second Critical Speeds of the HP Spool.

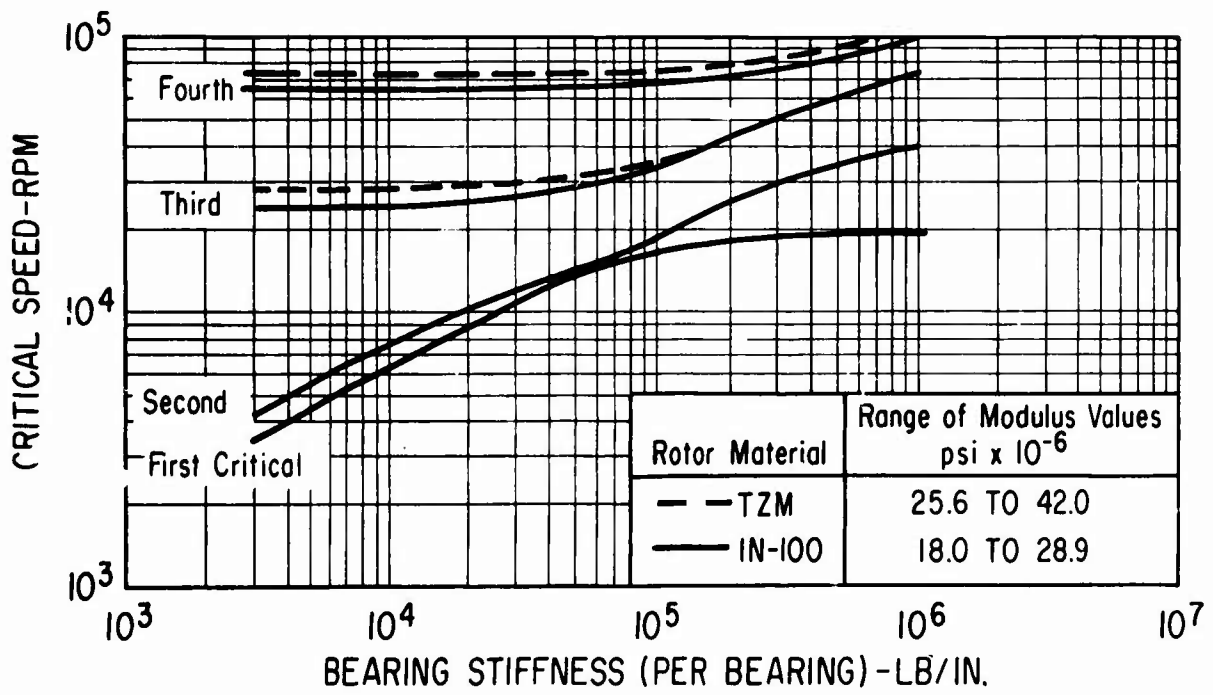


Figure 48. Critical Speed Map for the LP Spool.

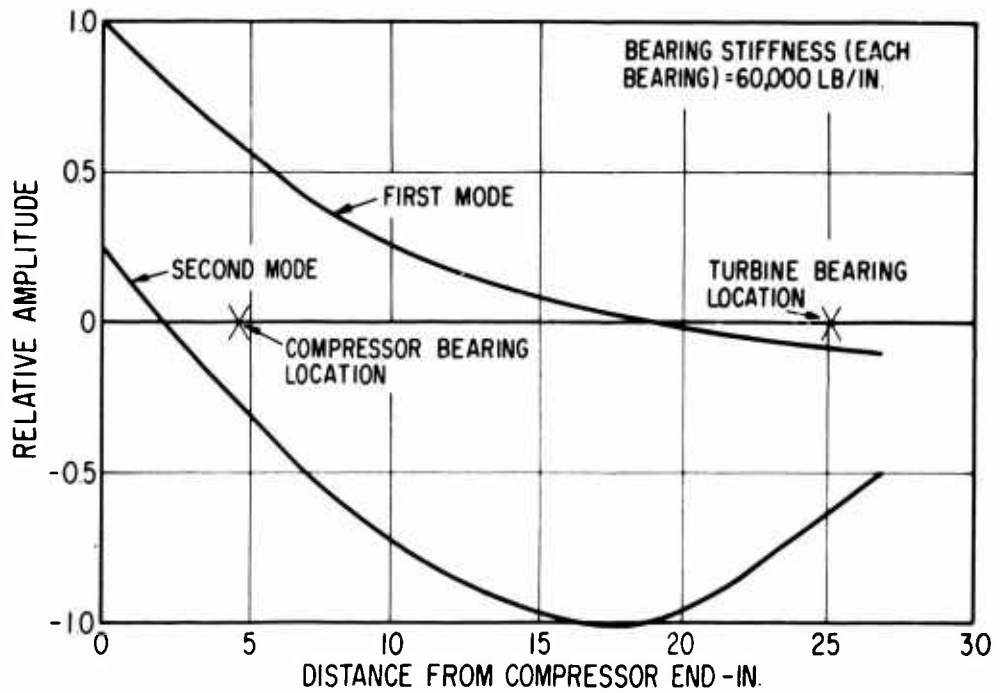


Figure 49. Undamped Mode Shapes for the First and Second Critical Speeds of the LP Spool.

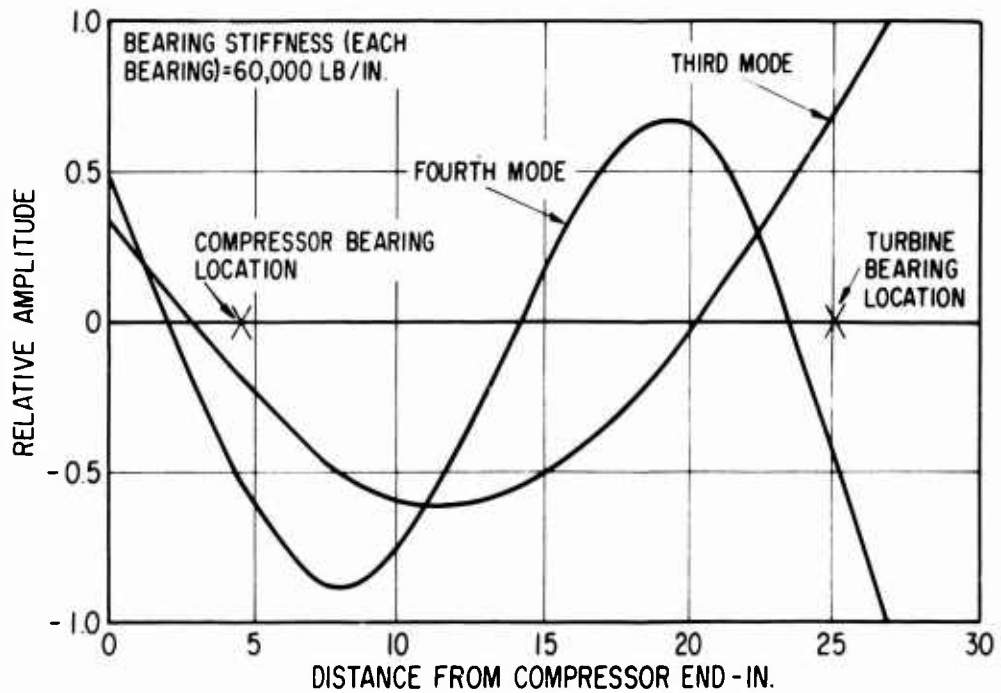


Figure 50. Undamped Mode Shapes for the Third and Fourth Critical Speeds of the LP Spool.

50,000 rpm, respectively. Efforts to increase shaft diameter were limited by the bore diameters of the HP-spool journal bearings, which were set at the largest size possible consistent with acceptable values of journal centrifugal growth and stress. Efforts to reduce shaft length were, of course, limited by HP-spool length. HP-spool length, in turn, was primarily determined by the journal bearing span required to reduce the gyroscopic bearing loads to acceptable levels. The LP-spool critical speeds are thus highly coupled to the HP-spool journal bearing design. Changes in LP-spool diameter and length for the purpose of raising the flexural critical speeds will adversely affect the performance of the HP-spool journal bearings.

Figure 48 represents the most recent effort to raise the LP-spool fourth critical speed out of the operating speed range by decreasing length and increasing diameter of the spool to the maximum extent possible. As will be seen from the rotor response results, this effort did not produce the total required increase. However, if the fourth critical speed could be increased by another 10,000 rpm, it appears that a satisfactory rotor response situation would be achieved, at least with respect to the fourth critical. (The third critical speed would still have to be contended with by working out satisfactory balancing and/or damping techniques.) Ways in which the fourth critical could be raised should be investigated further. The most promising approach appears to be an increase in shaft diameter at the point where the shaft passes through the hub of the HP turbine. This, however, would require a larger hub diameter for the turbine, which in turn would increase turbine stresses. Hence, design of the HP turbine would be intimately involved in this approach. A second approach which should give some improvement is reduction of overhung mass at the two ends of the shaft, particularly at the turbine end. It is felt that design optimization in these two areas would accomplish the desired increase in the fourth critical speed.

The LP spool would still, however, have to operate through and above the third critical speed. This represents an operating condition which has not yet been demonstrated with gas-bearing turbomachinery. Further discussion of this problem area is given in the "LP-Spool Unbalance Response" subsection of this chapter.

UNBALANCE RESPONSE

The most common form of undesirable rotor motion is synchronous whirl resulting from excitation of the transverse critical speeds of the rotor in its rigid or flexible beam modes. The excitation most commonly derives from mechanical unbalance of the rotor, although other forms of excitation are possible.

A series of unbalance rotor response calculations was performed for both the HP and LP spools using MTI computer program PN 365. This is a very complete rotor response program which includes the following effects:

1. Gyroscopic stiffening

2. Variable rotor geometry, including variable values of density, dynamic modulus, Poisson's ratio, and cross-section shape factor
3. Rotor elasticity
4. Bearing radial and angular stiffness (eight coefficients per bearing)
5. Bearing radial and angular damping (eight coefficients per bearing)
6. Bearing mass
7. Bearing support stiffness and damping
8. Completely general designation of the unbalance condition existing within the rotor

The program can also handle the simultaneous response solution for two separate rotors interconnected by stiffness and damping elements.

Output from the program includes the following:

1. All data needed to define the steady-state response orbit at each rotor station (the orbit being, in general, an ellipse)
2. Maximum and minimum values of dynamic bending moment, bending stress, dynamic shear, and shear stress at each rotor station
3. Maximum values of transmitted force at each bearing
4. Maximum eccentricity of the journals relative to the bearings (which, when subtracted from radial clearance, gives minimum bearing film thickness)

Program PN 365 is a powerful rotor dynamics design and analysis tool, and it has been proven by numerous experimental tests to give accurate results when correct values of bearing stiffness and damping are used. In fact, the program, in conjunction with test data, currently provides the best means for verifying new analytical procedures for calculating dynamic stiffness and damping properties of bearings.

A flexure-mounted three-pad pivoted-pad bearing has 12 degrees of freedom. That is, it requires, in general, 12 coordinates to define completely the position of the three pads at any instant of time. Rather than incorporate a complete 12 degree-of-freedom dynamic system at each bearing location in the rotor response model, effective values of bearing stiffness and damping for the bearings are separately computed by MTI program PN 409 (this program is briefly described in the "Journal Bearing Design Studies" chapter of this report). These computations, made as a function of speed, include the effects of flexure stiffness, pad mass and mass-moments of inertia, and gas film stiffness and damping. Four dynamic stiffness and four dynamic damping coefficients are computed for the completely assembled bearing at its

specified operating condition. These coefficients define the effective stiffness and damping of the complete bearing as seen by the journal under synchronous whirl conditions.

An example of the stiffness and damping functions for the HP-spool bearings under 1-g load conditions is given in Figures 51 and 52. The negative values for some of the dynamic stiffness and damping coefficients may seem rather unusual, as indeed they are in terms of conventional bearing design. However, the reason for these negative coefficient values is physically explainable when it is realized that the flexure-mounted pads introduce additional resonance characteristics to the bearings. When the natural frequencies of the pad-flexure systems are sufficiently close to (but still above) synchronous rotor frequency, motions of the pads can be greater than, although still in phase with, motions of the journal. Such a condition can give rise to negative dynamic bearing coefficients.

HP-Spool Unbalance Response

The unbalance response characteristics of the HP spool were examined using two rotor-unbalance models. These are shown in Figure 53 and were selected to correspond to the two rigid-body critical-speed mode shapes for the HP spool. The "in-phase" unbalance model corresponds to the translatory mode, while the "out-of-phase" unbalance corresponds to the conical mode. A total mass-moment unbalance of 0.002 ounce-inch was used, this being an achievable level of residual unbalance using in-place balancing techniques.

Figure 54 shows the response of the HP-spool turbine-end bearing to the two conditions of unbalance. The calculations were made using the effective stiffness and damping functions of Figures 51 and 52. These functions correspond to normal operation of the HP spool under gravity load conditions. It is seen that maximum journal amplitude occurs at the 80,000-rpm overspeed condition during excitation by the in-phase unbalance condition. However, actual response amplitude (amplitude being maximum excursion of the journal from its static eccentricity position) is less than 10 microinches, a most acceptable condition. Similar results were obtained for the compressor-end bearing responses. Maximum journal amplitude again occurred with the in-phase unbalance, and was less than 10 microinches. These results indicate that a high degree of balance is not essential for good operation of the HP spool.

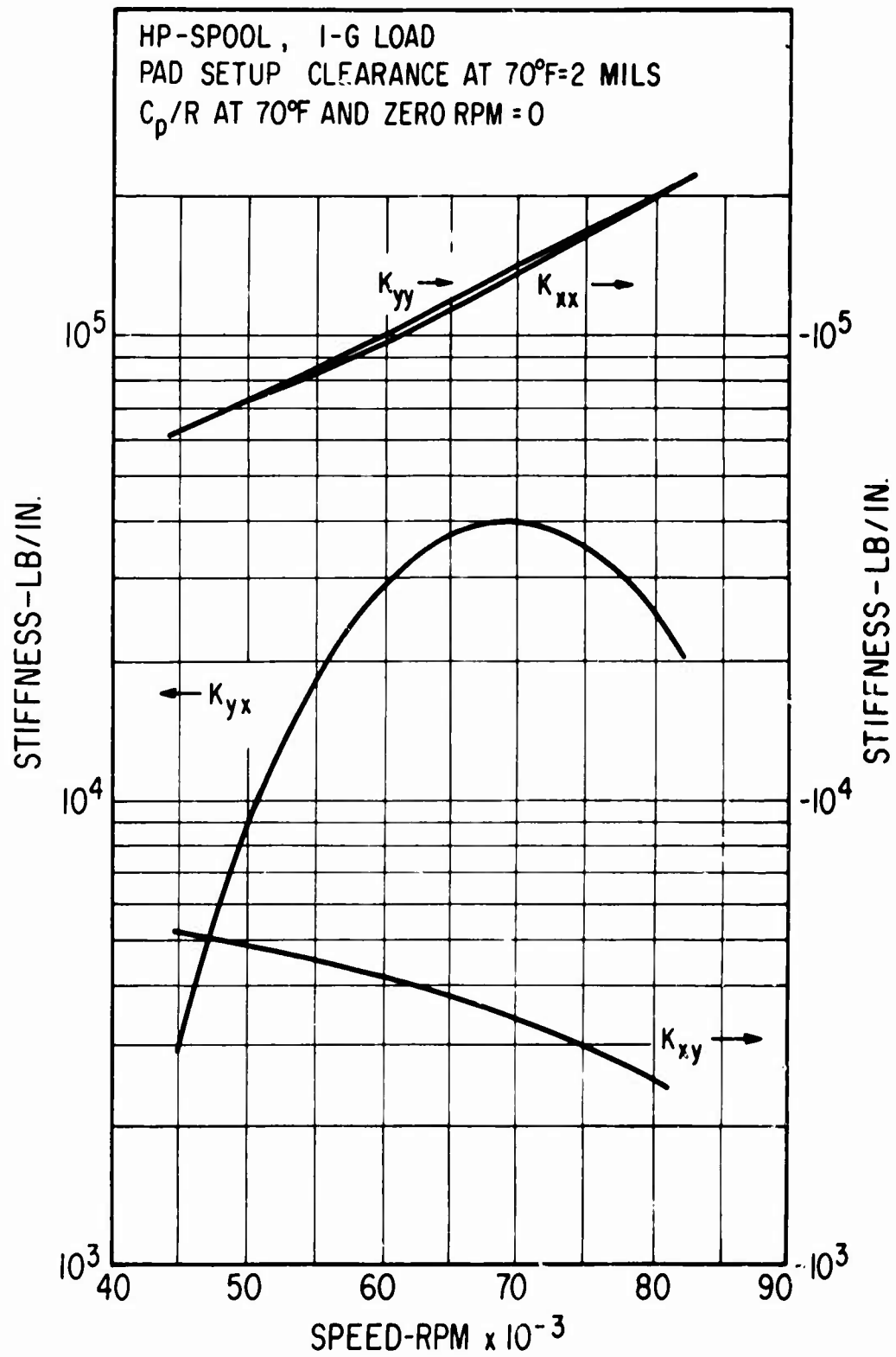


Figure 51. Effective Dynamic Stiffness Coefficients for the HP-Spool Journal Bearings Under 1-G Load Conditions.

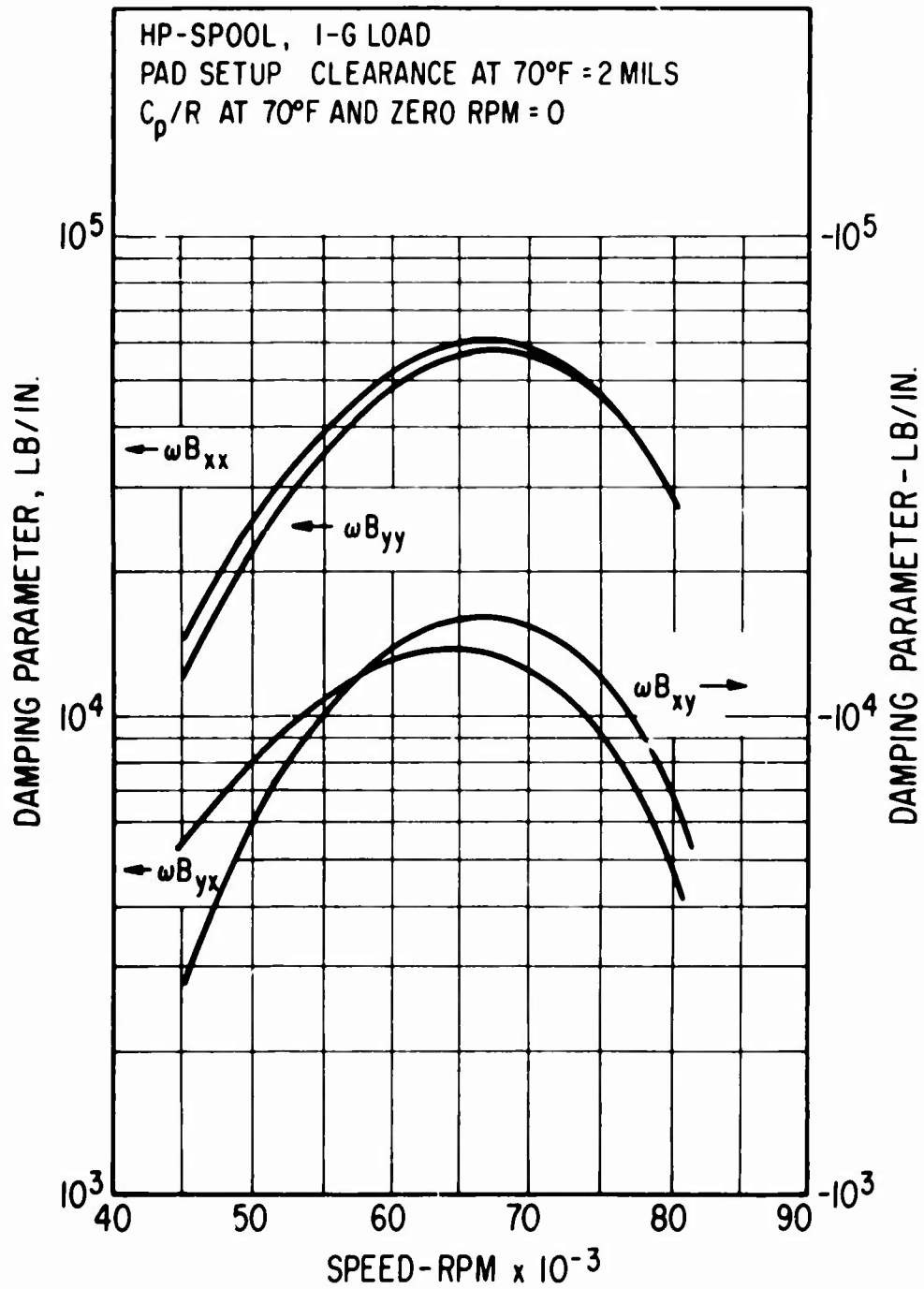


Figure 52. Effective Dynamic Damping Parameters for the HP-Spool Journal Bearings Under 1-G Load Conditions.

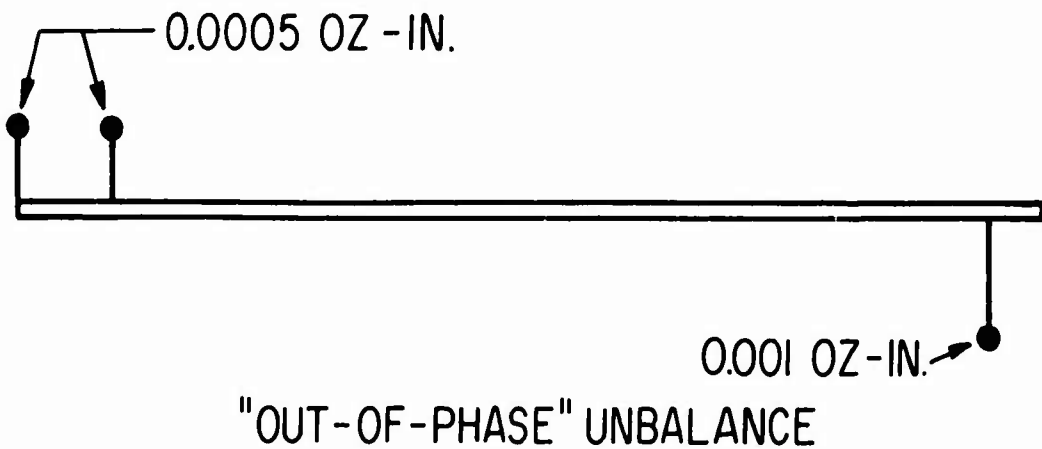
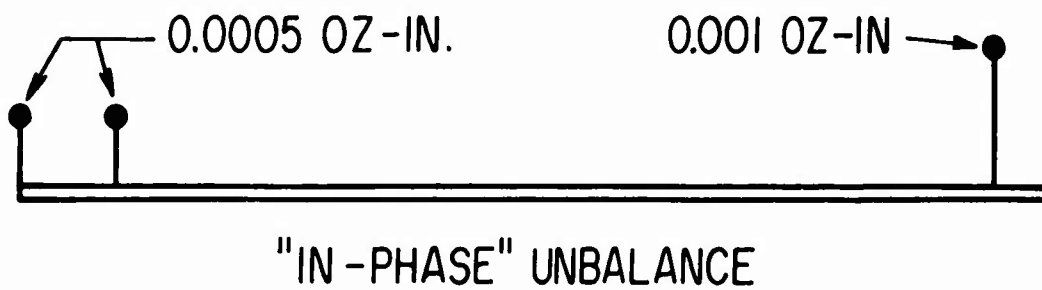
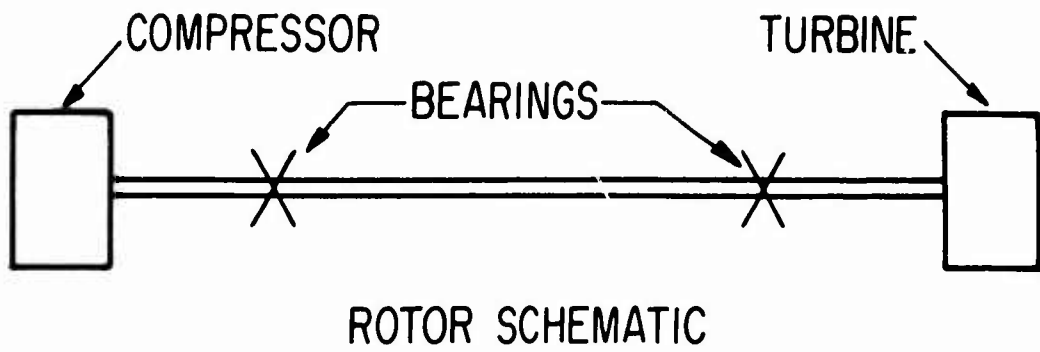


Figure 53. Mass-Moment Unbalance Models Used to Investigate the Unbalance Response Characteristics of the HP Spool.

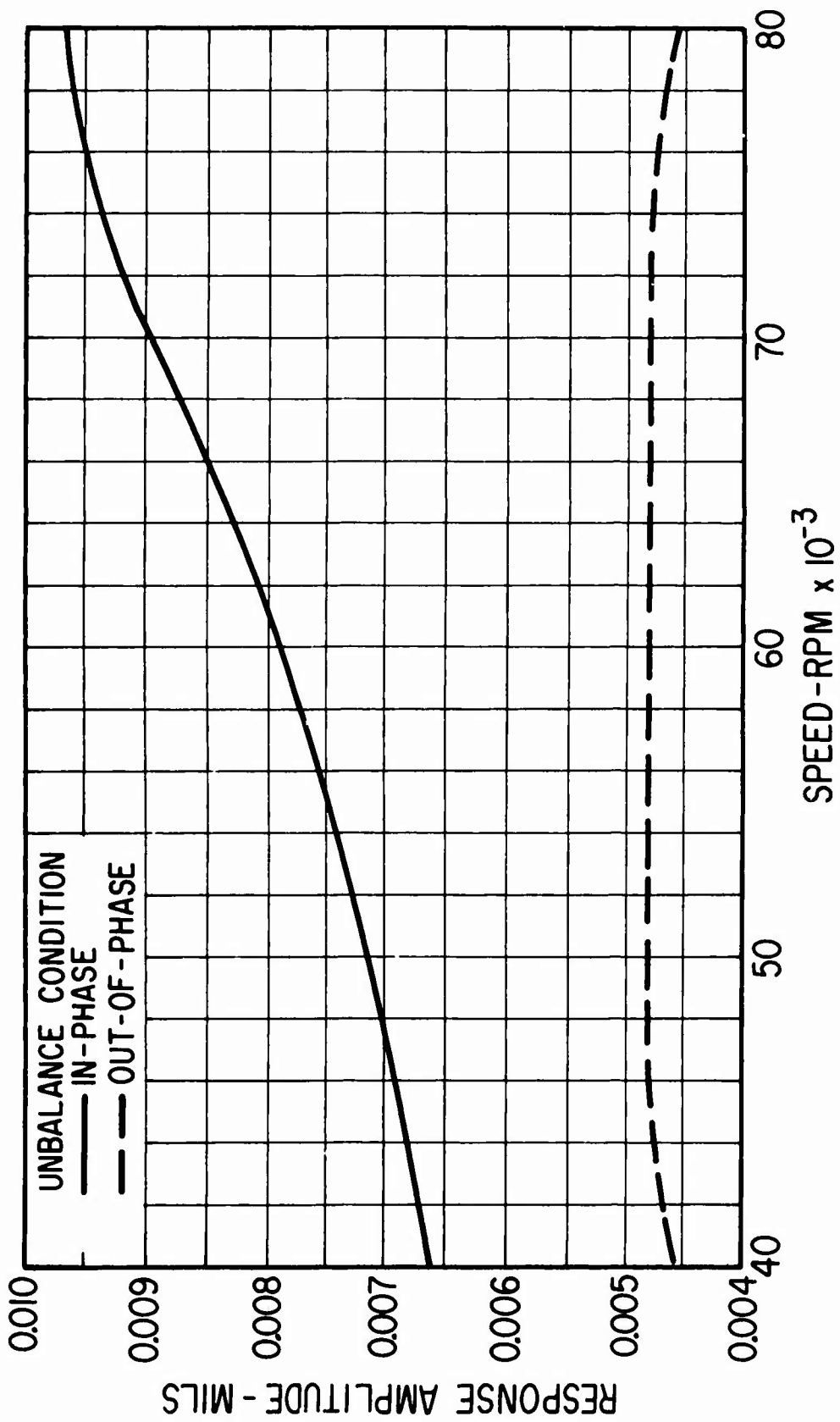


Figure 54. Unbalance Response of the HP-Spool Turbine-End Journal to the Mass-Moment Unbalance Conditions of Figure 53.

LP-Spool Unbalance Response

Figure 55 shows the two conditions of mass unbalance used to investigate the synchronous response characteristics of the HP spool. The "out-of-phase" unbalance configuration was chosen to strongly excite the third critical speed. A total mass-moment unbalance of 0.003 ounce-inch was used for both the "in-phase" and the "out-of-phase" condition.

Figure 56 shows displacement response of the turbine-end journal bearing at normal gravity-load operating conditions. Maximum response amplitudes occur at 28,500 rpm; that is, at the third critical speed. Out-of-phase unbalance produces the largest amplitudes. However, the in-phase condition also produces large amplitudes. In other words, the third critical speed will be quite responsive to most unbalance conditions.

The actual range of peak response values is 0.2 to 0.6 mil. This means that the unbalance orbit would have a major diameter of 0.4 to 1.2 mils. Under perfectly balanced conditions, diametral clearance of the bearing at 28,500 rpm would be in excess of 2.0 mils (see Figure 38). At first glance, then, it would appear that the bearing clearance is greater than the unbalance orbit and bearing rubs should not occur. In actuality, however, comparison of statically calculated clearances with the dynamic journal orbit does not give an accurate indication of bearing film thickness conditions when the pads are elastically mounted. The use of pad flexures introduces additional degrees of freedom into the overall rotor-bearing system, with the net result that the pads also undergo dynamic responses in the radial direction. The amplitude and phase of the radial pad motions depend upon the relationship of rotative (excitation) frequency to the natural frequencies of the rotor-bearing system. Minimum bearing film thickness in turn depends on the relative motion between the journal and the pads, and hence on the amplitude and phase of each pad relative to its journal.

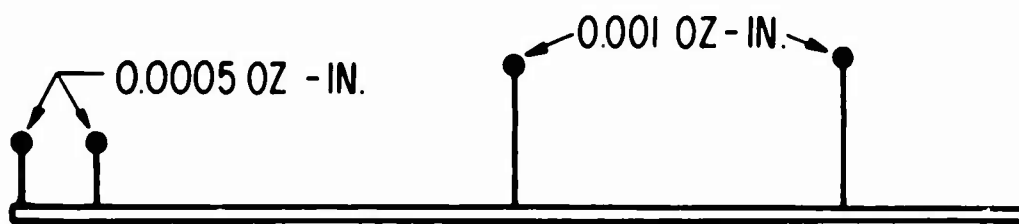
Although the LP-spool journal bearing designs were not optimized, preliminary analysis of the pad dynamics indicated that radial motions of the pads will be in phase with the journal motions and that amplitudes of the pad motions will be within ± 20 percent of the journal amplitudes. In other words, the pads will track the radial motions of the journal, and minimum film thickness will not vary more than 20 percent from the static clearances which would be obtained with a perfectly balanced shaft.

It would appear therefore that the LP spool can operate without danger of bearing contacts at the 1.2-mil unbalance orbit condition obtained at the third critical speed. However, the effects of critical speed orbits must also be considered from six additional machine design aspects:

1. Flexure fatigue stress
2. Pivot fatigue stress
3. Flexure dynamic forces transmitted to the bearing housings



ROTOR SCHEMATIC



"IN-PHASE" UNBALANCE



"OUT-OF-PHASE" UNBALANCE

Figure 55. Mass-Moment Unbalance Models Used to Investigate the Unbalance Response Characteristics of the LP Spool.

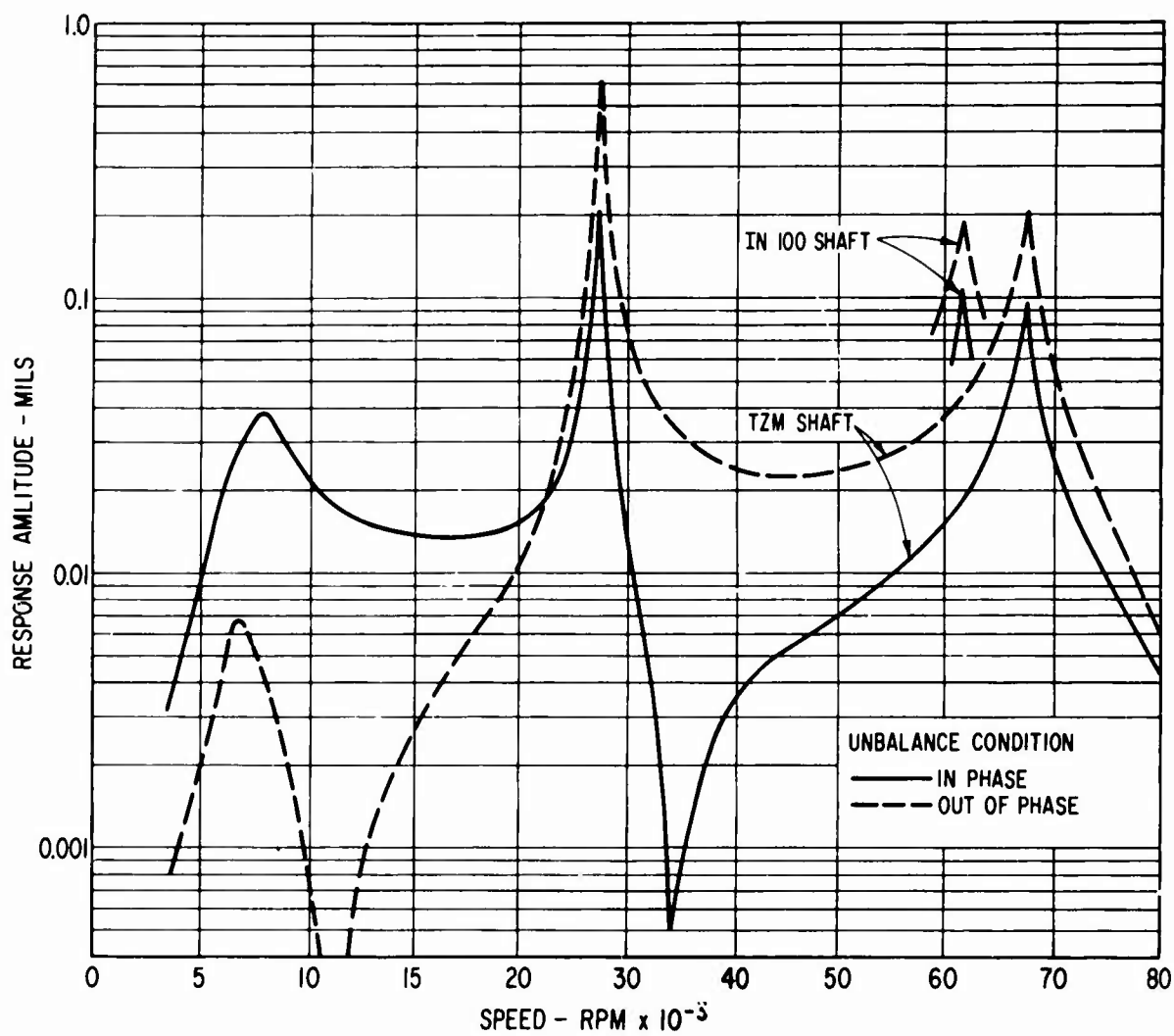


Figure 56. Unbalance Response of the LP-Spool Turbine-End Journal to the Mass-Moment Unbalance Conditions of Figure 55.

4. Shaft bending stresses (which will also be dynamic in nature if the unbalance orbits are elliptical)
5. Labyrinth seal clearances
6. Thrust bearing film thickness (lateral resonances of the rotor will always interact with the thrust bearing except for the special, and infrequent, case where the shaft deflection curve is parallel to the line of journal centers at the thrust bearing attachment point)

Conditions 1 and 6 above would be the most critical problem areas for the LP spool at a 1.2-mil journal orbit condition. Condition 3 would likewise probably be undesirable. Although an optimized design study of the LP-spool system is required, it is probably safe to say that the 1.2-mil orbit condition is too large for good machine design practice. Based on gas-bearing turbomachinery experience to date, a maximum orbit size of approximately 0.5 mil would probably be acceptable.

Unless some relatively simple and reliable means can be found for increasing damping in the LP-spool rotor-bearing system, reduction of the maximum unbalance response amplitude at the third critical will have to be achieved by rather fine balancing of the LP spool. However, since the spool operates in a flexible, rather than a rigid, condition, multiplane, rather than two-plane, balancing techniques will be required. By careful selection of the balance planes, it may be possible to achieve satisfactory balance with only three planes. If not, four or possibly five balance planes will be needed. Total unbalance moment would have to be reduced to approximately 0.0015 ounce-inch, which represents about the limit of the best commercially available balancing machines. Unquestionably, final balance would have to be checked, and probably trimmed, with the LP spool completely assembled on its bearings in the engine casings.

To the best of the author's knowledge, there has been no instance of a gas-bearing machine operating through its third critical speed. This is not to imply that it cannot be done, but rather that it has so far always been possible to achieve rigid shaft designs for which balancing techniques are relatively simple and well developed. However, with constantly increasing speeds, it is becoming more and more difficult to design rigid shafts. The near-future need for proven and practical techniques for balancing flexible shafts has been recognized and work to this end has been started by MTI [31]. The LP spool represents an application where it will be impossible to achieve a rigid-shaft design. Future development of a successful LP-spool gas-bearing system will thus be dependent upon the availability of practical techniques for flexible-shaft balancing.

Achievement and maintenance of good LP-spool balance are two different problems. The first, of course, is related to the balancing process. Maintenance of balance, however, will be primarily a function of mechanical design. The problem here will be to assure that there can be no gross mass shifts due to poor design of wheel attachment methods, etc., and no dissymmetry mass shifts due to thermal distortions or unsymmetrical creep of high-temperature parts.

Returning to Figure 56, it is seen that the fourth critical speed resonance occurs almost exactly at design speed when the shaft is made of IN-100 alloy. If made of TZM refractory alloy, the fourth critical is raised approximately 5,000 rpm and hence coincides essentially with LP-spool overspeed. Although the response amplitudes at the fourth critical are somewhat smaller than those at the third critical, it is considered to be very undesirable to have a critical speed in close proximity to either design speed or overspeed. Accordingly, every effort should be made to increase the fourth critical speed by 10,000 rpm. Possible ways to achieve this increase were mentioned in the "LP-Spool Critical Speeds" subsection of this chapter.

Finally, Figure 56 indicates a definite resonance in the range of 5,000 to 10,000 rpm due to the first and second critical speeds. The response amplitudes, however, are significantly smaller than those which occur at the third and fourth criticals. Individual response peaks for the first and second criticals are not observed due to the small separation between these criticals (approximately 1000 rpm; see Figure 48). These criticals should present no problem.

The unbalance response amplitudes for the LP-spool compressor-end bearing are shown in Figure 57. In this case, the maximum amplitudes occur at the fourth critical speed and have approximately the same values as were calculated for the turbine-end bearing. The resonant amplitudes due to the first and second criticals are considerably higher than those calculated for the turbine-end bearing.

Although there are differences in response amplitudes for the compressor and turbine-end bearings, the basic nature of the response curves is the same. The conclusions pertaining to shaft balancing requirements and the desirability of increasing the fourth critical speed, as presented in connection with the turbine-end bearing, are equally as valid with respect to the compressor-end bearing. The most significant difference between the two bearings is that the compressor-end bearing is less sensitive to the third critical speed resonance. This can be seen from the undamped mode shape for the third critical speed shown in Figure 50. Figure 50 also indicates that the midshaft response orbits should be approximately the same as the turbine-end bearing orbits. The response calculations confirmed this fact.

The cause of the large LP-spool critical speed resonances is, of course, insufficient damping. Only gas-film damping in the two journal bearings was considered for the unbalance response calculations. The principal damping coefficients for the film are shown as a function of speed in Figure 58. One possible means to increase damping is to add a third bearing at roughly the midshaft position of the LP spool. This bearing would thus have to operate at the relative speed of the HP and LP spools. Although a mechanical design study of such an arrangement was not made, the effect of such a bearing was investigated theoretically. It was assumed that the third bearing would have the same amount of damping as shown in Figure 58. The results of the calculation showed that the response amplitudes at the third critical speed would be reduced by a factor of approximately two. Amplitudes at the first, second, and fourth criticals were also reduced, but

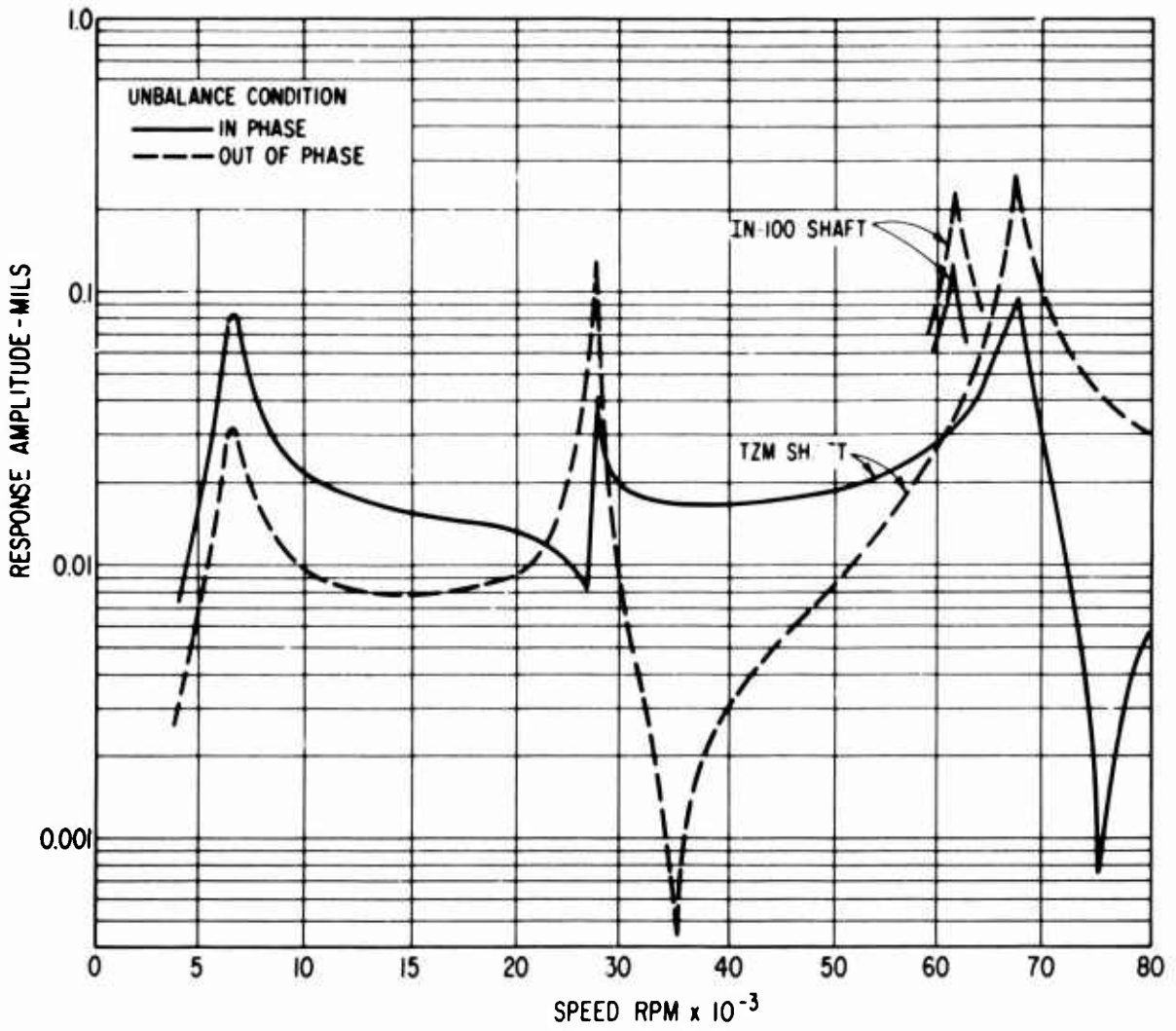


Figure 57. Unbalance Response of the LP-Spool Compressor-End Journal to the Mass-Moment Unbalance Conditions of Figure 55.

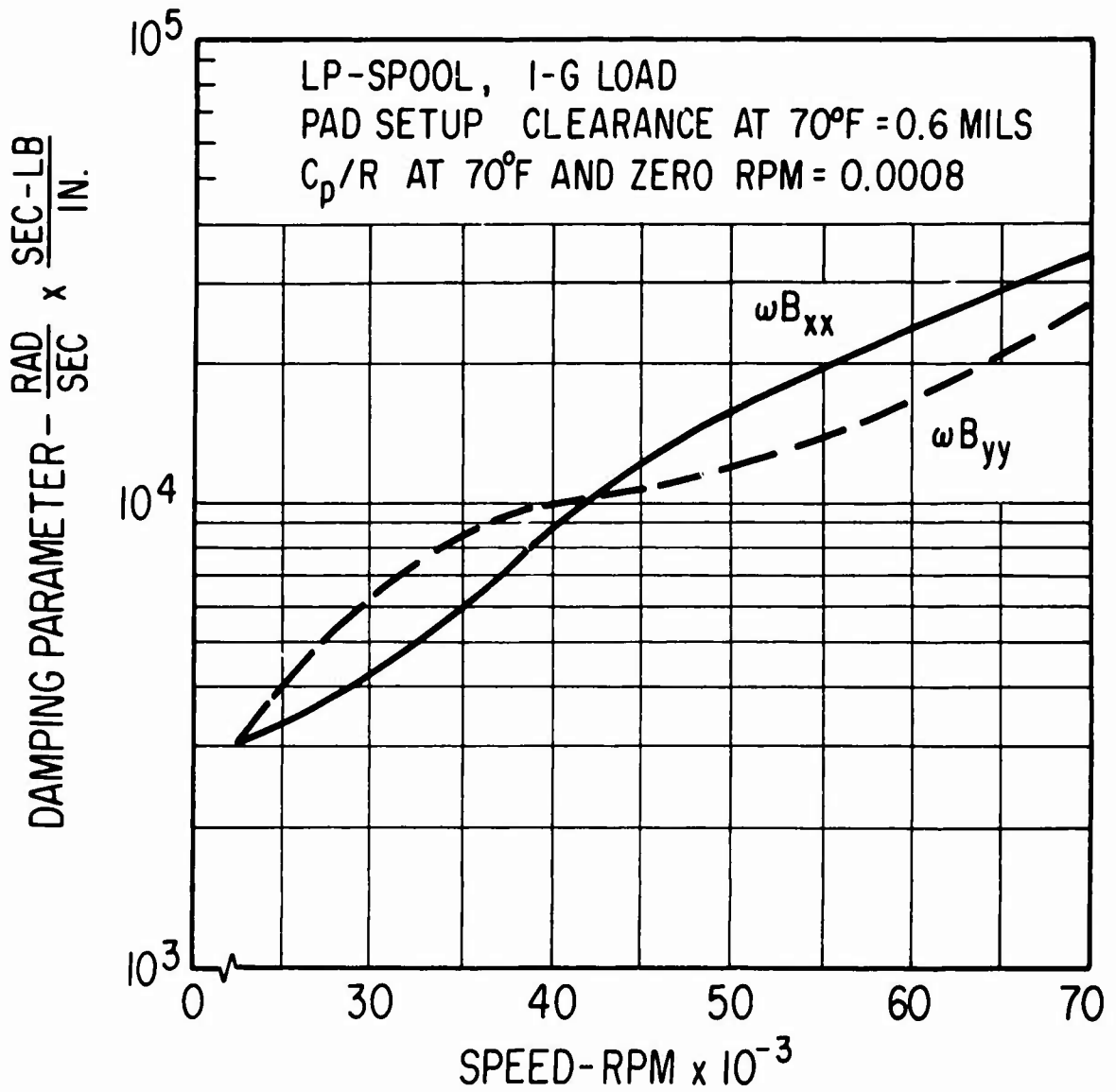


Figure 58. Effective Dynamic Damping Parameters for the LP-Spool Journal Bearings Under 1-G Load Conditions.

not as much. However, since the first and second criticals present no problem, and since the fourth critical can (hopefully) be raised out of the operating speed range, the addition of a third bearing offers a theoretically feasible way of greatly reducing the LP-spool unbalance response problem. Further design study should be made of the mechanical feasibility of this approach.

It was stated on page 12 that there are at least two other mechanical arrangements of the gas generator which seem to offer potential advantages over the Phase VI gas-generator arrangement (shown in Figure 2) which was the basis for the rotor dynamic calculations presented here. One of these is a single shaft, rather than a two shaft, arrangement. It is possible that a single-shaft arrangement might be designed such that the shaft behaves as a rigid body throughout the engine speed range, or at most would have to operate through only one flexible-shaft critical speed. In this case, the LP spool, and its associated rotor dynamic problems, would be eliminated.

PAD DYNAMICS

At this time, the interactions between pad dynamics and the overall dynamic performance of a rotor supported by gas-lubricated pivoted-pad journal bearings are not well understood. The reason for this is twofold. First, pivoted-pad gas bearings have been used only since the early 1960's. Second, only within the past three years has it been observed that large-amplitude subsynchronous rotor whirl may occur with this type of bearing. From a dynamical standpoint, the individual pivoted-pad segments and the rotor comprise a mechanical system having many degrees of freedom. The pads are coupled to the rotor via the gas films, and to the bearing housings via the flexure supports. Rigorous analysis of the response characteristics of this system (which may be of a synchronous or nonsynchronous, stable or unstable nature) entails simultaneous solution of a complex system of equations. Because of the magnitude of this analysis task, various approaches to the response prediction problem are currently being independently pursued by several investigators [15, 32]. One of these approaches should ultimately lead to positive conclusions about the significance of pad dynamics in the overall picture of rotor-bearing system response.

At the present time, however, one must resort to simple pad-dynamics criteria. These criteria have evolved on the basis of intuition and a small amount of experimental data. In essence, each pad is considered as an isolated 4-degree-of-freedom system which can have translational motion in the radial direction, and rotational motion in three directions about the pivot point. The rotations are referred to as roll, pitch, and yaw rotations. Pitch rotation occurs about an axis through the pivot and parallel to the shaft axis. Yaw motion occurs about an axis passing through the pivot and perpendicular to the pad surface. The roll axis likewise passes through the pivot and is orthogonal to the pitch and yaw axes.

The pad is acted upon by radial, roll, pitch, and yaw gas-film forces and moments, and by radial flexure forces. Dynamic motions of the journal are

assumed to be the independent forcing functions acting on the pad system. (This assumption, of course, is the one which reduces a very complex rotor-bearing system to a number of relatively simple single-pad systems. It is also the assumption, however, which makes it impossible to predict the true rotor-bearing system nonsynchronous response and stability characteristics.) It is then assumed that the journal and pad motions are sufficiently small that the gas film can be represented by 16 stiffness and damping coefficients. As a result of these assumptions, each pad system can be reduced to two 2-degree-of-freedom analytical models which have closed-form solutions for the case of periodic journal excitation.

With regard to design criteria for the pads, a reasonable argument can be made for requiring the natural frequencies of the simple pad systems to be well above operating speed, although hopefully not an integer multiple of running speed. This criterion accomplishes two things. First, it assures that simple resonances of the pads will not occur. Second, it assures that the pads will follow (track) the dynamic motions of the journal. In this latter respect, tracking ability is important primarily in the radial, pitch, and roll directions. Journal-induced yaw motions of a pad are insignificant in a two-bearing machine unless the rotor operates through a critical speed which produces a sizeable amount of shaft bending.

In all of MTI's turbomachinery developments using gas-lubricated pivoted-pad journal bearings, the theoretical natural frequencies of the pads in the radial, pitch and roll directions have exceeded running frequency by at least 10 percent, and usually by 30 percent. In all instances, whirl-free stable rotor operation was obtained. In one instance where controlled testing was possible, subsynchronous whirl could be induced by increasing the bearing clearance [7]. The effect of increasing the clearance was, of course, a reduction in film stiffnesses and hence in pad natural frequencies. Unfortunately, the experiment was not pursued to the point of recalculating the theoretical pad frequencies at the onset of whirl. Accordingly, it still is not known whether the natural frequency criterion is really a necessary condition for whirl-free operation.

The unloaded pad (or pads) in a pivoted-pad bearing will have the greatest film thickness and hence the lowest film stiffness values and natural frequencies. Figure 59 shows frequency ratio plots for the unloaded pads of the HP-spool journal bearings under 1-g and maximum load conditions. Frequency ratio in this case is pad natural frequency divided by spool speed, both quantities being expressed in the same frequency units. The loads were specified to act directly on one pivot. Thus, Figure 59 represents conditions of the largest possible film under an unloaded pad. It is seen that under 1-g loads, the radial, roll and pitch frequencies are always above running frequency throughout the operating speed range. The pitch frequency is the lowest, being only 8 percent above running frequency at 70,000 rpm. Under maximum load conditions, the pitch frequency drops to within ± 2 percent of running frequency between 58,000 to 75,000 rpm.

For the 1-g load condition, natural frequencies of the loaded pad for the HP spool were slightly higher than those of the unloaded pads shown in Figure 59. At the maximum load condition, the radial pitch and roll natural

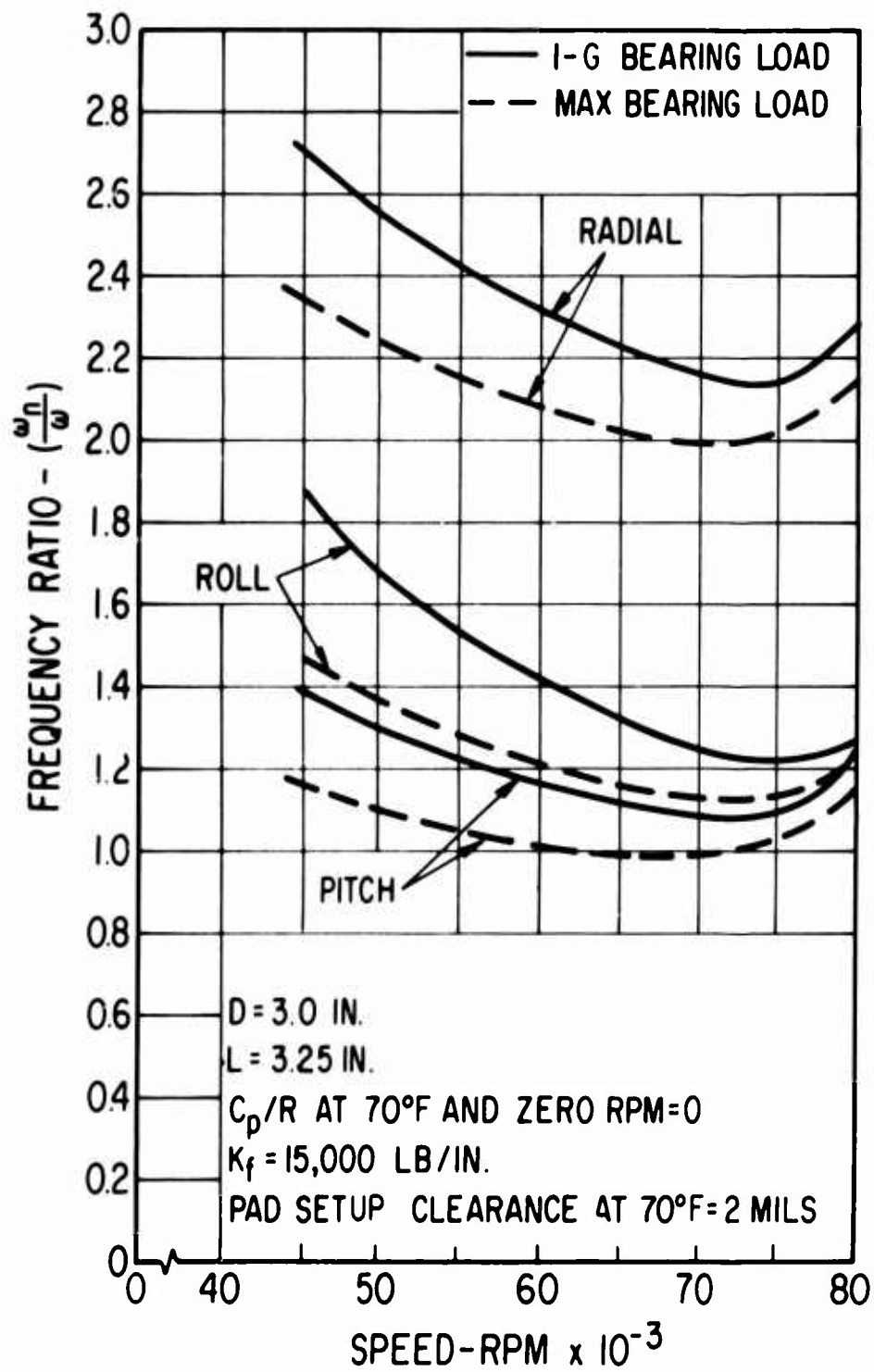


Figure 59. Natural Frequency Ratios for the Unloaded Pads of the HP-Spool Journal Bearings Under 1-G and Maximum Load Conditions.

frequencies of the loaded pads were all above 100,000 rpm.

It would appear that further optimization of the journal bearing designs could produce an increase in the pitch frequency of the unloaded pads. In particular, the moment of inertia of the pads about the pitch axis could be reduced by a gradual reduction in pad thickness from the pivot point out to the leading and trailing edges of the pad, rather than use a constant-thickness pad as was assumed in the calculations.

Although pitch frequency of the unloaded pads was lowest at the condition of maximum bearing load, it was found that the total calculated damping of the bearing was approximately three times greater at maximum load than it was at 1-g load. Since damping is believed to play a vital role in rotor stability, the increased damping may offset any detrimental effect of the low pitch frequency of the unloaded pads. Data given in Reference 17 show a significant increase in whirl threshold speed when rotor orientation is changed from vertical to horizontal. This may reflect the effect of greater total bearing damping resulting from the increased damping obtained from the loaded films.

Overall, the pad dynamics data for the HP spool are generally the same as those obtained with previous successful developments. Some increase in the pitch natural frequencies via a reduction in pitch inertia of the pad appears to be desirable, although perhaps not necessary. However, based on the present lack of proven analysis techniques for predicting threshold of non-synchronous whirl, final assessment of the pad dynamics situation must be made by actual test, preferably by a rotor-bearing system simulator test.

Since the pivoted-pad journal bearing designs for the LP spool were not optimized to the extent of the HP-spool bearings, the pad dynamics situation for the LP spool was not analyzed.

ROTOR STABILITY

As mentioned previously, the fractional-frequency whirl and stability characteristics of rotors supported by gas-lubricated pivoted-pad bearings are not yet well understood from a theoretical standpoint. That fractional-frequency whirl can occur has been verified by recent test data from two gas-bearing machines.

Test data reported in Reference 7 show that for one particular bearing design, the threshold of fractional-frequency whirl occurred at a rotor speed of approximately 0.5 times the apparent first critical speed of the rotor-bearing system. By contrast, it has been shown both experimentally and analytically that the threshold speed of rotors running in rigidly mounted, full-circular, self-acting and hybrid gas bearings usually occurs at a factor of approximately two times the first critical speed [33, 30]. Thus, if comparable values of bearing stiffness can be obtained, the experimental data suggest that rotors running in pivoted-pad bearings can operate stably at several times higher speeds than those running in full-circular types of bearings. This capability to operate stably at higher speeds was, of

course, the primary advantage of the pivoted-pad bearing which led to its initial use in gas-bearing turbomachinery in the early 1960's.

The radial gas-film stiffness for each pad of the HP-spool journal bearings was calculated at 1-g and maximum load conditions. The lowest values of film stiffness were found to occur with the unloaded pads at maximum load conditions. At 70,000 rpm, the minimum value of film stiffness was 251,000 pounds per inch. If this stiffness value is interpreted, for the moment, as the effective bearing stiffness, Figure 46 indicates that the first critical speed of the HP spool would occur at 20,000 rpm. Based on measured values of threshold-speed factor obtained from the previously referenced test data, the threshold speed for fractional-frequency whirl would lie somewhere between 80,000 and 110,000 rpm; in other words, above running speed. Similar checks throughout the HP-spool speed range showed that the threshold speed would always lie above running speed.

The above procedure of using film stiffness values for a single pad would be a conservative estimate of total bearing stiffness if the bearing pivots were rigidly supported. The estimates of threshold speed would therefore also be conservative. However, for the HP-spool application, the pivots for each pad must be individually mounted on flexures so that the bearing can accommodate journal centrifugal growth and differential thermal expansions. Furthermore, stiffness of each flexure will be only 5 percent or so of the gas film stiffness. Unfortunately, the effect of low-stiffness flexures, if any, on the threshold speed value is unknown at this time. Although the experimental threshold speed data of Reference 7 were obtained using flexure-supported pivoted-pad bearings, there were significant differences between these test bearings and the proposed HP-spool bearings. First, the test bearings had four, rather than three, pads per bearing. Second, two different flexure designs were used in each test bearing. The two loaded pads were supported by identical flexures having stiffnesses approximately equal to the gas film stiffness. The two unloaded pads, however, were supported by identical flexures of considerably lower stiffness, being approximately 10 percent of the gas film stiffness.

Since experimental threshold speed data have been published for only one bearing design, and since this design differs considerably from the HP-spool bearing designs, it is not possible to draw any substantiated conclusions about stability of the HP spool. Because of the present lack of verified analytical procedures for predicting the threshold of fractional-frequency whirl in pivoted-pad bearings, the stability situation must be assessed experimentally. For this purpose, full-scale rotor-bearing system simulators should be used to eliminate any uncertainties about extrapolating test results to larger sizes or higher speeds. Since rotor stability is, of course, a prerequisite for satisfactory HP- and LP-spool operation, this matter must receive immediate attention in any future phase of work related to the feasibility demonstration of the design concepts outlined in this report.

CONCLUSIONS AND RECOMMENDATIONS

To the extent that it is presently possible to make a quantitative analytical assessment, the results of this study indicate that gas lubrication of an advanced 4.5-pound-per-second, two-spool gas generator is technically feasible. However, there are two critical areas where feasibility could not be quantitatively assessed due to the lack of proven analytical techniques and sufficient test data. These areas are rotor-bearing system stability, and adequacy of bearing structural and coating materials at high-temperature, high-stress conditions, such as will exist in the HP-spool turbine-end journal. To complete the basic feasibility assessment as rapidly and conclusively as possible, it is recommended that experimental investigations of these two areas be undertaken using full-scale test rigs representative of the Phase VI design of the HP spool.

If the recommended stability and bearing material investigations result in positive feasibility conclusions, the following developments will be required to implement the gas-bearing approach:

1. A noncontacting face seal for the LP-spool thrust balance piston to greatly reduce LP-spool leakage flow.
2. Practical flexible-shaft balancing, and perhaps damping, techniques for the LP spool. (In all probability, this development would also be required for an oil-lubricated LP spool.)
3. A reliable automatic pressure-limit regulator for the journal bearing cavities to minimize labyrinth seal leakage.
4. A compact, high-speed accessory package which can be directly driven from the compressor end of the LP spool. (Work to this end has already been started by USAAVLABS. Such a package would, of course, also be compatible with an oil-lubricated engine.)
5. A small auxiliary compressor to be incorporated on the HP spool for additional pressurization of the thrust bearing supply gas. A regenerative compressor appears to be most suitable for this requirement.
6. Possibly an automatic thrust bearing air-flow control to prevent excessive cooling, and resultant thermal distortion, of the HP-spool thrust bearing under maximum thrust load conditions. The need for such a control could be experimentally assessed, using the same test rig, in parallel with the above recommended rotor stability investigation.

In all of the above-listed development areas, some design technology already

exists. Hardware development with respect to Items 1, 4 and 5 is currently being pursued, although not specifically for the herein discussed engine application. Extension of the design technology (where necessary), and development of satisfactory techniques and hardware, should not pose significant obstacles to timely development of a gas-lubricated gas generator. However, positive verification of feasibility from the standpoints of rotor stability and bearing materials (as mentioned above) should be obtained before proceeding with the required development tasks.

SPECIFIC CONCLUSIONS

The following conclusions apply specifically to the 4.5-pound-per-second gas-generator configuration. In all probability, these conclusions apply throughout the 3- to 6-pound-per-second flow range. However, further study would be needed to confirm this point.

Journal Bearings

1. On the basis of an experimentally verified analytical design criterion, conventional full-circular externally pressurized journal bearings are not feasible for the present gas-generator application because of stability problems. To overcome this problem, it would be necessary to develop a "constant or controlled clearance bearing" and/or a reliable high-temperature damping mechanism which could suppress the onset of fractional-frequency whirl. Whether a practical mechanism to supply the required amount of damping could be developed is a question which was not investigated.

From a load capacity standpoint, an auxiliary compressor would be required for additional pressurization of the journal bearings.

2. Self-acting pivoted-pad journal bearings can theoretically carry the maximum dynamic bearing loads if ambient pressure around the bearings is maintained at HP-compressor discharge pressure for low and intermediate engine power levels. At rated and near-rated power conditions, full HP-compressor discharge pressure is not required and bearing ambient pressure should be limited to about 130 psia so as to minimize labyrinth seal leakages.
3. Load capacity calculations for the pivoted-pad bearings included effects of thermal distortions resulting from air cooling of the bearings. The use of helically grooved air-flow passages under the journals is a feasible way to limit thermal distortions to an acceptable level.
4. Pivoted-pad journal bearings are known to have appreciably better stability characteristics than externally pressurized bearings; for this reason they have been used extensively in

gas-bearing turbomachinery. However, although some analytical work is being done on the stability of such bearings, this work has not yet been subjected to experimental verification nor reduced to an easily useable form. For these reasons, it is concluded that the HP-spool configuration of the Phase VI gas-generator design should be subjected to experimental investigation of stability characteristics.

5. Flexure support of each pad segment of the pivoted-pad journal bearings is a feasible way to accommodate journal centrifugal growth and differential thermal expansion of the bearing parts. The flexures will not load the pads against the journals at low or zero-speed conditions. Hydrodynamic startup of the bearings is therefore feasible and desirable.
6. Pivoted-pad bearings, on the basis of extensive operating experience, are known to be quite tolerant of environmental dirt and debris. In MTI's experience, no failure of a pivoted-pad journal bearing has ever occurred, for any reason, in field service. In one case, customer acceptance tests required injection of significant amounts of carbon-graphite particles into the machine during operation. Although accumulations of these particles were subsequently found in static areas of the bearing cavities, no malfunction of the bearings was ever observed. On the basis of this and other experiences, it is not felt that any particularly exotic procedures will be required to keep dirt and debris out of the bearing cavities.
7. Because of their segmental and pivot-support features, pivoted-pad bearings can readily self-align. Hence, problems of maintaining precise mechanical alignment between the hot and cold ends of the machine are greatly alleviated. Pivots have been extensively tested at temperatures up to 1400^oF under simulated pad motions, for periods of 2000 hours, with no sign of pivot damage.
8. The question of structural and surfacing materials for the HP-spool turbine-end journal is crucial. Data relative to 1000-hour creep rates, dimensional stability, corrosion resistance, and coating bond strength must be obtained at the actual operating conditions of the journal. Subsequent to these tests, assuming that satisfactory materials are found, high-speed rub compatibility between the journal and pads must be determined. Existing test data (see Appendix III) suggest that the material requirements can be met. However, the operating conditions of the HP-spool turbine-end bearing are severe from a materials standpoint, and testing is essential to establish feasibility.

Thrust Bearings

1. Externally pressurized thrust bearings are required to carry the maximum dynamic thrust loads. The only stipulation which must be made is that the engine not be operated at less than 15 percent of rated power during an arrested landing.

Self-acting types of thrust bearings are not feasible.

2. An auxiliary compressor is required to achieve sufficient supply pressure for the externally pressurized thrust bearings. This compressor should ideally be an integral part of the HP spool. A regenerative type of compressor represents a feasible means for achieving the required 1.7 pressure boost.
3. For engine startup, an external source of pressurized air will be required for the thrust bearings. If startup is accomplished by mechanical drive of the spools via the accessory power-take-off shaft, an 80- to 100-psi external source of air would be required for the thrust bearings. In this mode of startup, the thrust bearings provide axial loading force to couple the HP and LP spools via friction or face-serrated drive surfaces. If direct air-drive of the HP spool could be used, and if it were a feasible way to accomplish startup, considerable reduction in thrust bearing supply pressure might be possible. This latter startup concept was not investigated.
4. The externally pressurized thrust bearings will have many relatively large feeding holes. Accordingly, standard high-temperature air filtering means should be sufficient protection against problems of dirt and debris.
5. If satisfactory structural and coating materials can be found for the HP-spool turbine-end journal bearings, thrust bearing materials should not be a problem.

Bearing Cooling

1. Cooling of the journal bearings can be conveniently accomplished using turbine cooling air. Helically grooved flow passages under the journals provide a feasible means for removing bearing friction losses without excessive thermal distortions.
2. The HP-spool turbine-end journal bearing will be the hottest bearing in the gas generator. Maximum bearing temperatures will occur at sea-level rated-power conditions. For the HP-spool turbine-end bearing, it would be desirable to operate with a maximum bearing temperature in the range of 1300°F and 1500°F to minimize thermal stresses in the turbine heat dam. However, to achieve reliable 1000-hour bearing life with present-day structural materials, maximum bearing temperature would have to

be limited to 1300°F. From a heat transfer standpoint, it appears feasible to achieve a design-point temperature anywhere in the range of 1200°F to 1500°F.

3. Air flow through the externally pressurized HP-spool thrust bearing, together with labyrinth seal leakage flow, is sufficient to remove the bearing friction losses with acceptable temperature rise. Actually, other modes of heat transfer will also exist.
4. Air flow through the externally pressurized LP-spool thrust bearing is not sufficient to remove the bearing friction losses. In this case, however, the second-stage axial compressor blades provide an excellent heat transfer path from the thrust runner to the compressor air flow. Therefore, cooling of this bearing should not be a problem.

Rotor Dynamics

1. The HP spool will behave as a rigid rotor. Synchronous unbalance response will not be a problem. Two-plane balancing techniques can be used. Normal standards of balancing for gas-bearing machinery will be sufficient. These standards are not difficult to achieve.
2. The LP spool will behave as a flexible rotor. Design speed will lie between the third and fourth flexural critical. (In a realistic sense, there are no "rigid" body criticals for the LP spool.) Practical multiplane balancing techniques will probably have to be developed. Because of assembly requirements, only the two ends of the spool will be available for final balance trim during the final stage of engine assembly. Additional study is needed to assess the feasibility of developing a practical balancing procedure for the LP spool. Several practically oriented multiplane balancing theories are now available, and existing computer programs can be used to perform an analytical feasibility study of this problem.
3. In addition to the problem of achieving satisfactory balance of the LP spool, the question as to maintenance of balance for the required time between overhauls must be studied. If maintenance of balance appears doubtful, due perhaps to thermal distortions or unsymmetrical creep, thought should be given to the use of additional means of damping. An intershaft bearing, for example, was found to appreciably suppress unbalance resonant amplitudes. Implementation of this approach, however, presents a mechanical design challenge.
4. It should be noted that the LP-spool unbalance response problem is not the result of using gas bearings. The same problem would exist with oil-lubricated bearings. Only if oil-film, rather than rolling-element, bearings were used might the problem be

somewhat less severe. Oil-film bearings, depending on size, might contribute more damping to the rotor.

5. Stability aspects were discussed under Item 4 of the journal bearing conclusions and hence will not be repeated here.

General Conclusions

1. The most severe operating condition for both the journal and the thrust bearings is engine idle under maximum dynamic load conditions. This is due to the low levels of engine pressures at idle speeds. The 25,000-foot maximum altitude condition is, therefore, the most severe idle condition.
2. There is a strong interaction between HP-spool dynamics and bore diameters of the HP turbine and HP compressor. Design of the HP turbine and compressor components for a two-spool gas-bearing engine should emphasize maximum possible bore diameters.
3. Aerodynamic thrust forces from turbine and compressor components must be minimized to the maximum extent possible by aerodynamic design. This is particularly important with respect to the LP spool. For the Phase VI gas-generator layout, it was necessary to add a thrust balance piston to this spool to reduce the net thrust loads to manageable values. However, in addition to being an extra part, the labyrinth seal for the balance piston has by far the largest leakage rate of all the engine seals. Reduction of the axial compressor thrust forces would permit reduction of the balance-piston diameter, which in turn would reduce seal losses.
4. Gas-seal losses for the HP spool are comparable to those for conventional single-spool low-pressure engines. Losses for the LP spool, however, are considerably higher. This is primarily the result of thrust-balance piston losses and the compressor-end journal bearing cavity losses. Careful attention should be given in future designs to the factors which determine seal radial clearance requirements and to ways of achieving more seal length. Consideration should also be given to the use of a non-contacting face seal for the LP-spool thrust-balance piston.

RECOMMENDATIONS

To complete this feasibility assessment, it is essential to obtain data relative to (1) rotor-bearing system stability and (2) adequacy of bearing structural and coating materials for the HP-spool turbine-end journal at the high-temperature, high-speed conditions which will exist. The writer believes that these data can most rapidly and conclusively be obtained by experimental means. Specifically, it is recommended that:

1. A full-scale rotor-bearing system simulator for the HP spool be built and tested to assess the rotor-stability question. The simulator should utilize the types of bearings recommended in this report.

At the same time and with little additional cost, the simulator could be designed to experimentally verify the load capacity of the journal and thrust bearings under the maximum specified load conditions. Although the analytical load capacity results are believed to be valid, self-acting pivoted-pad journal bearings have never been operated at the high eccentricity conditions required for this application. Experimental verification of high-eccentricity load capacity is therefore quite important.

The simulator should be operated cold; i.e., simulation of aerodynamic temperatures is not important to the test objectives. However, the bearing cooling techniques must be incorporated into the simulator design. Although bearing temperature levels are a strong function of aerodynamic temperatures, bearing temperature gradients are primarily a function of bearing friction losses and bearing cooling technique. Since bearing load capacity is a strong function of bearing temperature gradients, the recommended simulator program would, of necessity, provide test verification of the bearing cooling concepts and the predictions of thermal distortions.

2. A second test rig be built to test full-scale models of the HP-spool turbine-end journal. Tests should be performed in air at 70,000 rpm and 1500°F. Purpose of the tests should be to evaluate various combinations of journal structural and coating materials with respect to the following:
 - a. Corrosion
 - b. Creep
 - c. Coating bond strength
 - d. Dimensional stability.

Short-term, intermediate-term, and 1000-hour tests should be performed.

The above test programs should answer the remaining basic feasibility questions relative to applying gas bearings to the 3- to 6-pound-per-second class of advanced aircraft engines. If the above tests are positive, the next question to be asked is, Do gas-lubricated bearings offer significant advantages over oil-lubricated bearings? To answer this question objectively, a similar type of design feasibility study would seem to be required for the oil-lubricated approach. Only by comparing results from the two studies could knowledgeable decisions be made as to the future course to be followed. Three alternatives would, of course, be possible: all oil-lubricated, all gas-lubricated, or a combination of oil- and gas-lubricated bearings. Once a decision is reached, a specific, phased (least risk), overall development program could rapidly be formulated based on the findings of the feasibility studies.

REFERENCES CITED

1. Sternlicht, Beno, GAS-BEARING TURBOMACHINERY, ASME Paper No. 68-Lubs-32, presented at the Lubrication Symposium, Las Vegas, June 17, 1968.
2. Curwen, P.W., EVALUATION OF GAS BEARINGS FOR USE IN NAVAL MACHINERY UNDER CONDITIONS OF FRAME OSCILLATION AND IMPACT, Mechanical Technology Inc., MTI Report 65TRI, prepared for Office of Naval Research under Contract Nonr-4358(00), January 1965.
3. Navy contract N000-14-66-C 282, EVALUATION OF GAS BEARINGS FOR USE IN NAVAL MACHINERY UNDER CONDITIONS OF HI-IMPACT, work being performed by Mechanical Technology Inc. for the Office of Naval Research, Washington, D.C.
4. Curwen, P.W., and Frost, A., AN INVESTIGATION OF THE PERFORMANCE OF GAS-BEARING MACHINERY SUBJECTED TO LOW-FREQUENCY VIBRATION AND SHOCK, paper presented at the 38th Shock and Vibration Symposium, May 1, 1968, to be published in The Shock and Vibration Bulletin No. 38 by the Naval Research Laboratory, Washington, D.C.
5. Schwarz, H., DESIGN OF FORCED-DRAFT BLOWER WITH STEAM-LUBRICATED JOURNAL AND THRUST BEARINGS, Mechanical Technology Inc; MTI Report 66TR61, prepared for the Office of Naval Research under contract Nonr-4966(00), Nov. 15, 1966.
6. Curwen, P.W., and Meacher, J.S., TURBOMACHINERY RESEARCH FOR NUCLEAR SYSTEMS, Mechanical Technology Inc.; AEC Report NYO-3237-10 (Special), U. S. Atomic Energy Commission, Washington, D.C., July 1968.
7. Curwen, P.W., RESEARCH AND DEVELOPMENT OF HIGH-PERFORMANCE AXIAL-FLOW TURBO-MACHINERY, VOLUME 2 - DESIGN OF GAS BEARINGS, Mechanical Technology Inc.; NASA Contractor Report CR-801, Lewis Research Center, Cleveland, Ohio, May 1968.
8. Curwen, P.W., Harmon, R.A., and Manning, G.B., A COMPARISON OF OIL AND GAS LUBRICATION SYSTEMS FOR CLOSED LOOP GAS TURBINE MACHINERY, ASME Paper No. 67-GT-9, presented at the 12th Annual Gas Turbine Conference and Products Show, Houston, Texas, March 5-9, 1967.
9. NASA Contract NAS 3-7629, SELECTION OF MATERIALS AND TESTING OF GAS-BEARING PIVOT CONFIGURATIONS FOR A HIGH-TEMPERATURE ARGON ENVIRONMENT AND OTHER TYPICAL BRAYTON CYCLE SYSTEM CONDITIONS, work being performed by Mechanical Technology Inc. for the Lewis Research Center, Cleveland, Ohio.

10. NASA Contract NAS 3-9433, DEVELOPMENT OF SELF-ACTING GAS BEARINGS FOR HIGH-TEMPERATURE OPERATION IN A NON-ISOTHERMAL ENVIRONMENT FOR ADVANCED GAS TURBINE MACHINERY, work being performed by Mechanical Technology Inc. for the Lewis Research Center, Cleveland, Ohio
11. Air Force Contract AF 33(615)-3235, HIGH-TEMPERATURE GAS LUBRICATION, work being performed by Mechanical Technology Inc for the Air Force Aero Propulsion Laboratory, Wright-Patterson Air Force Base, Dayton, Ohio.
12. Richardson, Harry L., and Tommasini, Rocco M., ADVANCEMENT OF SMALL GAS TURBINE ENGINE ACCESSORY TECHNOLOGY, Curtiss-Wright Corp.; USAAVLABS Technical Report 67-13, U.S. Army Aviation Materiel Laboratories, Fort Eustis, Virginia, April 1967, AD 652896.
13. Malanoski, S.B., EXPERIMENTS ON AN ULTRASTABLE GAS JOURNAL BEARING, ASME Paper No. 66-Lub-6, 1966.
14. Gunter, E.J., Jr., Hinkle, J.G., and Fuller, D.D., DESIGN GUIDE FOR GAS LUBRICATED TILTING PAD JOURNAL AND THRUST BEARINGS WITH SPECIAL REFERENCE TO HIGH SPEED ROTORS, The Franklin Institute Research Laboratories; AEC Report No. NYO-2512-1, U.S. Atomic Energy Commission, Washington, D.C.
15. Lund, J.W., CALCULATION OF STIFFNESS AND DAMPING PROPERTIES OF GAS BEARINGS, ASME Paper No. 68-Lubs-19, presented at the Lubrication Symposium, Las Vegas, Nev., June 17, 1968.
16. Curwen, P.W., Bjerlkie, J.W., Jones, H.F., McLaughlin, D.W., Smith, L.F., and Smith, V.J., DESIGN AND DEVELOPMENT OF A GAS-BEARING BRAYTON CYCLE TURBOCOMPRESSOR, Mechanical Technology Inc.; AEC Report NYO-3237-1, U.S. Atomic Energy Commission, Washington, D.C., March 1, 1965.
17. Waters, W.J., and Freche, J.C., A HIGH STRENGTH NICKEL-BASE ALLOY WITH IMPROVED OXIDATION RESISTANCE UP TO 2200 DEG F, ASME Paper No. 67-GT-1, presented at the Gas Turbine Conference, Houston, Texas, March 5-9, 1967.
18. HIGH-TEMPERATURE HIGH-STRENGTH NICKEL BASE ALLOYS, Revised Edition, The International Nickel Company, Inc., 67 Wall Street, New York, N.Y., 1964.
19. CREEP-RUPTURE DATA ON THE 0.5% TITANIUM-MOLYBDENUM ALLOY AT 1000° TO 24000°F, Climax Molybdenum Company, 1270 Avenue of the Americas, New York, N.Y., Sept. 1957.
20. Peterson, M.B., Arwas, E.B., Gray, S., Murray, S.F., Lund, J.W., INTERIM REPORT, ANALYTICAL AND EXPERIMENTAL INVESTIGATION OF GAS BEARING TILTING PAD PIVOTS, Mechanical Technology Inc.; MTI Report 67TR84, prepared for the NASA-Lewis Research Center under contract Nas 3-7629, Nov. 1967.

21. Murray, S.F., and Peterson, M.B., MATERIAL CONSIDERATIONS FOR HIGH TEMPERATURE TILTING PAD GAS BEARINGS, ASME Paper No. 68-Lubs-34, presented at the Lubrication Symposium, Las Vegas, Nev., June 17, 1968.
22. Grover, H.J., Gordon, S.A., and Jackson, L.R., FATIGUE OF METALS AND STRUCTURES, Battell Memorial Institute; NAVWEPS Report 00-25-534, Bureau of Naval Weapons, Department of the Navy, Washington 25, D.C., June 1960, p. 127.
23. Sternlicht, Beno, DESIGN AND APPLICATION OF GAS BEARINGS, ASME Paper No. 64-MD-3, presented at the Design Engineering Conference and Show, Chicago, Illinois, May 11, 1964.
24. Rieger, N.F., DESIGN OF GAS BEARINGS - 1967, VOLUMES I AND II, Notes supplemental to the RPI-MTI course on gas bearing design, Mechanical Technology Inc., 1967.
25. Pan, C.H.T., and Sternlicht, B., THERMAL DISTORTION OF SPIRAL-GROOVED GAS-LUBRICATED THRUST BEARING DUE TO SELF-HEATING, Transactions of the ASME, Vol. 89, Series F, No. 2, April 1967.
26. Meacher, J.S., EXPERIMENTAL TEST AND EVALUATION OF A GAS-BEARING BRAYTON CYCLE TURBOCOMPRESSOR, Mechanical Technology Inc; AEC Report NYO-3237-8, U.S. Atomic Energy Commission, Washington, D.C., Oct. 6, 1967.
27. Meacher, J.S., EXPERIMENTAL TEST AND EVALUATION OF A GAS-BEARING BRAYTON CYCLE TURBOCOMPRESSOR, Mechanical Technology Inc.; AEC Report NYO-3237-6, U.S. Atomic Energy Commission, Washington, D.C., Aug. 26, 1966.
28. Frost, A., Lund, J.W., and Curwen, P.W., RESEARCH AND DEVELOPMENT FOR A HIGH-PERFORMANCE TURBOALTERNATOR AND ASSOCIATED HARDWARE, VOLUME 2 - DESIGN GAS BEARINGS, Mechanical Technology Inc., NASA Contractor Report CR- , Lewis Research Center, Cleveland, Ohio, Aug. 1968.
29. Zabriskie, W., and Sternlicht, B., LABYRINTH-SEAL LEAKAGE ANALYSIS, ASME Paper No. 58-A-118, Presented at annual meeting, New York, N.Y., Nov. 30, 1958.
30. Wilson, D., and Murray, S.F., GAS LUBRICATION RESEARCH FOR 1900 F NON-ISOTHERMAL OPERATION; BEARING DISTORTION EFFECTS ON PERFORMANCE AND HIGH TEMPERATURE MATERIAL INVESTIGATIONS, Mechanical Technology Inc; Technical Report AFAPL-TR-67-57, Part I, Air Force Aero Propulsion Laboratory, Wright-Patterson Air Force Base, Dayton, Ohio, May 1967.
31. Rieger, N.S., COMPUTER PROGRAM FOR BALANCING OF FLEXIBLE ROTORS, Mechanical Technology Inc.; MTI Report No. 67TR68, prepared under NASA contract NAS 3-10926 for the Lewis Research Center, Cleveland, Ohio, Sept. 15, 1967.

32. Elrod, H.G. Jr., McCabe, J.T., and Chu, T.Y., DETERMINATION OF GAS-BEARING STABILITY BY RESPONSE TO A STEP-JUMP, Transactions of the ASME, Vol. 89, Series F, No. 4, Oct. 1967.
33. Lund, J.W., A THEORETICAL ANALYSIS OF WHIRL INSTABILITY AND PNEUMATIC HAMMER FOR A RIGID ROTOR IN PRESSURIZED GAS JOURNAL BEARINGS, Transactions of the ASME, Vol. 89, Series F, No. 2, April 1967.
34. Futral, Samuel M., Jr., and Wasserbauer, Charles A., OFF-DESIGN PERFORMANCE PREDICTION WITH EXPERIMENTAL VERIFICATION FOR A RADIAL-INFLOW TURBINE, Lewis Research Center; NASA Technical Note TN D-2621, National Aeronautics and Space Administration, Washington, D.C., February 1965.
35. Johnsen, Irving A. and Bullock, Robert O. (editors), AERODYNAMIC DESIGN OF AXIAL-FLOW COMPRESSORS, REVISED, Lewis Research Center; NASA Publication SP-36, National Aeronautics and Space Administration, Washington, D.C., 1965.
36. HASTELLOY X, bulletin prepared by the Stellite Division of Union Carbide Corporation, October, 1964.
37. Wilson, D. and Murray, F., GAS LUBRICATION FOR 1900°F NON-ISOTHERMAL OPERATION — SECOND SEMI-ANNUAL PROGRESS REPORT, Mechanical Technology Inc.; MTI Report 67TR64, prepared for the Air Force Aero Propulsion Laboratory, Wright-Patterson Air Force Base, Dayton, Ohio, Sept. 30, 1967.
38. EVALUATION STUDY OF HASTELLOY X AS A NUCLEAR CLADDING — QUARTERLY PROGRESS REPORT, 1 OCTOBER THROUGH 31 DECEMBER 1966, Aerojet-General Corporation; Aerojet-General Report No. AGN-8214, prepared for the U.S. Atomic Energy Commission under contract AT(04-3)-368, Project Agreement No. 6.
39. EVALUATION STUDY OF HASTELLOY X AS A NUCLEAR CLADDING — QUARTERLY PROGRESS REPORT, 1 JANUARY THROUGH 31 MARCH 1967, Aerojet-General Corporation; Aerojet-General Report No. AGN-8224, prepared for the U.S. Atomic Energy Commission under contract AT(04-3)-368, Project Agreement No. 6.
40. Rauch, H.W., Sr., Sutton, W.H. and McCreight, L.R., SURVEY OF CERAMIC FIBERS AND FIBROUS COMPOSITE MATERIALS, Space Sciences Laboratory, General Electric Co.; Technical Report AFML TR-66-365, Air Force Systems Command, Research and Technology Division, Wright-Patterson Air Force Base, Ohio, October 1966.
41. Fox, G.R. and Murray, S.F., GAS BEARING DEVELOPMENT PROGRAM, General Electric Company; Final report for Contract AF 33-038-21102, Req. No. 192(ANPG)05582, October 28, 1958.

42. Ingham, H.S. and Shepard, A.P., FLAME SPRAY HANDBOOK - VOL. III, PLASMA FLAME PROCESS, Westbury, Long Island, New York, Metco Inc., 1965.
43. AEC Contract AT(30-1)-3839, STEAM LUBRICATION OF TURBOMACHINERY, work being performed by Mechanical Technology Inc. for the U.S. Atomic Energy Commission, Washington, D.C.
44. Macks, E.F., GAS LUBRICATION OF RADIAL AND THRUST BEARINGS AT HIGH TEMPERATURES, HIGH SPEEDS, AND LOW LUBRICANT FLOW RATES, Airglide Laboratories; WADD Report No. TR 61-83, Wright-Patterson Air Force Base, Ohio, February 1961.
45. Drescher, H., SPECIAL FEATURES OF SELF-ACTING AIR BEARINGS AND THEIR EFFECT ON PRACTICAL APPLICATION, Gas-Lubricated Bearings (First International Symposium), document No. ACR-49, published by the Office of Naval Research, Department of the Navy, Washington, D.C., October, 1959, pp. 319-345.
46. Adams, C.R., STEP GAS BEARINGS, SAE Journal, June 1960, pp. 29-31.
47. Murray S.F. and Peterson, M.B., THE SELECTION AND EVALUATION OF MATERIALS AND LUBRICANT FILMS FOR GAS-LUBRICATED GYRO BEARINGS, Mechanical Technology Inc; MT Report 64TR1, prepared for Director, SP-24, under Contract Nobs-88615 (FBM), June 6, 1964.
48. Trugman, L.A., SOME TESTS ON HYDRODYNAMIC GAS BEARINGS AT NORMAL AND ELEVATED TEMPERATURES, Lubrication Engineering, Vol. 21, No. 4, April 1965, p. 138.
49. Patterson, A.G., THE EVOLUTION AND DESIGN OF AN AERODYNAMIC GAS BEARING, Paper No. 1, Gas Bearing Symposium, University of Southampton, England, March 1965.
50. Lund, Jorgen W., THE STABILITY OF AN ELASTIC ROTOR IN JOURNAL BEARINGS WITH FLEXIBLE, DAMPED SUPPORTS, ASME Paper No. 65-APM-8, presented at the Western Conference of the Applied Mechanics Division, Los Angeles, Calif., Aug. 30, 1965.
51. Wilcock, D.F., Bjerklie, J.W., and Cheng, H., DESIGN OF FLOATED SHOE CLOSE CLEARANCE SEALS FOR SUPERSONIC JET ENGINE COMPRESSORS, Transactions of the ASME, Vol. 90, Series F, No. 2, April 1968, pp. 500-509.
52. Cheng, H.S., Chow, C.Y., and Wilcock, D.F., BEHAVIOR OF HYDROSTATIC AND HYDRODYNAMIC NON-CONTACTING FACE SEALS, Transactions of the ASME, Vol. 90, Series F, No. 2, April 1968, pp. 510-519.

APPENDIX I
AERODYNAMIC ANALYSIS OF THE TURBINE
AND COMPRESSOR COMPONENTS

INTRODUCTION

Before the bearing-system and rotor-dynamic design studies for the gas generator were begun, it was necessary to establish the weights, sizes, and speeds of the aerodynamic components. In addition, static pressures and blade forces were required as a function of speed to enable thrust loads to be predicted. Static pressures were also required (as a function of speed) to determine ambient and differential pressures which would be available for bearing design purposes.

Starting from the specified gas-generator design-point conditions (as defined on page 9), the following aerodynamic studies are necessary to obtain the required data:

1. Design-point thermodynamic analysis
2. Optimization study of components
3. Sizing of compressor and turbine components
4. Component performance prediction
5. Off-design matching analysis
6. Calculation of off-design static pressures and total temperatures
7. Calculation of blade forces.

To reduce the considerable amount of aerodynamic analysis required for Steps 2, 3, and 4 above, the following data were provided by USAAVLABS:

1. A design configuration of a two-stage, 3-to-1 pressure-ratio axial compressor, together with a predicted performance map for the compressor.
2. A performance map for a single-stage, 6-to-1 pressure-ratio centrifugal compressor.
3. A design configuration for a radial turbine.

Extensive use was made of these data to obtain predicted performance of the axial and centrifugal compressor components, as well as to size the axial compressor, for the gas generator.

It was recognized that the use of USAAVLABS data in this manner would not result in an optimized aerodynamic design for the specific 4.5-pound-per-second application, nor would the predicted overall engine performance

characteristics be exactly right. Nonetheless, this approach to the aerodynamic design was judged to be adequate for the purpose of the study, which, of course, was to determine the feasibility of applying gas bearings to advanced gas generator engines. Use of the USAAVLABS data, having been recently generated under USAAVLABS contracts for development of advanced turbine and compressor components, should constitute a reasonable basis for definition of rotor-bearing system requirements for advanced two-spool engines in the 3-to-6-pound-per-second airflow range.

The following sections of this appendix document and discuss the seven aerodynamic analysis steps as performed for the gas-generator application.

AERODYNAMIC ANALYSIS

Throughout the following sections of this appendix, the specific assumptions used are stated. The general assumptions of the overall study were as follows:

1. Constant turbine efficiencies
2. Constant fuel-air ratio of 0.035 for determination of gas properties
3. Constant percentage of bleed flow
4. Negligible inlet and duct losses.

Design Point Thermodynamic Analysis

The design-point engine parameters, as specified in the contract Statement of Work, are given in Table I.

During a preliminary aerodynamic study of the gas generator (i.e., during Phase I of the contract), no obviously significant effect of flow range (within the specified limits of 3 to 6 pounds per second) was identified with respect to either aerothermo aspects of turbine and compressor design or mechanical and dynamic aspects of rotor-bearing system design. Since the Army has potential engine applications over the complete 3-to-6-pound-per-second flow range, a 4.5-pound-per-second design-point was selected so that a minimum of extrapolation would be required to extend the final results of the study to either extreme of the 3-to-6-pound-per-second flow range. All aerodynamic results reported in this appendix are based on a 4.5-pound-per-second design-point flow.

For the design-point thermodynamic analysis, the following specific assumptions were used:

1. Disc friction and bearing losses 2 percent of gas-generator turbine power

- | | |
|---------------------------------|--|
| 2. Gas bearing air requirements | negligible with respect to compressor design-point flow |
| 3. Inlet and duct losses | assumed to be included in component efficiencies |
| 4. Radial turbine efficiency | 85 percent (This results in an efficiency of 86.5 percent for the axial turbine based on the specified overall turbine efficiency of 86 percent) |
| 5. Component efficiencies | assumed to be based on total-to-total conditions |

The results of the design-point thermodynamic analysis, based on the above assumptions, are summarized in Table XV.

Component Optimization Study

As mentioned in the Introduction to this appendix, an extensive aerodynamic effort to optimize the gas-generator components (particularly the compressors) was circumvented by use of the following data provided by USAAVLABS:

1. The two-stage 3-to-1 pressure-ratio axial compressor
 - a. A dimensional sketch
 - b. A predicted performance map
 - c. Velocity diagrams.
2. The single-stage 6-to-1 pressure-ratio centrifugal compressor

A measured performance map.
3. The radial single-stage turbine

A dimensional sketch.

The USAAVLABS compressor data were generated under recent USAAVLABS contracts and have been assumed to represent current advanced state of the art. As will be seen in following sections of this appendix, these data were used for sizing of the gas-generator compressor components and for predicting off-design performance. The radial turbine data, however, were used only to justify the selection of the turbine detailed configuration; namely, the use of a highly scalloped turbine disc. Disc scalloping of a radial turbine or compressor component is common practice in gas-bearing machinery as a means of reducing differential pressure forces acting on the disc.

TABLE XV. COMPONENT DESIGN-POINT CONDITIONS						
	STATION*					
	(1) Axial Compressor Inlet	(2) Centrifugal Compressor Inlet	(3) Combustion Chamber Inlet	(4) Radial Turbine Inlet	(5) Axial Turbine Inlet	(6) Power Turbine Inlet
P_T -psia	14.7	44.1	264.5	256.5	108.4	78.1
T_T -°R	520	753	1352	3460	2958	2781
W-lb/sec	4.50	4.50	4.19	4.34	4.65	4.65
HP/lb	79.4	201.0	—	223.0	79.8	285.0**
<p>*Station numbers correspond to similarly numbered stations on the compressor and turbine meridional views of Figures 60 and 61 .</p> <p>**This value was specified by the contract Statement of Work. However, it appears that up to 320 HP per pound of air may be realizable from the power turbine.</p>						

Sizing of Compressors and Turbines

Axial Compressor

The two-stage axial compressor data supplied by USAAVLABS were based on a design flow of 5.0 pounds per second. To scale the compressor size for 4.5 pounds per second, a sizing scale factor of 0.949 was used (scale factor = $\sqrt{4.5/5.0}$). Figure 60 shows the axial compressor design scaled down to 4.5 pounds per second. The new design speed was obtained by dividing the original speed by the scale factor. Hence, $N = 59600/0.949 = 62,800$ rpm.

Centrifugal Compressor

The centrifugal compressor data supplied by USAAVLABS were likewise based on a flow rate slightly different from that of the present gas generator. A scale factor was accordingly computed for the compressor data as follows:

$$\text{Scale Factor} = \sqrt{\frac{W_1}{W_2} \frac{P_2}{P_1} \sqrt{\frac{T_1}{T_2}}} \quad (3)$$

Subscripts 1 and 2 refer to conditions for the gas-generator compressor and the USAAVLABS compressor data respectively. Using the resulting scale factor, the USAAVLABS data gave the following values for the gas-generator centrifugal compressor:

Compressor tip diameter = 7.50 inches

Speed = 63,100 rpm.

In the event that a smaller size and weight compressor might be advantageous from the standpoint of rotor dynamic and bearing system design (which was intuitively felt to be the case prior to start of the actual mechanical design study), the compressor size was also scaled for the maximum speed value permitted by the contract Statement of Work. The resulting alternative design values were as follows:

Compressor tip diameter = 6.65 inches

Speed = 70,000 rpm.

Aerodynamic calculations for the compressor inducer indicated that this change in size and speed was entirely reasonable.

Figure 60 shows the meridional view of the centrifugal compressor for the 70,000 rpm design-point speed. The inducer inlet area is sized to accommodate an absolute Mach number of 0.5 to allow some acceleration in the S-duct.

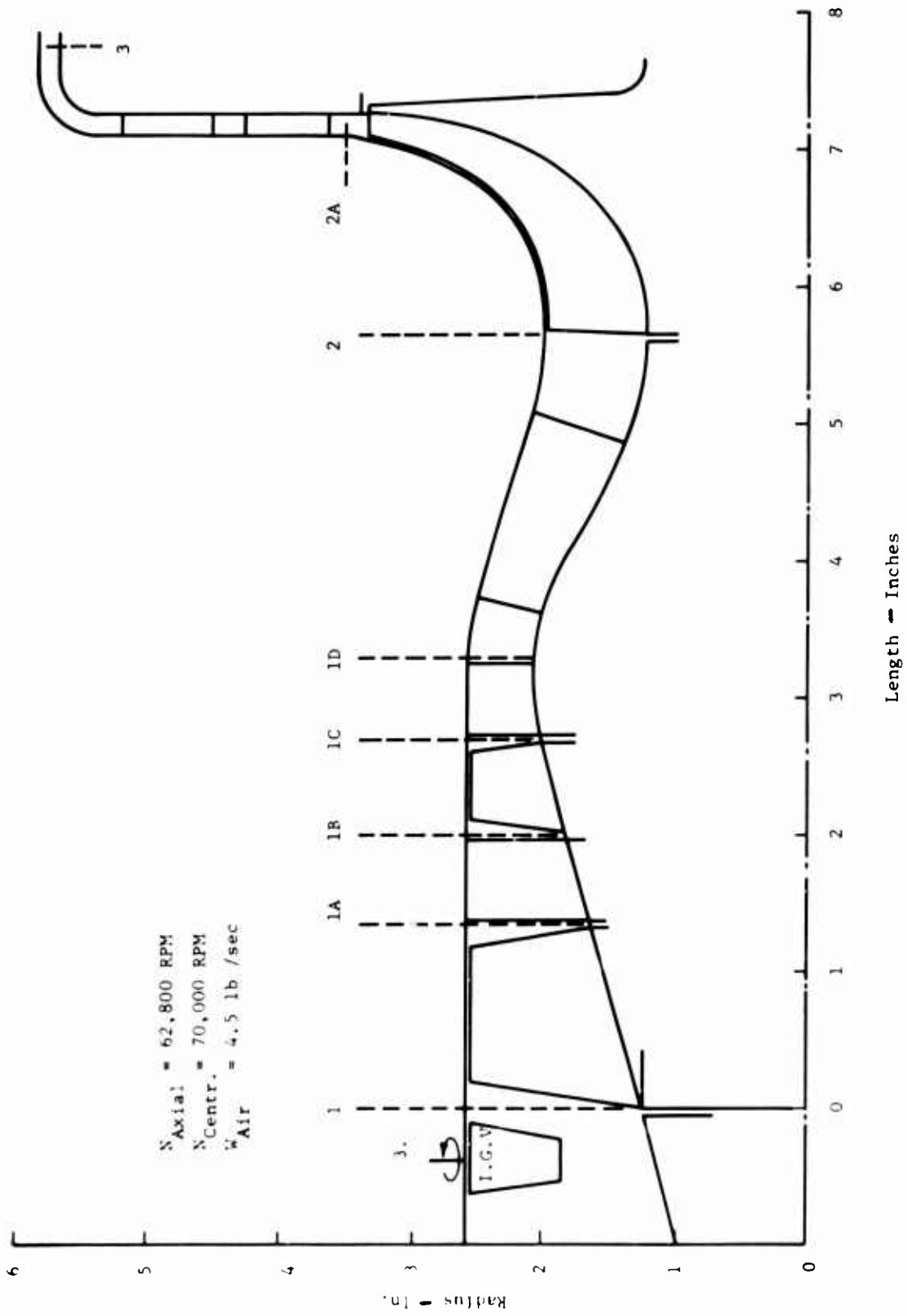


Figure 60. Meridional View of Axial and Centrifugal Compressor Stages.

Radial Turbine

Using a HP (high-pressure) spool design speed of 70,000 rpm, the radial turbine was sized on the basis of centrifugal compressor power requirements, bleed flow, and bearing losses. A minor degree of freedom existed in the design of the exducer.

Using a velocity ratio of $U/C_0 = 0.7$, a nozzle angle of 70 degrees, a meridional velocity ratio of 1.1, and a minimum hub radius of 1.5 inches, the radial turbine configuration appears as shown in Figure 61. The basic proportions (but not the absolute dimensions) of the configuration are similar to those of the radial turbine configuration supplied by USAAVLABS.

Axial Turbine

The design-point speed for the LP (low-pressure) spool, as determined from the axial compressor sizing calculations, was 62,800 rpm. For the required work output of the axial turbine, there was considerable freedom for design optimization.

The design was chosen to have only 10 percent reaction at the hub. This reaction is sufficient to ensure acceptably high efficiency. The advantages obtained from the low hub reaction are

1. Low weight
2. Low blade root temperature
3. Low blade pressure drop and, hence, low differential pressure (thrust load) across the turbine disc

The configuration of the axial turbine is shown in Figure 61.

Component Performance Prediction

Axial Compressor

The compressor performance map for the two-stage axial compressor was obtained by replotting the map supplied by USAAVLABS, using the appropriate mass-flow scale factor of 0.90. As mentioned previously, the corrected value of design speed was 62,800 rpm. All other values remained the same.

Figure 62 shows the axial compressor map, as scaled from the USAAVLABS data, for the 4.5-pound-per-second gas-generator.

Centrifugal Compressor

The performance map for the single-stage centrifugal compressor was likewise obtained by replotting the USAAVLABS map, using the appropriate mass-flow scale factor. However, since the USAAVLABS map is a

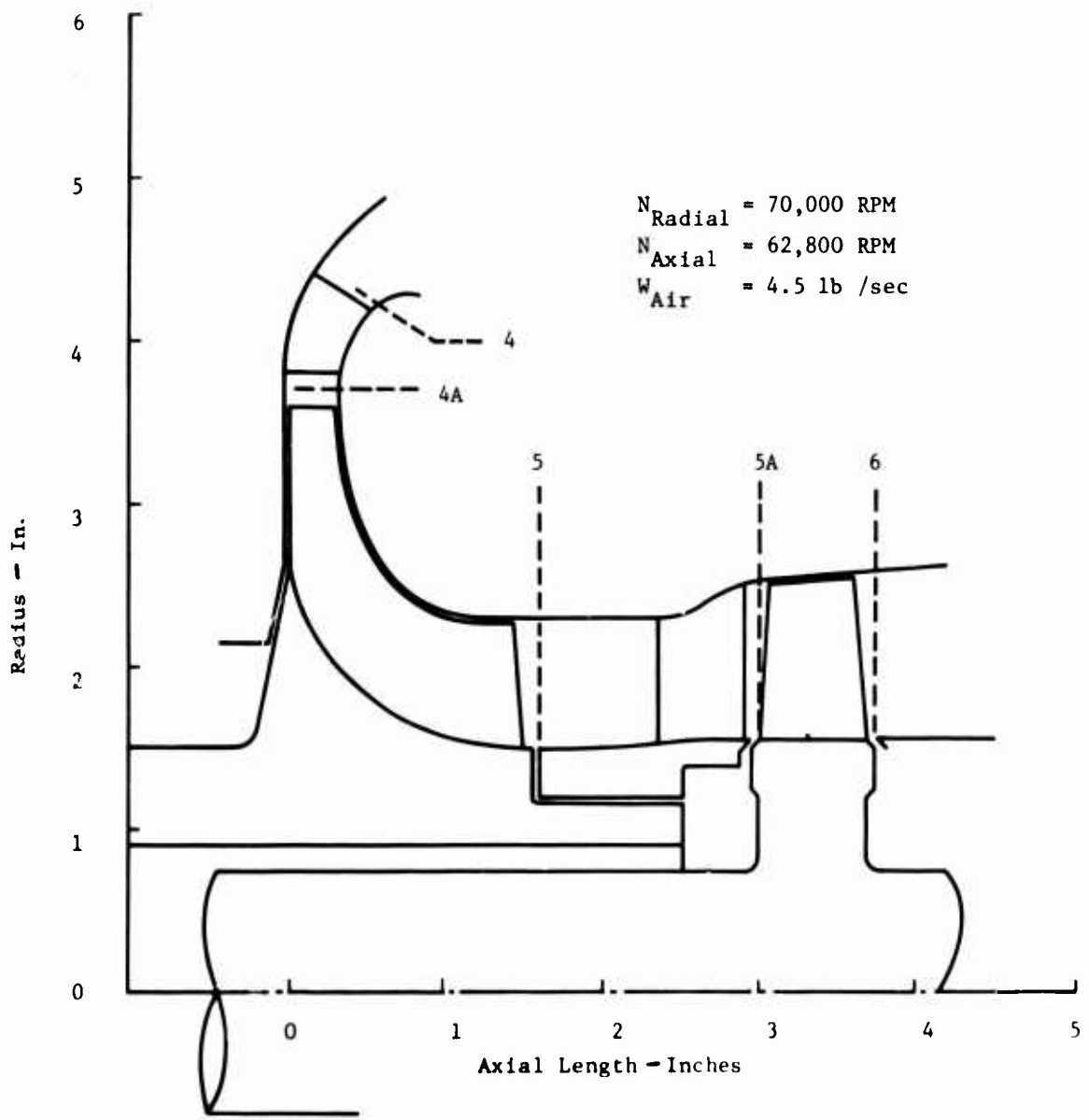


Figure 61. Meridional View of Radial and Axial Turbine Stages.

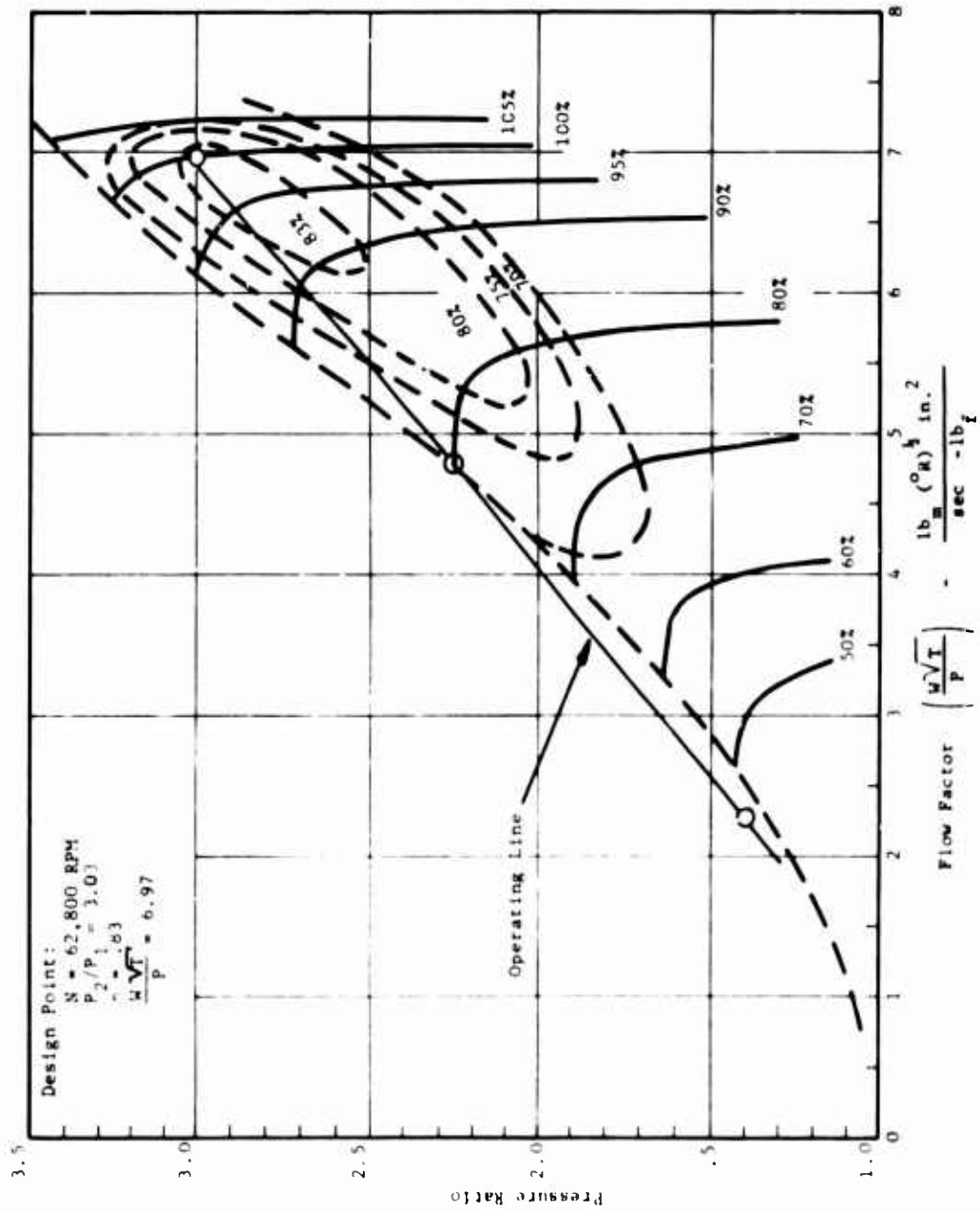


Figure 62. Two-Stage Axial Compressor Map (design-point flow equals 4.5 pounds per second).

classified document, a figure of the scaled centrifugal compressor map for the gas-generator could not be included in this report.

Radial Turbine

In order to simplify the turbine-to-compressor matching analysis (for which the component performance maps were required), it was assumed that the radial turbine flow characteristic could be represented as a single curve of pressure-ratio versus flow-factor. To obtain a realistic curve, a radial turbine test characteristic, as obtained by NASA and given in Figure 7 of Reference 34, was used. The 60-percent speed line of that characteristic corresponds to the required radial turbine pressure ratio. The mass-flow factor was scaled to match the flow condition of the gas-generator.

Figure 63 shows the result of replotting the NASA turbine characteristic to represent the radial turbine characteristic for the gas-generator.

Axial Turbine

Since the axial turbine is designed with impulse blading near the hub, it was assumed that the axial turbine characteristic could be represented by a nozzle characteristic. Figure 64 shows the assumed axial turbine characteristic.

Power Turbine

Because of the high pressure ratio available to the power turbine, its characteristic should conform to a multistage turbine. For this reason, the multistage characteristic shown in Figure 338 of Reference 35 was used as a typical example. This curve was scaled to match the design flow factor for the power turbine.

Figure 65 shows the power turbine characteristic that was used for this analysis.

Use of a single curve to represent turbine characteristics for a component matching analysis is a frequently used approximation; it was certainly adequate for the purpose of the present study.

Off-Design Matching Analysis

At this point, sufficient information was available to perform an off-design compressor-turbine matching analysis. The objective was to find the operating lines of the engine on the compressor maps, so that off-design conditions could be found for various power settings.

Assumptions

1. Constant turbine efficiencies

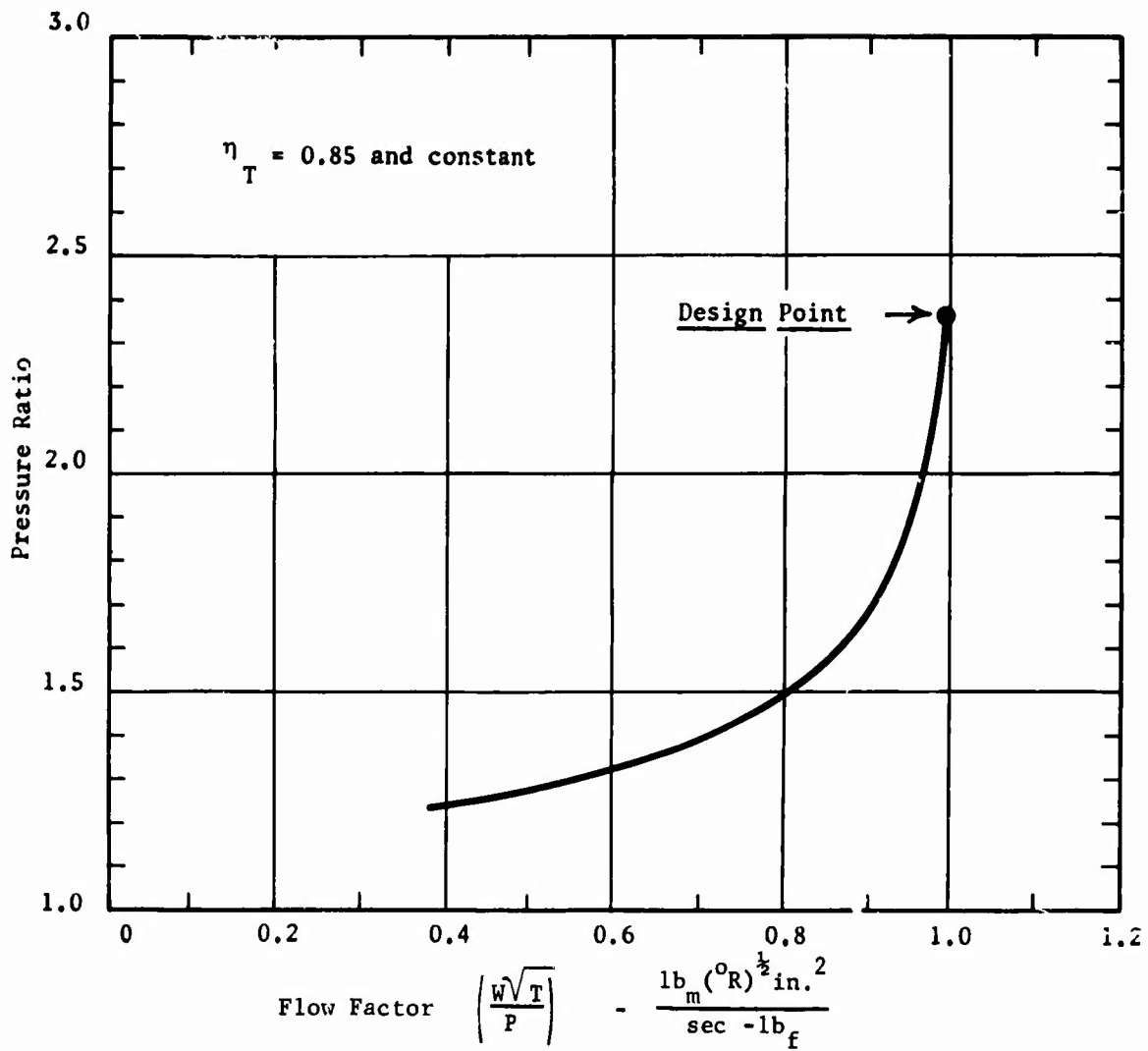


Figure 63. Radial Turbine Characteristic.

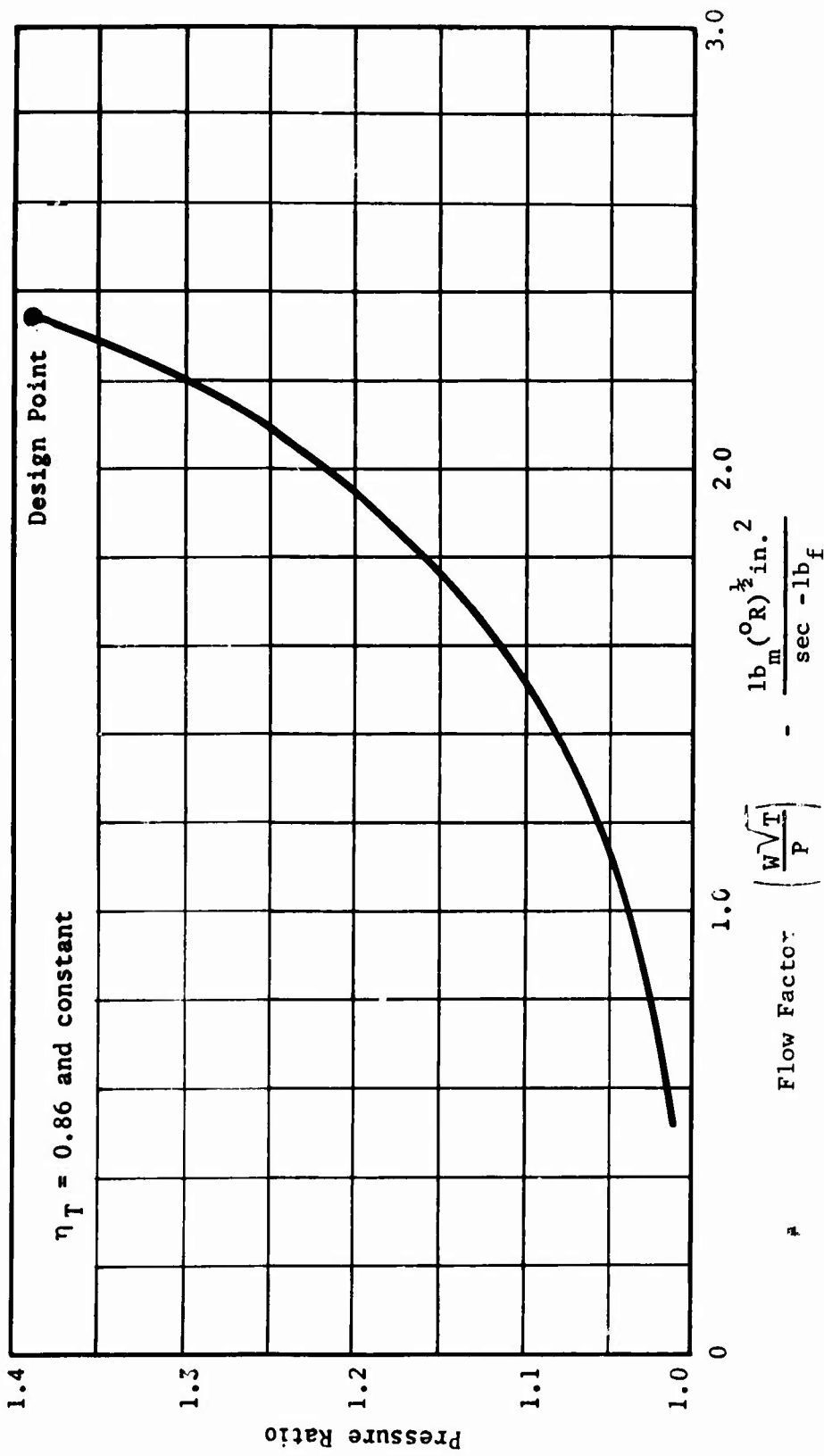


Figure 64. Axial Turbine Characteristic.

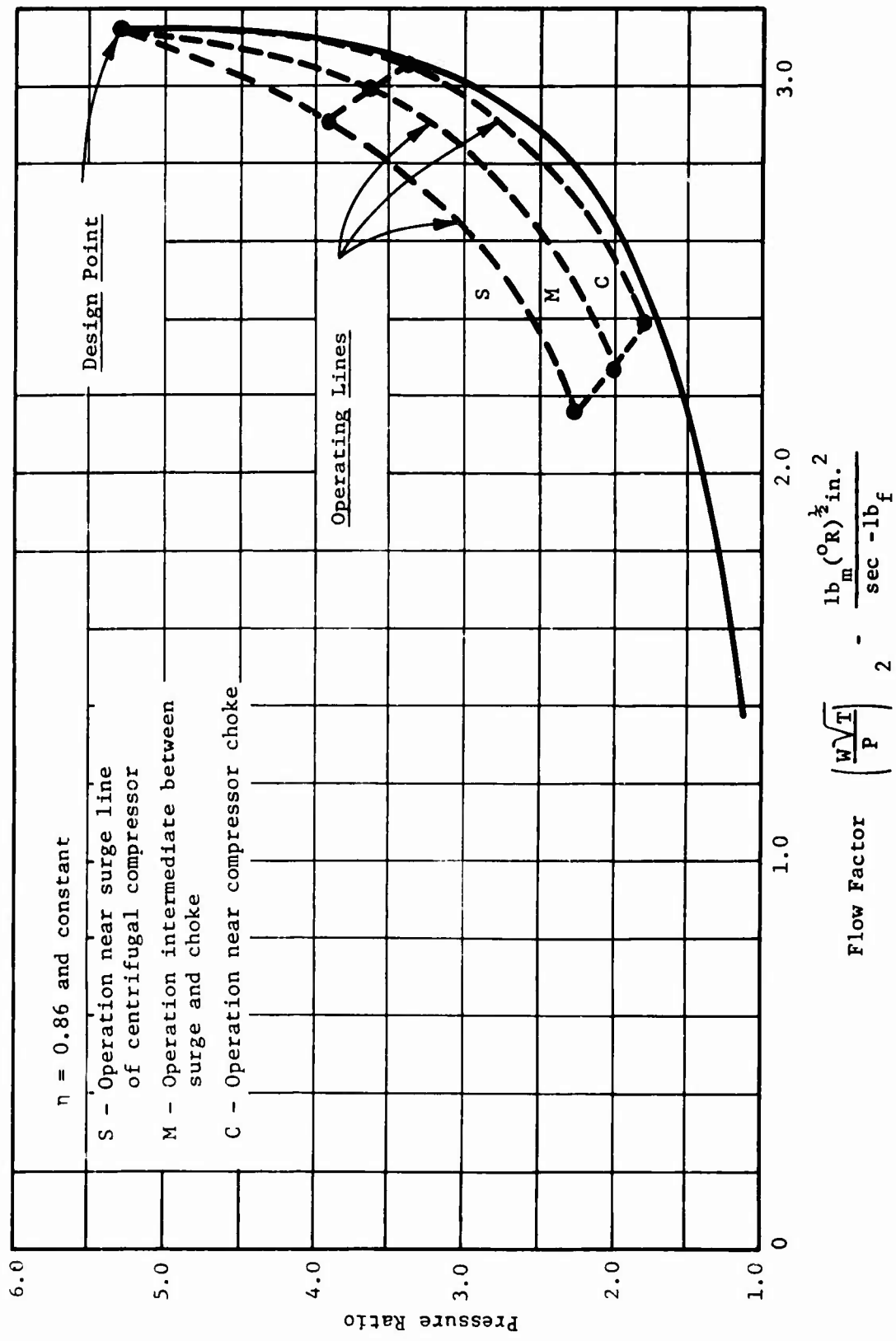


Figure 65. Power Turbine Characteristic.

2. Constant combustion fuel-air ratio
3. Constant percentage bleed

Procedure

The following step-by-step procedure was followed for the off-design calculations.

High-Pressure Spool

1. Three assumed operating lines were drawn on the HP-compressor map, passing through the design point.
2. A point was selected on the intersections of one of the operating lines and a constant speed line.
3. The HP-compressor work was calculated at the selected point.
4. A ratio of T_2/T_4 was assumed.
5. The HP-turbine work (including losses) was calculated.
6. Values of $W_4\sqrt{T_4}/P_4$ and P_4/P_5 were calculated for the HP turbine.
7. Steps 4, 5, and 6 were repeated until the values of $W_4\sqrt{T_4}/P_4$ and P_4/P_5 defined a point on the HP-turbine characteristic of Figure 63.
8. HP-spool pressure ratio, P_5/P_2 , and temperature ratio, T_2/T_5 , were then calculated.
9. The values of P_5/P_2 and T_2/T_5 were plotted as a function of $W_2\sqrt{T_2}/P_2$.
10. Steps 1 through 9 were then repeated for other points on the initially assumed operating lines.

The result of Step 9 above was plots of HP-spool temperature and pressure ratios corresponding to each of the three assumed compressor operating lines. The plots are shown in Figure 66. Figure 67 shows the plots of T_2/T_4 for the same three assumed operating lines.

Low-Pressure Spool

1. A point on one of the corrected-speed lines of the LP-compressor map was selected.
2. LP-compressor work and flow parameter $W_2\sqrt{T_2}/P_2$ were calculated.

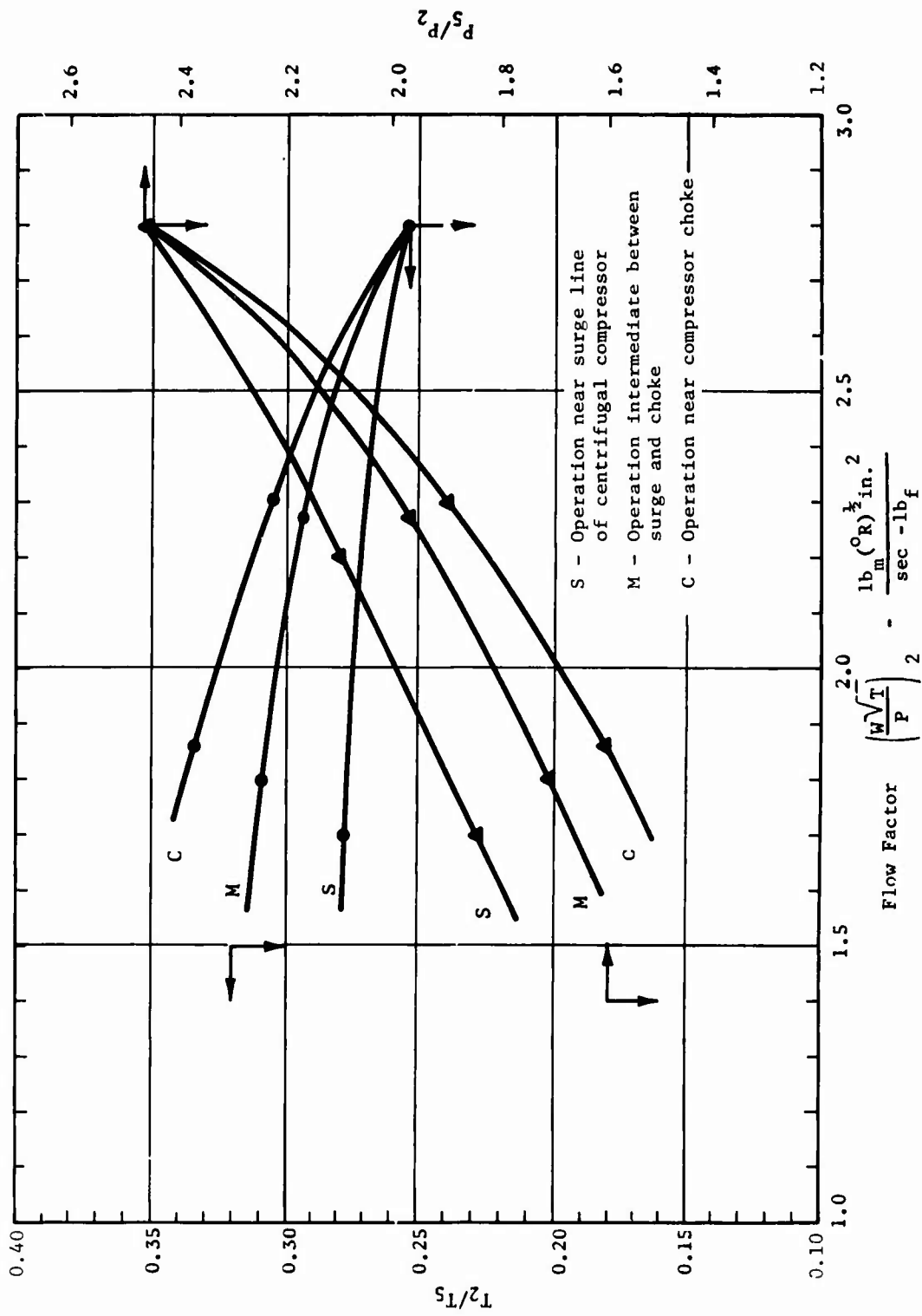


Figure 66. HP-Spool Pressure Ratio and Temperature Ratio Characteristics for Three Operating Lines.

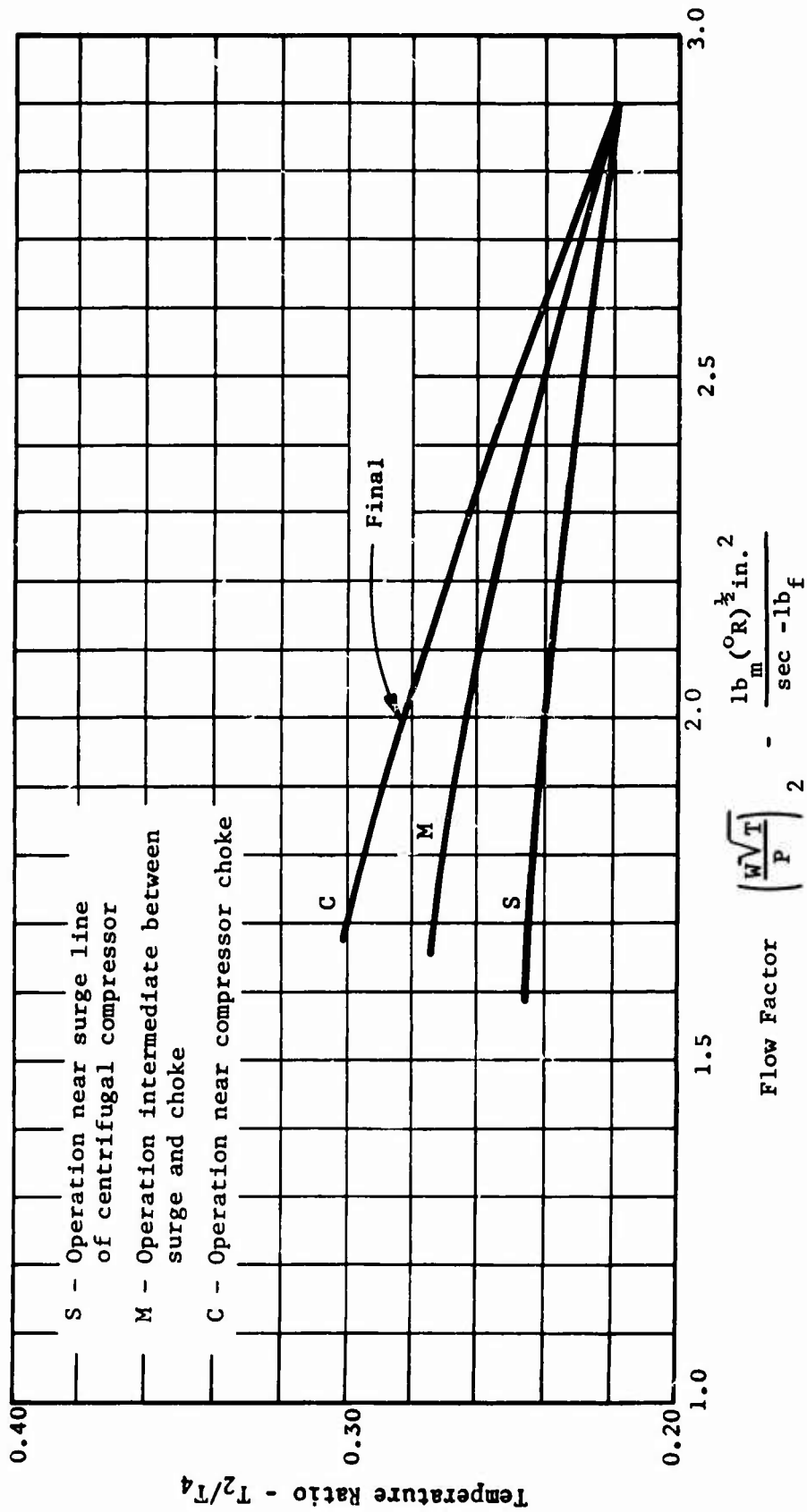


Figure 67. HP-Spool Compressor Inlet to Turbine Inlet Temperature Ratio.

3. Values of P_2/P_5 and T_2/T_5 were determined from Figure 66 for the value of LP-compressor $W_2\sqrt{T_2}/P_2$.
4. LP-turbine work (including losses and bleed flow) was calculated.
5. Values of $W_5\sqrt{T_5}/P_5$ and P_5/P_6 were next calculated for the LP turbine.
6. Steps 1 through 5 were then repeated until the values of $W_5\sqrt{T_5}/P_5$ and P_5/P_6 defined a point on the LP-turbine characteristic of Figure 64.
7. Steps 1 through 6 were then repeated for other corrected-speed values on the LP-compressor map.
8. Steps 1 through 7 were repeated such that three operating lines could be drawn on the LP-compressor map corresponding to the three operating lines initially assumed on the HP-compressor map.
9. Finally, LP-turbine exit pressure, P_6 , and exit temperature, T_6 , were calculated.

Power Turbine

1. Values of $W_6\sqrt{T_6}/P_6$ and P_6/P_1 were calculated for the power turbine.
2. Three operating lines, corresponding to the three initially assumed operating lines for the HP compressor were then plotted on the power turbine operating map.
3. By interpolating or extrapolating back from the three operating lines on the power turbine map, a new operating line can be defined on the HP-compressor map which corresponds quite closely to the power turbine characteristic.
4. The complete matching analysis is then repeated, starting with the newly defined operating line on the HP-compressor map (and perhaps one other). The analysis is repeated as many times as necessary until the final operating line on the power turbine map coincides with the actual power turbine operating line.
5. When the above iteration procedure is completed, the final operating lines can be drawn on the compressor maps.

For the gas-generator analysis, it was found that one of the initially assumed operating lines on the HP-compressor map gave a close fit to the power turbine characteristic (line "C" of Figure 65). Accordingly, it

was not necessary to go through additional iterations of the complete matching analysis.

After the engine operating line on the various component maps was established, values of speed, total pressure, and total temperature for various shaft horsepower values could be determined. These results are shown in Figures 68, 69, and 70.

The final operating line for the axial (or LP-spool) compressor is plotted on the compressor map on Figure 62. It is seen that the operating line runs into the surge region at partial power settings. This problem can be taken care of in various ways, one of which is variable inlet guide vanes to the axial compressor. Detailed analysis of such guide vanes was outside the scope of this analysis. Such analysis, however, would not alter the present results appreciably.

Calculation of Off-Design Static Pressures

Axial Compressor

In order to find the static pressure between blade rows, the thermodynamic analysis had to be extended. By assuming an equal work split between the two axial stages, and an efficiency of 84 percent for the first stage, the pressure ratios for the first and second stages were found to be 1.83 and 1.64, respectively. It was further assumed that this pressure-ratio split would be maintained at off-design conditions. On this basis, the off-design total pressure at the second-stage inlet was determined and plotted as curve 1B on Figure 71. The stator inlet total pressures were determined by assuming a 0.98 recovery value for the stators. These pressures are plotted as curves 1A and 1C on Figure 71.

The static pressures at off-design are a function of Mach number and total pressures. It was assumed that the Mach number would be proportional to the speed, which is a reasonable approximation. The Mach numbers at design point were given on the velocity diagrams provided by USAAVLABS. Using these values, and ratioing proportional to speed, the static pressures at off-design could be calculated along the hub profile of the axial compressor. The resulting static pressures at sea-level conditions were replotted against power setting and are shown on Figure 72.

Centrifugal Compressor

In a similar way the static pressures at the centrifugal compressor inlet and the diffuser inlet were calculated. The total pressure at the diffuser inlet was determined from a diffuser recovery curve as a function of diffuser inlet Mach number. Results of these calculations at sea-level conditions are shown in Figures 73 and 74.

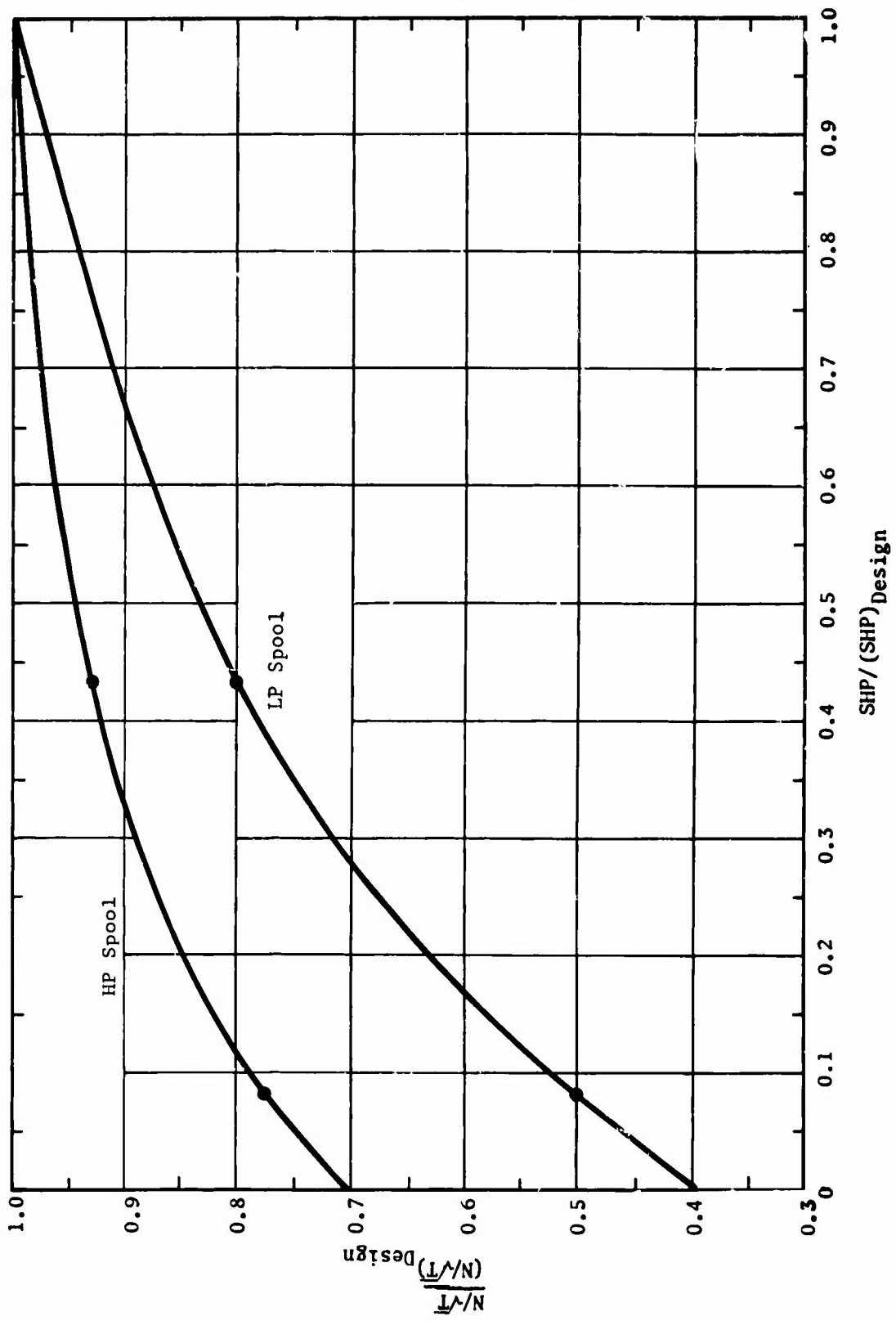


Figure 68. Part-Load Speeds at Sea Level.

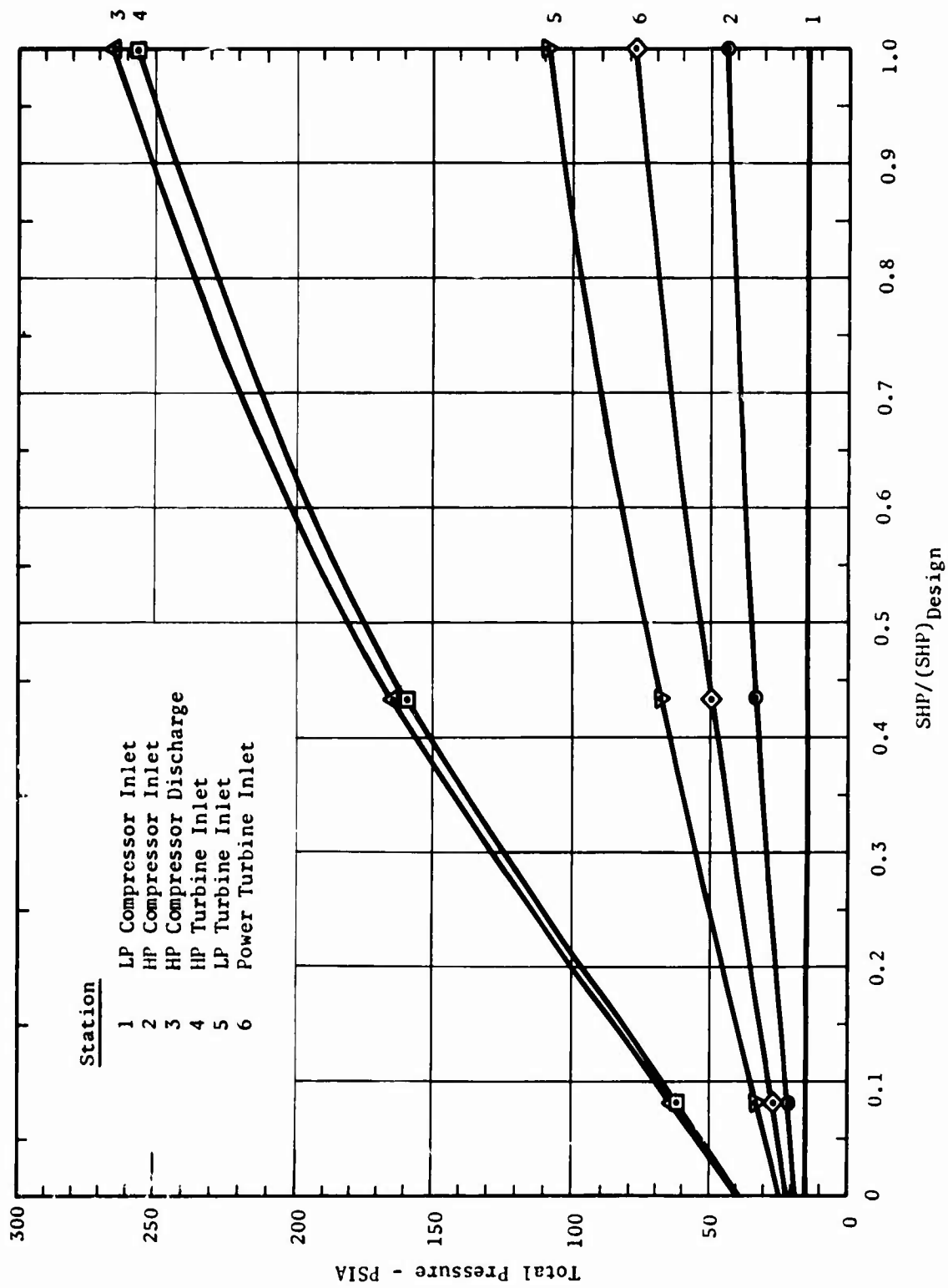


Figure 69. Part-Load Total Pressures at Sea Level.

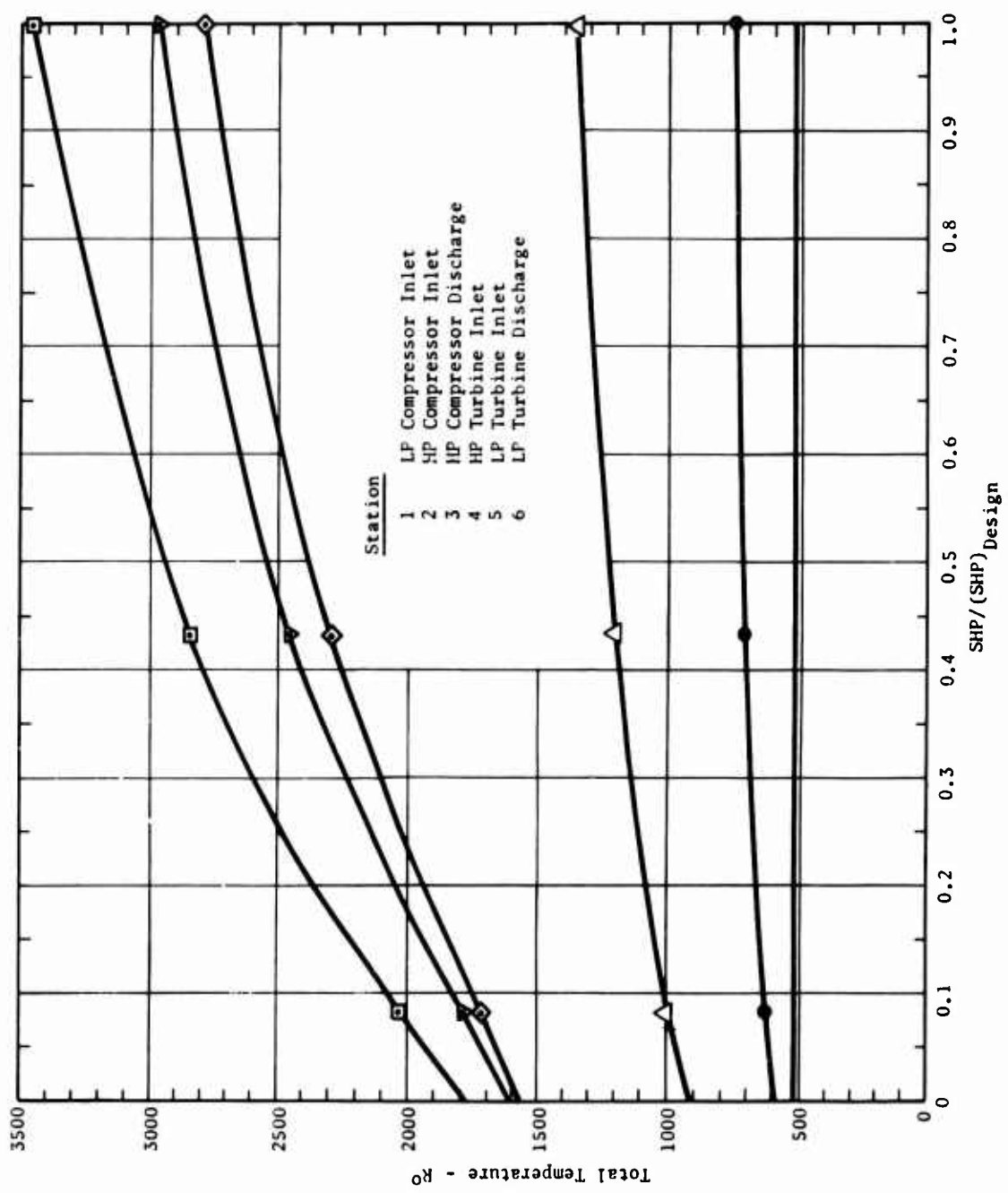


Figure 70. Part-Load Total Temperatures at Sea Level.

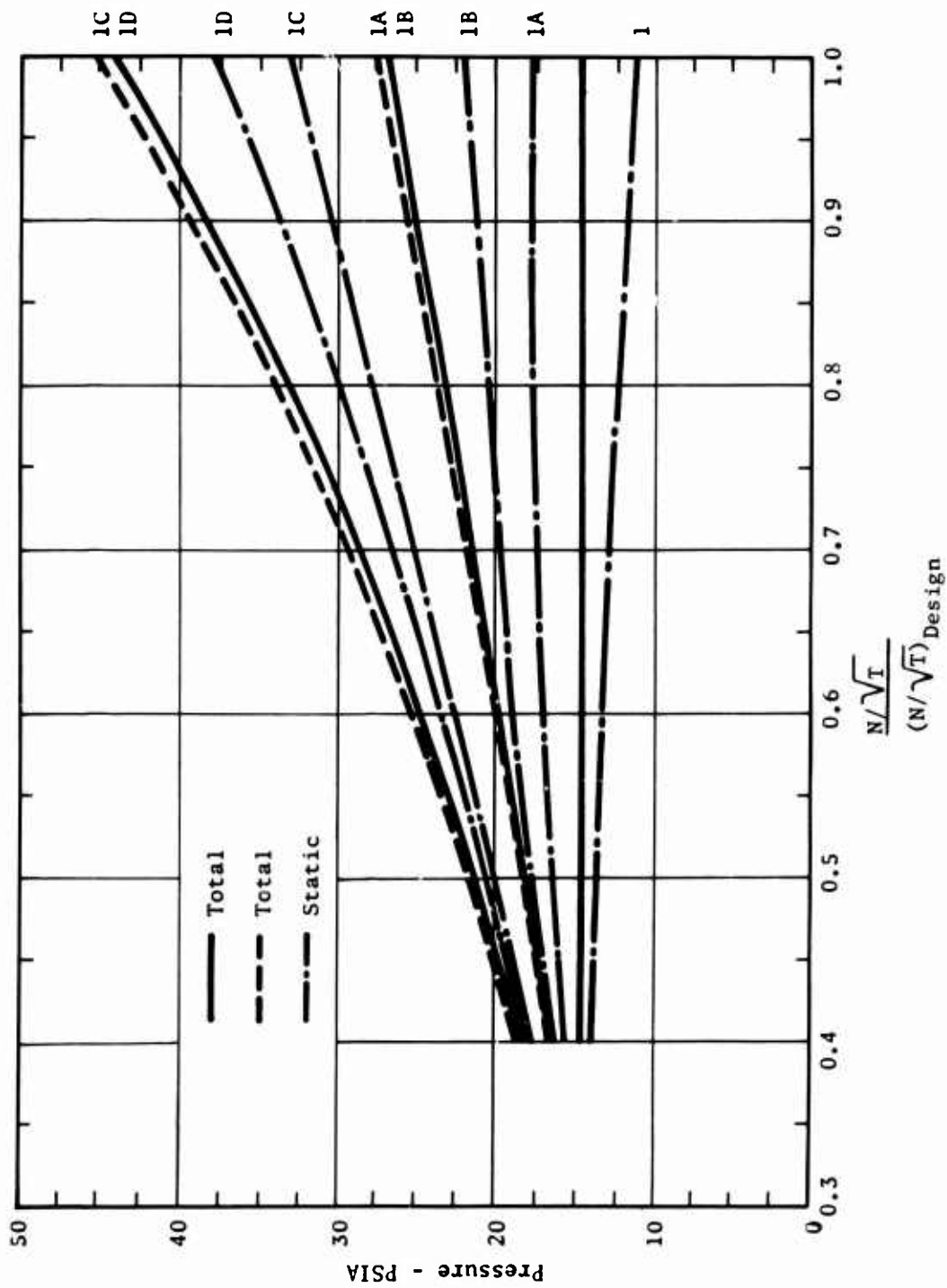


Figure 71. Total and Static Pressures for the P-Spool Axial Compressor at Sea Level.

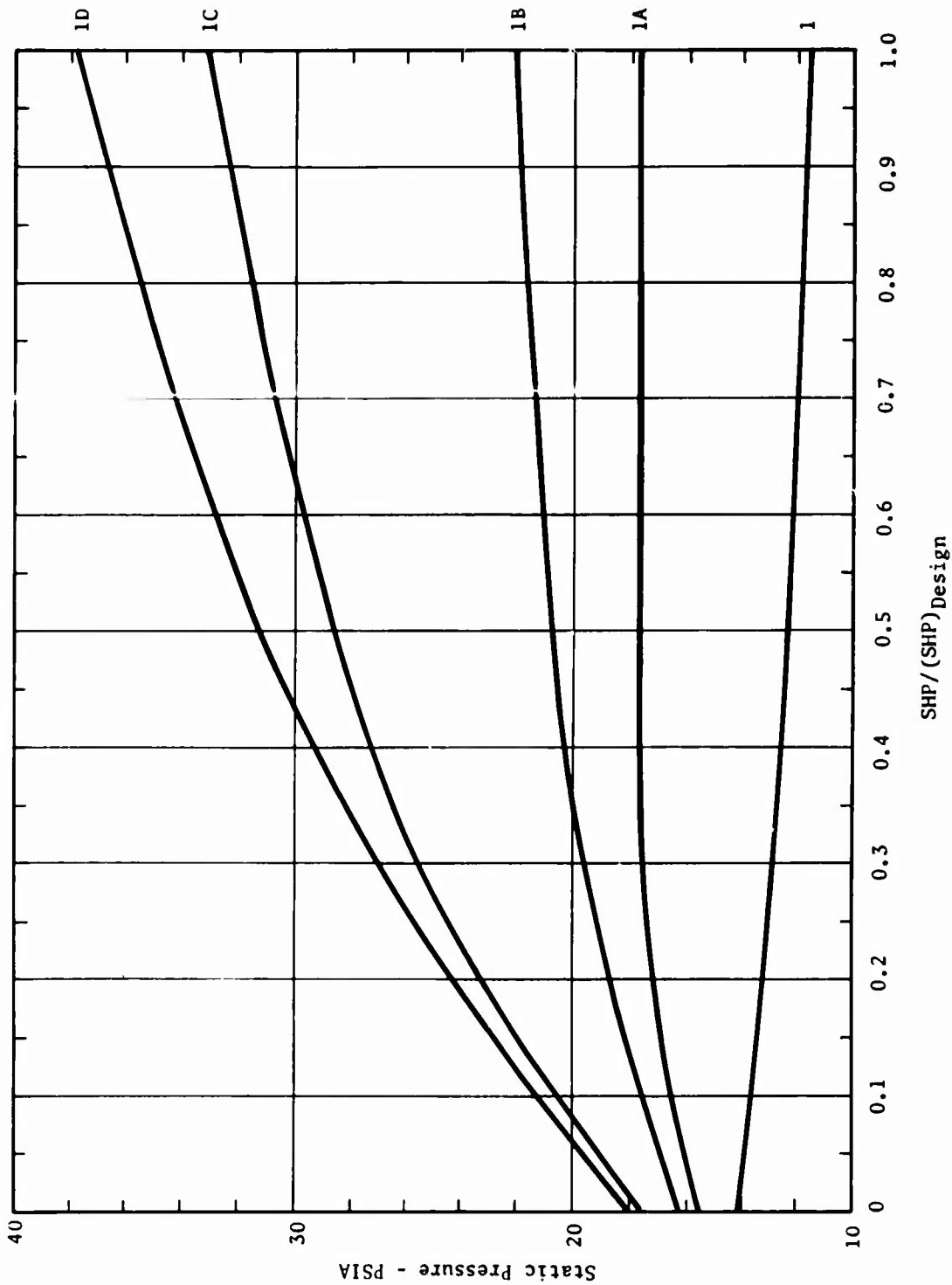


Figure 72. Part-Load Static Pressures for the HP-Spool Axial Compressor at Sea Level.

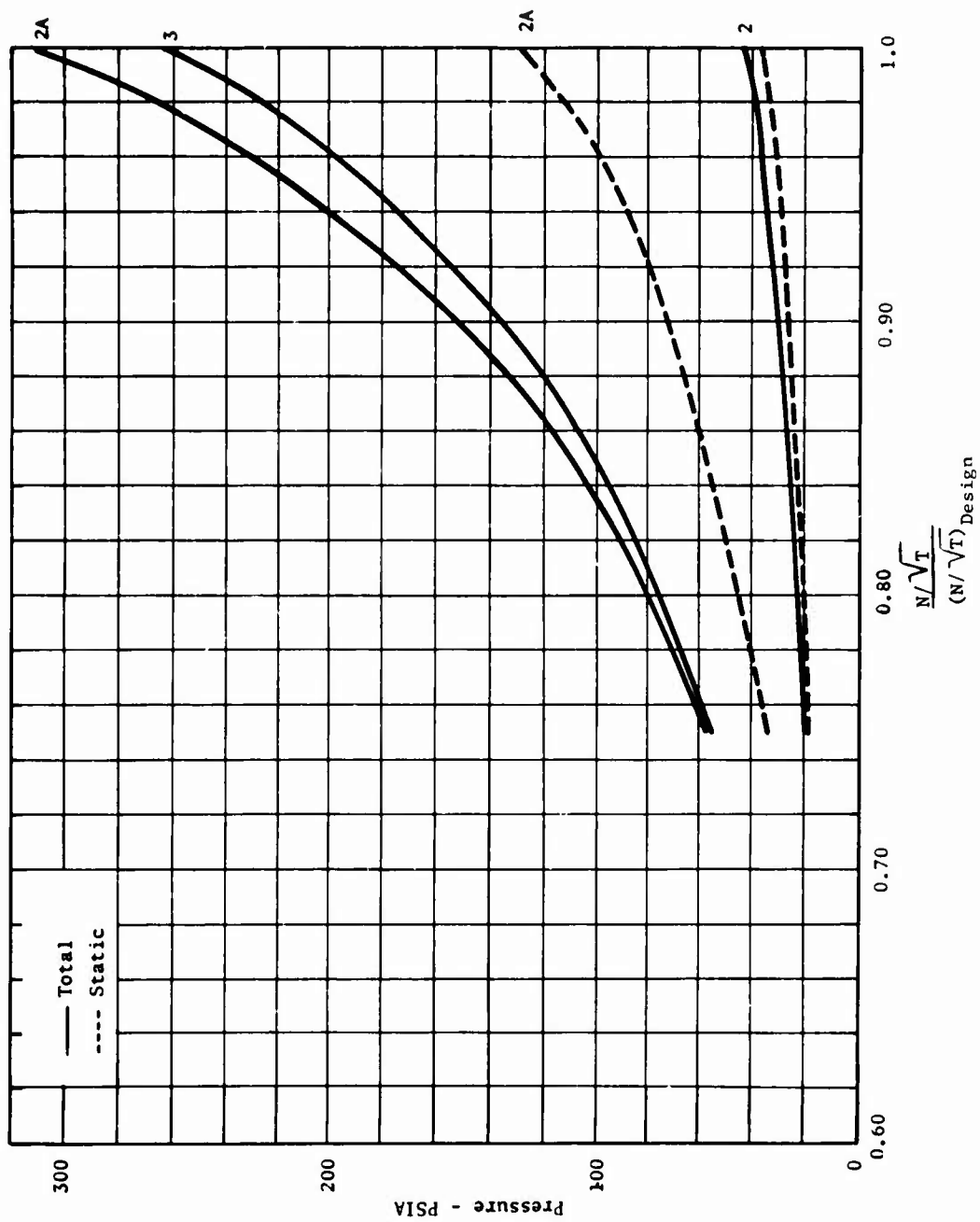


Figure 73. Total and Static Pressures for the HP-Spool Centrifugal Compressor at Sea Level.

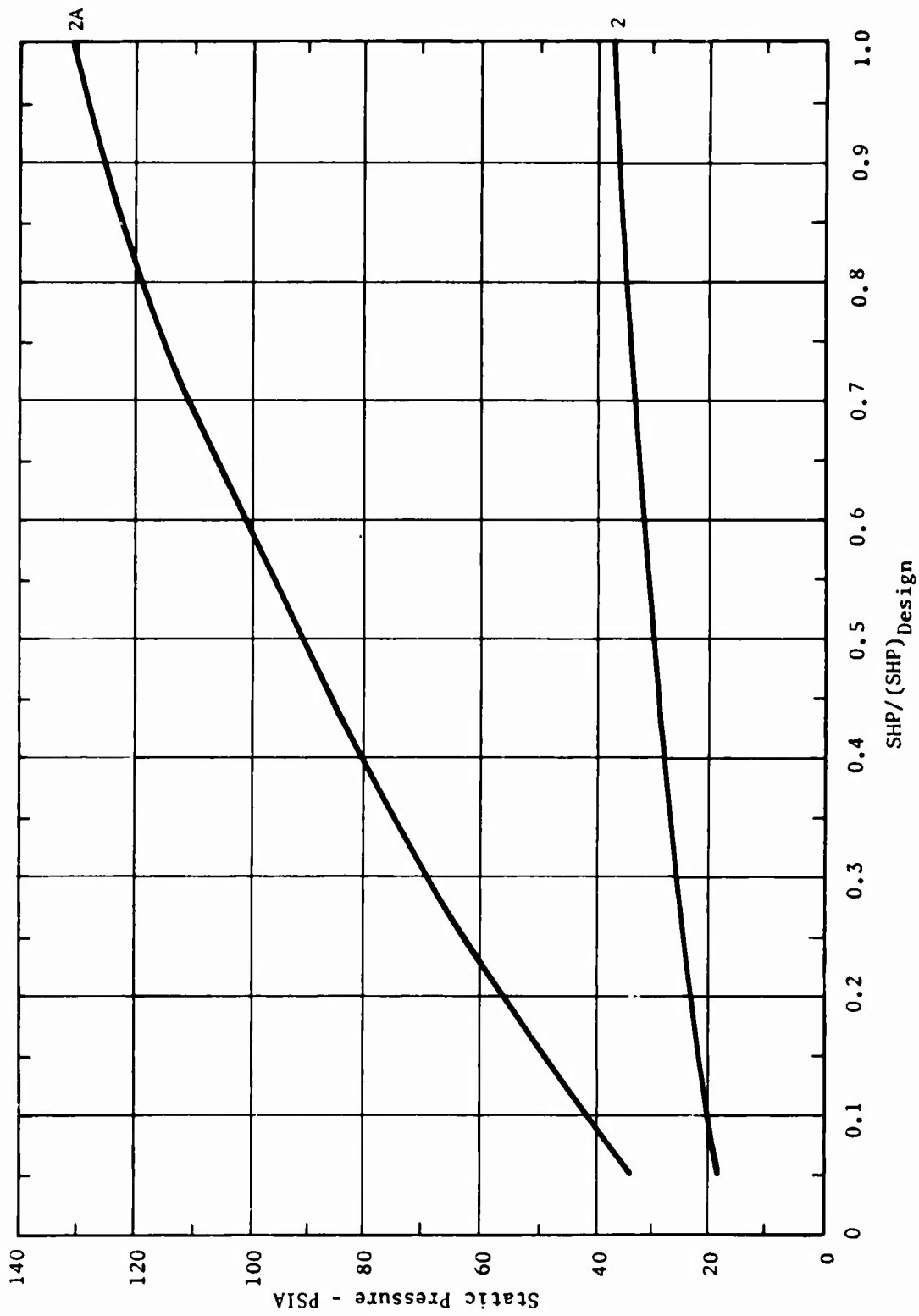


Figure 74. Part-Load Static Pressures for the HP-Spool Centrifugal Compressor at Sea-Level.

Radial Turbine

The design-point total and static pressures through the radial turbine were calculated during the component sizing study. It was not possible to use the same off-design analysis procedure for the turbines as was used for the compressors, because the temperature changes in the turbines for off-design operation are quite large. Instead, it was assumed that the ratio of nozzle static pressure drop to stage total pressure drop would be constant at off-design conditions, as would also the ratio of exit velocity head to stage pressure drop. These assumptions were based on the assumption that the velocity triangles would not change at off-design conditions. Based on the above reasoning, the static pressures at off-design were determined. The resulting static pressures at the hub profile are plotted against power setting in Figure 75 for sea-level conditions.

Axial Turbine

A procedure identical to that used for the radial turbine was used to determine the static pressures in the axial turbine. Results are plotted in Figure 75 for sea-level conditions.

In addition to off-design static pressures at sea-level conditions, pressures and engine speed data were generated as a function of shaft horsepower for the maximum altitude condition of 25,000 feet. These data are shown in Figures 76, 77, and 78.

Calculation of Thrust Forces

The net thrust loads on the HP and LP rotors can be considered as the sum of (1) differential pressure forces acting on the compressor and turbine discs and (2) differential pressure blade forces. To calculate the disc forces once seal locations are defined, the static pressure data of Figures 71 through 78 are used. The following paragraphs describe the calculation of blade forces.

Blade Forces

In order to find the blade forces, the average static pressures between blade rows and the effective blade areas must be determined.

It is assumed that the static pressures between stages do not vary with radius. This is a reasonable assumption if no whirl components are present. However, the static pressure between rotor and stator of a stage is not constant; it is therefore necessary to calculate the tip static pressure at these locations (i.e., at locations 1A, 1C, and 5A of Figures 60 and 61).

For the axial rotor it is assumed that the tips of the rotors have approximately 85 percent reaction, which is constant at off-design

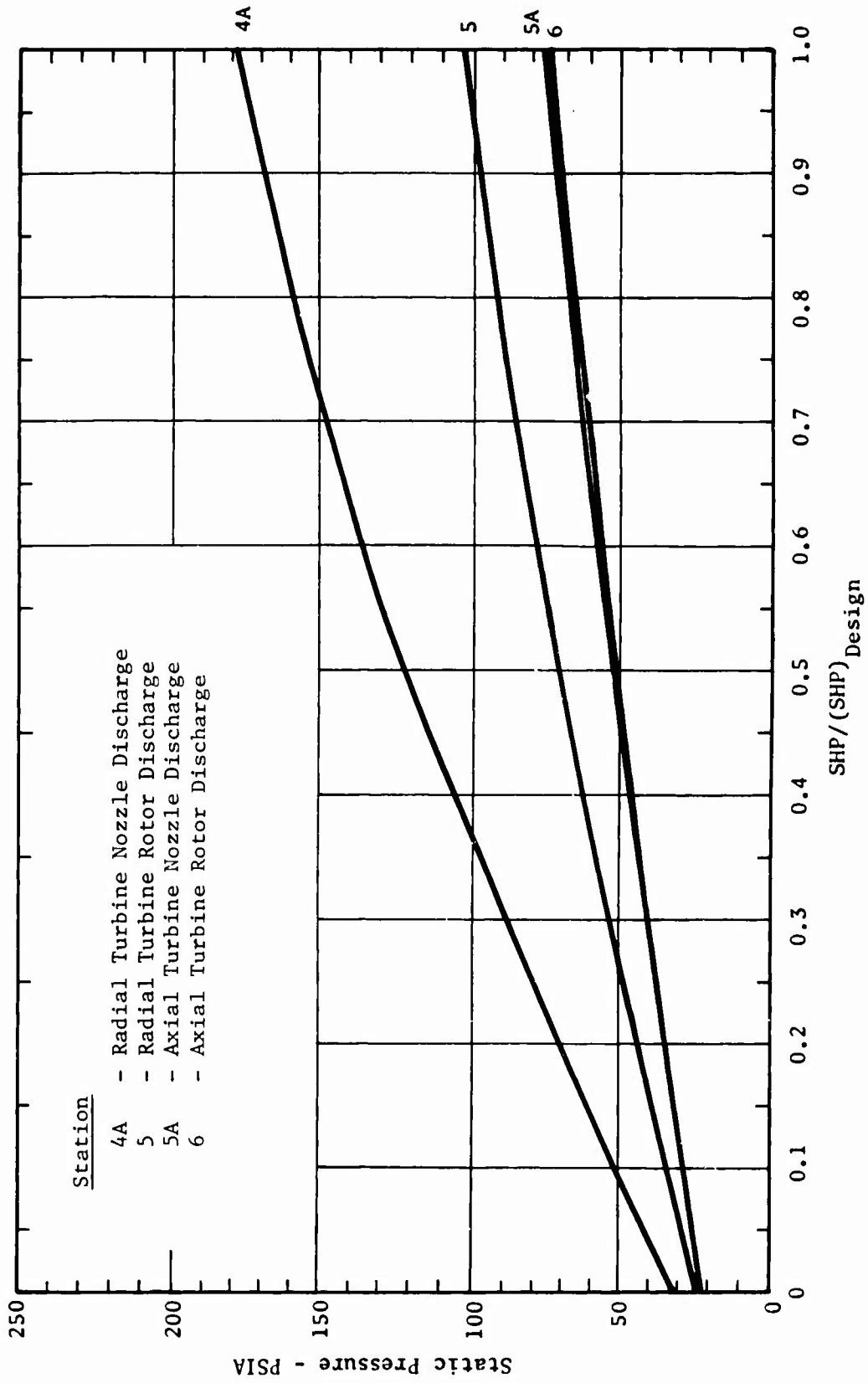


Figure 75. Part-Load Static Pressures for the HP- and LP-Spool Turbines at Sea Level.

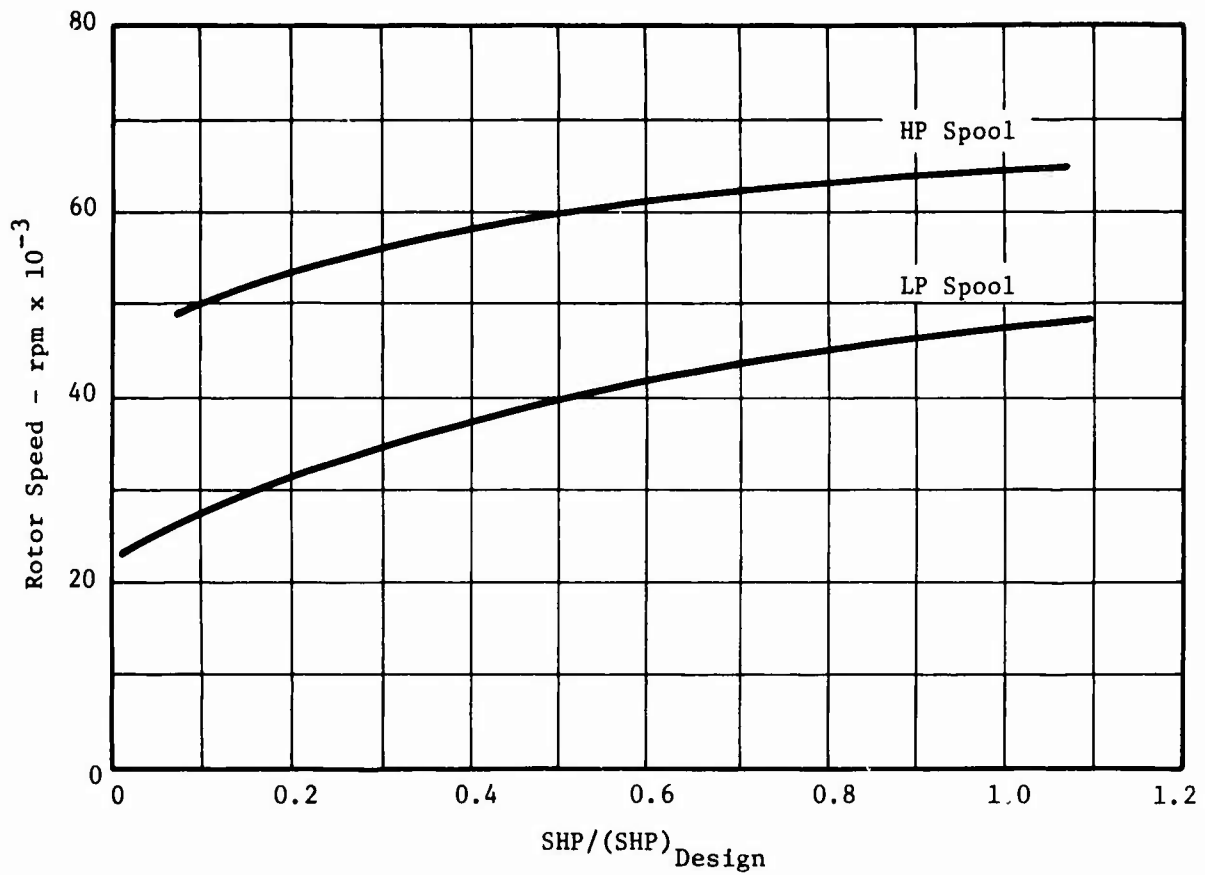


Figure 76. Part-Load Speeds at a 25,000-Foot Altitude.

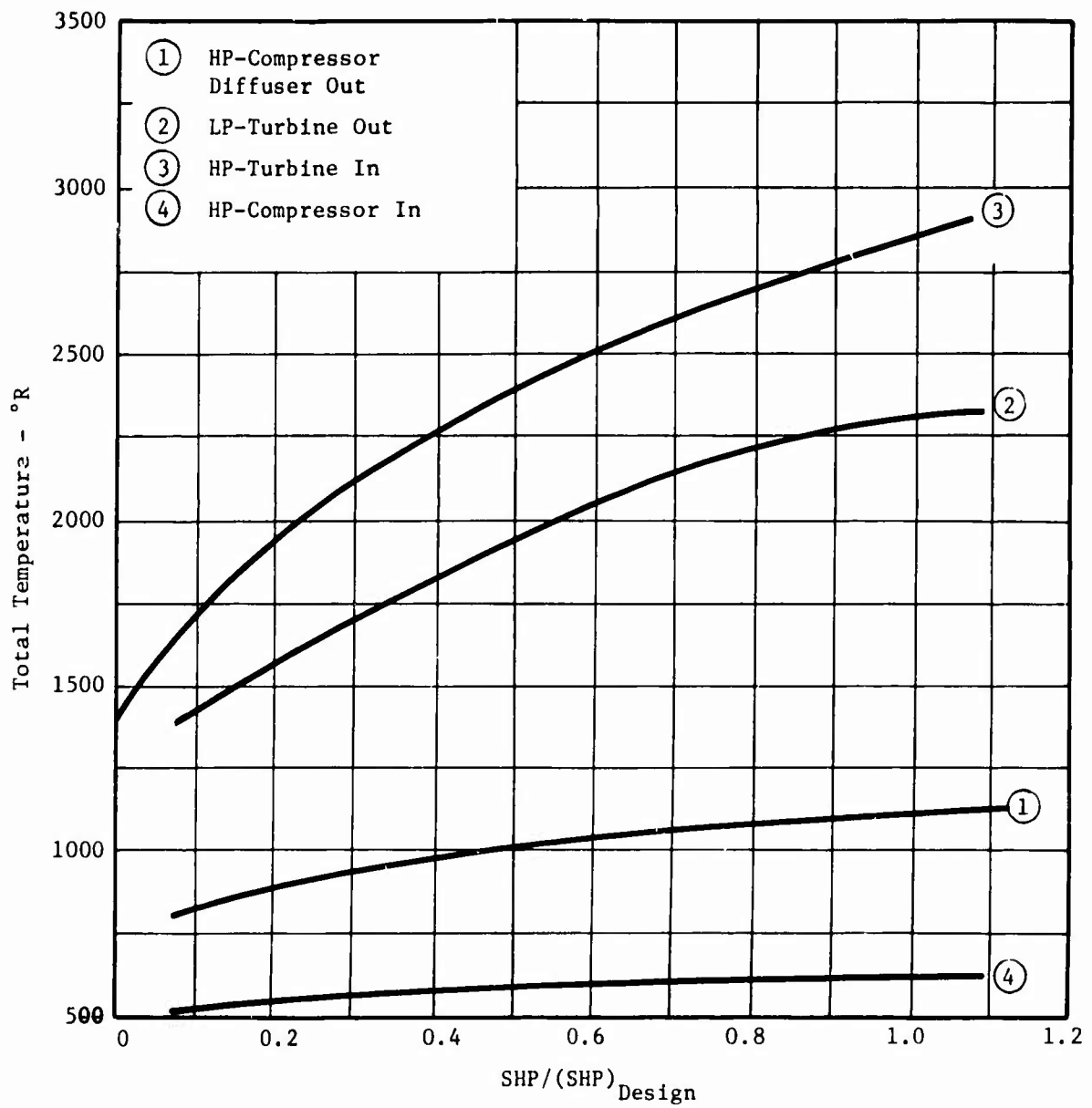


Figure 77. Part-Load Total Temperatures at a 25,000-Foot Altitude.

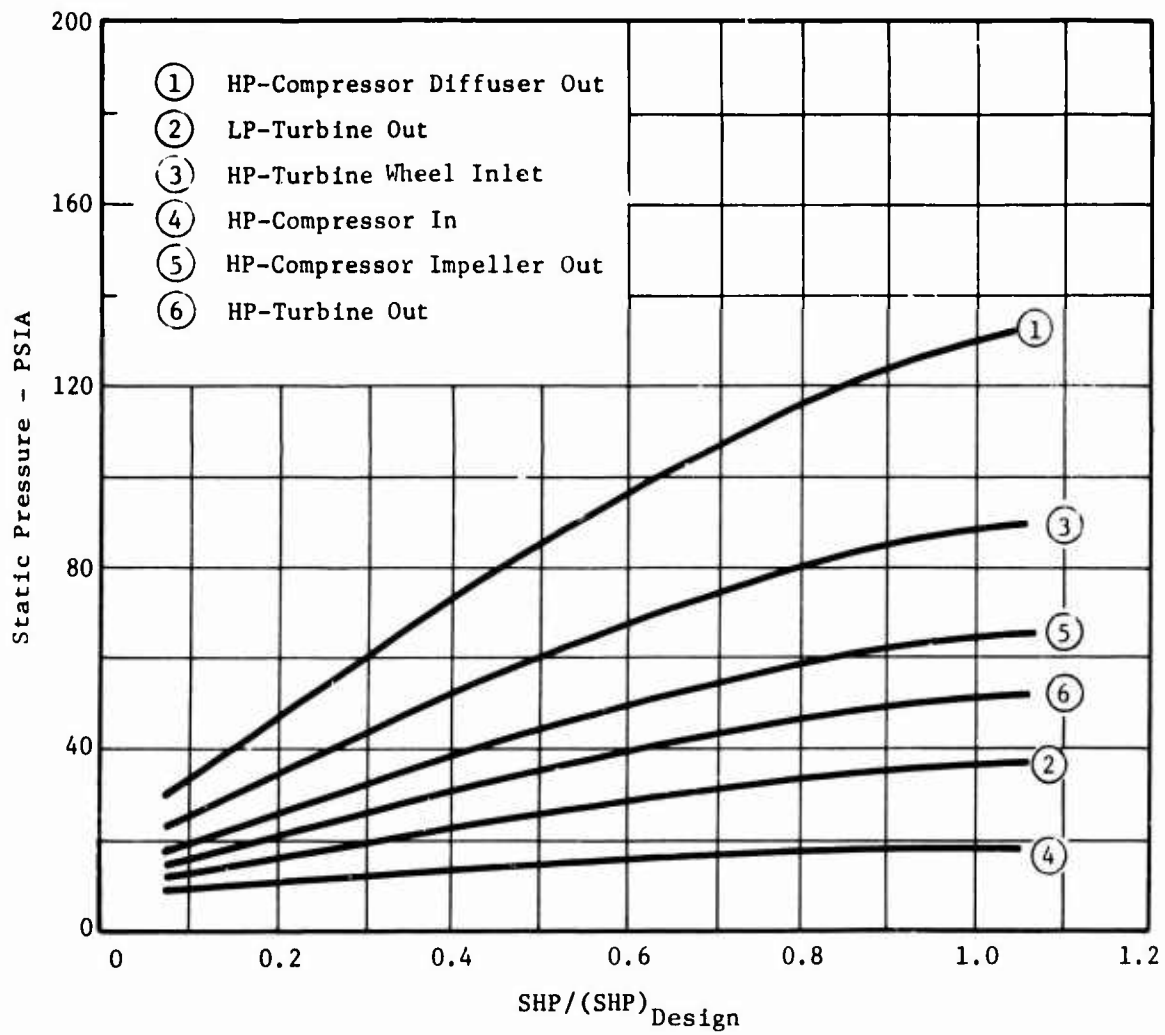


Figure 78. Part-Load Static Pressures at a 25,000-Foot Altitude.

conditions. From this, the tip static pressure can be easily calculated, since

$$\frac{(\Delta P_s)_{\text{Rotor Tip}}}{(\Delta P_s)_{\text{Stage}}} = 0.85$$

For the axial turbine, a procedure was followed similar to the calculation of the hub static pressure. The blade forces were then determined by multiplying the effective annulus areas by the average static pressures on these areas. Results of these calculations for sea-level and 24,000-foot-altitude conditions are shown in Figure 79.

The pressure force on the face of the centrifugal impeller was calculated by assuming that the static pressure increases with the square of the radius. The pressure was then integrated over the face area. Results of this calculation for sea level are plotted on Figure 80.

The face force on the radial turbine was calculated in a manner similar to that used for the centrifugal impeller. Results of this calculation for sea-level and 25,000-foot-altitude conditions are shown on Figure 80.

CONCLUSION

Although a fairly extensive aerothermodynamic analysis was performed to evaluate off-design static pressures for the gas generator, it should be remembered that only a minimal effort was permissible to extract required information. Some of the assumptions used in the analysis would not be acceptable in a rigorous analysis, but they are sufficiently accurate for the purpose of this study.

For other values of design mass flow, new component dimensions can be easily calculated by scaling Figures 60 and 61, using a linear scale factor equal to the square root of the mass flow ratio:

$$\text{Scale Factor} = \sqrt{\frac{\text{New mass flow}}{\text{Original mass flow}}} \quad (4)$$

Speeds are calculated by dividing the original speed by the same scale factor.

All pressures and temperatures are independent of the scaling.

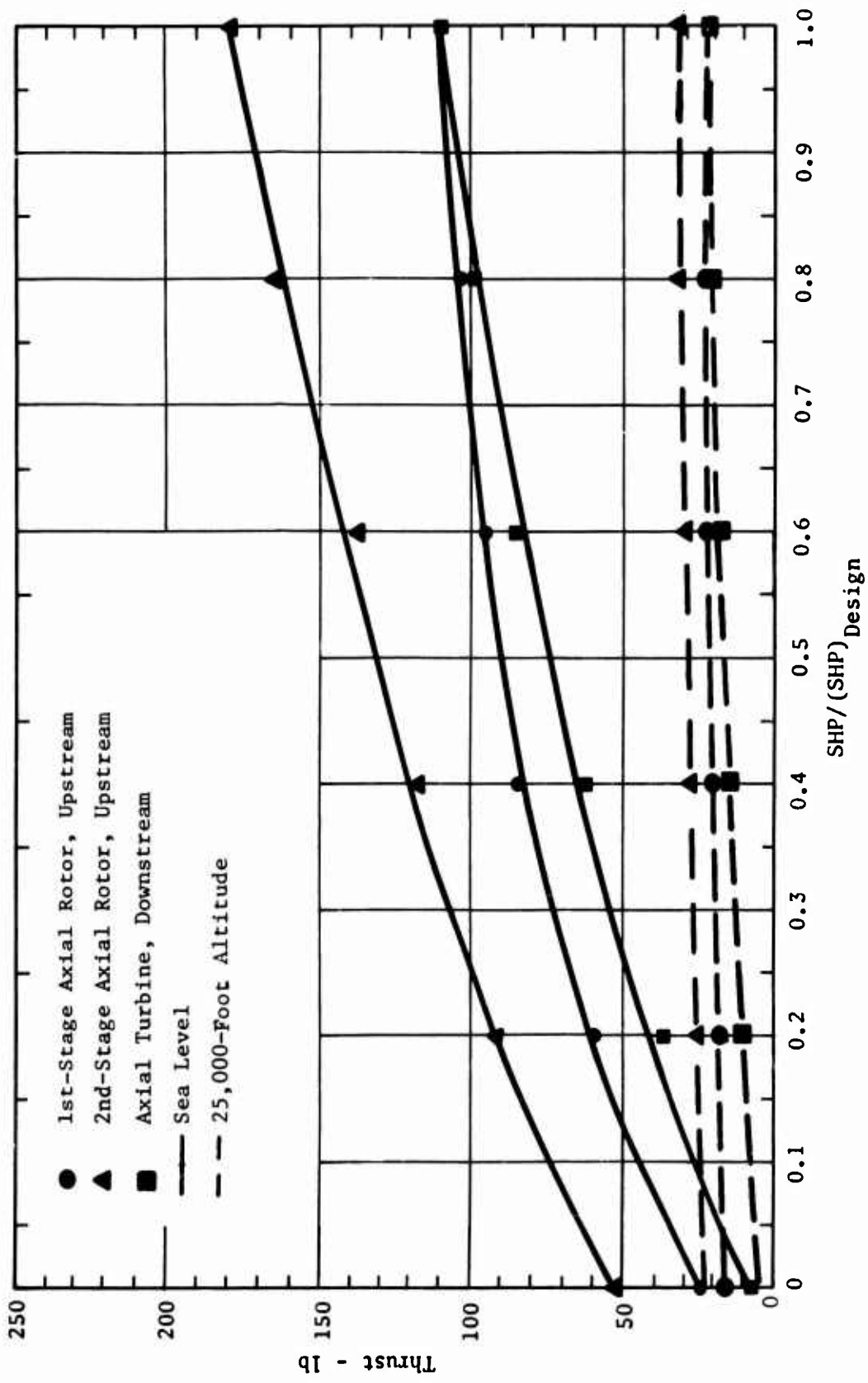


Figure 79. Part-Load Blade Forces for the LP-Spool Axial Compressor and Turbine Stages.

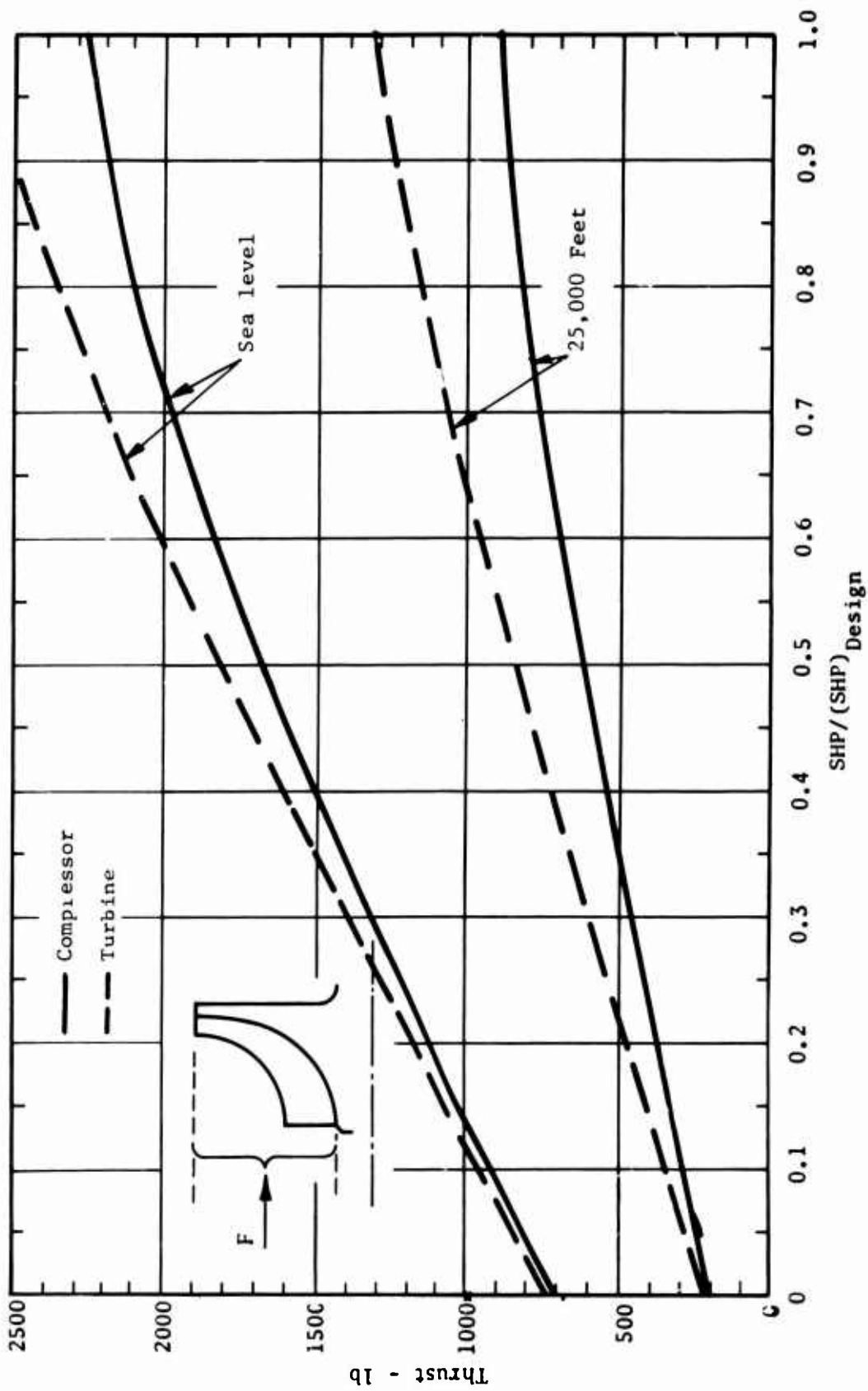


Figure 80. Part-Load Blade-Side Impeller Disc Forces for the HP-Spool Radial Compressor and Turbine Stages.

APPENDIX II
STATUS OF MATERIAL TECHNOLOGY FOR
HIGH-TEMPERATURE GAS BEARINGS

The development of gas-lubricated bearings for practical machinery applications has progressed rapidly in the last ten years [1]. Each success has increased the level of confidence in the reliability of this type of bearing. Problems which seemed almost insurmountable in the beginning, such as the apparent need for dirt-free gas environments, and the development of wear-resistant surfaces which could survive dry rubbing contacts with no significant wear or surface damage, have been largely overcome. It has been found that certain types of bearings, particularly pivoted-pad bearings, can tolerate airborne debris without failure. This is apparently due to the fact that there are surface interruptions which permit debris to escape. The self-aligning capability of this type of bearing probably also contributes to its ability to resist damage from particles which enter the clearance spaces.

The advances which have been made in the development of wear-resistant surfaces are described in more detail later in this appendix.

Gas bearings have evolved from the state of being delicate laboratory curiosities to a point where they can be applied with confidence in high-speed machinery. Both design and materials technology have played major roles in these successes.

In spite of these advances, there are still many problems which must be resolved. Of these, the temperature barrier is one of the most important. Theoretically, the performance of a gas bearing should improve with increasing temperature since the viscosity of the gas also increases. However, from a practical standpoint, high-temperature operation presents a number of problems in material selection. The purpose of this discussion is to summarize the current status of our knowledge of gas-bearing materials, and to point out where better materials or new design concepts will be required.

DISCUSSION OF REQUIREMENTS

In a study of this type, it is difficult, as well as undesirable, to separate materials and design problems into rigid and separate categories. One of the primary objectives of this appendix is to point out where materials problems exist so that the design engineer can factor them into his thinking. Ultimate solution to the problems may well require the use of new or improved materials, new design concepts, or, more likely, some combination of both.

The following list indicates the several characteristics of materials which are of greatest importance in gas-bearing design. The order of the listing is not significant; depending on the application, any one or a combination of these characteristics might constitute the predominant design problem.

1. Dimensional Stability
 - a. Metallurgical Stability
 - b. Resistance to creep or centrifugal growth
2. Adequate control of thermal expansion coefficients
3. Corrosion and erosion resistance
4. Good sliding compatibility, both under start-stop conditions and during high-speed runs
5. Adequate fabrication techniques
6. Suitable thermal conductivity

The proposed gas-bearing operating conditions for the gas-generator application are presented in previous sections of this report. The following paragraphs discuss each of the above material characteristics from the standpoint of high-temperature bearing design and they point out the areas where the proposed operating conditions may present materials problems which are beyond the current state of the art.

DIMENSIONAL STABILITY

Metallurgical Stability

In any fluid-film bearing, uniformity and constancy of the bearing surfaces are important. This is particularly so with gas bearings, where relatively large bearings and small film clearances are encountered. Consistent, reliable gas-bearing operation typically requires that parts be manufactured to tolerances of 50 to 100 microinches with respect to surface profile. In some cases, this degree of accuracy can be achieved and maintained only by (1) careful selection of materials and (2) by using the proper heat treatments to minimize residual stresses which might be left from machining operations and to obtain the most metallurgically stable condition.

Dimensional stability must be considered as a factor in any gas bearing application where temperatures above 1000°F might be encountered. Data which are available from alloy suppliers on the proper techniques of heat treating high-temperature alloys are directed mainly toward maximizing strength rather than achieving dimensional stability. In the temperature range from 1100°F to 1600°F, many superalloys undergo age-hardening effects which can result in dimensional changes.

MTI has been working under both Air Force [11] and NASA [10] contracts on the selection of materials for use in gas bearings operating from 70°F to 1400°F. The Air Force work is directed toward operation of externally pressurized (hydrostatic bearings in air. Hastelloy X was selected as

the most promising alloy because of its outstanding oxidation resistance and adequate high-temperature strength. It also appeared to be promising from a standpoint of dimensional stability because the material is not supposed to age-harden to any appreciable extent. According to the supplier [36], optimum properties are developed by a solution heat-treatment at 2150°F, followed by a water quench. Aging is not specified by the supplier since exposure to high temperatures does not appreciably change the properties of the alloy. However, it is reported to be possible to increase the hardness from R_B 90 to R_B 104 by aging for 100 hours at 1350°F.

A number of dimensional stability tests on Hastelloy X were made at MTI to determine what changes would occur as the result of various heat treatments. It was found that when the solution-treated alloy was heated at 1100°F for 120 hours, there was a very uniform shrinkage of about 0.4 mil/inch. If the alloy was solution-treated at 2150°F and age-hardened for 100 hours at 1400°F, there was still a uniform shrinkage on the order of 80 microinches (0.08 mil) per inch when the part was cooled and then heated for 120 hours at 1100°F. Further studies have shown that the alloy continues to change dimensions at a slow rate [37]. Recent work at Aerojet-General, which was reported in References 38 and 39, has shown that at high temperatures, in the range of 1300° to 1800°F, metallurgical changes were still taking place in Hastelloy X after 10,000 hours. Since dimensional changes result from metallurgical changes, it is likely that the material was still changing shape even after this long period of time.

This dimensional instability is not unique to Hastelloy X. It is believed that most of the so-called superalloys will show some degree of dimensional instability at high temperature. Those superalloys which contain aluminum and titanium are strengthened primarily by precipitation of a face-centered cubic-ordered phase known as γ' , with composition Ni_3Al , Ti. In addition, refractory metals such as chromium, molybdenum, and tungsten are added as solid solution hardeners. The presence of the latter may lead, however, to pronounced carbide formation, as these alloys generally contain 0.05 to 0.25 percent carbon. These carbides are of two general types: M_6C and $M_{23}C_6$. Furthermore, an excess of refractory metal additions often leads to formation of intermetallic compounds such as Laves, μ , or sigma phases. These have been termed TCP compounds, the designation standing for "topologically close packed". These phases generally appear as thin plates which nucleate on carbides. They are hard and brittle, and they lead to accelerated high-temperature rupture failures, as well as low-temperature brittleness. The exact nature of the metallurgical changes will depend on the initial solute content, heat treatments, and exposure times and temperatures. Some alloys, such as Hastelloy X and its variants, Hastelloy X-280 and R-235, are considered to be non age-hardening because aluminum and titanium are not included, and therefore γ' cannot form. This, however, overlooks the possibility of chromium or molybdenum carbide formation, since these alloys also contain about 0.10 percent carbon.

Apart from the appearance of new phases after long aging times, existing precipitates coarsen while others may disappear entirely with time. The result is that the structure of the nickel and cobalt-base superalloys is

probably inherently unstable for exposure times of thousands of hours. These microstructural changes will be reflected in the dimensional stability of bearing materials from this group of alloys.

This conclusion has been reinforced by the results of a preliminary series of tests on the dimensional stability of various alloys which were conducted at MTI:

<u>Alloy</u>	<u>Evaluation Temperature, °F</u>
Haynes 25, solution treated	1400
Rene 41	1400
TD nickel	1400
4340 steel	900
A-286 stainless	900
Hayes 25, cold worked	900

One-hundred-hour tests were conducted, at temperature, using an argon atmosphere to inhibit oxidation. With the exception of the TD nickel, which was very stable, all of these alloys changed in dimensions. In every case, the changes were in the direction of shrinkage and were on the order of 0.0001 to 0.0003 inch per inch. These specimens are now being examined by metallographic techniques to determine what structural changes have taken place. Considerably more effort is required in this area to determine the effect of temperature and time on the stability of these alloys.

There is still the possibility that these alloys might be useful in gas bearings. Many alloys appear to change dimensions very uniformly, generally in the direction of shrinkage. As long as the rate and magnitude of these changes are known, it should be possible to compensate for them in the design. For example, the dimensional changes which were measured in the study of Hastelloy X all showed that a very uniform shrinkage was taking place. This was illustrated by a test in which a plug and bushing were made from Hastelloy X and age-hardened. The OD of the plug and the ID of the bushing were coated with a plasma-sprayed ceramic, and the surfaces were finish ground so that the plug fit into the bushing with a diametral clearance of 0.0005 inch. The purpose of this test was to determine qualitatively if the journal and bushing, having clearance at room temperature, would undergo some reversible dimensional change or warpage when the parts were hot, which might prevent journal rotation until the parts had been cooled down again.

The plug could easily be rotated in the bushing at room temperature. After several days in the furnace at 1400°F, it was possible to reach into the furnace and easily rotate the plug while the parts were hot. A photograph of these specimens (after these initial tests) is shown in Figure 81.

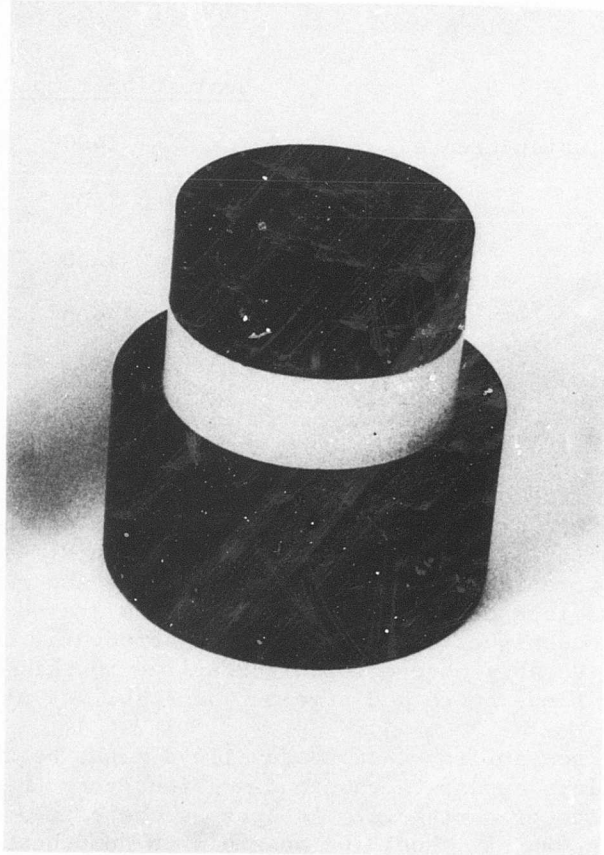


Figure 81. Plug and Bushing Set Used for Dimensional Stability Tests.

These specimens were left in the furnace and exposed for over 5000 hours to temperatures ranging from 900° to 1400° F. The plug was still a close-slide fit in the bushing, both at room temperature and at 1400° F. This does not mean that dimensional changes were necessarily negligible. Both the plug and the bushing may have changed significantly. But, if such changes did occur, they were uniform and little or no warpage occurred.

One approach to minimizing dimensional changes lies in the technology of dispersion-hardened or high-strength fiber-reinforced metals. For example, TD nickel which is 98 percent nickel with 2 percent thoria dispersed in the matrix should be a very stable material since there is no interaction between the nickel and the thoria even at extremely high temperatures. Some preliminary results which have been obtained on the NASA program [10] at 1400° F in argon do indicate that such a TD nickel is stable, at least during short time (100 hour) tests.

This particular alloy would not have adequate oxidation resistance for use in air at 1400° F, but there are chrome-nickel alloys of this type which should be more suitable. These dispersion-hardened alloys do not have outstanding strength in the low-temperature range (up to about 1500° F). However, at temperatures of 1800° F and above, they are superior to the more conventional superalloys.

MTI has successfully used TD nickel for a finned heat exchanger in a 60,000-rpm rotor of a gas-bearing turbocompressor developed for NASA [7]. Nevertheless, it should be noted that some metallurgists do not recommend the dispersion-hardened alloys for high-temperature rotating components. They feel that these alloys, in their present state of development, are not consistent enough in strength characteristics. This appears to be mainly a manufacturing and quality assurance problem which should be resolved with further development work.

The fiber or whisker-reinforced composites, which are discussed briefly in the next section, also offer promise that this problem of dimensional stability may be largely eliminated. As is the case with the dispersion-hardened alloys, interactions should not occur between the metal matrix and the reinforcing material to cause dimensional changes.

If ceramics or cermets were to be used for the turbine bearing parts, the problem of dimensional stability might not be as critical. However, even here nothing should be taken for granted. Since ceramics are bonded by solid-state diffusion between discrete particles, it is obvious that changes can still take place at high temperatures. This could lead to grain growth or grain boundary changes which could have a significant effect on dimensions. The same general comments apply to cermets.

Resistance to Creep or Growth

In this application, it is essential that the designer make provisions for centrifugal growth of the shaft. Figure 23 shows some typical curves of radial growth as a function of speed for a 3-inch-diameter shaft. Means

must be developed to compensate for this growth, even in the compressor section. Normally, small high-speed shafts will grow on the order of 0.0005 to 0.001 inch, but the calculated radial growths for the large shafts required in this application will range from 0.002 to 0.003 inch at a speed of 70,000 rpm.

Where very high-speed high-temperature operation is required, stress-to-rupture data are essential since this type of operation may impose a rigid limit on life. This is particularly true for the turbine bearing. Table XVI lists some typical physical properties for a few candidate alloys which are currently being used or have been suggested for turbine applications.

As shown in Figure 21, average tangential stresses in the bearing journals will be of the order of 60,000 to 70,000 psi at 70,000 rpm. High-strength alloys will thus be required for satisfactory 1000-hour life. The current temperature limits for available alloys at these stress levels are roughly as follows:

<u>Alloy types</u>	<u>Limiting temperature range, °F*</u>
Conventional superalloys (Inconel X, Waspalloy, Rene 41, etc.)	1000 - 1200
High-strength superalloys (Inco 713, Udimet 700, IN-100, etc.)	1200 - 1400
Refractory alloys (TzM)	1400 - 1500

In an actual engine application, it is obvious that 1000-hour stress-rupture would not be used as a design criterion when 1000 hours of reliable bearing life are desired. Actual operating temperatures would have to be less than those indicated above. How much less, however, is a question which cannot be answered at this time. Test data from actual high-speed high-temperature test journals must first be obtained.

High-temperature strength is one area where substantial breakthroughs could reasonably be expected in the next few years. At the present time, there is a prodigious amount of effort being devoted to the use of whiskers and fibers for metal reinforcement [40]. Major emphasis is being placed on the following reinforcing materials:

Silicon carbide whiskers

α - alumina whiskers

Graphite yarn

* Based on 1000-hour stress-rupture life.

TABLE XVI. PHYSICAL PROPERTIES OF SOME CANDIDATE ALLOYS FOR HIGH-SPEED, HIGH-TEMPERATURE GAS BEARINGS							
Alloy	Modulus of Elasticity (Room Temp)	Density	Tensile Strength	0.2% Yield 10 ³ psi	Stress Rupture Life, 1000 hrs 10 ³ psi	Thermal Expansion in./in./°F x 10 ⁻⁶	Thermal Con- ductivity Btu/hr/sq ft °F/ft
TZM (Mo Base)	46 x 10 ⁶	0.37	83 x 10 ³ at 1600°F	67 at 1800°F	64 at 1600°F	2.7	80 at 1600°F
Udimet 700 (Ni Base)	32 x 10 ⁶	0.286	130 x 10 ³ at 1500°F	110 at 1500°F	62 at 1400°F	8.35 70° - 1400°F	14 at 1600°F
S - 816 (Co Base)	35.2 x 10 ⁶	0.313	73 x 10 ³ at 1500°F	40 at 1500°F	21 at 1500°F	9.3 70° - 1800°F	13 at 1300°F
TD Nickel (Ni+2ZHO ₂)	30 x 10 ⁶	0.322	28 x 10 ³ at 1400°F	26 at 1600°F	16 at 1400°F	8.5 70° - 1000°F	27 at 1500°F
Hastelloy X	28.5 x 10 ⁶	0.297	50 x 10 ³ at 1400°F	27 at 1400°F	18 at 1350°F	8.9 70° - 1500°F	12 at 1100°F
Al ₂ O ₃	50 x 10 ⁶	0.129	34,000	-	-	4.3	10.7 (200°F)
K162B	59 x 10 ⁶	0.216	112,000	-	20 at 1800°F (100 hrs life)	3.7	-
IN-100 (Ni base cast alloy)	31.2 x 10 ⁶	0.280	128 x 10 ³ at 1600°F	101 at 1600°F	55 at 1500°F	8.8 70° - 1600°F	-
Inco 713C (Ni - base cast alloy)	29.8 x 10 ⁶	0.286	135,400 at 1600°F	72 at 1600°F	44 at 1500°F	8.63 70° - 1600°F	18 at 1600°F

Boron filament

Boron carbide whiskers

Many of these reinforcing agents have extremely high tensile strengths, ranging from 3×10^5 psi to values greater than 1×10^6 psi, and moduli from 25×10^6 to 70×10^6 psi. By suitable fabrication techniques, it is possible to make metallic reinforced structures which translate a large percentage of this strength into the composite. When the amount of effort being applied to this development is considered, it seems reasonable to anticipate that materials will be available in a few years with much higher strength properties than are possible today.

ADEQUATE CONTROL OF THERMAL EXPANSION COEFFICIENTS

In any high-temperature gas-bearing system, the designer must make provisions to compensate for the effect of thermal gradients on bearing clearances. Even for the case of the compressor journal, where the temperature range covers a span of only 800°F , some compensation may be required.

If it should prove to be necessary to use ceramics or cermets for the turbine journal bearings, formidable problems in design would result. Most of these ceramics and cermets have characteristically low values of thermal expansion. Some typical values are listed below:

<u>Material</u>	<u>Coefficient of Thermal Expansion, in./in.-$^\circ\text{F}$</u>
Hot-pressed Al_2O_3	4.3×10^{-6}
Cemented titanium carbide	3.7×10^{-6}
Silicon carbide	2.1×10^{-6}
Metal bonded Al_2O_3	4.7×10^{-6}

When one considers that these materials will have to be attached to high-temperature metallic alloy structures with characteristic expansion values of 8 to 9×10^{-6} in./in.- $^\circ\text{F}$, it is obvious that serious thermal stress problems can result. The only metallic alloys that have low coefficients of expansion are the refractory metal alloys based on molybdenum, tungsten, and columbium. These alloys are expensive, difficult to fabricate, and unsuitable for use in air at high temperatures (above 1000°F) unless they are protected from oxidation.

CORROSION AND EROSION RESISTANCE

Corrosion Effects

There is an extensive amount of information in the literature on the corrosion resistance of high-temperature alloys in air. In a negative way, these data are useful because they indicate the materials which would not be suitable for gas bearings. However, experience has shown that the information cannot be applied directly to the bearing design problem because there is not enough data on dimensional changes which result from oxide film growth. For example, Hastelloy X is claimed to be oxidation-resistant to at least 1800°F in air. This is very misleading. Hastelloy X forms a tenacious oxide film at 1400°F which has a significant thickness, on the order of tenths of mils. For most applications, this is of no consequence since the film does not spall after thermal cycling. However, in gas bearings it does represent a dimensional change. At 1400°F and above, the oxide film on Hastelloy X could cause a significant change in bearing clearances unless provision is made to compensate for this in the design. Based on past experience and previous attempts to find oxidation resistant materials, it appears that there is no presently existing alloy which is sufficiently oxidation resistant for use in gas bearings at temperatures above 1600°F.

At a temperature level of about 1200° to 1300°F, most of the superalloys will form an oxide film of significant thickness (in excess of 0.0001 inch). At 1400°F, some of the superalloys with relatively poor oxidation resistance will begin to show scaling, powdering, or spalling of the oxide after thermal cycling. At temperatures of 1600°F and above, oxide film buildup will become a very serious problem in maintaining bearing clearances. Past work [41] has shown that Inco 702 is an outstanding choice for oxidation resistance at temperatures up to 1600°F. If not the best, it is certainly very close to being the top choice. However, this alloy is readily available only in sheet stock. Of the superalloys which are commercially available, Hastelloy X and Inco 718 appear to show the most promise, and both of these alloys will form oxide films of significant thickness even at 1400°F. Several techniques can be used to minimize this problem:

Preoxidation of Critical Parts

Preoxidation helps to maintain dimensions since these alloys form protective films which follow a parabolic rate law. Once a protective oxide layer has been formed, subsequent oxidation of the material depends on the rate of diffusion of oxygen, or of diffusion of substrate metal atoms, through the oxide layer.

Surface Diffusion Treatments

Surface diffusion treatments, such as chromizing or aluminizing, offer some hope of reducing the oxidation to a more acceptable level. These

surface treatments should be studied more extensively to determine how well this technique can be applied to gas-bearing machinery.

Plasma Sprayed Coatings

MTI has done some limited evaluation work on the effectiveness of plasma-sprayed coatings in inhibiting oxidation. These coatings are not really oxidation barriers because they are porous, but the test results do indicate that they will slow the rate of oxidation and minimize dimensional changes caused by the buildup of oxide films. For example, two Hastelloy X shafts, 1.0 inch nominal diameter, were solution-treated and age-hardened for 100 hours at 1400°F. These shafts were then ground to finish dimensions. One shaft was coated with Al₂O₃ and finish ground so that the coating was 0.003 inch thick. The other shaft was not coated. These shafts were measured and were then heated in air for various periods of time. At intervals, the shafts were cooled and the dimensions were rechecked. The results were as follows:

	<u>Total change in diameter after 390 hours at 1100°F</u>	<u>Total change in diameter after 645 hours at 1400°F</u>
Uncoated Hastelloy X	- 65 microinches	+ 150 microinches
Hastelloy X with 0.003" Al ₂ O ₃ surface coating	- 90 microinches	- 82 microinches

To interpret these results, it is important to note that there are two events occurring simultaneously. First, the Hastelloy X parts are gradually decreasing in size because of aging effects. Second, the parts are gradually increasing in size because of the formation of a surface oxide film. At 1100°F, the oxide film on the Hastelloy X still shows interference colors, indicating that the film is extremely thin. Thus, the major change is due to metallurgical effects. Both shafts show a decrease in size. At 1400°F, the oxide film on Hastelloy X is black and polished, indicating that the film has significant thickness. Thus, there are two competing changes taking place: shrinkage due to aging, and growth due to oxide formation. The uncoated Hastelloy X shows a diametral growth of 0.00015 inch, while the Al₂O₃ coating prevents the buildup of an oxide film.

Some studies have been made to evaluate plasma-sprayed self-bonding coatings as a means of protecting molybdenum from oxidation in high-temperature air [42]. In those tests, a nickel aluminide coating 0.010 to 0.020 inch thick protected molybdenum from catastrophic oxidation for over 200 hours in air at 2000°F. Improved coatings of this type might provide adequate oxidation barriers which would make it possible to take advantage of the high-temperature strength of TZM molybdenum in this application. The nickel aluminide coating would

provide an excellent base for a thin, wear-resistant cermet coating on the journal surfaces.

If ceramic parts, such as Al_2O_3 , were to be used, there would be no problem of oxidation. However, most of the cermets, or self-bonded materials such as silicon carbide, will form oxide films of significant thickness at high temperature. Once again, it must be noted that when a supplier speaks of oxidation resistance, this term should be treated with caution. Many of these materials will oxidize readily, but the supplier may be thinking in terms of protective oxide film which will inhibit further oxidation after it has been formed.

Erosion Resistance

Erosion damage is generally confined to externally pressurized (hydrostatic) bearing applications. A high-velocity flow of hot gas passing through small orifices and impinging against a mating bearing surface can result in changes in the diameter or shape of the orifice, or it can cause degradation of the mating surface. This damage may be caused by solid, contaminant particles being carried through the gas supply system, or it can be caused by corrosive attack between the gas and the bearing or shaft material, and subsequent spalling of this corrosion film. The former can be avoided by maintaining a clean supply system and by the use of filters; the latter, by choosing corrosion-resistant materials. If a clean gas supply system is used, and if there is no reaction between the gas and any of the components, then erosion will not be a problem.

Tests which have been made using a 1200°F air stream impinging on an Inconel X surface have shown that a considerable "buildup" in the oxide layer can occur around the area of impingement. This "buildup" is probably due to the cracking of the protective oxide film. At velocities of 500 ft/sec, a gas stream will exert considerable pressure against the surface. If this pressure varies, the oxide film will crack and increased corrosion will be observed. A secondary effect may result from the fact that particles of oxide spalled from the surface will increase the erosion as well as close up the bearing clearances. Many high-temperature materials form several oxides. These are not necessarily bonded firmly to the surface. For example, Inconel X forms a powdery oxide on the surface on top of the corrosion-resistant film. This powdery film can be easily wiped away and would serve as a source of erosion in itself. There is little that can be done to combat this type of erosion damage on metals other than to select the most corrosion resistant materials or materials which form very tightly-adherent oxide films.

At MTI, some work has been done to evaluate the use of plasma-sprayed coatings as a means of preventing erosion damage. Tests have been run using 1000°F air impinging against flat surfaces which have been coated with 0.003 inch of various hard-surface coatings. The self-bonded oxide coatings stood up very well under these conditions. Cermet coatings behaved in the same way as metals; i.e., those cermets with the most

corrosion-resistant metal binders showed the least amount of damage. In those tests, the orifices were type 347 stainless steel, and only the impingement surfaces were protected by the coatings.

Similar tests are now being run with saturated steam at 300°F under an AEC Contract [43]. In these tests, the orifice is metallic, but the surface of the orifice plate and the impingement surface are both coated.

Problems were encountered when ceramic coatings were used on the orifice plate. The coating flaked away around the orifice. Figure 82 shows the appearance of the orifice before and after the test. The metal-bonded cermets were much more effective, and no chipping or erosion was observed around the orifice when these coatings were used. Some damage was observed on all of the impingement surfaces, but this was not unique to the plasma-sprayed coatings; even solid Stellite showed damage.

An examination was also made of a cermet-coated journal surface that had actually been run on externally pressurized steam bearings. The results of that examination showed that the damage which was observed in the static erosion test was much worse than that on the journal surface. Part of the difference was due to the fact that erosion damage was localized in the static test. In a practical application, the impingement area is always changing as the bearing rotates. Another, and probably more important, consideration was the fact that the static test was being run under choked flow conditions, whereas the flow in the actual bearing was always subsonic.

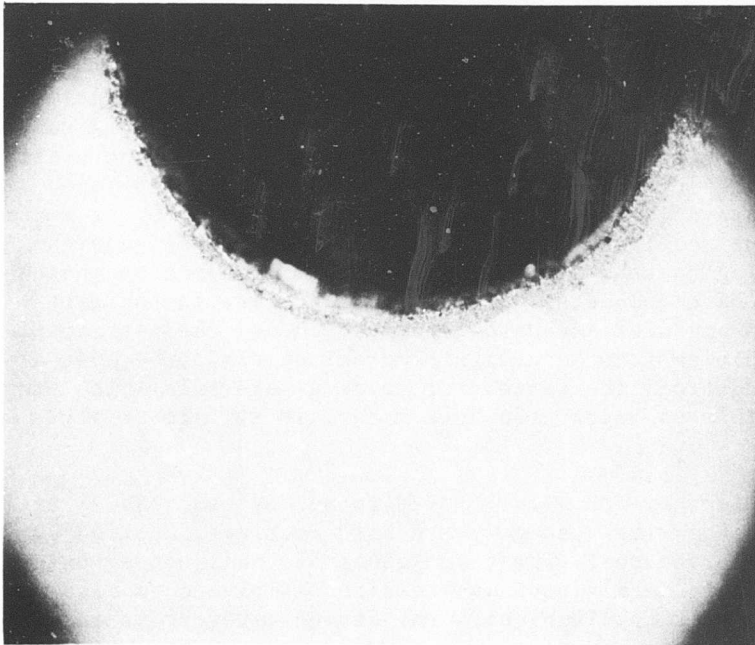
The erosion test results indicated that cermet coatings, particularly metal-bonded tungsten carbide and metal-bonded chrome carbide, were promising enough to warrant long-term evaluations in actual bearings. A 500-hour bearing test is now being planned as the next step.

SLIDING COMPATIBILITY

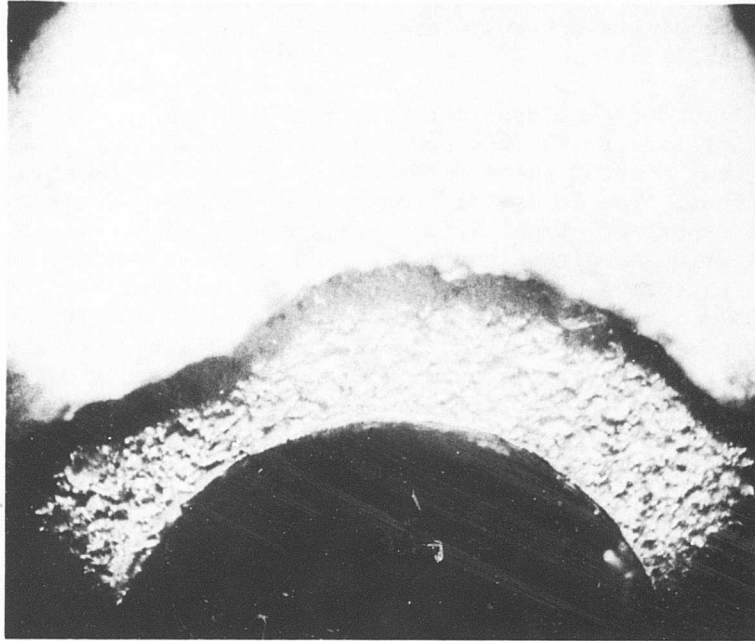
The problem of sliding compatibility in gas bearings was badly neglected until recently. The reason for this neglect is not hard to understand. Since the bearing surfaces were supposed to be separated and supported by a film of gas, it was natural to relegate sliding behavior to a very secondary role. In most of the early machinery, hydrostatic jacking was also used to lift the shaft, at least for starts and stops, thus eliminating any problems of sliding contacts. In addition, most of these machines were laboratory demonstration models, which were never designed for high reliability.

Emphasis on the sliding behavior of gas-bearing materials was the result of several factors, including the following:

1. The trend toward self-acting hydrodynamic bearings.
2. A number of premature failures, which were caused by damage to bearing surfaces during assembly or by momentary rubs due to unstable operation.



Before Test



After Test

Figure 82. Orifice Erosion Damage Caused by 300°F Steam.

3. The need for greater reliability in practical machinery.
4. The realization that gas-bearing machinery would have to be capable of withstanding shock and vibration with resulting contact in many applications.

Very little has been published in the open literature on gas-bearing material combinations. References 44 through 49 describe some material experience in this area, but most of these were bearing design rather than bearing material evaluations. The loads, lift-off speeds, number of starts and stops, etc., are not reported. Table XVII lists a number of materials which have been used in various applications in England, France, and the United States. With the exception of the DU, the carbon graphites, and the solid lubricant films, none of these material combinations could survive a high-speed rub, and most of them had limited start-stop capability. The DU was difficult to bond to the substrate material (particularly if curved surfaces were involved) and made very unreliable gas bearings. The solid lubricant films had limited wear life and could be applied effectively on steel or bronze surfaces only. The carbon graphites present differential thermal-expansion problems when utilized with normal materials of construction.

Solid ceramics or cermets have been used to solve this problem of sliding behavior, particularly in liquid-metal lubricated bearings, but, as noted before, these materials are very difficult to mount in practical machinery. Generally, sleeves of the material are used for the journal surfaces, and the bearings are made of the solid ceramic or cermet. The tasks of compensating for differential thermal expansion and making attachments to the structure are formidable.

In the MTI gas-bearing work, the following approach to this problem of material selection has been adopted. One base alloy, with adequate strength, corrosion resistance, and dimensional stability, is selected for the shaft, the bearings, and any other critical structural members. Then, surface coatings are used to achieve good sliding compatibility and any other surface properties which might be required. This approach minimizes many design problems, such as matching parts for differential thermal expansion and the mounting or positioning of components. Its chief value lies in the fact that it gives the design engineer adequate leeway to choose the best available materials without having to make design compromises simply because of sliding behavior. In addition, the variety of coating materials which are available makes it possible to select the best materials for almost any environment.

The coating materials which have thus far proved to be most successful fall into two categories. In the first category are hard coatings, applied by flame or plasma-spraying processes. These are generally self-bonded oxides or cermets, although certain metals such as Stellite or molybdenum also look promising for particular applications. The second category is made up of solid-lubricant coatings.

Special test techniques have been developed to evaluate these coatings under

TABLE XVII. MATERIAL COMBINATIONS WHICH WERE USED IN EARLY GAS BEARING WORK

Shaft Material	Bearing Material	Temperature Limitations	Application	Experience
1. Hardened Steel	Leaded bronze	250°F	Hydrostatic Bearings	Limited sliding compatibility. Failures at high speeds.
2. Hardened metals or hard chrome plate	Carbon-graphites or metal-filled carbon-graphite	To 1000°F, depending on grade	Hydrodynamic	Excellent slow-speed sliding behavior. Occasional failures at high speed. Poor thermal expansion characteristics.
3. Hard metal surfaces	Metals with thin resin bonded solid lubricants	To 600°F	Hydrostatic and hydrodynamic	Excellent as long as coating was intact. Limited wear life.
4. Nitrided Nitralloy	Same as shaft	To 800°F	Same as above	Unreliable, random failures.
5. Hard Metal Surfaces	DU* bonded to metal	500°F	Same as above	Difficult to retain DU. Limited load-carrying capacity. Excellent sliding behavior.
6. Hardened tool steel	Same as shaft	700°F	Hydrostatic	Poor sliding behavior.
7. Stellite	Hard chrome plate	800°F	Hydrodynamic	Good for starts and stops.
8. Hard, lapped chrome plate	S-Monel	700°F	Hydrodynamic	Good for starts and stops. Quality of Monel was critical.
9. Hard Metal Surface	Meehanite	350°F	Hydrodynamic	Good for starts and stops. Poor corrosion resistance.

*Proprietary composite made by sintering bronze particles on steel sheet and impregnating pores with Teflon and lead.

realistic bearing conditions. In the past, the selection of gas-bearing material combinations has been made using test data from conventional friction and wear bench tests. While these tests have been found to be useful for screening candidate materials, experience has shown that they do not truly simulate the problems encountered in a gas bearing. Some materials have given excellent results, even at high sliding velocity, in bench test machines. However, when these same materials were used in an actual gas bearing, catastrophic failures took place during high-speed runs.

The reason for this behavior is understandable. First, in a gas bearing the effect of wear or surface damage on bearing operation is the primary consideration. This is not predictable in any way from sliding bench tests. Second, the sliding conditions are different in gas-lubricated bearings since sliding contact will normally occur only for short time periods. In sliding bench tests, there may be some initial surface scoring which is smoothed over with time. Bench test data may thus appear satisfactory, while in a bearing test, failure can result. The amount of the clearance and the geometry of the bearing will ultimately determine the amount and type of damage or loose debris which may be tolerated without seizure.

As a result of this experience, a gas-bearing test has been developed to evaluate promising materials under realistic bearing conditions. Specialized instrumentation is used to measure the important variables in these tests. Essentially, this equipment measures the effect of sliding contact on the performance of a hydrodynamic bearing.

Bearing Test Equipment

A photograph of the test rig is shown in Figure 83. Figure 84 shows a schematic of the rig. Essentially, it consists of a stub test shaft 1.5 inches in diameter, which is overhung on a high-speed ball-bearing pedestal. A single, hydrodynamic, pivoted-pad bearing is deadweight loaded against this shaft. A ball and socket pivot on the back of the pad provides for self-alignment.

To monitor the performance of the pivoted-pad test bearing, two capacitance probes are mounted on the pad, one on each side of the pivot point. The signals from these probes are fed through two proximity meters into an oscilloscope. Running film thickness and wear can be measured with this system. In Figure 85, a composite photograph of typical oscilloscope traces is shown. The "zero line" is set at the beginning of the test, while the bearing is stationary on the shaft. The two upper signal traces show that the pad was running on an average film thickness of approximately 200 microinches and that the pad is tilted about 60 microinches off horizontal. When the bearing or shaft becomes worn, the probe signals on the stationary bearing will be displaced below the "zero line" at zero speed. This is a very accurate means of measuring the total wear in a bearing system.

Both start-stop and high-speed rub tests have been run at temperatures up to 500°F [7]. The equipment was then modified for an Air Force

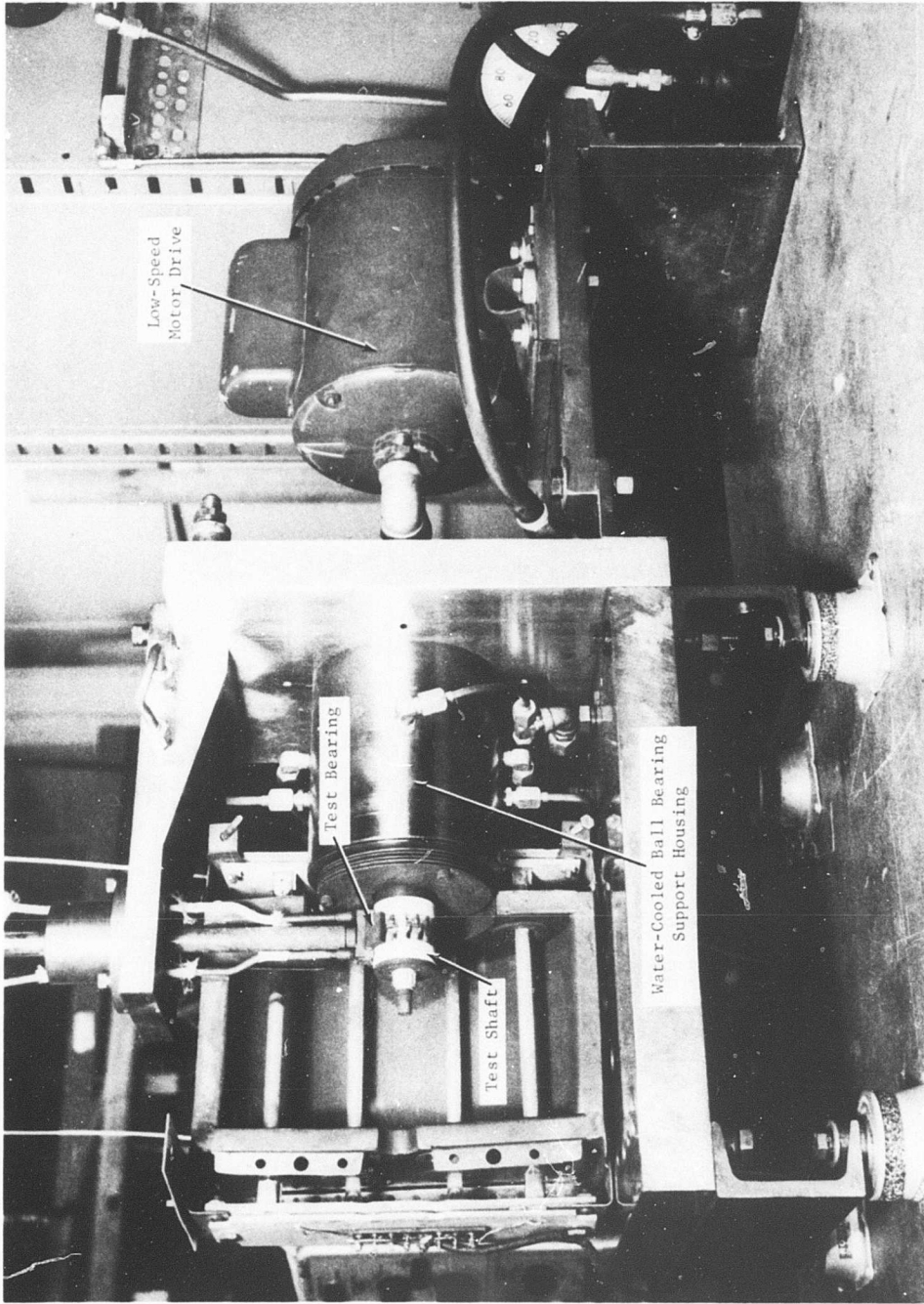


Figure 83. High-Temperature Hydrodynamic Bearing Test Rig for Materials Evaluations.

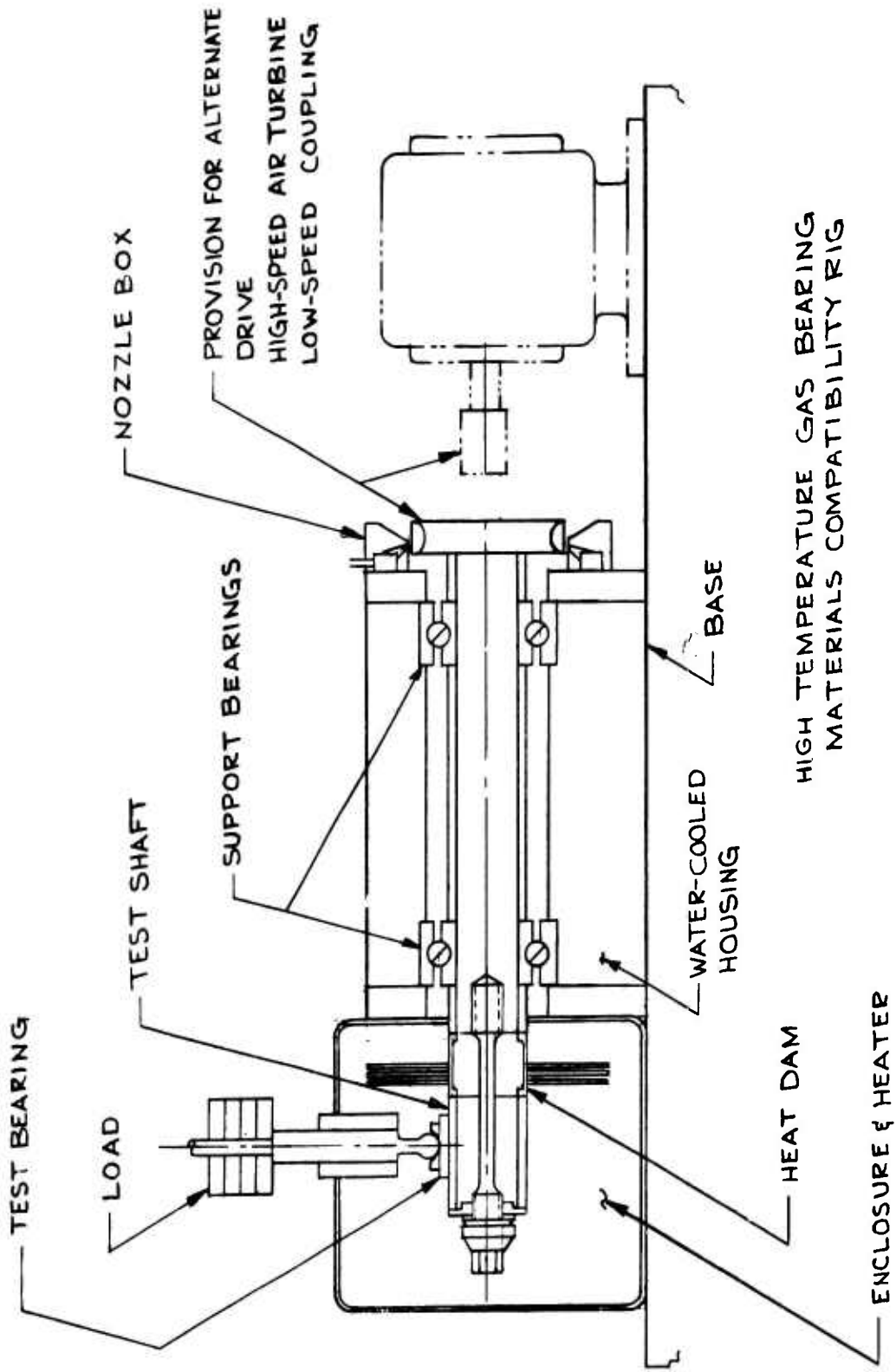
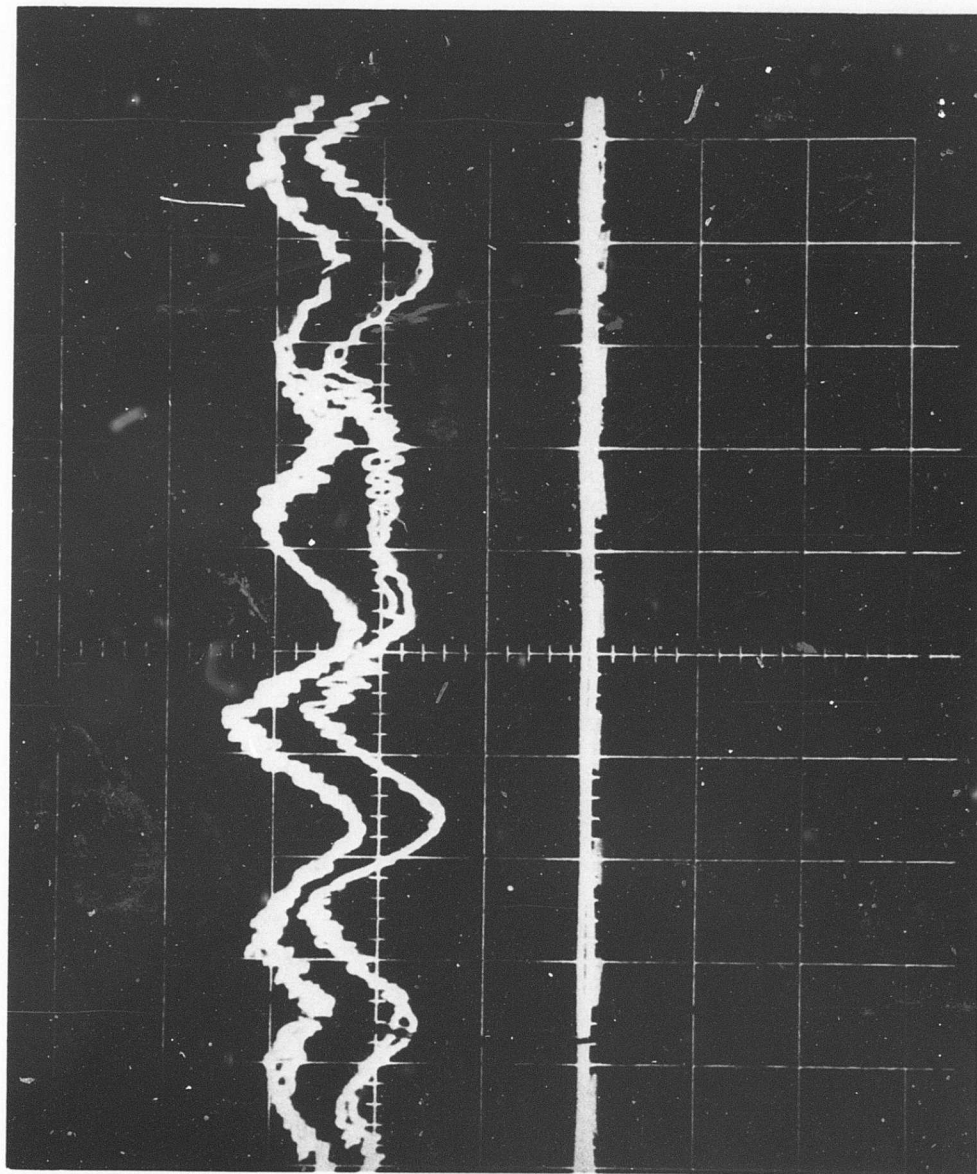


Figure 84. Schematic of Bearing-Materials Test Rig



RUNNING FILM
THICKNESS

ZERO LINE

Figure 85. Oscilloscope Traces of Film Thickness Signals
From Bearing Materials Test Rig.

program [11], to evaluate the sliding behavior of coatings in air at 1400°F, and also for a NASA study [10], to evaluate various combinations in argon at 900°F and 1400°F.

The same general test procedure is used for all of these evaluations. This procedure consists of running 1000 start-stop tests at some desired stress level, temperature, and environment. A program timer is used to turn on the drive motor, run the test for 5 seconds at a speed of 3400 rpm, then shut off the motor and allow the shaft to coast to a dead stop. This sequence is repeated until 1000 starts and stops have been accumulated. Observations are made at periodic intervals to see if the running film thickness has changed and to determine if the probe signals on the stationary bearing indicate wear. At the end of the test, the bearing and shaft are examined and photographed.

Those combinations which show promise are then evaluated in high-speed rub tests. These tests are run by bringing the shaft up to a stable operating speed of 60,000 rpm and then imposing a series of shock loads on the test pad by means of a hinged, weighted arm. At each impact, the pivoted-pad probe signals indicate that the pad has actually contacted the shaft. If the pad is still operating satisfactorily after the first series of impacts, weight is added to the hinged arm to increase the load, and a new series of shock tests are made.

	<u>Number of Drops</u>	<u>Load</u>	<u>Drop Height</u>	
First Series	50	1 pound	1 inch	Proceed if performance is satisfactory
	20	3 pounds	1 inch	Disassemble and examine
Second Series	10	5 pounds	1 inch	Proceed if performance is satisfactory
	10	7 pounds	1 inch	Disassemble and examine

Oscillograph traces, taken during these tests, are used to determine the time in contact. These traces showed that the actual time in contact between the bearing and the shaft during each shock test varied from 0.03 to 0.05 second, regardless of the weight applied.

In the initial phases of the bearing material evaluations [7], the following combinations were evaluated:

<u>Bearing (Pad) Surface</u>	<u>Journal Surface</u>	<u>Test Temp.</u>	<u>Environment</u>
1. Resin bonded MoS ₂ solid lubricant film*	Hardened steel	75°F 300°F	air argon
2. Plasma-sprayed chrome oxide**	Same as bearing	75°F 300°F 500°F	air and nitrogen argon argon
3. Flame-plated nickel-bonded tungsten carbide**	Flame plated Al ₂ O ₃ ²	75°F 300°F	air argon
4. Flame-plated nickel-bonded tungsten carbide**	Same as bearing	75°F	air
5. Hardened M-50 tool steel	Flame-plated cobalt-bonded tungsten carbide**	500°F	argon

Of the above material combinations, the following were found to be promising for start-stop tests. They are listed in order of decreasing effectiveness:

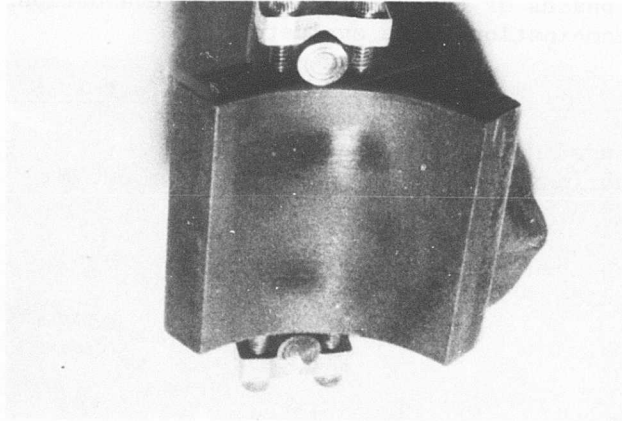
<u>Bearing Surface</u>	<u>Journal Surface</u>
1. Plasma-sprayed chrome oxide	Same as bearing
2. Flame-plated nickel-bonded tungsten carbide	Flame plated Al ₂ O ₃
3. Same as 2 above	Same as bearing
4. Resin bonded MoS ₂	Hardened steel

In the high-speed tests, only the self-mated chrome oxide showed real promise. This coating was able to survive over 100 high-speed rubs at various shock loads without any apparent damage. The contact areas were smooth and highly polished, as shown in Figure 86. By way of contrast, Figure 87 shows the severe abrasion which occurred with the tungsten-carbide-coated pad running against the Al₂O₃ coated journal.

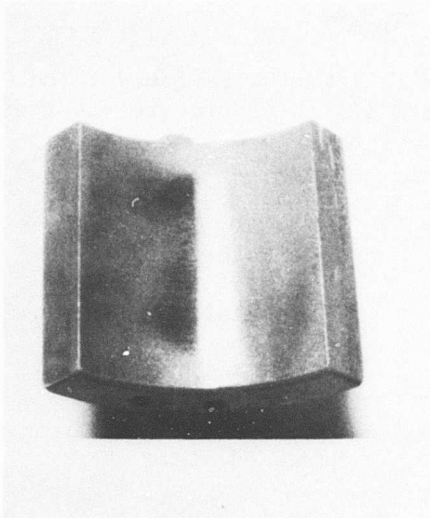
* This coating was lapped down to a thickness of 0.0001-0.0002 inch before testing.

** These were coatings, 0.003 inch thick, on metal substrates.

NOT REPRODUCIBLE



(a) PAD AFTER FIRST SERIES OF HIGH-SPEED RUBS

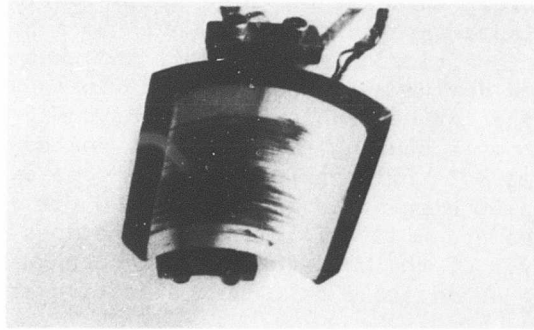


(b) TEST PAD

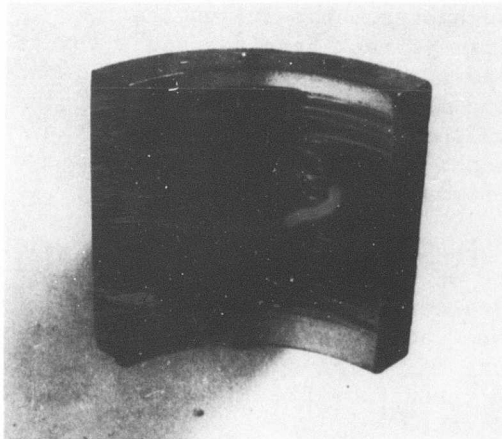


(c) TEST SHAFT

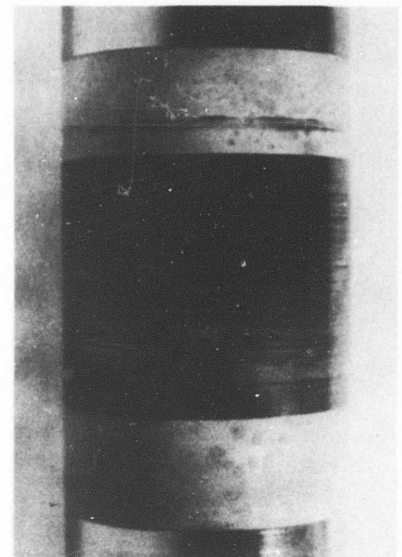
Figure 86. Bearing Surfaces of Test Pad and Journal After High-Speed Contacts (Plasma-Sprayed Chrome-Oxide Coating on Both Pad and Journal).



(a) CARBIDE PAD AFTER FIRST SEQUENCE OF SHOCK LOADS



(b) CARBIDE PAD



(c) Al_2O_3 SHAFT

Figure 87. Bearing Surfaces of Test Pad and Journal After High-Speed Contacts (Nickel-Bonded Tungsten-Carbide Coated Pad Versus Al_2O_3 Coated Journal).

The resin-bonded MoS₂ film was very effective as long as the film remained intact but, in both the start-stop tests and the high-speed run tests, metal transfer and scoring was noted before the end of the run. It was felt that the use of a solid-lubricant film applied over one of the plasma-sprayed coatings would be a better approach. This would reduce the friction considerably and thus minimize the amount of heat generated during a high-speed run. In many cases, it would also reduce starting torque problems in hydrodynamic bearing systems. Figure 88 shows a bearing pad which was coated with chrome oxide plus a resin-bonded MoS₂ film on top of the chrome oxide. This pad was subjected to 100 high-speed runs at 48,000 rpm in air. The original grinding marks are still visible, and there does not appear to have been any wear. Even if the MoS₂ coating had been worn away, the chrome oxide coating would still have been effective in preventing surface damage.

It is important to note that further evaluations have been made using the straight chrome oxide coating in full-scale journal and thrust bearing tests. This work is being done under a Navy contract [3] to determine how well gas bearings can stand up to shock-test impacts under simulated shipboard conditions. In this test rig, which is shown in Figure 89, a 2.375-inch-diameter motor-driven shaft, weighing 65 pounds, is mounted on two journal bearings and a thrust bearing. The shaft is brought up to a speed of 8000 rpm, and impact loads are applied to the base of the machine by means of a pendulum hammer. Accelerometers, mounted on the machine casing, sense the acceleration levels to which the machine is subjected. Capacitance probes are used to monitor the performance of the bearings.

Gas-lubricated journal and thrust bearings, coated with chrome oxide, have been subjected to 1300 impacts of 40 g's on the casing without destroying the bearings. Both hydrostatic and hydrodynamic bearings were evaluated. A photograph of one set of the hydrodynamic bearing pads and journals is shown as Figure 90. Talysurf traces of the wear areas show only a slight change in surface finish. The hydrostatic bearings were in even better condition.

Several gas-bearing machines have also been built using chrome oxide coated bearings. In no case have any problems been encountered with these machines because of the coatings.

The results of the initial work on the single, pivoted-pad bearing showed that many of the hard-coated materials were able to survive the 1000 start-stop tests with little or no measurable surface damage. However, in the high-speed run tests, it was found that any bearing material which was metallic or contained a metallic binder (such as the nickel-bonded carbide) would transfer metal to the journal surface. This transferred metal then caused scoring or welding. The results are not too surprising, since the sliding velocities and loads are very high. For example, at 60,000 rpm, with a 1.5-inch-diameter shaft, the sliding velocity is about 390 feet per second under loads as high as

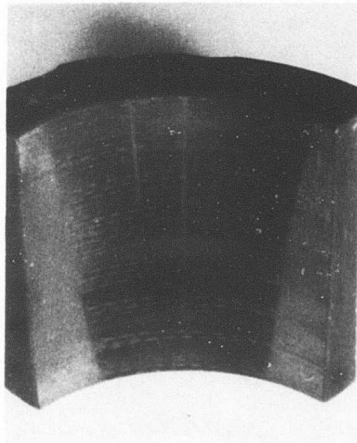


Figure 88. Surface of Test Pad After 100 High-Speed Rubs at 48,000 RPM in Ambient Air (Pad Surface Coated With 0.003 Inch of Plasma-Sprayed Chrome Oxide plus 0.0001 Inch of Resin-Bonded MoS_2).

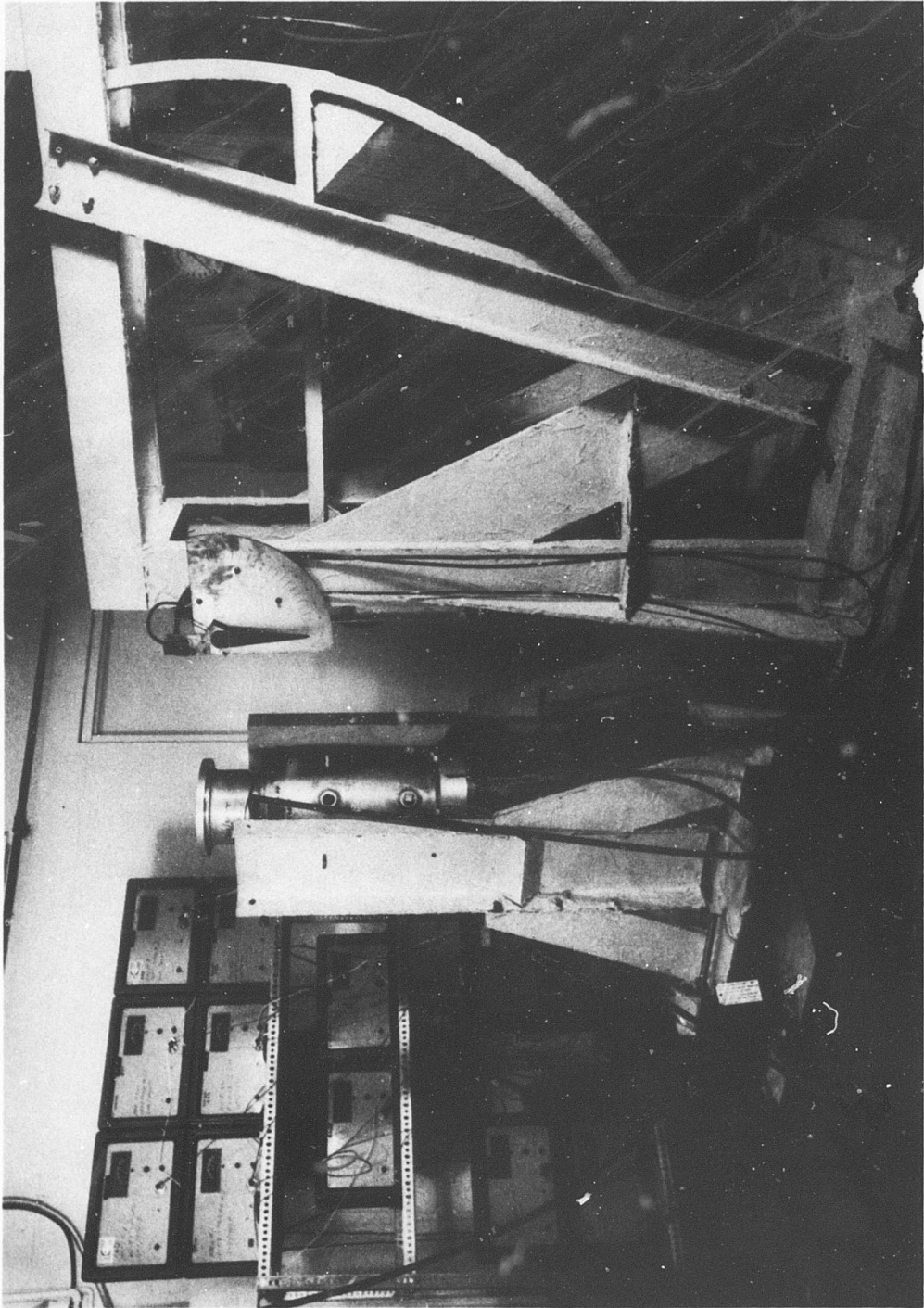


Figure 89. Gas-Bearing Test Machine Mounted on Shock Test Stand.

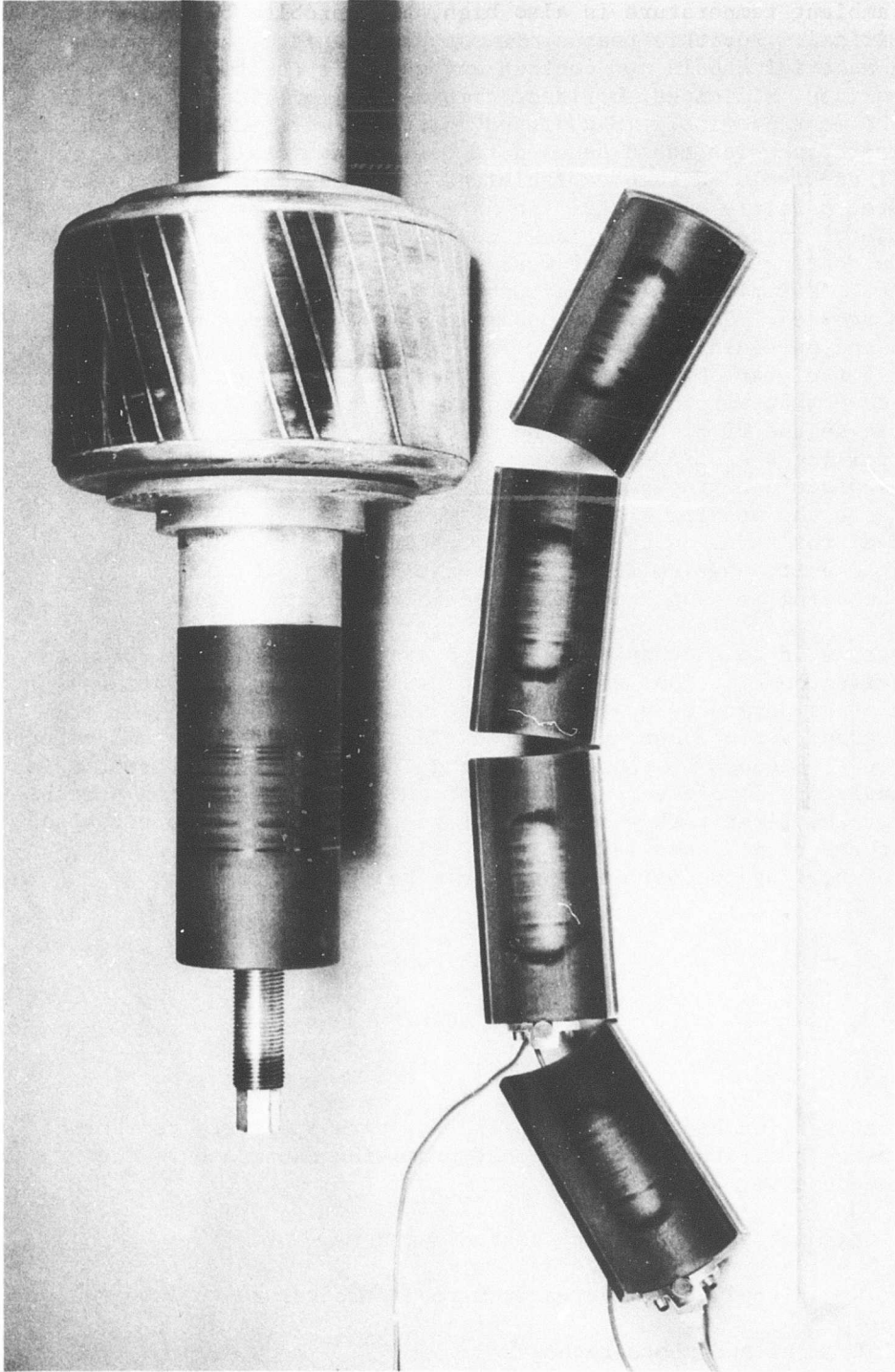


Figure 90. Chrome-Oxide Coated Journal and Hydrodynamic Pivoted-Pad Bearing Segments From Gas-Bearing Test Machine After 1300 Impacts on the Shock Test Stand.

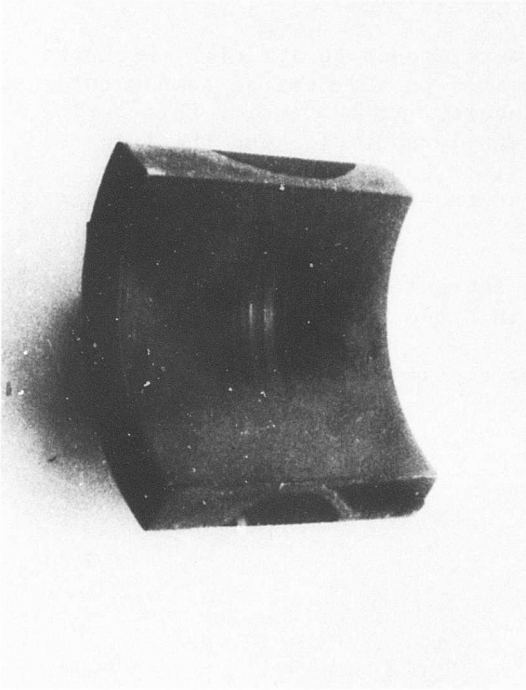
50 to 100 g's. Sufficient heat is generated, even in a fraction of a second, to bring the surfaces up to the melting point of the metal. If the ambient temperature is also high, this problem becomes even more critical. For this reason, it was hypothesized that the ideal coating material should not contain any metallic constituent. Self-bonded oxides, silicides, borides, carbides, or nitrides seemed to offer the most promise. In addition, attempts were made to establish other criteria which could be used to define the ideal coating combination. These included such variables as hardness, density, crystal structure, particle size, etc. To date, none of these has been found to be useful in defining the ideal coating. It has been established that the coating material must wear in the form of fine, discrete particles. Materials which fracture and produce large agglomerates must be avoided. However, the conditions which control the wear process and particle size are not really defined. Density is known to affect the wear characteristics of the coatings. It has been found in one case that very dense coatings are not as effective as coatings with some degree of porosity. The porosity could be part of the key to controlling the size of the wear particles. In addition, the pores in the surface can trap particles and minimize the amount of loose material in the bearing clearance. Figure 91 shows the results of high-speed rub tests on chrome oxide coatings of different densities. The high-density coating shows considerable abrasion, while the low-density coating is smooth and polished in the contact area.

A new series of bearing materials tests are currently in progress to find coating combinations which will be suitable for applications running at temperatures up to at least 1400°F [10] and [11], in both air and argon. Since chrome-oxide coatings are limited to temperatures below 900°F, because of thermal spalling at higher temperatures, this work involved a complete reappraisal of the requirements of a suitable coating. The first task was to select coatings which could withstand temperatures of at least 1400°F in an oxidizing (air) environment. A number of coating compositions were selected for evaluation:

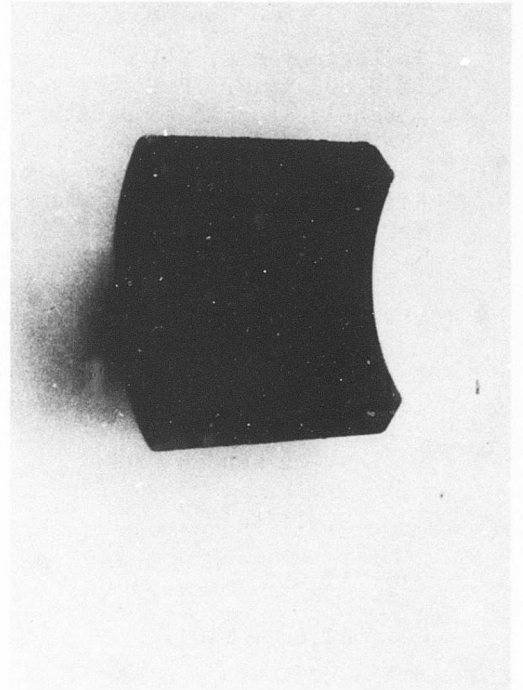
$\text{Cr}_2\text{O}_3 + \text{Al}_2\text{O}_3$	Ni-Cr bonded Cr_3C_2
Al_2O_3	Arc sprayed Stellite 6
$\text{Al}_2\text{O}_3 + \text{TiO}_2$	MoSi_2

These coatings, on Hastelloy X substrates, were subjected to thermal cycle tests in air to select the most promising candidates. The test procedure was as follows:

1. Examine and photograph coated surfaces
2. Run five 24-hour cycles from room temperature to 1000°F
3. Examine and photograph



High-Density Coating



Low-Density Coating

Figure 91. Surface Appearance of Chrome-Oxide Coated Pads With Different Density Coatings (Both Pads Subjected to 100 High-Speed Rubs at 48,000 RPM in Air).

4. Run five more cycles to 1200°F
5. Examine and photograph
6. Run five more cycles to 1400°F
7. Examine and photograph

Continue to at least 1800°F or until all coatings have failed.

In these tests, all of the coatings were ground to a finish thickness of 0.003 inch. The specimens were heated to the desired temperature and held at this temperature for 16 hours. At the end of this period, the power to the furnace was automatically shut off, and the furnace was cooled by blowing compressed air into the bottom of the chamber. After 8 hours, the air was cut off and the furnace was turned on again for the next cycle.

Photographs of typical specimens are shown in Figures 92 and 93. The results of the tests are summarized in Table XVIII.

Based on these results, the following coatings were selected for evaluation in the bearing test rig:

Ni-Cr bonded Cr_3C_2

Stellite 6

Al_2O_3

$\text{Al}_2\text{O}_3 + \text{TiO}_2$.

At this point, more thought was given to the hypothesis that self-bonded ceramic coatings were the most likely materials to resist high-speed rubs, and it was decided that orientation effects should also be important. The reasoning behind this was as follows:

If the bearing pad is impacted against the journal, the contact area on the journal continuously changes as the shaft rotates. However, the contact area on the pad is essentially fixed. This means that thermally induced sliding effects can be appreciably different depending on whether the metallic constituent is on the bearing and the nonmetallic coating is on the journal, or vice versa.

One of the goals of the bearing tests was to establish the validity of this argument.

Start-Stop Tests Results at 1400°F

The following coating combinations were selected for evaluation in air at 1400°F.

NOT REPRODUCIBLE

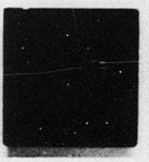
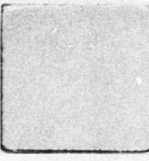
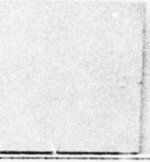
Al_2O_3	NUMBER OF CYCLES	$Al_2O_3 + TiO_2$
 Light, smooth coating	Before test	 Dark, smooth coating
 No damage	After five cycles from 80° to 1000°F	 No damage
 No damage	After five cycles from 80° to 1200°F	 Very light spalling along edges. Coating changing color
 No damage	After five cycles from 80° to 1400°F	 Coating is now cream color. More spalling on edges
 No damage	After five cycles from 80° to 1600°F	 Coating almost completely gone
 Coating almost completely gone	After five cycles from 80° to 1800°F	Not Run

Figure 92. Effect of Temperature Cycling on Adherence of Coatings on Hastelloy X (Al_2O_3 and $Al_2O_3 + TiO_2$ coatings; no undercoating).

NOT REPRODUCIBLE

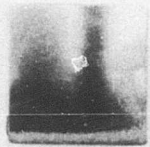
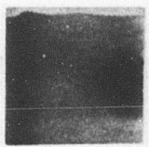
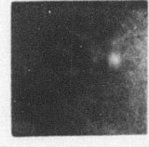
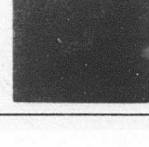
ARC SPRAYED STELLITE	NUMBER OF CYCLES	Ni-Cr BONDED Cr_3C_2
 Metallic appearance	Before test	 Metallic appearance
 Light oxide film	After five cycles from 80° to 1000°F	 Light, spotty oxide film
 Dark green oxide film	After five cycles from 80° to 1200°F	 Oxide film becoming more uniform
 Oxide film becoming powdery	After five cycles from 80° to 1400 °F	 Same as above
 Same as above	After five cycles from 80° to 1600°F	 Oxide film turning dull
 Same as above	After five cycles from 80° to 1800°F	 Uniform dull oxide
 Very thick loose oxide	After 1/2 hour at 1950°F	 Uniform dull oxide

Figure 93. Effect of Temperature Cycling on Adherence of Stellite and Nickel-Chrome Bonded Chrome Carbide on Hastelloy X.

TABLE XVIII. THERMAL CYCLE TEST RESULTS FOR VARIOUS BEARING COATING MATERIALS

Linde LS-6 (Stellite)	Still intact but badly oxidized after the 1800°F thermal cycles
Linde LC-1-C (Cr_3C_2 + Ni-Cr Binder)	Still intact, oxidized after the 1800°F thermal cycles
Linde LA-2 (Al_2O_3)	Spalled completely after the 1800°F thermal cycles
Heanium Blue (Al_2O_3 + TiO_2)*	Spalled after the 1800°F thermal cycles. Undercoating was no help.
Linde LA 7 (Al_2O_3 + TiO_2)	Starting to spall on edges after the 1200°F thermal cycles.
Linde LC-5 (Cr_2O_3 + Al_2O_3)	Same as LA-7
Plasma-sprayed Cr_2O_3 *	Starting to spall at corners after 1000°F thermal cycle. Undercoat was no help.
Plasma-sprayed MoSi_2	Attacked at 1200°F
* Tested with and without metallic undercoat.	

<u>Bearing (Pad) Coating</u>	<u>Journal Coating</u>	<u>Reason for Selection</u>
1. Al ₂ O ₃	Al ₂ O ₃	Nonmetallic coating
2. Al ₂ O ₃ + TiO ₂	Al ₂ O ₃ + TiO ₂	Nonmetallic coating
3. Stellite 6	Al ₂ O ₃	Effect of orientation
4. Al ₂ O ₃	Stellite 6	Effect of orientation
5. Ni-Cr bonded Cr ₃ C ₂	Al ₂ O ₃	Effect of orientation
6. Al ₂ O ₃	Ni-Cr bonded Cr ₃ C ₂	Effect of orientation

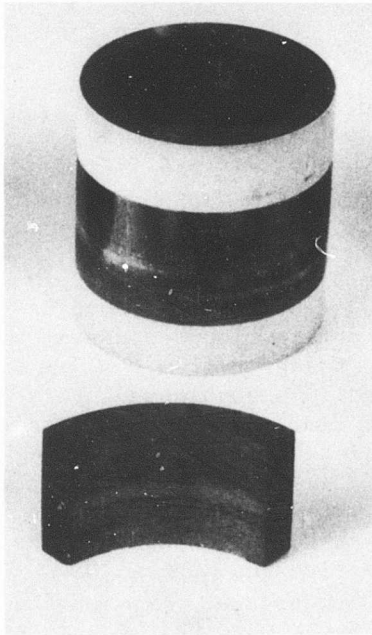
The self-mated Al₂O₃ combination wore at an extremely high rate although the bearing performed well as long as the coating was intact (about 300 starts and stops). The self-mated Al₂O₃ + TiO₂ coating ran very well for about 250 starts and stops, then performance deteriorated rapidly. It was later found that the coating had separated from the substrate in the loaded zone of the bearing pad.

The tests on the effect of orientation yielded very interesting and significant results. As long as the bearing surface was the non-metallic coating, in this case Al₂O₃, metal transfer was reduced appreciably. The Al₂O₃-coated bearing running against the Ni-Cr bonded Cr₃O₂ journal was a particularly good combination. Figure 94 shows the difference in transfer characteristics between the two orientations. The Al₂O₃-coated bearing running against Stellite 6 or the journal did not show as dramatic an improvement because of oxide film buildup on the Stellite. However, it was still considerably better than the Stellite-coated bearing versus the Al₂O₃-coated journal.

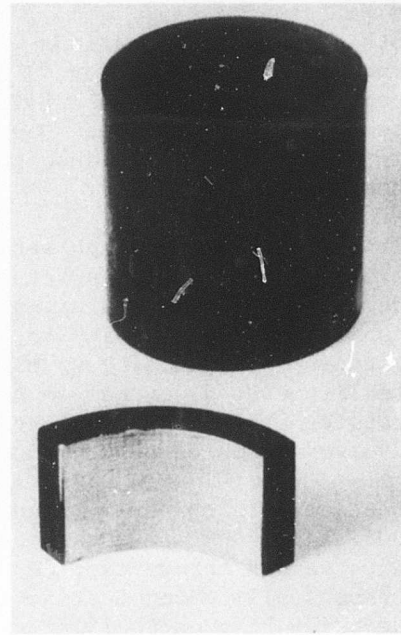
High-Speed Rub Tests

The purpose of the high-speed rub tests was to ensure the ability of the coating to survive an instantaneous high-speed contact. Experience has indicated that occasional high-speed rubs, due to unexpected acceleration or shock loads, can induce momentary contacts. In most bearing support systems, the presence of a low friction lubricant inhibits permanent damage. Since, in this case, a gas film separates the moving surfaces, rupture of the film could result in permanent damage unless the coating materials provide adequate protection.

A 30,000-rpm operating speed and a 1400°F ambient temperature were selected to evaluate these coatings. At this speed, the partial arc gas-bearing test pad was supported on a self-generated gas film of approximately 0.001 inch. The pad was preloaded to a unit loading of 2.5 psi. The pad was instrumented with capacitance probes to monitor the gas film. At this steady-state condition, the pad was subjected to instantaneous shock loads sufficient to rupture the film as observed from the pad instrumentation.



Al_2O_3 Coated Shaft vs Ni-Cr
Bonded Cr_3C_2 Coated Pad.



Ni-Cr bonded Cr_3C_2 coated
Shaft vs Al_2O_3 coated Shaft.

Figure 94. Effect of Orientation on Al_2O_3 Versus Cr_3C_2 .

The following material combinations were evaluated:

<u>Bearing (Pad)</u>	<u>Journal</u>
1. Al_2O_3 coating	Ni-Cr bonded Cr_3C_2 coating
2. Al_2O_3 coating	Stellite 6 coating

Both of these combinations withstood the 50 drops of 1 pound from a height of 1 inch. The Al_2O_3 versus the Cr_3C_2 failed after 6 drops of 3 pounds from a height of 1 inch, and the Al_2O_3 versus Stellite 6 failed after 13 impacts with the 3 pound weight. Figures 95 and 96 show the appearance of the specimens after these high-speed tests.

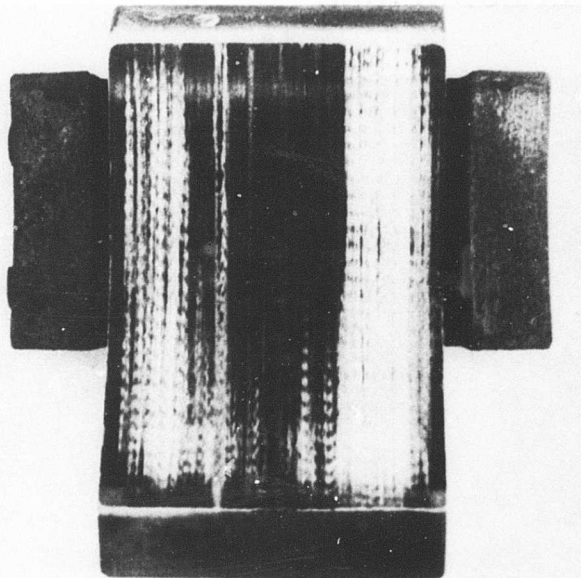
Although the differences were small, it did appear that the Al_2O_3 versus Stellite 6 was a better combination for high-speed rub performance in air. In the start-stop tests, the Al_2O_3 - Stellite 6 combination was a second choice to the Al_2O_3 - Cr_3C_2 combination because of a tendency for an excessive amount of oxide to transfer from the Stellite-coated journal to the Al_2O_3 -coated pad. At high speed, this transfer still occurred, but the short contact time and the high speeds involved produced a much more adherent and polished film.

Subsequent tests were run under NASA contract [10] at temperatures of 900°F and 1400°F in an argon environment. These tests showed that the Al_2O_3 versus chrome carbide was much more effective than the Al_2O_3 versus Stellite combination in a nonoxidizing atmosphere. Apparently, the oxide film on Stellite plays a major role in protecting the sliding surfaces, particularly during high-speed rubs.

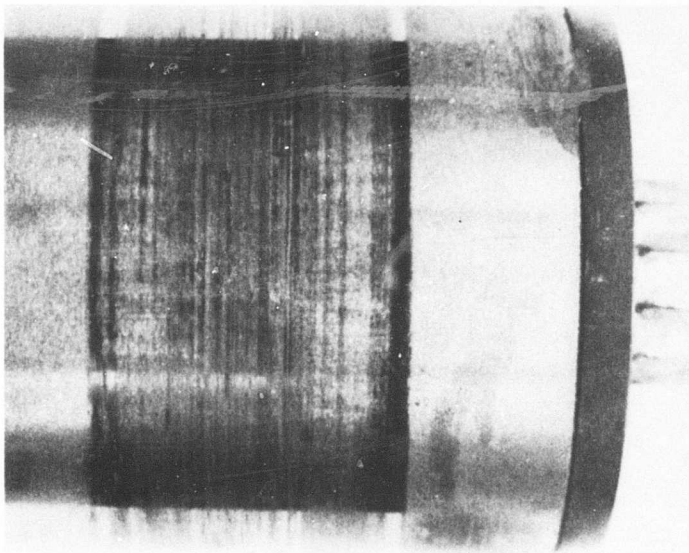
A substantial improvement in the results of these tests could probably be realized by the use of a solid lubricant film applied over the plasma coatings on the bearing and journal. In the air tests, failure was caused by minute fractures in isolated areas on the Al_2O_3 coating. Talysurf traces showed that these failures took place within the coating rather than at the bond between the coating and the substrate. This could be the result of an interaction between the Al_2O_3 coating and the oxide films on the journal surfaces.

The use of solid ceramics or cermets for the bearing surfaces would seem to offer a good alternative to the use of the plasma coatings for obtaining good sliding behavior, if means can be developed for holding these solid parts. However, this may not be as good an approach as it seems to be at first sight. Many of these materials are not as wear or damage resistant as the manufacturer's claims imply. Furthermore, most of the combinations which are known to be effective have metal-bonded tungsten carbide as one of the members. This carbide is limited to temperatures below 900°F in air because of oxidation. Thus, it is evident that this approach also offers many difficulties.

NOT REPRODUCIBLE



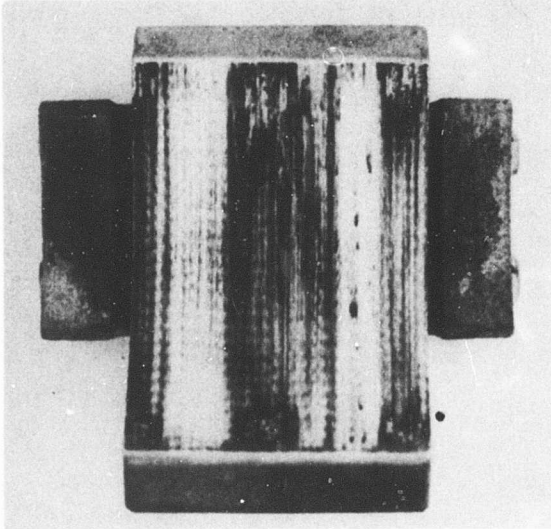
2.5 Magnification



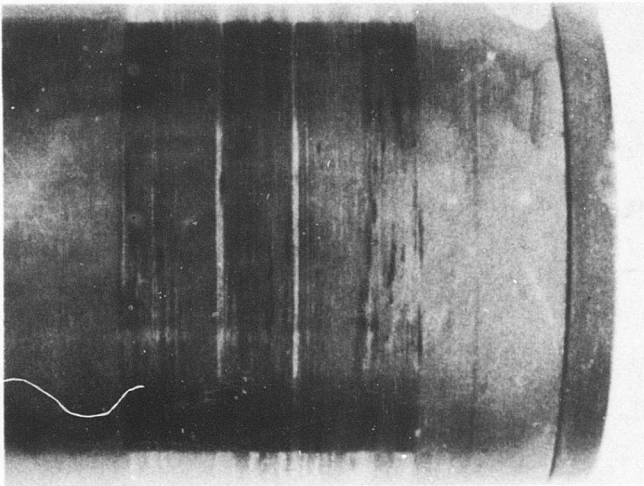
2.5 Magnification

Figure 95. Al₂O₃ Coated Pad Versus Stellite 6 Coated Journal After High-Speed Rubs at 1400°F in Air.

NOT REPRODUCIBLE



2.5 Magnification



2.5 Magnification

Figure 96. Al_2O_3 Coated Pad Versus Chrome Carbide Coated Journal After High-Speed Rubs at 1400°F in Air.

ADEQUATE FABRICATION TECHNIQUES

The most important questions in this area are:

1. Can the bearing design be made by available techniques with the materials which have been selected?
2. Has an adequate manufacturing sequence for material processing been established with suitable provisions for quality control?

It is difficult to make general comments on these items without having a specific bearing design available, but certain points should be borne in mind.

Bearing Design

First, with regard to the bearing design, any steps which are taken to improve the sliding behavior of bearings invariably place limitations on the basic design concepts. For example, if plasma-sprayed coatings are to be used for surface protection, provision must be made for applying the coatings to the bearing surface. It is very difficult to spray coatings on the ID of a bore unless the L/D ratio is less than 1 and the bore is greater than 2 or 3 inches. This is because the adherence of the coating is strongly dependent on the angle at which the spray impacts against the surface. Ideally, the best condition is a perpendicular impact. This can be done with pivoted-pad bearings because each pad can be coated individually, but full sleeves are a problem. Orifices in the bearing surface also required special techniques. The orifice must be plugged during spraying and then the plugs must be removed without damaging the edges of the coating. Teflon, graphite, brass, and aluminum have all been used to protect the orifices.

Grooving is almost impossible to achieve on the ID of a coated sleeve bearing. If grooving is required, it should be applied to the OD surface of the journal. Photo-etching techniques can be used on many cermets since these are electrical conductors, but no way has been developed to etch ceramic coatings such as chrome oxide or Al_2O_3 .

Thrust bearings are relatively simple to groove, even when plasma-sprayed coatings are used. A negative mask can be placed over the thrust bearing surface and the bearing can then be coated. When the mask is removed, those areas which were exposed form the lands and dam areas, and the areas which were covered form the grooves. The coating is then ground back until the proper groove depth has been achieved. Figure 97 shows typical thrust bearing patterns which were fabricated using this technique.

Solid ceramics or cermets are much more difficult to fabricate, especially when grooves or orifices must be used. Abrasive blasting or photo-etching techniques can generate grooves or lands, but orifices are a serious and

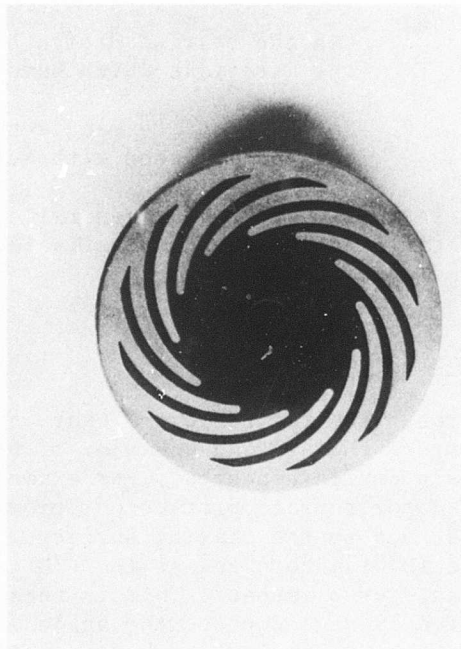
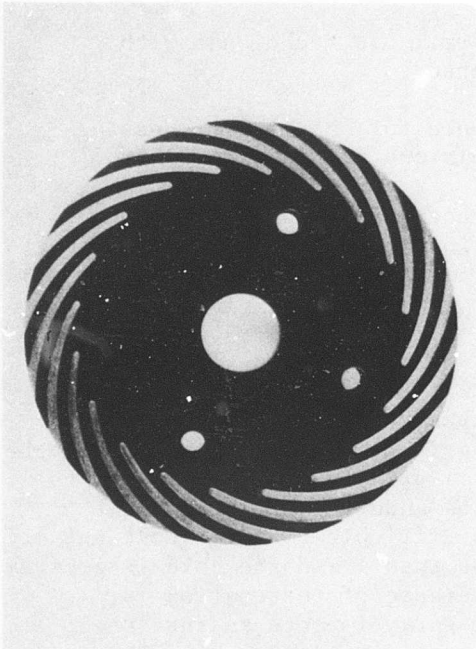


Figure 97. Typical Self-Acting Thrust-Bearing Groove Patterns Formed by Applying Plasma-Sprayed Coatings Through A Mask.

expensive problem. Again, it must be noted that the techniques for retaining ceramic parts present difficult design problems.

Surface finish plays an important role in determining the effectiveness of material combinations. There appears to be an optimum roughness in the range from 4-8 rms. Greater values of roughness will promote material transfer. Lower values represent additional cost with no apparent benefit.

Manufacturing and Quality Control

In spite of the fact that processing sequences are almost universally used to set down a step-by-step procedure for manufacturing parts, it is surprising to note the number of times that the sequence fails to satisfy the basic goals. This is particularly true when coatings are used, whether these be solid lubricant films or the plasma-sprayed hard coatings. The coating process, and the grinding and lapping of these coatings, is practically the last step in manufacturing, yet many vendors end up with a heat treatment or brazing or plating procedure after the coating has been applied. Even if the coating can tolerate these conditions, it presents the possibility that the coating could be damaged in a way which would not be readily detected.

This brings up the problem of quality control, which is one of the greatest drawbacks to the use of plasma deposition. Plasma coating is a fairly recent development, at least as a standard manufacturing process and, like electroplating, it has been developed primarily as a "job shop" operation. There is a large and serious lack of basic information concerning the mechanisms by which these coatings adhere and cohere. In addition, quality control procedures leave much to be desired. There are standard techniques available for evaluating coatings but these are primarily destructive tests. For example, tensile tests and bend tests are used to evaluate the bond strength of the coating, and metallographic sections can be made to inspect the bond between the coating and the substrate. However, these tests must be made on specimens which have been coated separately. The results may or may not be representative of the condition of the actual machine part.

In recent years, a number of techniques have been developed to determine bonding effectiveness of coatings by nondestructive methods. These include the following:

1. Ultrasonic pulse-echo and phase detection bond test
2. Eddy current flux field applications
3. Thermal or infrared evaluation.

Ultrasonic

Ultrasonic pulse-echo testing introduces a high-frequency, short-duration burst of sonic energy into any material exhibiting the

correct values of Young's modulus, density and Poisson's ratio. One of several piezo-electric crystalline elements can be used as the ultrasonic vibration transducer: quartz, lithium sulphate, lead zirconate, and barium titanate, to name a few. Because of the short wavelengths at the ultrasonic frequencies (1.0 megacycles-25.0 megacycles), the wave is unable to bridge the air interface existing between the crystal face and the entrant surface of the test sample. However, a layer of water, oil, or other suitable liquid "couples" the ultrasonic vibrations into the test piece. The waves are then free to travel through the part at extremely high velocities; for example, 5.0×10^5 cm/sec in steel. The path of the wave is regarded as being rectilinear and will reflect from other air interfaces within the sample, following the dictates of Snell's law of reflection and refraction of light waves. The returning vibrations are electronically detected, amplified, and finally applied to a cathode ray tube as "pips" or "indications". The analogy would be to a sonar device.

A poor bond immediately adjacent an entrant surface would represent an air interface and would cause the wave to reflect at an inappropriate time. This ill-timed reflection would be easily identifiable as such.

Eddy Current

If a test coil or probe is excited with an alternating current of a suitable frequency, an alternating magnetic field of this frequency is thus created in the vicinity of the coil. When a metal part is brought into juxtaposition, eddy currents are induced in the part since the part may be considered as an infinite number of conductors, each of which is crossed by the time-varying electromagnetic flux lines. This characteristic is analogous to the development of a secondary voltage in a transformer.

These eddy currents set up electromagnetic fields of their own. The fields partially cancel the original coil field, yielding a resultant field. This resultant field interacts with the coil current and associated flux linkages to create a specific coil impedance for the part under test. Four fundamental properties of any material affect the eddy current distribution in a part; conductivity, permeability, size (diameter, mass or thickness), and homogeneity. Metallurgical and physical variations will cause changes in one or more of these fundamental properties and will therefore affect the probe impedance.

It may be expected that lack of bonding, constituting an air impedance, will have a significant effect on those four parameters.

Infrared or Thermal

In performing this test, a radiant heat source is made to cast a uniform heat spot over a fixed area of the part being investigated. After a predetermined heating period, the heated region is scanned by an infrared radiometer, which measures temperatures at a pattern

of points covering the region. The scan is made rapidly compared with the heating rate, so that the temperature pattern remains essentially unchanged during the scanning process.

In the heating period before temperature measurement, the heat flows from the surface into the test sample at a rate dependent upon internal characteristics of the material.

A discontinuity in the structure, such as an unbonded area, will retard the heat flow, causing the heated surface to rise rapidly in temperature.

Anyone of these three techniques could be used as a nondestructive test, but some further development effort is necessary to bring the technique up to the level of a practical standard test.

In order to achieve any real degree of optimization in the use of plasma coatings, there are a number of basic questions which must be at least partially answered.

1. What is the effect of application techniques on coating density, and what is the effect of density on sliding behavior?

There are already some guidelines which can be used to answer this question, but some optimization work would be necessary for any specific coating composition.

2. What is the effect of substrate composition on adherence?

Until a few years ago, it was generally believed that these coatings were only mechanically bonded to the substrate. This has now been modified since it is apparent that solid-state bonding is at least partially responsible for coating adherence. However, there has been very little work done to understand the mechanisms involved. The coatings appear to bond reasonably well on a variety of substrate alloys such as aluminum, titanium, ferrous, and nickel-base alloys (stainless steels, etc.). However, there are no data available to show if one specific type of coating adheres more strongly to one type of alloy than another.

3. What is the effect of powder composition on the coherence of the coating?

This is a particularly interesting problem for the self-bonded oxide coatings such as Al_2O_3 or chrome oxide. The individual oxide particles must be bonded together through some form of a sintering process, yet there has been no effort to determine how this is done. The purity of the original powder would be a critical item in determining the mechanical strength of the particle-to-particle bonds.

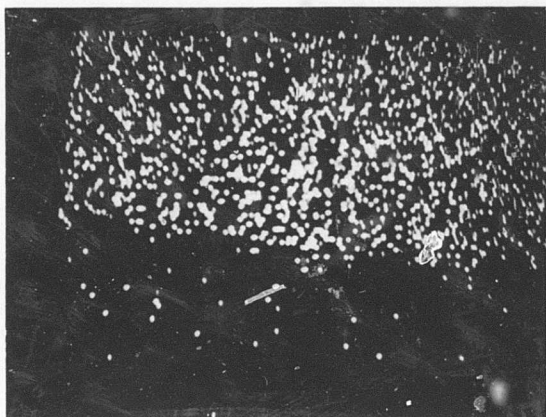
An interesting observation was made at MTI when chrome oxide was evaluated for suitability in NaK. At 200°F, the chrome oxide coating was not affected by the liquid metal; at 600°F, the coating disintegrated because the NaK dissolved the interface between the original particles. The individual particles were not affected. This suggests that the bond is a vitreous phase composed of impurities which probably have a different composition and melting point from the pure chrome oxide. A better understanding of these cohesive bonds might make it possible to specify what the chrome oxide powder composition should be. This result also furnishes a possible explanation for the fact that chrome oxide is not suitable for use at temperatures above 900°F. If cohesion is the result of a low melting glass phase between the particles, then the coating could disintegrate at high temperature, even though chrome oxide itself should not be affected.

Fundamental studies of the questions listed above are essential to understand and predict the behavior of coatings. MTI has recently installed a plasma-spray facility to study these factors under controlled conditions. Unless more effort is concentrated in this area, plasma coatings will never be able to achieve the kinds of reliability and assurance which would enable the engineer to use them with confidence. Metallographic techniques are being used in conjunction with electron probe work to determine the composition of the coating and the nature of the interface. Some typical photographs are shown in Figures 98 and 99. This type of basic work, coupled with the work which is being done in the bearing evaluations, should represent a substantial contribution to the state of the art.

THERMAL CONDUCTIVITY

To date, there has been very little practical hardware built for high temperature usage. For this reason, the problem of thermal conductivity has been largely ignored. However, this could be a critical problem, especially in thrust bearings operating under nonisothermal conditions. Thermal gradients can cause crowning and a substantial reduction in load-carrying capacity. Most of the superalloys and high-temperature stainless steels are poor from a standpoint of thermal conductivity and would show appreciable warpage or crowning. Some of the refractory metals such as tungsten, molybdenum, and columbium have high thermal conductivities and adequate strength for use at high temperature. However, these metals must be protected against oxidation.

This problem will not be easy to solve, and it will require a combined effort between design and materials technology.

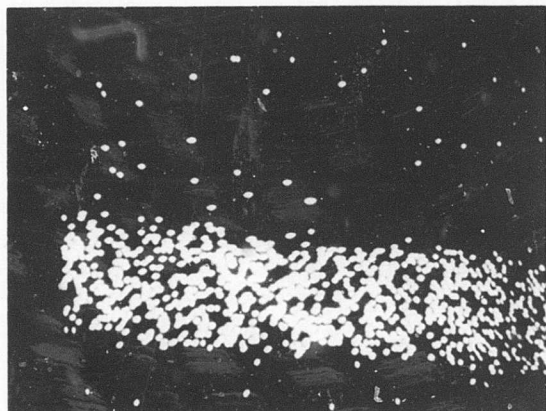


a) $K\alpha$ line for iron

Steel Substrate

Stellite Coating

Mounting Plastic



b) $K\alpha$ line for cobalt

Steel Substrate

Stellite Coating

Mounting Plastic

Figure 98. Preliminary Electron-Probe Patterns From Cross Section of Stellite Coating on Steel Substrate.

'NOT REPRODUCIBLE

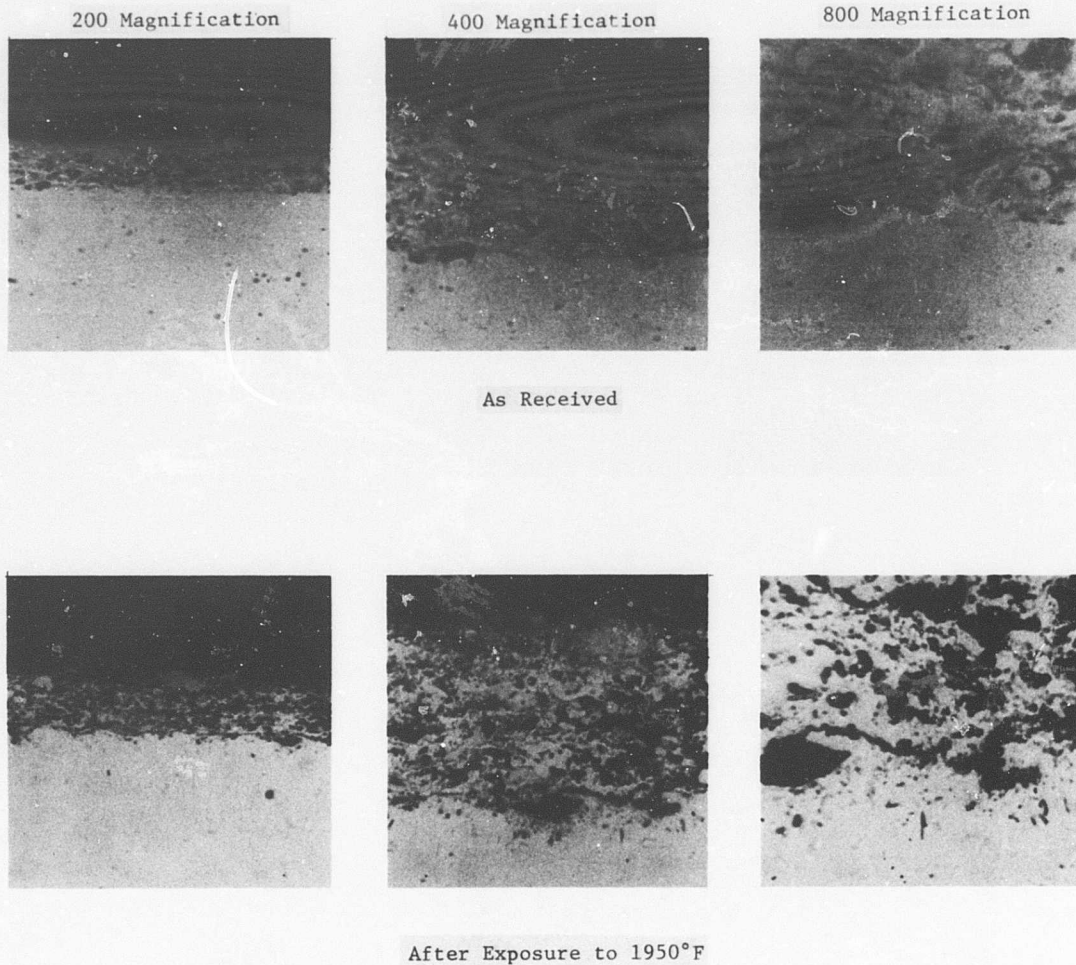


Figure 99. Cross Sections of Chrome Carbide Coating Before and After High-Temperature Tests.

SUMMARY

The objective of this discussion was to sum up the state of the art on materials for high-temperature gas bearings in advanced gas-turbine engines. The approach which is recommended by MTI is to use suitable high-temperature high-strength alloys for the journal and bearing parts, and to rely on plasma-sprayed hard coatings to achieve good surface properties, particularly sliding compatibility.

There is a state-of-the-art ceiling of 1400° to 1500°F, which limits maximum bearing temperature for the gas-generator application. This is set by the following considerations:

1. Stress-rupture life of available journal materials. At the present time, a temperature range from 1400° to 1500°F appears to be the upper limit for the proposed engine design. The 1500°F limit would apply to a 2.625-inch-diameter journal rotating at 70,000 rpm. For a 3-inch-diameter journal, the 1400°F temperature limit would apply.
2. Oxidation characteristics of high temperature alloys. For gas bearing applications, many of the superalloys are limited to temperatures below 1500°F because of the formation of poorly adherent oxide films. Even the most oxidation resistant alloys will probably be limited to temperatures of about 1600°F. Above this level, the oxide films become excessively thick and would be a source of loose debris, particularly in hydrostatic bearings. Coatings or diffusion treatments to inhibit oxidation could reduce this limitation, but these techniques would have to be evaluated to determine how well they apply to gas bearings.
3. Availability of wear-resistant plasma-sprayed coatings. Up to 1600°F, there are suitable coatings. Above this temperature level, problems of thermal spalling and oxidation will drastically limit the available choices. None of the base alloys would have satisfactory resistance to sliding damage if they are used in the uncoated condition.

Provision must be made in the bearing design concepts to provide compensation for the following effects:

1. Centrifugal growth of the rotating journals
2. Thermal gradients along the shaft
3. Formation of oxide films
4. Changes in dimensions of the base alloys as a result of metallurgical reactions at high temperature.

In addition, thermal conductivity of the materials will be an important factor in thrust bearing design. Under nonisothermal conditions, there will be problems with dishing or crowning of the thrust bearings. This distortion can be minimized by using alloys of high thermal conductivity, but these alloys are all very susceptible to high oxidation rates. The solution to this problem must be a joint effort by both design and materials technology.

In summary, 1400° to 1500°F appears to be the practical upper limit for the gas-generator turbine-end bearings. It should be noted that this limit could be increased by a significant amount in the next few years by development work which is now in progress. For example, advances in the technology of fiber-reinforced or dispersion-hardened alloys could raise the stress-rupture life and decrease the importance of compensation for centrifugal growth or dimensional changes. Also, the problem of oxidation could be virtually eliminated by advances in the oxidation barrier coatings.

APPENDIX III
ANALYSIS OF EXTERNALLY PRESSURIZED JOURNAL BEARINGS

INITIAL SCREENING STUDY

As described on page 32 of this report, the HP-spool turbine-end journal bearing was selected for the purpose of a comparative analysis and evaluation of various journal bearing designs. This appendix describes the initial screening study and the detailed analyses performed for the full-circular externally pressurized type of journal bearing.

For initial screening purposes, a preliminary layout configuration of the gas generator was used to establish the bearing requirements. (This configuration is documented on MTI drawing SK-D-2806.)

The following design-point conditions were defined:

$$N_{\text{design}} = 63,100 \text{ rpm}$$

$$W_{\text{max design}} = 320 \text{ lb}_f$$

$$m = 7 \text{ lb}_m$$

where

$$N_{\text{design}} = \text{design-point shaft speed}$$

$$W_{\text{max design}} = \text{maximum design-point bearing load}$$

$$m = \text{rotating mass per bearing}$$

In order to include centrifugal growth effects on bearing performance, the following assumptions were made:

$$R_i/R_o = 0.87$$

$$E \begin{cases} = 30 \times 10^6 \text{ psi (100}^\circ\text{ to 1000}^\circ\text{F)} \\ = 20 \times 10^6 \text{ psi (1000}^\circ\text{ to 2000}^\circ\text{F)} \end{cases}$$

where

$$R_i = \text{journal inside radius, in.}$$

$$R_o = \text{journal outside radius, in.}$$

$$E = \text{journal modulus of elasticity, psi}$$

Fractional Frequency Whirl

It is well known that a rotor supported in full-circular fluid-film journal bearings is susceptible to a particular form of instability commonly called "fractional frequency whirl". The instability manifests itself as a violent rotor vibration when rotor speed exceeds a particular value denoted as the "instability threshold speed" or, simply, the "threshold" speed. Successful application of externally pressurized bearings requires that the rotor-bearing system be designed such that shaft speed will always be less than the threshold speed at all possible operating conditions. The following paragraphs give a brief description of the design criterion and analysis procedures used to assess the fractional frequency whirl characteristics of the HP spool when supported by externally pressurized bearings.

From a simplified standpoint, the rotor-bearing system can be thought of as a mechanical spring-mass system. The spring, in this case, would represent the combined effective stiffness of the bearing lubricant film and the bearing support structure. The lubricant film, and perhaps the support structure, would also contribute some damping to the system. Neglecting damping for the moment, the natural frequency of the spring-mass system can be expressed (again on a simplified basis) by:

$$\omega_n = \sqrt{\frac{K g}{m}} \quad (5)$$

where ω_n = natural frequency, rad/sec

K = combined effective stiffness, lb/in.

g = gravitational constant = 386 lb_m-in./lb_f-sec²

The natural frequency, ω_n , is commonly called the transverse critical speed of the rotor.* If the rotor-bearing system is excited by a forcing function at or near a frequency of ω_n , resonant vibration of the rotor will occur. The most common form of excitation is that which is due to mechanical unbalance of the rotor. In the absence of significant damping (which, unfortunately, is the usual case with gas bearings), unbalance will cause large amplitudes of synchronous rotor whirl when rotor speed equals ω_n .

It has been shown, both analytically and experimentally [30,33], that the threshold speed for fractional frequency whirl of a full-circular, externally pressurized, rigidly mounted gas bearing generally occurs when rotor speed approaches twice the first critical speed of the rotor-bearing system. That is,

$$\omega_t \cong 2 \sqrt{\frac{K_b g}{m}} \quad (6)$$

*In an actual rotor-bearing system there are an infinite number of possible natural frequencies; that is, transverse critical speeds. However, only the lowest critical speed (frequently referred to as the first critical speed) is of importance from the standpoint of fractional frequency whirl. Equation (5) will thus be interpreted here as the lowest critical speed.

where

ω_t = threshold speed for fractional frequency whirl, rad/sec

K_b = bearing (gas film) stiffness, lb/in.

Although Equation (6) represents a simplified approach to predicting the instability threshold speed, experience has shown that this approach provides a reasonable basis for design evaluation purposes. To provide adequate safety margin for whirl-free operation, Equation (6) was modified to the following "design criterion" form:

$$\omega \leq 1.9 \sqrt{\frac{K_b g}{m}} \quad (7)$$

where

ω = rotor speed, rad/sec

Equation (7) requires that rotor speed never be greater than 1.9 times the first critical speed of the rotor-bearing system. If this requirement can be achieved, whirl-free rotor operation should be realized. A more convenient form of Equation (7) for the purposes of this discussion is:

$$N \leq 357 \sqrt{\frac{K_b}{m}} \quad (8)$$

where

N = rotor speed, rpm.

Bearing Stiffness

Bearing stiffness is a function of bearing design and operating parameters, and it will be a maximum at one operating condition only. In lieu of a rigorous analysis, it is possible to obtain a conservative (i.e., somewhat low) estimate of bearing stiffness from the following equation:

$$K_b \cong \frac{\Delta P L D}{3C} \quad (9)$$

where

$\Delta P = P_s - P_a$, psi

P_s = bearing supply pressure, psia

P_a = bearing ambient pressure, psia

L = length of bearing, in.

D = diameter of bearing, in.

C = bearing radial clearance, in.

The variable in Equation (9) is the constant 1/3, which will actually increase to a maximum of 1/2 at optimum conditions.

Equation (9) gives the static stiffness of the bearing. Dynamic squeeze film effects will result in an increase in stiffness of approximately 10 percent. This, however, was neglected for the initial design study.

A quick estimate of bearing load capacity can be made using the static stiffness:

$$W = K_b e = K_b \epsilon C \quad (10)$$

where

W = bearing load, lb

ϵ = bearing eccentricity ratio ($\frac{e}{C}$)

e = bearing eccentricity, in.

Using the expression for K_b given by Equation (9), we obtain

$$W = \frac{\Delta PLD\epsilon}{3} \quad (11)$$

Assuming an eccentricity ratio of 0.9 and a projected bearing area of 12 square inches, it is found from Equation (11) that a 90-psi differential pressure would be required to carry a 320-pound bearing load. However, hydrodynamic effects at the high eccentricity ratio condition would tend to decrease this pressure requirement.

With an approximate expression established for bearing stiffness, the bearing stability criterion can now be expressed as follows:

$$N \leq 357 \sqrt{\frac{\Delta PLD}{3C_m}} \quad (12)$$

Review of the initial gas-generator layout drawing indicated that HP-compressor discharge and inlet pressures would be a logical choice for bearing supply and ambient pressures, respectively. However, both of these pressures, as well as the radial clearance of the bearing, would vary as a function of speed. Figure 100 shows the variation of P_s and P_a with speed as obtained from the aerodynamic analysis of Appendix I. Radial bearing clearance, including the effects of journal centrifugal growth, was expressed by the following equation:

$$C = C_1 - \frac{\rho \omega^2 R_o^3}{4Eg} \left[\left(\frac{R_1}{R_o} \right)^2 (3 + \nu) + 1 - \nu \right] \quad (13)$$

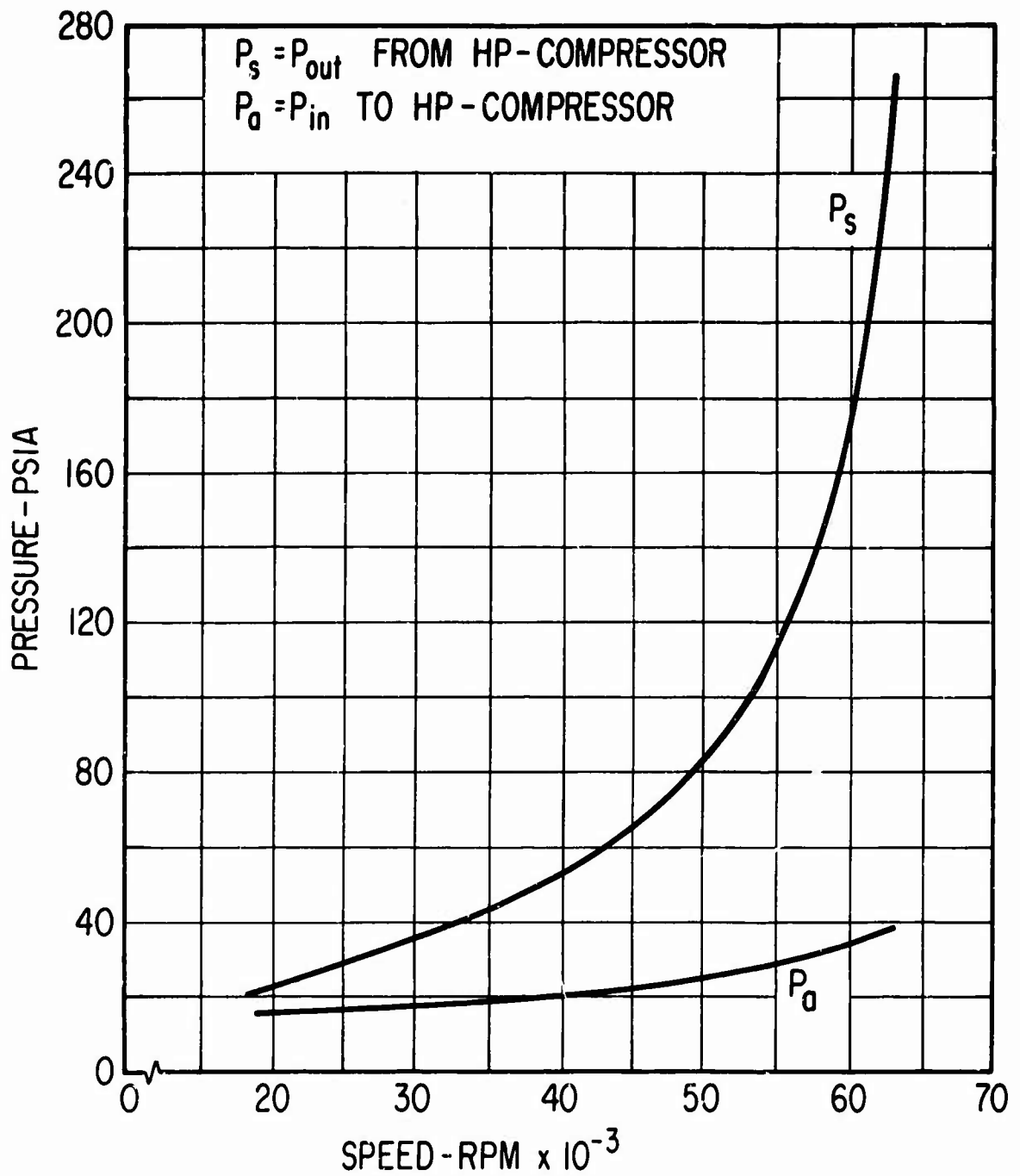


Figure 100. Inherently Available Supply and Ambient Pressures as a Function of Speed for the Externally Pressurized HP-Spool Turbine-End Journal Bearing.

where

C_1 = zero-speed radial clearance, in.

ρ = mass density of journal structural material, lb/in.³

ν = Poisson's ratio for the journal structural material
($\nu = 0.3$ in this study).

A value for C_1 as a function of journal diameter was established by specifying that the radial clearance at 70,000 rpm (i.e., at overspeed) should be 0.001 inch. By substituting the appropriate values for R_1/R_0 , E , ν , ρ , and g into Equation (13), the following expression for C as a function of shaft speed and journal diameter was obtained:

$$C = 0.001 + D^3 (1.88 \times 10^{-4} - 3.84N^2 \times 10^{-14}) \quad (14)$$

The above expression for C was then substituted into Equation (12), and Equation (12) was solved for the ratio of L/m .

$$\frac{L}{m} \geq \frac{3 \left[0.001 + D^3 (1.88 \times 10^{-4} - 3.84N^2 \times 10^{-14}) \right] N^2}{(357)^2 \Delta P D} \quad (15)$$

The minimum allowable ratio of bearing length to rotating mass supported by the bearing was then calculated as a function of bearing diameter (D) and speed (N), using Equation (15) and Figure 100. Figure 101 shows the results of this calculation. Also plotted on Figure 101, for comparative purposes, are data for constant bearing clearance; that is, neglecting the effect of journal centrifugal growth.

The results plotted on Figure 101 give considerable insight into the problem of designing externally pressurized bearings which will operate stably in the gas generator. Consider first the curves for a constant clearance bearing. The shape of the curves reflect the increase in compressor discharge pressure, and hence bearing ΔP , with increasing speed. Between 50,000 and 55,000 rpm, a significant change in slope is apparent due to the rapid increase in compressor discharge pressure at this point. It is clear that the smaller the L/m ratio, the larger is the rotating mass which can be stably carried on a bearing of fixed length. It is likewise clear from Figure 101 that the L/m ratio is inversely proportional to bearing diameter for constant clearance conditions. In other words, if the bearing clearance can be held constant, the bearing threshold speed increases with increasing diameter.

Now consider the data reflecting radial clearance changes with speed; that is, where journal centrifugal effects are included. In this case, the effect of bearing diameter on stability is exactly opposite to the results for a constant clearance bearing. It is seen from Figure 101 that the amount of rotating mass which can be stably supported by a bearing of fixed length will decrease with increasing bearing diameter (assuming that

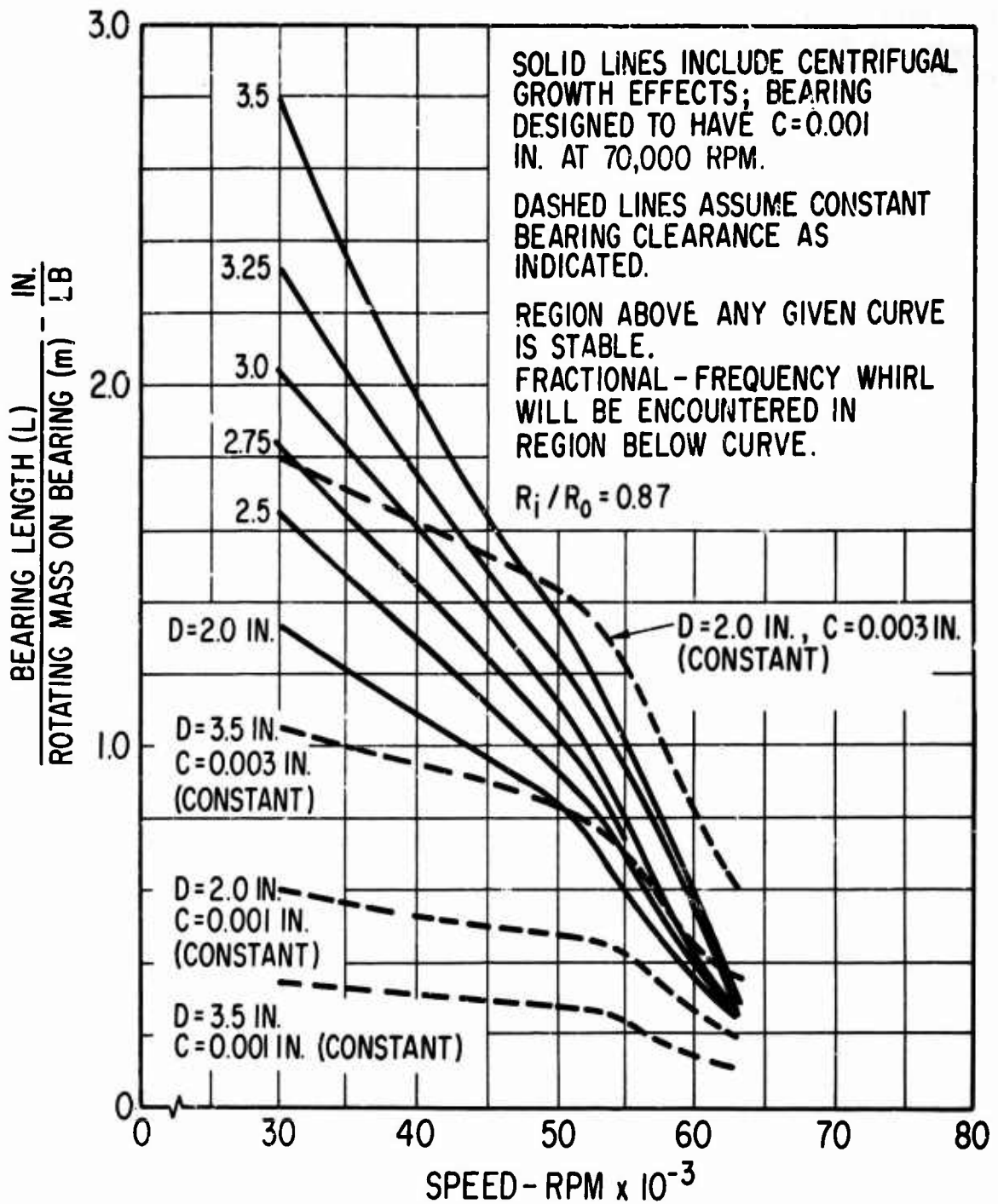


Figure 101. Stability Map for Externally Pressurized Full-Circular Journal Bearings, Based on Pressure Schedules of Figure 100, Showing Effect of Journal Size and Journal Centrifugal Growth.

the ratio of R_1/R_0 is held constant). In other words, the effect of centrifugal growth requires that bearing diameter be reduced if an increase in the stability threshold speed is required. However, static load capacity is reduced as bearing diameter is reduced. Thus, the requirements of static load capacity and stable operation are conflicting in the presence of centrifugal growth effects.

It is seen from Figure 101 that the differences in L/m ratio between the various curves are most pronounced at speeds below 50,000 rpm. At speeds above 50,000 rpm, the differences are considerably less since the rapid increase in bearing ΔP tends to minimize the effect of clearance changes.

With respect to the gas generator design, the initial layout, together with engineering judgement based on previous experience, established that the maximum bearing length should not exceed 6 inches. Two 6-inch bearings would necessitate a rotor length in excess of 12 inches. Minimum possible rotating mass per bearing under these conditions was estimated to be 6 pounds. Thus, the largest achievable value of L/m was established to be approximately 1.0. Figure 101 indicates that for an L/m ratio of 1.0, a 3-inch-diameter bearing would probably operate stably if bearing clearance could be maintained constant at approximately 0.002 inch. However, in the presence of centrifugal growth effects, the bearing diameter would have to be reduced to about 1.5 inches to achieve stability over the complete speed range. From a load capacity standpoint, a 3-inch-diameter by 6-inch-long bearing would easily be able to carry the maximum bearing loads. However, the load capacity for a 1.5-inch-diameter bearing would be marginal.

Conclusions of Initial Screening Study

As a result of the initial screening study, it was concluded that the externally pressurized bearing should be studied further in a more rigorous manner. However, it was recognized that stability would be a serious problem because of the centrifugal growth effects. Further, it was felt that the bearing length should be reduced as much below 6 inches as possible for various practical reasons, among these being manufacturing and thermal distortion problems. Accordingly, it was decided that the next phase of the design analysis should include studies of the following:

1. Reduction of the amount of bearing clearance change due to centrifugal growth either by reducing the bore diameter of the journal or by designing a "constant clearance" bearing; that is, a bearing which would automatically compensate for centrifugal growth.
2. Supplying the bearing with additional pressure beyond that available from the HP compressor at speeds below 55,000 rpm. This might be accomplished with a small auxiliary regenerative compressor built into the gas generator.

DETAILED STUDY OF EXTERNALLY PRESSURIZED JOURNAL BEARINGS

Additional survey-type calculations for the HP-spool turbine-end journal bearing were performed to determine reasonable means for implementing the conclusions reached during the initial screening study. These calculations established the following bearing parameters:

$$D = 3.0 \text{ in.}$$

$$L = 3.25 \text{ in.}$$

$$R_i/R_o = 0.433$$

In addition, it was established that a regenerative compressor having a pressure ratio of 1.8-to-1 would be feasible for additional pressurization of a small bleed flow from the HP-compressor discharge for bearing supply purposes. Finally, since it would be necessary to consider performance at both sea level and 25,000 feet altitude, temperatures and pressures of the bearing supply gas were determined for these two conditions. Figures 102 and 103 show pressures and temperatures, respectively, at sea level and 25,000 feet.

The nondimensional bearing feeding parameter for determination of bearing stiffness is designated Λ_s :

$$\Lambda_s = \frac{6\mu n a^2 \sqrt{RT}}{P_s C^3 \sqrt{1 + \delta^2}} \quad (16)$$

where

μ = viscosity of supply gas, lb-sec/in²

n = number of bearing feeder holes

a = feeder hole radius, in.

R = gas constant, in.²/sec²-°R

T = supply gas temperature, °R

$\delta = a/2C$

In order to minimize thermal gradients in the bearing film region, a double-plane admission bearing was selected. This means that instead of a single row of feeding holes located in the center-plane of the bearing, two rows of feeding holes were used, located in planes at the one-quarter and three-quarter length positions along the bearing. To avoid pneumatic hammer, feeding holes drilled directly through the bearing sleeve (referred to as inherently compensated orifices) were selected rather than pocket or groove-type feeders. Although the pocket design improves bearing

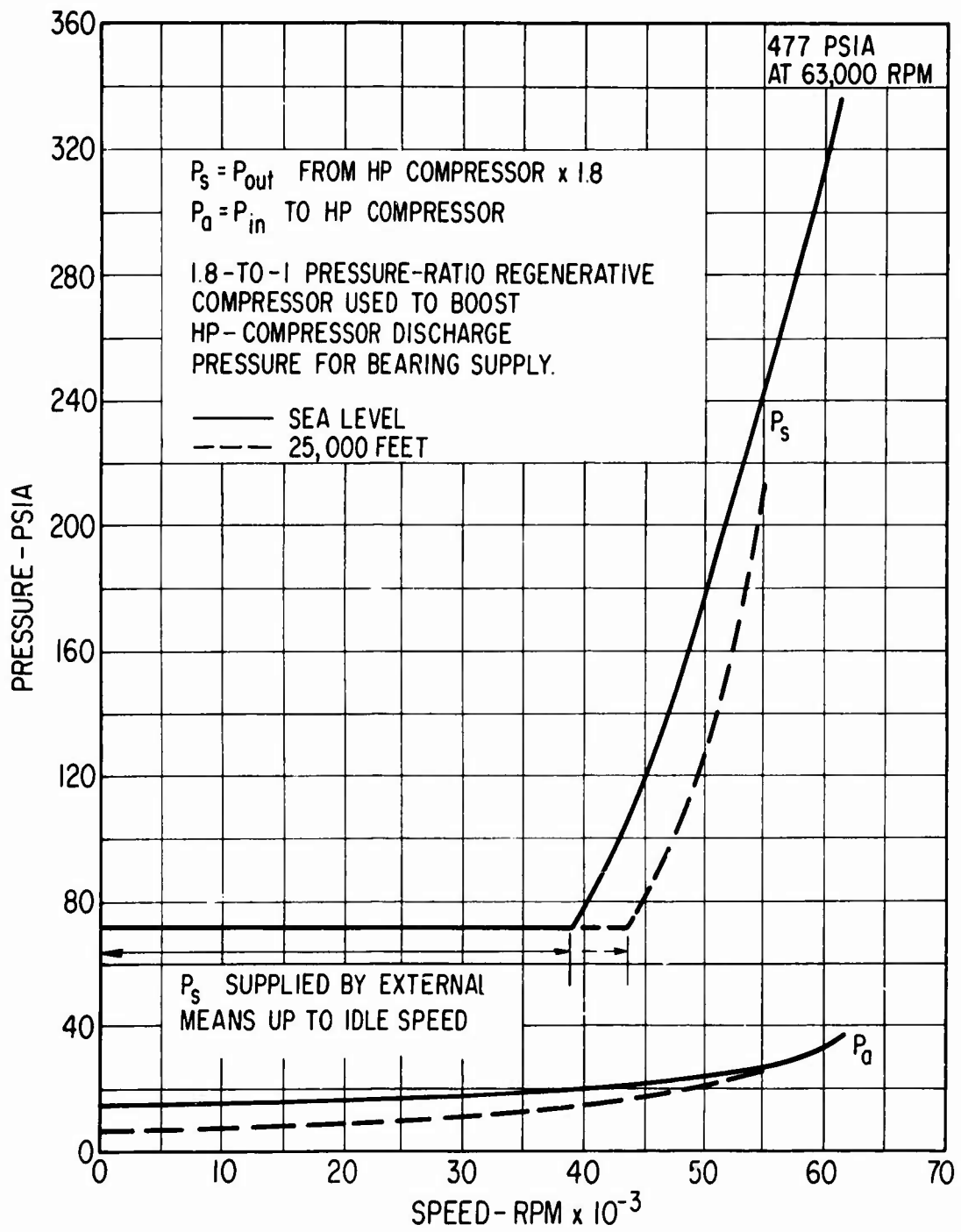


Figure 102. Supply Pressure (With Auxiliary Compressor Boost) and Ambient Pressure as a Function of Speed for the Externally Pressurized HP-Spool Turbine-End Journal Bearing.

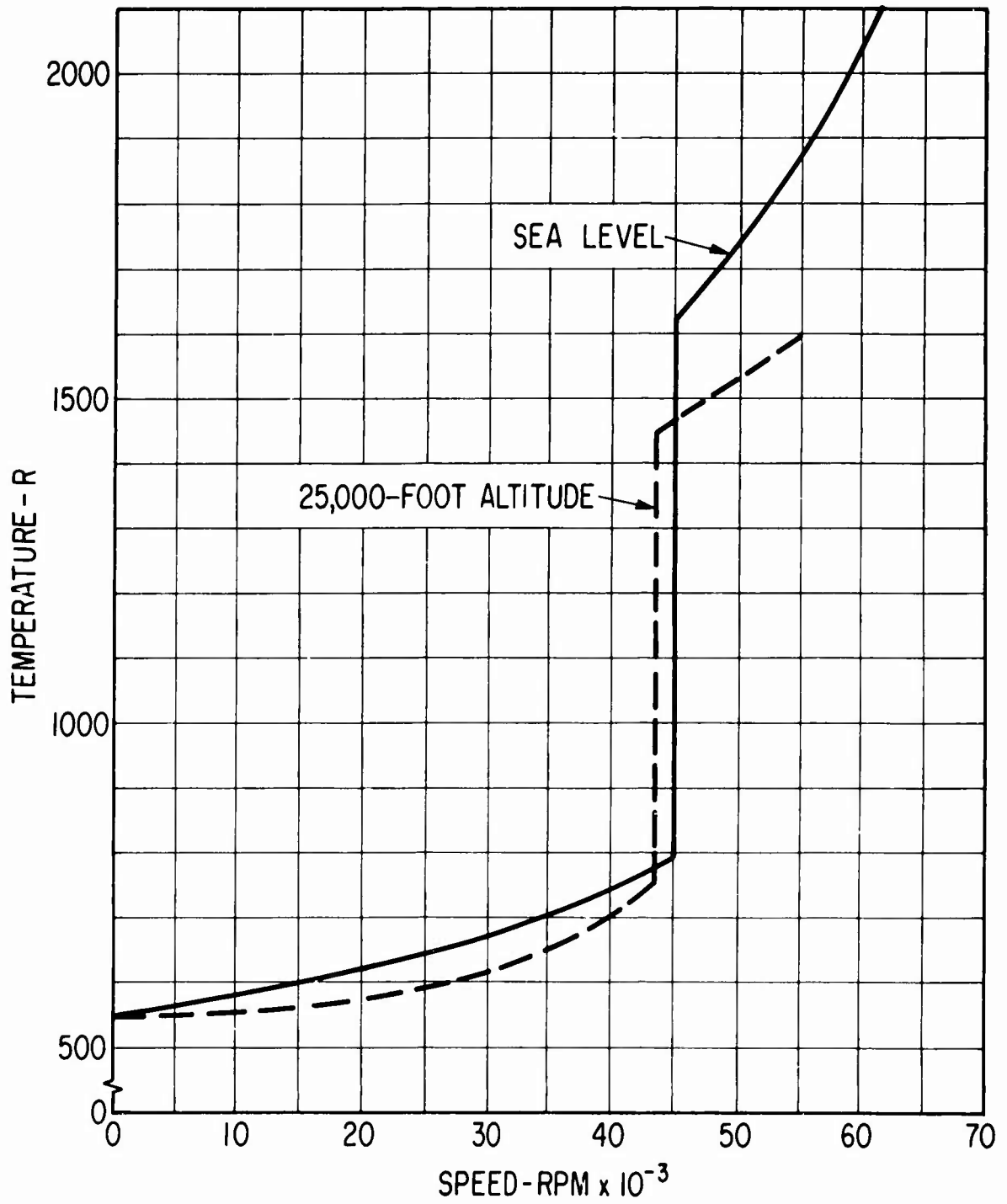


Figure 103. Temperature of Supply Gas as a Function of Speed for the Externally Pressurized HP-Spool Turbine-End Journal Bearing.

stiffness, the high bearing eccentricities anticipated under gyroscopic loading, together with the variations in clearance due to centrifugal growth, make it difficult to preclude pneumatic hammer from this design. The inherently compensated orifice design does not encounter this instability.

A constant bearing supply pressure of 72 psia was assumed to be available during startup. This pressure would be provided from a pressurized reservoir or an auxiliary compressor externally located from the gas generator. Subsequent to engine light-off and attainment of idle speed, the bearing supply air would be taken from the internally provided regenerative compressor. As will be seen shortly, the idle condition is the most severe from the standpoint of bearing stability. Above this speed, supply pressure increases and radial clearance decreases, both effects tending to improve bearing stability. The bearing design was consequently optimized for maximum stiffness at the most severe operating condition; namely, engine idle at a 25,000-foot altitude.

The first attempt at a bearing design was based upon noncompensation of the journal centrifugal growth. The known or chosen parameters of the design were as follows:

$$a = 0.012 \text{ in.}$$

$$E = 20 \times 10^6 \text{ psi}$$

$$n = 32$$

$$N = 43,400 \text{ rpm}$$

$$P_a = 18 \text{ psia}$$

$$P_s = 72 \text{ psia}$$

$$R = 2.47 \times 10^5 \text{ in.}^2/\text{sec}^2\text{-}^\circ\text{R}$$

$$T = 760^\circ\text{R}$$

$$\rho = 0.28 \text{ lb/in.}^3$$

$$\mu = 3.4 \times 10^{-9} \text{ lb-sec/in.}^2$$

The variation of bearing radial clearance was then calculated as a function of speed. Figure 104 shows the clearance schedule on the basis of a 1-mil minimum clearance at sea-level design speed. At HP-spool idle speed of 43,400 rpm (25,000-foot altitude), Figure 104 gives the minimum and maximum bearing clearances as 1.95 and 2.55 mils respectively. The value of bearing feeding parameter, Λ_s , was then calculated from Equation (16) and found to be 0.403. Once the feeding parameter was known, static bearing stiffness was determined from gas-bearing design charts similar to those given in Section 5 of Reference [24]. To correct the static

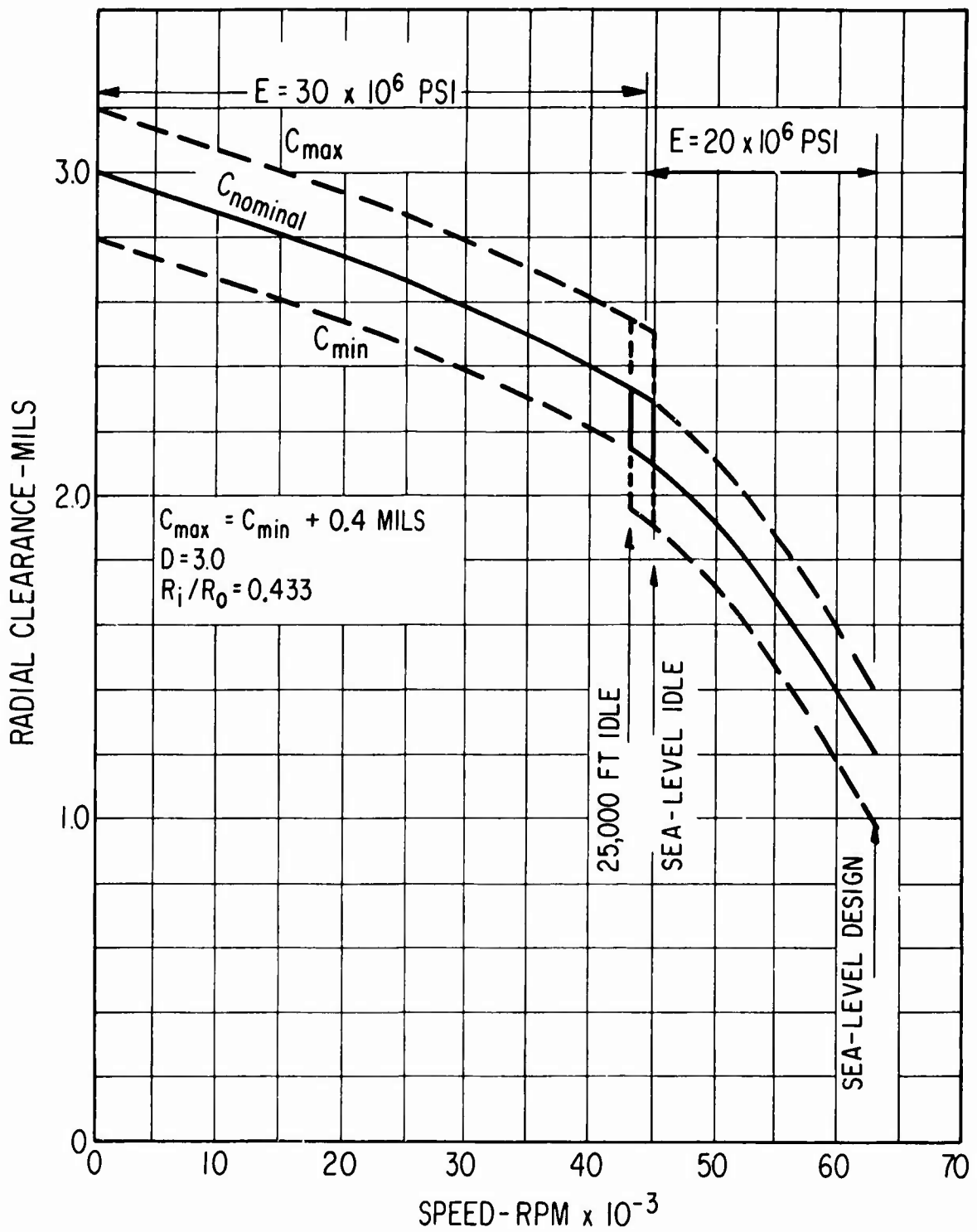


Figure 104. Variation in Radial Clearance as a Function of Speed for the Externally Pressurized HP-Spool Turbine-End Journal Bearing.

stiffness value for dynamic squeeze film effects, the dimensionless squeeze film number, σ , was computed as follows:

$$\sigma = \frac{12\mu\nu}{P_a} \left(\frac{R_o}{C} \right)^2 \quad (17)$$

where

ν = vibration frequency, rad/sec

With the squeeze film number determined, the correction factor for dynamic bearing stiffness was likewise determined from design charts given in Reference 24. The stability threshold was then calculated, using the dynamic stiffness, from Equation (8).

In addition to stability characteristics, the bearing load capacity was also determined. Both hydrostatic and hydrodynamic contributions to load capacity were included. The design parameter used to evaluate hybrid* bearing performance is the bearing compressibility number, Λ :

$$\Lambda = \frac{6\mu\omega}{P_a} \left(\frac{R_o}{C} \right)^2 \quad (18)$$

Once again, design charts given in Reference 24 were utilized to obtain values of hybrid load capacity.

Results of the Detailed Design Study

Using the procedures outlined above for determining bearing stability and load capacity, the characteristics of a hybrid bearing at a 25,000-foot altitude were calculated. The calculations were made, taking into account the effect of reasonable manufacturing tolerances on actual radial clearance. That is, maximum and minimum values of threshold speed and load capacity were calculated assuming that the actual radial clearance could vary ± 0.0002 inch from the nominal clearance schedule plotted in Figure 104. The results of the stability and load capacity calculations are shown in Figure 105. The stability data are plotted as a ratio of threshold speed to operating speed. A ratio of 1.0 or greater is required for stability. Load capacity is presented as the load which will produce a minimum film clearance of 0.0005 inch.

*A hybrid bearing is one in which both hydrostatic and hydrodynamic effects contribute to overall bearing performance.

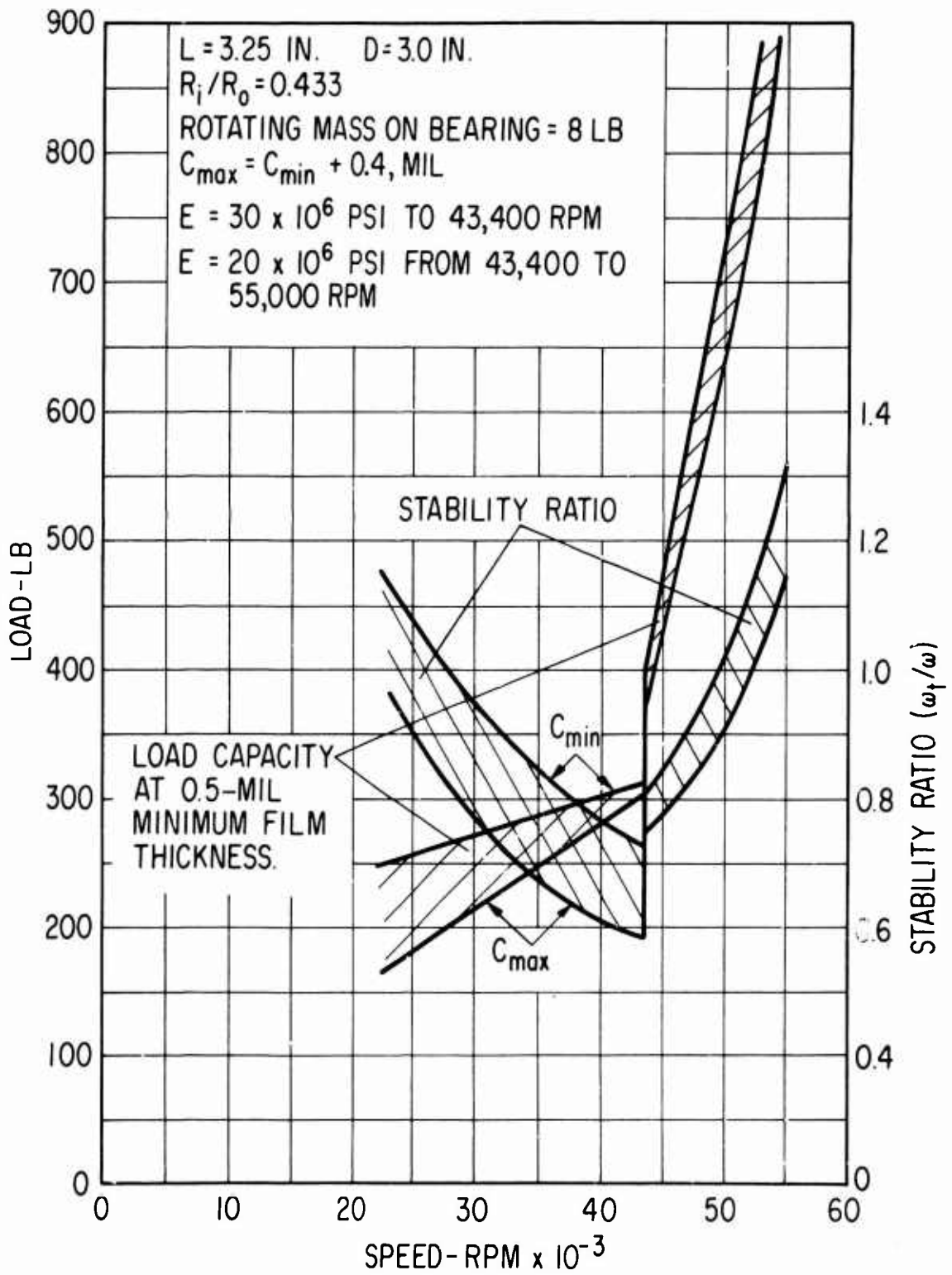


Figure 105. Stability Map and Load Capacity for the Refined Design of the Externally Pressurized HP-Spool Turbine-End Journal Bearing.

Before discussing the implications of Figure 105, additional explanation of the stability ratio data is in order. Calculation of the instability threshold speed from Equation (8) is valid if the first critical speed of the rotor-bearing system can truly be closely predicted by Equation (5). In essence, Equation (5) is the natural frequency equation for a symmetrical rigid beam having mass $2m$, symmetrically mounted on two identical springs, each spring having stiffness K . The natural frequency given by Equation (5) is thus called the translatory critical speed of a rigid rotor.

However, there is another vibrational degree of freedom for the symmetrical beam system defined above. This is the rotational, or angular, degree of freedom about a transverse axis passing through the center of mass of the beam. In the parlance of rotor dynamics, the natural frequency of the beam in the rotational mode is called the conical critical speed. The ratio of the conical critical speed to the translatory critical speed can be calculated from the following equation:

$$\frac{\omega_{nc}}{\omega_{nt}} = \sqrt{\frac{M \ell^2}{4(I_t - 2I_p)}} \quad (19)$$

where

ω_{nc} = conical mode critical speed, rad/sec

ω_{nt} = translatory mode critical speed, rad/sec

M = total mass of the shaft, lb

ℓ = bearing span, in.

I_t = transverse mass moment of inertia of the shaft about its cg, lb-in.²

I_p = polar mass moment of inertia of the shaft, lb-in.²

From the initial layout of the gas generator it was determined that

M = 16 lb

ℓ = 7 in.

I_t = 431 lb-in.²

I_p = 16.5 lb-in.²

Using these values in Equation (19) gave

$$\frac{\omega_{nc}}{\omega_{nt}} = 0.704$$

In other words, for the initial layout of the HP spool, the conical rigid-body critical speed would be approximately 30 percent lower than the translatory critical. (This result was subsequently confirmed by the rigorous critical speed results plotted in Figures 46 and 47.) Since the criterion for achieving whirl-free operation requires that rotor speed never be greater than 1.9 times the first critical speed of the rotor-bearing system, and since the conical critical speed would be the first critical, the final calculation of threshold speed was obtained by multiplying the values obtained from Equation (8) by the factor 0.704. These corrected values of threshold speed were used to obtain the stability ratio data plotted on Figure 105.

If the load capacity data of Figure 105 is compared to the maximum resultant loads which could be imposed on the bearing (Figure 13), it is seen that the 3-inch-diameter by 3.25-inch-long bearing (with additional pressure boost) can easily carry the specified loads. From a stability standpoint, however, Figure 105 shows that the bearing design does not satisfy the fractional-frequency-whirl criterion in the speed range of 22,000 to 52,000 rpm. In other words, the HP spool would be unstable (in fact, could not run) over most of the required operating range of the gas generator.

It is seen from Figure 105 that the lowest value of the stability ratio occurs at idle speed (43,400 rpm). It was decided to determine what minimum value of bearing stiffness would be required to raise the stability ratio to a value of 1.0 at this speed. Accordingly, Equation (8) was rearranged to solve for K. (The 0.704 factor was also properly inserted to account for the fact that the first critical speed was a conical, rather than a translatory, critical.) The resulting values of minimum bearing stiffness are tabulated below for several values of bearing rotating mass.

<u>Rotating bearing mass (lb)</u>	<u>Bearing stiffness required for stability at 43,400 rpm (lb/in.)</u>
10	293,000
9	278,000
8	262,000

The achievable stiffness from a 3-inch-diameter by 3.25-inch-long bearing at 25,000-foot-altitude engine-idle conditions was then computed as a function of bearing clearance. The results of this calculation, which included squeeze film effects, are shown on Figure 106. To achieve the stiffness values required for stability, it is apparent from Figure 106 that the radial clearance must be maintained between 0.7 and 0.8 mil for a 10-pound rotating mass per bearing. If the mass per bearing drops to 8 pounds, the radial clearance may be increased to 1.0 mil.

From 45,000 to 63,000 rpm, Figure 104 shows that the change in radial clearance due to centrifugal growth would be 0.9 mil. Therefore, it

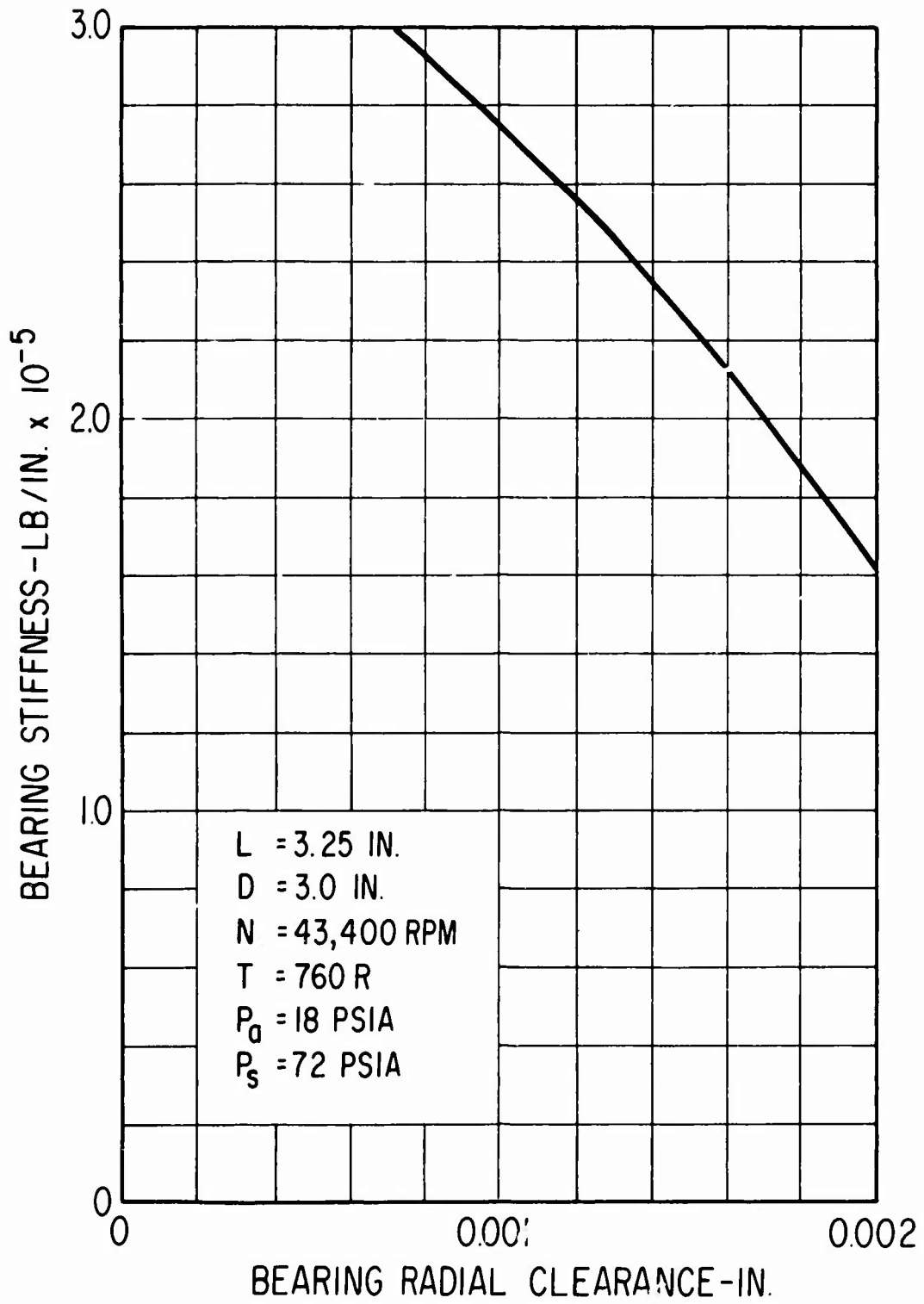


Figure 106. Achievable Bearing Radial Stiffness (Including Squeeze Film Effects) as a Function of Bearing Radial Clearance.

is evident that a radial clearance of 0.8 to 1.0 mil at 43,000 rpm would not be possible unless the bearing could be designed to automatically compensate for the centrifugal growth; that is, unless some means could be provided to achieve a more-or-less constant clearance bearing. In addition to centrifugal growth, thermal distortions and differential expansions will also induce variations in effective bearing clearance. The problem of achieving accurate control of the small bearing clearances which are required for stability becomes a very serious and difficult design problem, considering the wide range of speeds and temperatures over which the HP spool must operate.

It is possible to increase the allowable clearance range by considering a bearing having orifice compensated (i.e., pocket) feeding hole geometry. A 143-percent increase in stiffness is possible with this type of feeding. The minimum allowable radial clearance could thus be increased to 1.65 mils. Although this clearance approaches a reasonable design, it is necessary to review the pneumatic hammer stability question to determine feasibility. This was done using the stability charts given in Reference 24. The bearing feeding parameter (Λ_s) varies approximately 3-to-1 over the full operating range. The bearing pressure ratio varies from 4-to-1 to 12-to-1 over the same operating range. A dimensionless volume ratio of 0.1 or less at all conditions indicated that the values of Λ_s for hammer-free operation would range from 0.95 to 2.85. At the higher values of Λ_s , however, a 25-percent reduction in bearing stiffness would occur. Thus a reduced radial clearance would be required to ensure freedom from fractional-frequency whirl. The net result is that no significant improvement in bearing design can be realized by using an orifice compensated, rather than an inherently compensated, bearing unless some means of alleviating the pneumatic hammer problem is found.

Finally, all of the above described analyses for threshold of fractional-frequency whirl were performed assuming rigidly supported bearings. It has been shown [50] that support flexibility, in the absence of sufficient damping, will always tend to reduce the threshold speed. For various reasons, the bearing supports in the gas generator must have flexibility, and it is not unlikely that the stiffness of the supports will be of the same order as, or less than, the stiffness of the bearings. Consequently, the stability ratio results plotted in Figure 105 are considered to be optimistic.

CONCLUSIONS

Detailed analysis of an externally pressurized bearing for the HP-spool turbine-end journal resulted in the following conclusions.

1. Direct pressurization of the bearing from HP-compressor discharge (assuming a bearing of reasonable size) would not be feasible due to a lack of sufficient bearing stiffness for stable operation. In addition, load capacity of the bearing would be marginal at a 25,000-foot altitude.

2. An additional 1.8-to-1 pressure boost for the bearing supply gas would be feasible using a small regenerative compressor. The regenerative compressor could be incorporated as an integral part of the HP-spool assembly. The additional pressure boost would provide more than enough bearing load capacity.
3. However, even with a 1.8-to-1 pressure boost, fractional-frequency whirl would still be encountered throughout most of the gas generator operating range unless bearing radial clearance could be held to approximately 0.001 inch or less. A problem arises in satisfying this clearance requirement because of radial centrifugal growth of the journal which, from idle to maximum design speed, would amount to 0.0009 inch. Absolute radial clearance for stable operation would thus vary from a reasonable 0.001 inch at idle to an impractical 0.0001 inch at maximum speed, unless some means for automatic compensation of centrifugal growth was provided by the bearing design. In other words, a more-or-less constant clearance bearing design could be a solution to the stability problem. Although there appear to be several ways by which such a bearing might be achieved, considerable design and development effort would be required to prove feasibility and, more importantly, reliability.
4. The effects of thermal distortions and differential expansions between the journal and sleeve would also compound the problem of maintaining the necessarily small clearances needed for stability.
5. The effect of bearing support flexibility would also lower the threshold speed for fractional-frequency whirl. This effect was neglected in the threshold analysis, thus making the stability problem even more severe than it already appears. It is theoretically true that the addition of damping to a bearing support system can raise threshold speed. However, considerable development effort would be required to develop a suitable damper (it would have to operate at temperatures up to 1500° or 1600° F), assuming, of course, that sufficient increase in threshold speed could be achieved via the damping route.
6. In light of the above summarized stability problem, it was concluded that the externally pressurized bearing was not well suited for the HP-spool turbine-end journal. Rather than proceed with the untried, and hence unproven, concept of a constant clearance bearing, it was decided that self-acting types of bearings should be reviewed first.

The above conclusions for the HP-spool turbine-end journal bearing apply equally as well to the compressor-end bearing. The only significant difference between the two bearings is that the temperature of the compressor bearing may be somewhat lower. This difference would not alter the above conclusions.

With respect to the LP spool, externally pressurized bearings again cannot be used because of stability problems. In this case, shaft flexibility, rather than centrifugal growth, is the main problem. Reference to the LP-spool critical speed plot of Figure 48 shows that as bearing stiffness becomes infinitely large, the first critical speed approaches an asymptotic value of 22,000 rpm. (This asymptotic value is the first flexural natural frequency of the LP spool taken as a simply supported shaft.) Consequently, regardless of the value of bearing stiffness, it would be impossible to raise the whirl threshold speed above 44,000 rpm. Since maximum speed of the LP spool is well above 44,000 rpm, it is clear that externally pressurized journal bearings would be unsuitable for this spool.

APPENDIX IV
ANALYSIS OF THE HERRINGBONE-GROOVED JOURNAL BEARING

To begin a design study of the herringbone-grooved journal bearing, it is first necessary to select the bearing member on which the herringbone pattern is to be applied, and then the type of pattern. For this analysis, the rotating journal was selected to be the patterned member from considerations of both maximum stability and ease of fabrication. A full, rather than partial, herringbone pattern was selected, again for reasons of maximum stability.

Stability maps for the herringbone-grooved bearing are given in Reference 24. The maps are plots of bearing compressibility number (Λ) versus mass parameter (\bar{v}_o). These parameters are defined as follows:

$$\Lambda = \frac{6\mu\omega}{P_a} \left(\frac{R}{C} \right)^2 \quad (20)$$

$$\bar{v}_o = \frac{g m_c \left(\frac{C}{R} \right)^5}{LD} \left(\frac{RP_a}{\mu^2} \right) \quad (21)$$

where

μ = viscosity of gas, lb-sec/in.²

ω = rotor speed, rad/sec

R = journal radius, in.

C = bearing radial clearance, in.

P_a = bearing ambient pressure, psia

m_c = critical bearing mass, lb

L = bearing length, in.

D = bearing diameter, in.

g = gravitational constant = 386 lb_m-in./lb_f-sec²

Values of Λ were calculated for the HP spool at a 25,000-foot altitude, based on a 3-inch-diameter by 3.25-inch-long bearing. Three values of bearing clearance were used: 0.001, 0.002, and 0.003 inch. A range of Λ values corresponding to the operating speed range of the HP spool was obtained for each clearance value. The stability map was then entered with the minimum and maximum values of Λ for each clearance condition, and the corresponding values of \bar{v}_o were picked off. Equation (21) was then solved

for m_c , the critical bearing mass. To achieve stable operation, actual bearing mass must not exceed m_c .

The results of this analysis were as follows:

	C = 0.001		C = 0.002		C = 0.003	
Λ	3.67	8.15	0.917	2.04	0.408	0.905
\bar{v}_o	6.00	5.40	18.500	9.00	40.000	18.500
$m_c - lb$	30.50	72.40	2.940	3.77	0.830	1.020

A very rapid reduction in critical bearing mass is seen to occur as clearance increases from 0.001 to 0.002 inch. This is the result of critical mass being a function of the fifth power of radial clearance. Since the HP spool would have a bearing mass of 8 to 10 pounds, it was clear that close control of radial clearance would be required. At idle speed, radial clearance would have to be less than 0.0015 inch, while at maximum speed a clearance of 0.0017 inch would be the limiting value for stability.

For the most optimistic design concept of the HP-spool journals, radial centrifugal growth would be 0.0009 inch from idle to maximum speed. Accordingly, radial assembly clearance of the bearing would have to be 0.0008 inch, a tight, but not unreasonable, manufacturing requirement. However, more realistic concepts of the HP-spool journals (e.g., as represented by the Phase VI gas-generator layout) would have radial centrifugal growths of 0.002 to 0.003 inch over the operating speed range. Under these conditions, stable design of a herringbone-grooved journal would be impossible unless, by some means, the bearing sleeve could be designed to compensate for changes in journal diameter, such as to maintain a more-or-less constant clearance condition.

Based upon experimental evaluations of the herringbone-grooved bearing, it appeared that the maximum gas-generator bearing loads could be carried at an eccentricity ratio of approximately 0.6. However, because of the stability problem, and the lack of any developed or obviously simple way to achieve a "constant clearance bearing", the herringbone bearing approach was judged to be in the same category as the externally pressurized bearing — perhaps it would be feasible with development, but only to be considered for this study if a better-suited bearing is not available.

APPENDIX V
AUXILIARY COMPRESSOR FOR THRUST BEARING PRESSURIZATION

As discussed in the "Thrust Bearing Design Studies" chapter, additional pressurization of thrust bearing supply air, above that which is available from the HP compressor, is required to support the maximum thrust loads. The additional pressure boost must be provided by a highly reliable auxiliary compressor. Ideally, the auxiliary compressor should be an integral part of the gas generator. A survey of various rotating compressor types was made. The regenerative compressor was identified as having the best potential for meeting both performance and reliability requirements. It appeared that pressure-rise and flow conditions could be met with a single-stage single-sided unit. Accordingly, a brief design study was made to confirm the feasibility of this type of compressor.

DESCRIPTION OF THE REGENERATIVE COMPRESSOR

Before proceeding to a discussion of performance characteristics for the gas-generator application, a brief history and description of the regenerative compressor may be of interest to the reader. The regenerative pump has been used for many years to pump liquids for special applications. Patent literature goes back as far as 1888. The pump has been given many other names, among these being turbine, traction, tangential, drag, vortex, and peripheral pump. Although the gross flow direction is peripheral, we at MTI believe that "regenerative" best describes the compression process.

The regenerative compressor has an impeller with basically radial blades extending inward from the tip a distance of about 50 percent of the radius. Axially disposed from the blades is a stationary annular passage. In communication with the annular passage are an inlet and an outlet. The inlet and outlet are separated by a dam, which blocks the annular passage and has a close side clearance with the impeller. The gross flow direction is peripheral, from the inlet to the outlet, in the direction of impeller rotation. The compressor can be considered, in effect, a multistage centrifugal because the flow in the channel enters the blading passages at the inner diameter and, due to centrifugal action, flows out at the tip at a higher tangential velocity. The exiting flow imparts momentum to the gas in the stationary channel, which is travelling at an average velocity less than that of the impeller. The gas then flows radially inward and reenters the impeller at the inner diameter. The pressure buildup around the periphery between the inlet and the outlet is sustained by the momentum exchange. The above description of regenerative operation is simplified, but it explains why it is possible to obtain head rise coefficients greater than U^2/g . Figure 107 shows a typical impeller configuration for a regenerative compressor.

Compared to the centrifugal compressor, the regenerative is characterized by a much higher rise coefficient, a lower flow, and a lower peak efficiency. For many low flow applications where rotational speed is limited, the regenerative compressor can be as efficient as a multistage centrifugal.

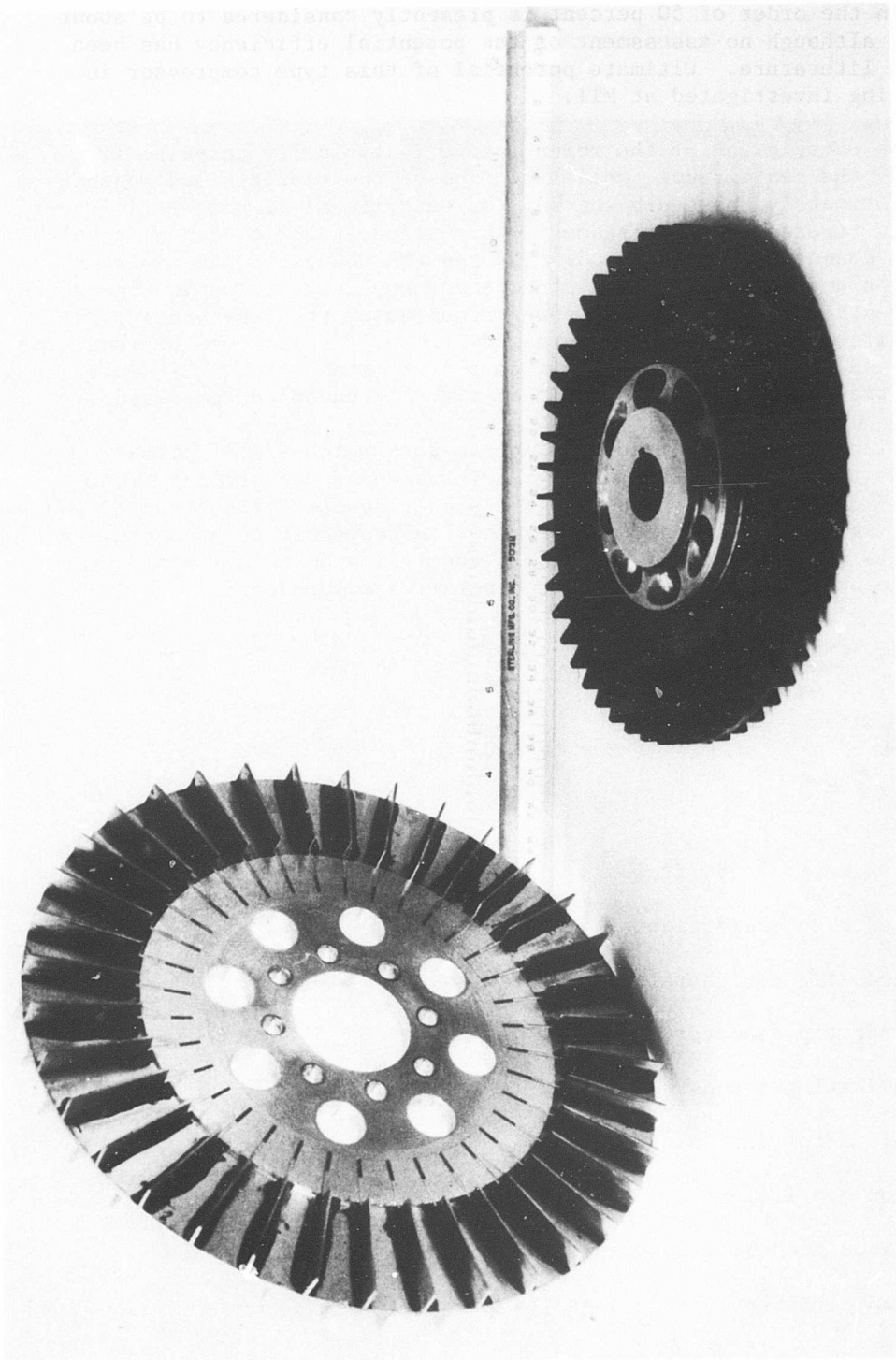


Figure 107. Typical Impeller Configurations for a Regenerative Compressor.

Efficiency in the order of 50 percent is presently considered to be about the maximum, although no assessment of the potential efficiency has been found in the literature. Ultimate potential of this type compressor is presently being investigated at MTI.

The head rise coefficient of the regenerative is typically three to five times that of the centrifugal, while the flow of the single-sided regenerative is approximately one-tenth that of the centrifugal at peak efficiency. By making the regenerative compressor double-sided, the flow can be doubled for the same channel size and speed. The general shapes of the important performance parameters versus flow at constant speed are shown in Figure 108. Unlike the centrifugal compressor, power required by the regenerative decreases significantly as flow is increased. Also, the flow can be completely shut off and pressure sustained — completely stall-free. Of course, temperature rise at zero flow is high, as with all uncooled compressors.

Figure 109 illustrates the dimensional parameters which are of primary importance to compressor performance. Performance of the regenerative compressor is usually shown in terms of a head rise coefficient and a flow coefficient, in the same manner as for other turbodynamic-type compressors, such as axials and centrifugals. At MTI, the following relationships are used to calculate performance of the regenerative compressor:

$$H = \frac{\psi U_t^2}{2g} \quad (22)$$

$$Q = 60\phi A_s U \quad (23)$$

where

H = isentropic head, ft-lb/lb

ψ = head rise coefficient

U_t = blade-tip peripheral speed (at diameter D), ft/sec

D = blade tip diameter, ft

g = gravitational constant = 32.2 ft/sec²

Q = inlet flow, ft³/min

ϕ = flow coefficient

A_s = stator channel flow area, ft²

U = mean peripheral blade speed (at diameter $D-d$), ft/sec

d = blade height, ft

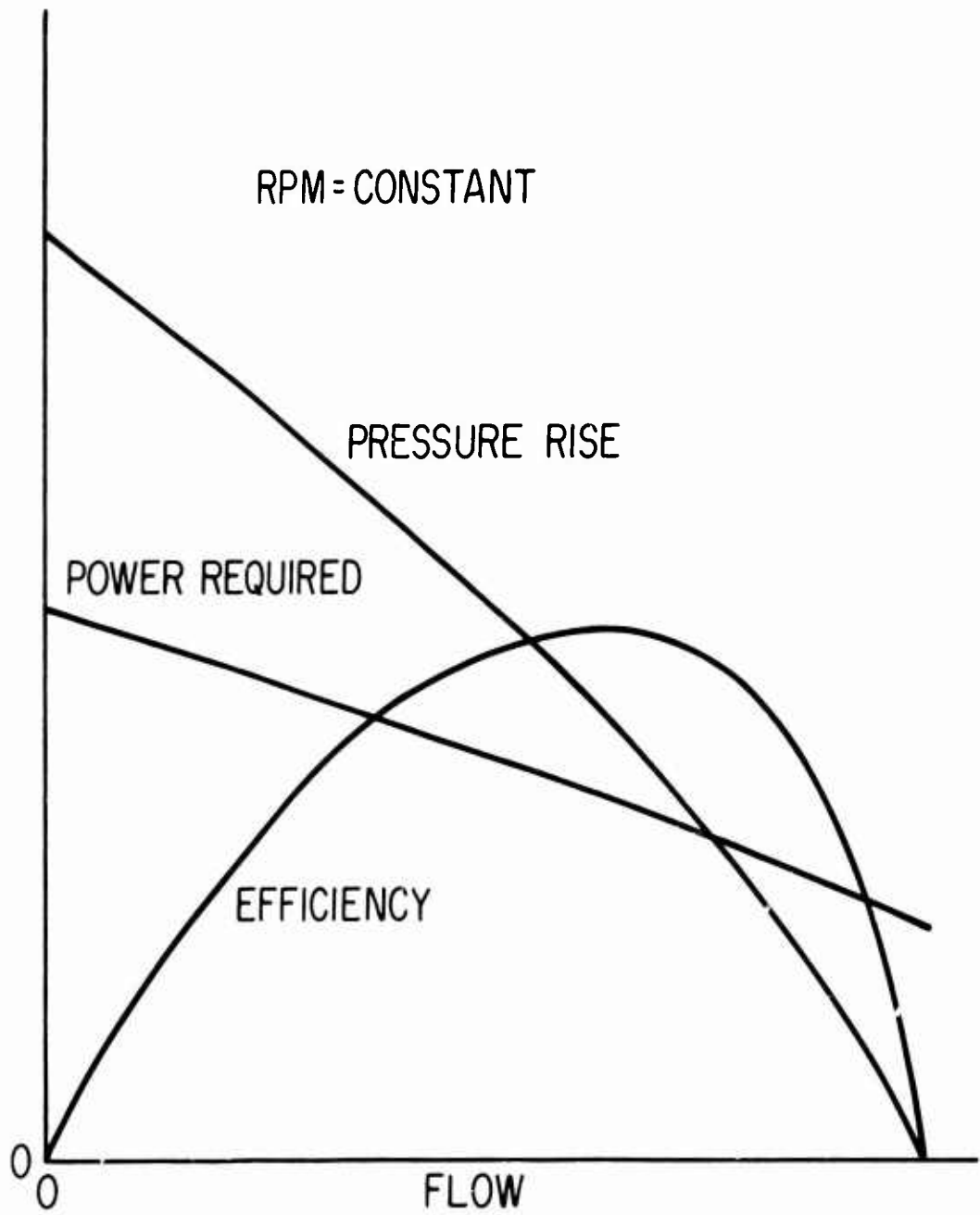


Figure 108. Performance Characteristics of a Typical Regenerative Compressor at Constant Speed.

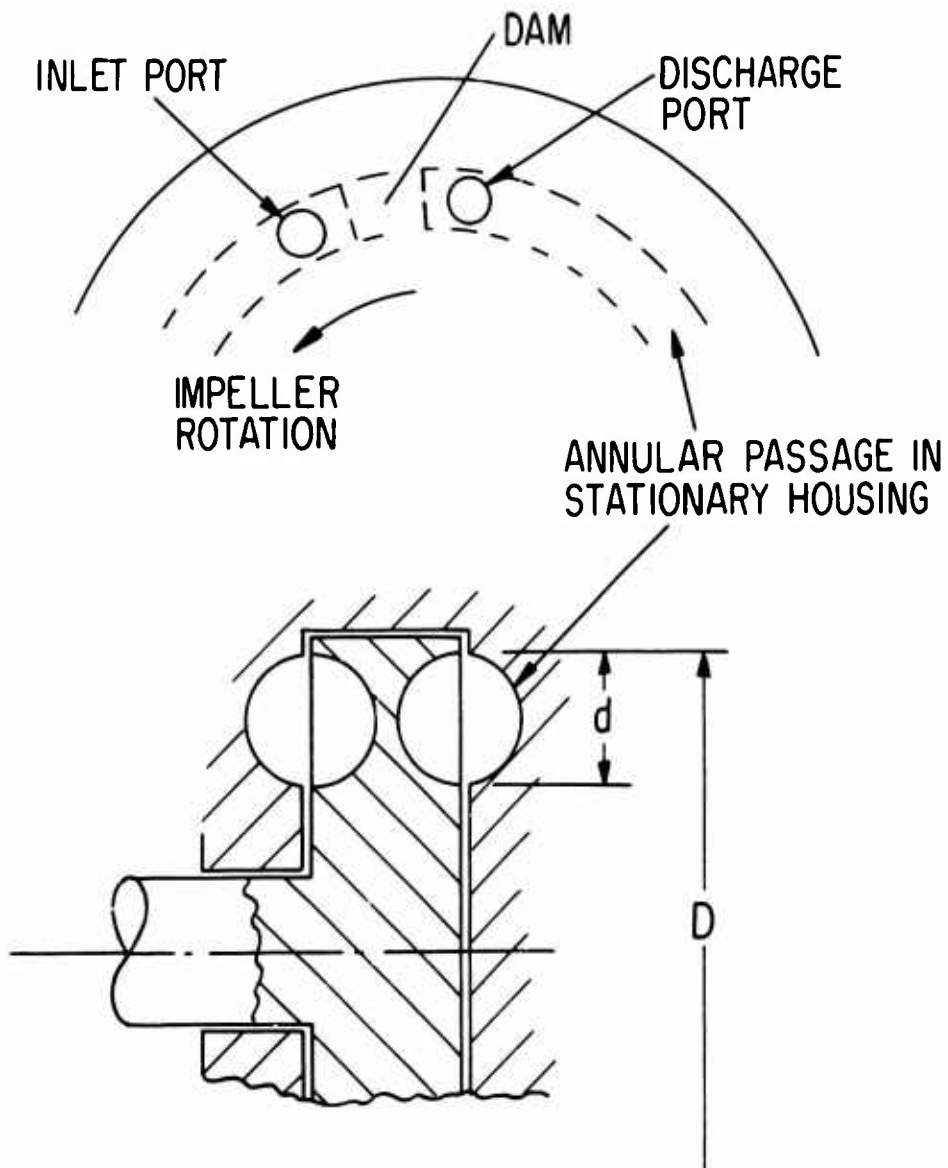


Figure 109. Important Dimensional Parameters of the Regenerative Compressor.

GAS-GENERATOR APPLICATION

Figure 110 shows plots of efficiency and head rise coefficient versus flow coefficient for a regenerative compressor developed by MTI. The compressor proposed for the gas generator would have characteristics similar to those of Figure 110.

Total flow for both the HP-spool and the LP-spool thrust bearings must be supplied by the regenerative compressor. The total flow requirements, including an allowance for leakage, are as follows:

<u>Flight Condition</u>	<u>Total Flow lb/sec</u>	<u>Density lb/ft³</u>	<u>Total Flow ft³/sec</u>
Sea level, rated power	0.09	0.27	0.34
25,000 feet, rated power	0.09	0.25	0.36
Sea level, idle speed	0.025	0.11	0.23
25,000 feet, idle speed	0.015	0.07	0.22

The compressor was assumed to be mounted on the HP spool to take advantage of the higher speeds and to obtain the required output head. Wheel geometry chosen for the initial performance study was as follows:

$$D = 0.3 \text{ ft}$$

$$d = 0.0392 \text{ ft}$$

$$A_s = 5.9 \times 10^{-4} \text{ ft}^2$$

Using the data of Figure 110, compressor performance was calculated for the four flow conditions listed above. Results of these calculations are given in Table XIX.

The required pressure boost for satisfactory thrust bearing operation varies from 1.7 at engine idle to 1.5 at rated power. Table XIX shows that these pressure ratios can be readily achieved, with additional margin for various feed-line pressure drops. In fact, at sea-level rated-power conditions, the pressure rise is too high, as is also the compressor temperature rise. Based on test experience, a 400°F temperature rise can be handled without difficulty. As temperature rise begins to exceed 400°F, the compressor design becomes more sophisticated as regards means to minimize thermal distortion of the stator. However, in this case the temperature-rise problem can be solved quite nicely. Head coefficient for a regenerative compressor can be reduced by increasing compressor flow, which in turn reduces

*The total flow for the HP- and LP-spool thrust bearings is actually obtained as a bleed flow from the discharge of the HP-spool compressor. The regenerator compressor acts only to increase pressure of this flow.

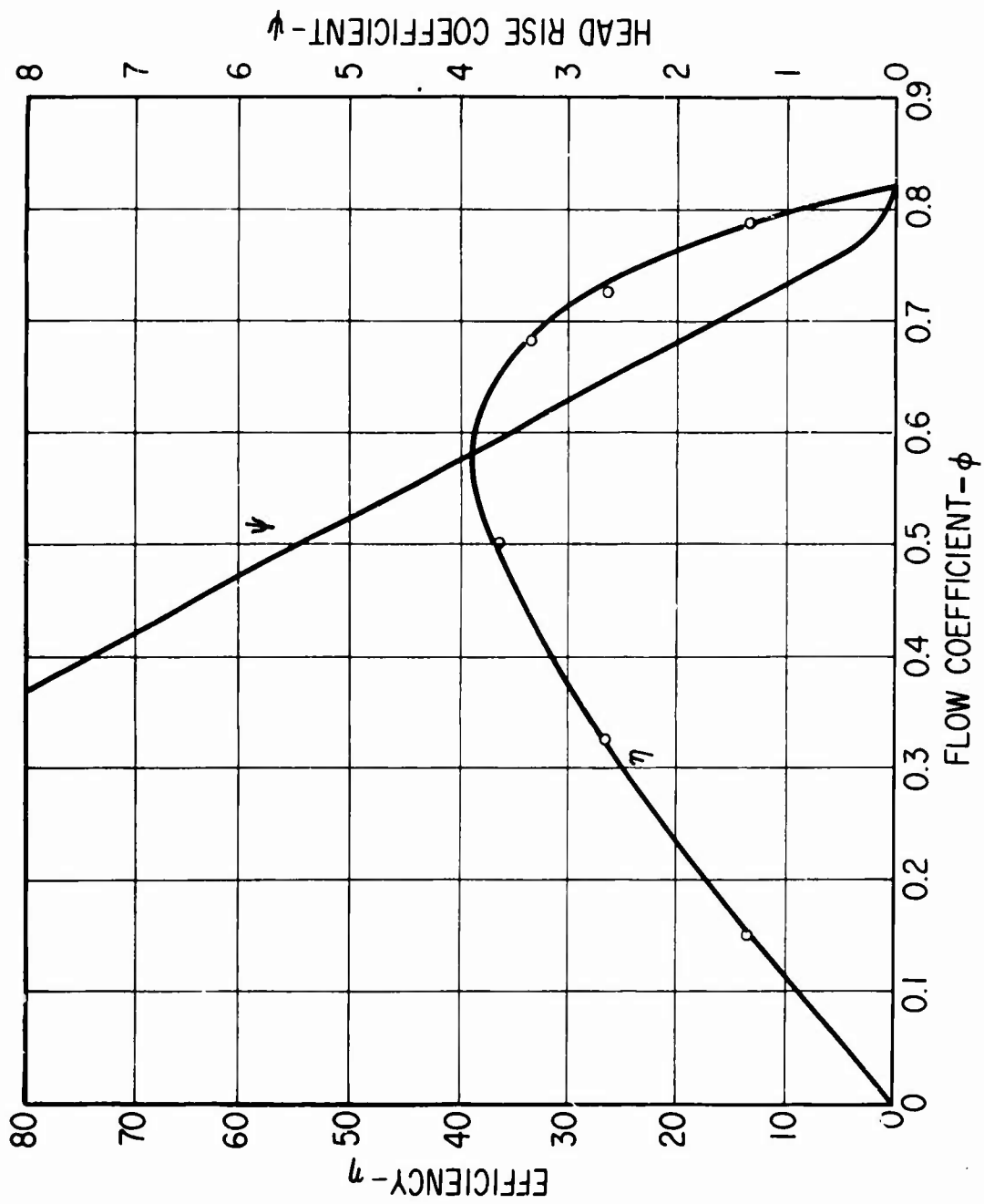


Figure 110. Efficiency and Head-Rise Coefficient for a Regenerative Compressor Developed by MTI (these characteristics are similar to those which would be required for the gas-generator application).

TABLE XIX. PERFORMANCE CHARACTERISTICS OF A PRELIMINARY
REGENERATIVE COMPRESSOR DESIGN

Flight Condition	Speed (rpm)	\bar{U} (ft/sec)	Q (ft ³ /sec)	ϕ	ψ	η (%)	H (ft)	$\frac{P_{out}^*}{P_{in}}$	ΔT (°F)
<u>Sea level</u>									
Rated power	70,000	960	0.34	0.60	3.5	39	66,000	2.24	920
Idle	49,000	675	0.23	0.58	3.9	39	36,000	1.94	492
<u>25,000 feet</u>									
Rated power		890	0.36	0.68	2.0	34	32,400	1.65	510
Idle	45,000	632	0.22	0.59	3.7	39	30,000	1.97	410

$$\frac{P_{out}^*}{P_{in}} = \left[\frac{H \left(\frac{\gamma-1}{\gamma} \right)}{RT} + 1 \right]^{\frac{\gamma}{\gamma-1}}$$

$$\Delta T = \frac{T_{in} H \left(\frac{\gamma-1}{\gamma} \right)}{\eta RT}$$

compressor power requirements and temperature rise. Flow can be increased by utilizing a pressure relief valve to limit low-altitude rated-power pressure boost factor to 1.7 or so. The relief valve would operate on differential pressure and hence could be set to function only at rated or near-rated power conditions at low altitudes.

This brief analysis indicates that the regenerative compressor is a feasible means of obtaining the required pressure boost for satisfactory thrust bearing operation. Design of the compressor should be optimized for best efficiency and best matching of flow and pressure-rise requirements to HP-spool operating speeds and pressures. Design emphasis should be placed on minimizing compressor temperature rise.

APPENDIX VI
SUMMARY OF DESIGN LAYOUTS PREPARED DURING THE FEASIBILITY STUDY

Numerous design sketches and layout drawings were prepared in the course of performing the herein reported feasibility study. For obvious reasons, the bulk of this report deals with the Phase VI gas-generator concept and layout.

This appendix briefly documents the other rotor-bearing systems and component arrangements which were considered during the study.

Table XX gives a summary of the most significant design sketches, with a brief description of the salient features of each concept and pertinent remarks about the concept.

TABLE XX. SUMMARY OF DESIGN SKETCHES FOR THE GAS-GENERATOR ROTOR-BEARING SYSTEM

Sketch No.	Name	Description	Remarks
SK-D-2738	1st configuration of rotor-bearing system for the gas generator	Closed-coupled HP-spool compressor and turbine are mounted between journal bearings. HP and LP spools are independently supported from engine casing via externally pressurized journal bearings. LP shaft runs through bore of HP shaft.	Function of drawing was to provide a basis for initial calculation of journal bearing loads and an initial assessment of rotor dynamics situation.
SK-D-2740	2nd configuration of rotor-bearing system	Similar to 1st configuration except that the LP spool is supported from the HP spool via self-acting journal bearings. The HP spool is supported from the engine casing via externally pressurized journal bearings.	This configuration imposes excessively high loads on the HP-spool bearings and is judged to be infeasible.
SK-D-2856	1st study of alternate arrangements of the aerodynamic components	Aerodynamic components all mounted on a single shaft; types of aerodynamic components and flow path arrangement are basically the same as above.	Qualitative assessment of this arrangement indicated that heat transfer, bearing design, and rotor dynamic problems should be less severe. Since design speed for both the HP and LP spools is nearly the same, aerodynamic feasibility of a single-shaft gas generator warrants further study. However, this arrangement was not pursued since the scope of the study was specifically limited to a two-shaft machine.

TABLE XX - Continued

Sketch No.	Name	Description	Remarks
SK-D-2857	2nd study of alternate arrangements of the aerodynamic components.	The LP-spool axial compressor and turbine stages were replaced by radial components.	The impetus for this arrangement study was an improved rotor dynamic situation. However, the arrangement was quickly ruled out because of the complex aerodynamic flow path and ducting requirements.
SK-D-2858	3rd study of alternate arrangements of the aerodynamic components	This arrangement had the HP shaft running through the bore of the LP shaft. Both spools were independently supported.	This arrangement gave maximum separation of the hottest and coldest parts of the gas generator and, hence, the smallest axial temperature gradients. The HP spool was also accessible for direct driving of engine accessories. Flow path and ducting problems, however, were complex.
SK-D-2959	3rd configuration of rotor-bearing system for the gas generator	Close-coupled HP-spool turbine and compressor components; HP spool supported from LP spool; geared accessory power take-off from HP spool.	This configuration resulted in a short machine and short flow path. However, the LP spool bearings were excessively overloaded, and significant advances in gear technology would be needed for the accessory drive.
SK-C-2803	1st layout of basic structure and casings for gas generator	Conical structure and toroidal combustor used.	Purpose of this layout was to identify any basic problem areas with respect to integrating the rotor-bearing system configurations into a practical engine structure. None were found.

TABLE XX - Continued

Sketch No.	Name	Description	Remarks
SK-D-2804	4th configuration of rotor-bearing system for the gas generator	This configuration is essentially the same concept as the 1st configuration (SK-D-2738) except that it reflects the results of the first theoretical design study of the externally pressurized journal bearings.	To achieve stability of the rotor, very long bearing lengths were required. This significantly increased the lengths of both the HP and the LP spools. These lengths were judged to be infeasible from a practical bearing design standpoint, as well as from a rotor-dynamic standpoint.
SK-D-2805	5th configuration of rotor-bearing system	This configuration shows the first use of an auxiliary regenerative compressor as an integral part of the HP-spool assembly.	The purpose of the auxiliary compressor was to provide a higher supply pressure for the externally pressurized journal bearings. However, even with increased supply pressure, the rotor stability criterion could not be satisfied.
SK-D-2806	6th configuration of rotor-bearing system	This configuration shows the first use of 3-inch-diameter journals for the HP spool. Previous configurations had used 2-to-2 $\frac{1}{4}$ -inch journals.	Increased journal diameter was required for higher load capacity and stiffness. Although this diameter was satisfactory for load capacity, the rotor stability criterion could not be satisfied.
SK-D-2956	7th configuration of rotor-bearing system	This configuration shows a "folded" heat dam concept for the HP spool.	Design of this heat dam was not very practical.
SK-D-2958	8th configuration of rotor-bearing system	First configuration to show overhung HP compressor and turbine arrangement.	Bearing materials study was completed at this point. Maximum allowable journal bearing temperature was established to be 1500°F for near-term future. This arrangement appeared to be the only sensible means for meeting the temperature limit.

TABLE XX - Continued

Sketch No.	Name	Description	Remarks
SK-D-2807	9th configuration of rotor-bearing system	This configuration shows a very thin shaft connecting the LP-spool turbine and compressor. The turbine and the compressor are individually supported by two journal bearings.	This arrangement required four, rather than two, journal bearings for the LP spool. This was considered to be somewhat complex.
SK-D-2808	10th configuration of rotor-bearing system	Concept same as 8th configuration except for increased diameter of LP shaft.	Large-diameter LP shaft improved LP-spool dynamics, but required a large bore in HP shaft. This in turn resulted in excessively high stresses and centrifugal growth in HP-spool journals.
SK-D-2809	11th configuration of rotor-bearing system	This configuration was made to evaluate design problems for a "low-speed" HP spool. Wheel diameters were increased to correspond to a 50,000-rpm design speed.	In spite of the lower speed, the stability criterion for a rotor supported by externally pressurized bearings could not be satisfied.
SK-D-2853	12th configuration of rotor-bearing system	This configuration shows an inverted bearing arrangement for the HP spool. The journals are stationary, and the bearing sleeves are mounted in the hubs of the turbine and compressor wheels. Externally pressurized bearings are used.	Centrifugal growth of wheels increases bearing clearance in this concept. In previous configurations, journal centrifugal growth decreased clearance. Although problems of stability still exist, this is an intriguing concept for future consideration. The stationary journal may allow practical

TABLE XX - Continued

Sketch No.	Name	Description	Remarks
SK-D-2883	13th configuration of rotor-bearing system	This configuration is the first design in which self-acting journal bearings were introduced. Otherwise, the concept is similar to the 8th rotor-bearing system configuration.	means for introducing bearing system damping which would improve rotor stability. Significant reduction in shaft length also appears possible. However, this concept was not pursued since it involved a number of new development areas which have not yet been demonstrated.
SK-D-2884	14th configuration of rotor-bearing system	This configuration shows an overhung HP-spool turbine, inboard turbine-end journal, radial compressor, outboard compressor-end journal, and a thrust bearing attached to the end of the shaft.	Results of initial load capacity and stability investigations with self-acting bearings were encouraging.
SK-D-2933	15th configuration of rotor-bearing system	This configuration shows a "high-speed" HP spool. Wheel diameters were decreased to correspond to a 70,000-rpm design speed.	Thrust bearing OD was incompatible with the aerodynamic inlet flow path to the radial compressor.
			Analysis indicated that the self-acting bearing design would favor high-speed operation.

TABLE XX - Continued

Sketch No.	Name	Description	Remarks
SK-D-2954	16th configuration of rotor-bearing system	A more refined version of the preceding configuration.	Long LP-spool shaft had four bending criticals within operating speed range.
SK-D-3058	LP turbine-end bearing region	Drawing shows details of bearing mount and flexure support for pivoted-pad bearing.	Analysis indicated the detail design features are feasible.
SK-E-3025	Advanced gas generator assembly	Drawing shows integration of rotor-bearing systems into gas generator assembly.	This drawing represents a cumulative result of the best features from all previous designs.

Unclassified

Security Classification

DOCUMENT CONTROL DATA - R & D		
<i>(Security classification of title, body of abstract and indexing annotation must be entered when the overall report is classified)</i>		
1. ORIGINATING ACTIVITY (Corporate author) Mechanical Technology Incorporated Latham, New York		2a. REPORT SECURITY CLASSIFICATION Unclassified
		2b. GROUP
3. REPORT TITLE FEASIBILITY OF GAS BEARINGS FOR SMALL HIGH-PERFORMANCE AIRCRAFT GAS TURBINES		
4. DESCRIPTIVE NOTES (Type of report and inclusive dates) Final Report		
5. AUTHOR(S) (First name, middle initial, last name) Peter William Curwen		
6. REPORT DATE March 1969	7a. TOTAL NO. OF PAGES 297	7b. NO. OF REFS 52
8a. CONTRACT OR GRANT NO. DAAJ02-67-C-0026	9a. ORIGINATOR'S REPORT NUMBER(S) USAAVLABS Technical Report 68-87	
b. PROJECT NO. Task 1G162204A01409		
c.	9b. OTHER REPORT NO(S) (Any other numbers that may be assigned this report)	
d.		
10. DISTRIBUTION STATEMENT This document has been approved for public release and sale; its distribution is unlimited.		
11. SUPPLEMENTARY NOTES		12. SPONSORING MILITARY ACTIVITY US Army Aviation Materiel Laboratories Fort Eustis, Virginia
13. ABSTRACT Future U. S. Army aircraft missions will require propulsion systems having significantly improved power-to-weight ratio and specific fuel consumption. To obtain these goals, simultaneous increases in engine operating pressures and temperatures are required. These ascending performance conditions, with accompanying high rotational speeds, will impose increasingly severe operating requirements on main engine bearings and seals. Because of the high temperatures and high speeds, conventional oil lubrication techniques may not be adaptable to the next generation of small engines. If this should be the case, new lubrication methods will be required. One such method is the air-lubricated (gas) bearing. This report presents the results of a comprehensive study, based on existing analytical techniques and test data, to assess the feasibility of, and to identify the problem areas related to, the application of gas bearings to an advanced two-spool gas generator. A 4.5-pound-per-second engine having the following gas-generator design-point operating conditions has been studied: turbine inlet temperature, 3000°F; compressor pressure ratio, 18:1; HP-spool speed, 70,000 rpm; and LP-spool speed, 62,800 rpm.		

DD FORM 1473

REPLACES DD FORM 1473, 1 JAN 64, WHICH IS OBSOLETE FOR ARMY USE.

Unclassified

Security Classification

Unclassified

Security Classification

14. KEY WORDS	LINK A		LINK B		LINK C	
	ROLE	WT	ROLE	WT	ROLE	WT
Gas Turbines Bearing Systems Gas Bearings Lubrication Systems						

Unclassified

Security Classification